NUMERICAL MODELLING OF SLAB-COLUMN JOINT OF RC FLAT PLATES

by

MOHAMMAD RAFIQUL ISLAM

MASTER OF SCIENCE IN CIVIL ENGINEERING (STRUCTURAL)

DEPARTMENT OF CIVIL ENGINEERING

BANGLADESH UNIVERSITY OF ENGINEERING AND TECHNOLOGY,

DHAKA, BANGLADESH

FEBRUARY, 2014

The thesis titled "NUMERICAL MODELLING OF SLAB-COLUMN JOINT OF RC FLAT PLATES" submitted by Mohammad Rafiqul Islam, Roll No: 100704320F, Session: October/2007; has been accepted as satisfactory in partial fulfillment of the requirement for the degree of Master of Science in Civil Engineering (Structural) on 11th February, 2014.

BOARD OF EXAMINERS

Dr. Tahsin Reza Hossain Professor Department of Civil Engineering BUET, Dhaka-1000.	Chairman (Supervisor)
Dr. A.M.M. Taufiqul Anwar Professor and Head Department of Civil Engineering BUET, Dhaka-1000.	Member (Ex-Officio)
Dr. Khan Mahmud Amanat Professor Department of Civil Engineering BUET, Dhaka-1000.	Member
Dr. Sharmin Reza Chowdhury Associate Professor Department of Civil Engineering Ahsanullah University of Science and Technology, Dhaka.	Member (External)

DECLARATION

It is hereby declared that except for the contents where specific references have been made to the work of others, the study contained in this thesis is the result of investigation carried out by the author. No part of this thesis has been submitted to any other University or other educational establishment for a Degree, Diploma or other qualification (except for publication).

Signature of the Candidate

_____

(Mohammad Rafiqul Islam)

CONTENTS

LIST OF FIGURES

LIST OF TABLES

NOTATIONS

σ_c	Compressive stress at any strain ε_c
σ_t	Tensile stress at any strain ε_t
σ_{cu}	Ultimate stress at compressive force
ε_{cu}	Ultimate strain at compressive force
σ_{tu}	Ultimate stress at tensile force
ε_{cr}	Cracking strain at tensile force
σ_{true}	True stress
ε_{true}	True strain
σ_{nom}	Nominal stress
ε_{nom}	Nominal strain
ε^t	True total strain
ε^{el}	True elastic strain
ε^{pl}	True plastic strain
E	Modulus of elasticity
E_c	Modulus of elasticity of concrete
E_{ci}	Modified parameter corresponds to E_c
E_s	Modulus of elasticity of steel
f'_c	Ultimate uniaxial compressive strength
f_r	Ultimate tensile strength (modulus of rupture)
f_y	Yield stress of steel
ε_{c1}	Strain at corresponding ultimate uniaxial compressive strength f'_c
ε_y	Strain at corresponding yield stress f_y
ν_c	Poisson's ratio for concrete
ν_s	Poisson's ratio for steel
w_c	Unit weight of the hardened concrete in pcf
γ_c	Decent function
G_{cl}	Constant crushing energy (19.0KN/m)
l_c	Characteristics length of the simulated or tested specimen
w	Crack opening according to(Hordijk, 1992)

w_c	Maximum crack opening (180μm) according to(Hordijk, 1992)
c_1=3, c_2=6.93	Free parameters determined experimentally by (Hordijk, 1992)
b_c=0.7, b_t=0.1	Damage parameters according to (Polling, 2000)
$\psi = 30^0$	Dilatational angle according to Lee (1998)
$fb_0/ fc_0 = 1.16$	Ratio of biaxial to uniaxial compressive strength according to Kupfer (1973)
K = 0.67	Second stress invariant ratio
e = 0	Eccentricity
μ = 0	Viscosity parameter
d	Damage variable
d_t	Tension damage variable
d_c	Compression damage variable
A_v	Area of shear reinforcement
ρ	Reinforcement ratio
ρ_b	Balance steel ratio
h	Total depth of slab
d	Effective depth of slab
c	Column dimension
A_c	Area of the critical section
V_n	Nominal Shear strength
k, α, β, ξ	Parameters
φ	Reduction factor
γ_f, γ_v	Fraction of unbalanced moment
M_u, M_{slab}	Unbalanced moment
FE	Finite Element
EXPT	Experimental
R.R.	Reinforcement Ratio (%)
W.R.	Without Reinforcement

ACKNOWLEDGRMENT

The author wishes to convey his profound gratitude to Almighty Allah for allowing him to bring this effort to fruition.

The author wishes to express his deepest gratitude to his supervisor Dr. Tahsin Reza Hossain, for his continuous guidance, invaluable suggestions, encouragement, generous help and unfailing enthusiasm at every stage of this study. His active interest in this topic and valuable advice was the source of author's inspiration.

The author is indebted to the Head of the Department of Civil Engineering, BUET for providing all the facilities of the department in materializing this work. The author gratefully acknowledges the cooperation of all concerned persons of the department, Civil Engineering Library, BUET Central Library and Computer Center for their assistance that were enjoyed by the author.

The author wishes to express his most sincere respect and gratitude to his family for their continuous encouragement and blessings and a constant source of inspiration throughout his life.

ABSTRACT

In the design of reinforced concrete flat plates, the region around the column always pose a critical analysis problem where punching shear failure occurs due to brittle nature of this failure mode. Column tends to punch through the slab because of the shear stresses that act around the perimeter of the column and develop a failure surface in the form of a truncated cone or pyramid shape. This punching shear failure is one of the topics of intensive research work in the recent years. The slab-column connection behaviour is also critical as it transfers combined gravity and lateral loads. The performance of slab-column connection has often been less than satisfactory under seismic action. This has prompted the design community to establish rather restrictive rules for flat plate system in earthquake prone region.

Before carrying out numerical model of slab-column connection, some existing literatures on the relevant field based on experimental investigation, analytical methods, numerical models and various codes of practice are thoroughly reviewed. A numerical model of slab-column joint of RC flat plate have been generated by using 'ABAQUS' software based on nonlinear finite element method. For nonlinear finite element analysis, material nonlinearity is modeled by considering the nonlinear effects due to cracking and crushing of concrete and yielding of steel reinforcement. A complete model requires the elastic properties, inelastic stress-strain relations and failure criteria of concrete. Regarding the concrete material behaviour, a nonlinear user-defined material approach based on the concrete damage plasticity model is used. On the other hand, reinforcing steel behaves as an elastic-perfectly plastic material.

A sensitivity analysis has been performed for mesh density to obtain a reliable solution. The numerical results of present finite element model have been verified with the experimental results and other numerical results. A satisfactory result has come in between the present numerical results and the experimental results or other numerical results which indicates the suitability and accuracy of present finite element model. All loads are applied in terms of displacement control criteria. A systematic parametric study of material and geometric parameters like concrete compressive strength, the amount of longitudinal reinforcement, yield stress of steel, effect of compression reinforcement, slab thickness, column dimensions and boundary conditions is carried out to identify the effects of different parameters on punching shear strength of flat plates. ACI 318-08/BNBC 2006 code provision is found to be more conservative in case of punching shear design of flat plates. It underestimates the influence of maximum material and geometric parameters to predict the actual punching capacity. Hence, a modification to the ACI 318-08/BNBC 2006 code equation has been discussed and verified against the results of present finite element results.

Four different slab-column joint of RC flat plates have been modeled numerically under different design specifications and analyzed to study the effects of different load combinations and loading sequence. The design and performance of these slabs have been discussed considering ACI 318-08/BNBC 2006 code provisions. It has been found that strength of slab-column connection improves if seismic design is performed. The performance of flat plate high-rise building structure with shear-wall has been checked under combined gravity and lateral loads considering different seismic zone. The percentage of moment transfer through different strip of slab is also analyzed under gravity and lateral loads.

Chapter 1

INTRODUCTION

1.1 Background and Present State of the Problem

Bangladesh and the northeastern Indian states have long been one of the seismically active regions of the world and have experienced numerous large earthquakes during the past 200 years. In geological point of view, part of Bangladesh is situated in moderate to high seismic zones. However, in the country a rapid urbanization is going on. With this, now-a-days flat plate structures are very much popular for its advantages regarding use and constructability. Flat plates, being thin members, are uneconomical from steel point of view, but they are economical in terms of formwork. Because formwork represents significant part of cost of reinforced concrete construction, economy of formwork often means overall economy. Reduced story height resulting from the thin floor, the smooth ceiling and the possibility of slightly shifting column location to fit the room arrangements are factors contributing in the overall economy and flexibility in architectural design. So it is important to understand the slab-column connection including punching shear behaviour at critical section of flat plates. However, flat plate as part of lateral load carrying system is not permitted in high seismic zone according to ACI 318 (2008)/BNBC (2006) as slab-column connection performance are not satisfactory in carrying seismic loads.

In the design of reinforced concrete flat plates, the regions around the column always pose a critical analysis problem. Column tends to punch through the flat plates, flat slabs and footings because of the shear stresses, which act in them around the perimeter of the columns. Shear failure, both beam and punching type are considered more dangerous than flexure failure. This is due to greater uncertainty in predicting shear failure, which is likely to occur suddenly with no advance warning of distress. When exposed to seismic loads, the performance of slab-column frames has often been less than satisfactory. Brittle punching failures of flat plates have

been observed during several earthquakes as documented by AISI (1964). This has prompted the design community to establish rather restrictive rules for flat plate systems in earthquake prone regions. It has also inspired researchers to start extensive experimental work and to develop new ways to make the connections stronger and more ductile in order to allow more widespread use of flat plate systems in seismic zones.

Large research efforts have been made in the past and are still being continued to develop methods for a reliable prediction of the punching shear capacity. Numerous tests [Gardner (1990), Elstner and Hognestad (1956), Bazant and Cao (1987)] have been carried out to evaluate the punching shear strength of slabs. Several theories have been put forward to estimate the strength observed in these tests. In Bangladesh, a number of research works on punching shear capacity of flat plates have been carried out. Alam (1997) presented punching tests conducted on reinforced concrete slabs with their edges restrained as well as unrestrained. Islam (2004) modelled numerically the punching shear behaviour of RC flat plates using finite element package 'ANSYS' and compared various test results with finite element analysis. As no such numerical work has been carried out for further research in the context of Bangladesh, it would be useful to conduct a nonlinear analysis to model the slab-column connection of RC flat plates.

1.2 Objectives with Specific Aims and Possible Outcome

The objectives of the present study are:

- To model numerically the slab-column connection with emphasis on punching shear behaviour of reinforced concrete flat plates subjected to lateral loads using nonlinear finite element method and validate the model against available experimental and numerical results.
- To carryout a parametric study to identify the effect of different parameters influencing the performance of slab-column connection of flat plate.

- To investigate the effectiveness of different Building Code provisions in predicting punching shear strength of flat plates due to both gravity and lateral load and propose possible improvements if any.

With successful completion of the above objectives, the behaviour of slab-column connection of flat plate is more clearly explained. A possible improvement on the punching shear prediction equations is also proposed to help designing the connection.

1.3 Methodology of Work

The modeling of reinforced concrete, to be employed in this work, use separate materials and elements for the concrete and steel reinforcement. In the discrete modeling of a RC slab, concrete is modeled by three-dimensional solid elements while the reinforcing steel is modeled by truss elements. The connectivity between a concrete node and a reinforcing steel node can be achieved by sharing the same node; hence perfect bond is assumed. The nonlinear effect due to the cracking and crushing of concrete and the yielding of steel reinforcement has been included. In this work, slab-column connection of flat plates is modeled numerically by using finite element package 'ABAQUS'. An incremental finite element technique is used which simulates the nonlinear load-deflection behaviour of reinforced concrete structure.

Results of the nonlinear finite element analysis are compared with some test results to ensure the acceptability of the numerical model used. A parametric study will be carried out to identify the effect of different material parameters mainly concrete strength, flexural reinforcement ratio and the yield strength of reinforcement and geometric parameters like span-depth ratio and the column size on the behaviour of the slab-column connection of flat plates. Explanation could be made on the behaviour of slab-column connection due to lateral load variation. Investigation should be made on different Building Code equations in predicting punching shear strength of flat plates due to both gravity and lateral load. A possible improvement

on the punching shear prediction equations would also be proposed to help designing the connection.

1.4 Outline of the Thesis

The thesis consists of 7 chapters. The current chapter is Chapter 1, which introduces the general background and present state of problem of this research work and summary of aims, objectives and methodology. Literature review and review of codes and theories for determining the punching shear capacity and lateral resistance of flat plates are described in Chapter 2. Chapter 3 describes the finite element modeling of reinforced concrete flat plates. Chapter 4 gives details of nonlinear FE analysis for determination of punching shear by 'ABAQUS'. Performance of the model is verified against different experimental results in this chapter too. Chapter 5 is dedicated to a thorough parametric study to identify the effects of material and geometric parameters on the punching shear capacity of flat plates. Investigation and findings of this chapter leads to recommendations on the choice of structural parameters to enhance the punching shear strength. It also presents a rationale for the punching shear prediction equation. Chapter 6 discusses on slab-column connection under seismic load. It describes the influence of flat plates having better lateral load carrying system under different seismic zone. The conclusions made from the study are presented in Chapter 7. This chapter also recommends future work for possible extension of the current study.

Chapter 2

LITERATURE REVIEW

2.1 General

Punching shear is one of the most critical phenomena for flat plate building systems due to the brittle nature of this failure mode. The region of a slab in the vicinity of a column could fail in shear by developing a failure surface in the form of a truncated cone or pyramid. This type of failure, called a punching shear failure, is usually the source of collapse of flat plate and flat slab buildings. Punching shear in slabs is a two-dimensional analog of shear in beam. The failure is a sudden rupture, which is not much restrained by the main reinforcement. Therefore the shear tends to reduce the ultimate load of the structure below its flexural capacity. It is one of topics of intensive research in recent years by various concrete structure researchers. Numerous tests have been carried out to evaluate the punching shear strength of slabs. Several theories have been put forward to predict the strength observed in these tests. This chapter summarizes the experimental investigations and analytical approach adopted by different researchers along with provisions of various building codes.

2.2 Punching Shear Mechanism

When a two-way slab is heavily loaded with a concentrated load or where a column rests on a two-way footing, diagonal tension cracks form that encircles the load or column. These cracks are not visible, except as flexural cracks. Such cracks extend into compression area of the slab and encounter resistance near the load similar to the shear-compression condition. The slab or footing continue to take load and finally the punching failure mechanism consists of the punching out a solid of revolution as a pyramid shape of concrete in the vicinity of column is adopted as indicated in Fig. 2.1, the surrounding slab remaining rigid. Diagonal cracks do not form further out from the load or column because of rapid increase in the failure perimeter. The initial diagonal cracks thus proceed to failure in punching shear type

of failure directly around the load. The slab is reinforced in such a way that flexural failure is prevented. This implies that a punching failure mechanism forms first before the yielding of the main reinforcement.

In compromising between initial cracking and the final shear condition at failure for different ratios between column (or load) dimension and footing (or slab) thickness, different codes recommend a single punching shear strength calculated at a pseudo-critical distance from the column face or edge of the load.

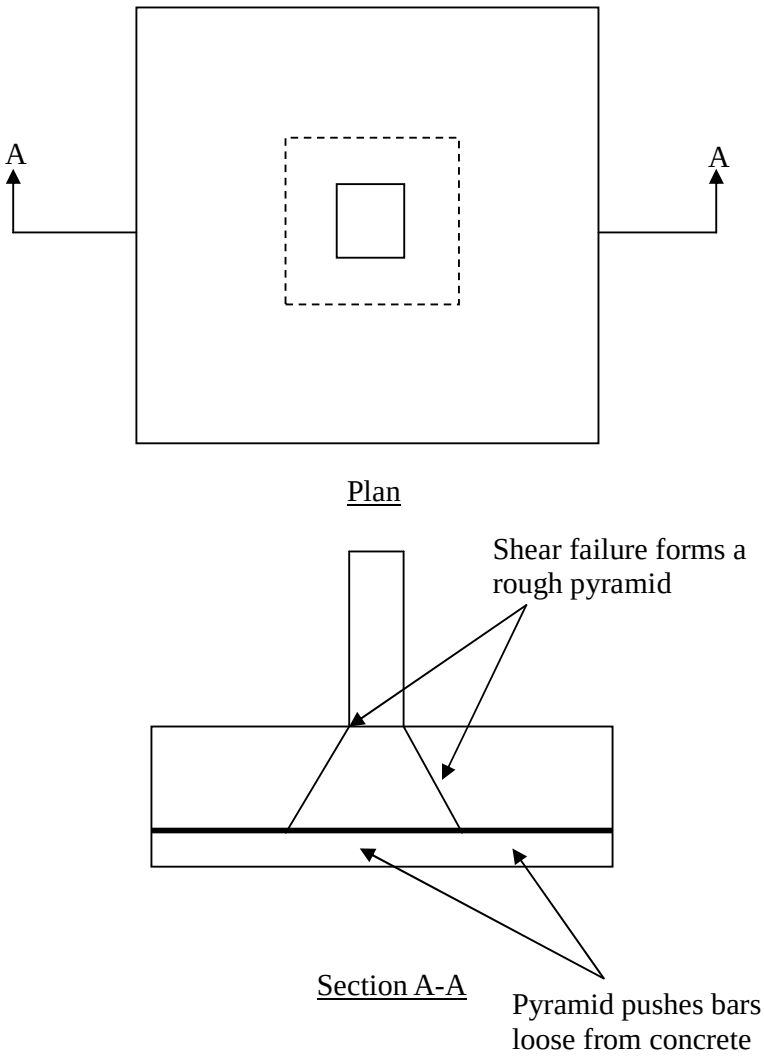

Figure 2.1 A square column tends to shear out a pyramid from a footing or flat plate

2.3 Experimental Investigations

Several experimental investigations have been carried out to evaluate the punching shear strength of flat plates and slabs. These investigation covers both concrete material and geometric parameters like concrete strength, influence of reinforcement type and ratio, column size, plate thickness, edge conditions etc. Some of these are briefly summarized in the following subsections.

2.3.1 Effect of concrete strength

Gardner (1990) presents the result of an investigation relating punching shear to concrete strength and steel ratio. It is concluded that the shear capacity is proportional to the cube root of concrete strength and steel ratio. It is also opined that the shear perimeter should be increased by using large columns and column capitals, if the punching shear capacity is in doubt. Elstner and Hognestad (1956) presented a research report on the methods and results of experimental work on the shearing strength of reinforced concrete slabs subjected to a centrally located concentrated load. The test findings show that the shearing strength of slabs is a function of concrete strength as well as several other variables like percentage of tension reinforcement, size of column, conditions of support and loading, distribution of tension reinforcement, and amount and position of shear reinforcement.

2.3.2 Size effect

Punching shear tests of geometrically similar reinforced concrete slabs of different sizes have been carried out by Bazant and Cao (1987). The test prediction summarized that the punching shear failure of slab without stirrup is not plastic but brittle. Results of an experimental investigation on the punching shear strength of reinforced concrete slabs with varying span to depth ratio have been summarized by Lovrovich and McLean (1990). It is reported that the ACI Code does not recognize span to depth ratio effects or the effects of restraining action at the support when treating punching shear in reinforced concrete slabs. It is also observed that

punching shear strengths are much greater than the values permitted by the ACI Code.

Broms (1990a) present a design method to predict the punching strength and deflection of flat plates at interior columns. Failure is assumed to occur when the compression zone of the slab in the vicinity of the column is distressed by either high radial compression stress or by a high tangential compression strain. Size effects and the effect of increasing concrete brittleness with increasing strength are both considered. The method showed excellent agreement with results from punching tests reported in the literature, with conditions ranging from ductile flexural failures to brittle punching failures, from small test specimens to a full-sized structure, and from symmetrical to unsymmetrical loadings.

2.3.3 Effect of shear reinforcement

Yamada, et al. (1991) performed a research programme for the determination of the effect of shear reinforcement type and ratio on the punching shear strength of monolithic slab column connections. The first type of shear reinforcement consisted of hat-shaped units, very advantageous from the points of view of prefabrication and field installation. The second type consisted of double-hooked shear bars, more difficult to install but with very efficient anchorage. Experimental results showed that the hat-shaped shear reinforcement was not effective because of lack of proper anchorage. Double-hooked reinforcement showed high effectiveness, which resulted in a considerable increment of the punching shear resistance of the connection. Olivera, et al. (2000) introduced a novel form of inclined stirrups and reported the results of test slabs with such reinforcement. Companion tests of slabs without shear reinforcement and slabs with vertical stirrups were also reported. The inclined stirrups were shown to function well and produced punching resistances superior to those obtained with vertical stirrups.

Four reinforced concrete slab-column sub-assemblies were subjected to a high intensity shear and moment transfer at the column-slab connections by Pillai et al.

(1982). The effectiveness of shear reinforcement in increasing the shear strength and preventing punching failure and in improving the ductility of the connections were assessed. It was found that shear reinforcement in the slab at the connections prevent punching failure and generally double their ductility. Ghoneim and MacGregor (1994a) presented the results of 19 tests of reinforced concrete plates simply supported on four edges. The plates were subjected to combined inplane compressive and lateral loads. The variables in the experimental investigation included the loading type, plate slenderness, inplane load level, aspect ratio, reinforcement ratio in the two orthogonal directions, and loading sequence. The test programme was successful in providing data relating to the behaviour of reinforced concrete plates under combined inplane compressive and lateral loads.

2.3.4 Edge condition effect

Alam (1997) presented punching tests conducted on reinforced concrete slabs with their edges restrained as well as unrestrained. The significant positive effect of edge restraint on the punching failure, resulting in enhancing the ultimate punching strength, has been noticed. Aghayere and MacGregor (1990a) presented the results of tests on nine reinforced concrete plates simply supported along four edges and subjected to combined uniaxial compression and uniform transverse loads. The results of the investigation led to the conclusion that the presence of an axial in-plane load can lead to a reduction in the transverse load capacity of a concrete plate. This reduction depends on the in-plane load level, the width to thickness ratio, the concrete strength, the amount of reinforcement, and the aspect ratio of the plate.

Kuang and Morley (1992) tested 12 restrained reinforced concrete slabs with varying span to depth ratio, percentage of reinforcement, and degree of edge restraint. It is reported that the punching shear strengths are much higher than those predicted by ACI 318 and BS 8110 codes. The study suggested that there is a definite enhancement in punching shear strength as the degree of edge restraint increases. The enhanced punching shear capacity was a result of compressive membrane action caused by restraining action at the slab boundaries.

2.3.5 Slab-column connection behaviour

Hammill and Ghali (1994) reported test results of five full-scale reinforced concrete flat plate connections with corner columns subjected to shear-moment transfer. The tests showed that the equations of the codes (ACI 318-89 and Canadian Standard CAN-A23.3-M84) are conservative and can be improved by addition of an appropriate equation for the fraction of the unbalanced moment resisted by eccentric shear stress. It is shown that the codes, or their commentaries, need to provide the equations necessary to determine the extent of the shear-reinforced zone for a corner column connection. Mortin and Ghali (1991) reported test results of six full-scale reinforced concrete flat plate connections with edge columns subjected to shear-moment transfer with and without shear reinforcement, to verify the effectiveness of the stud shear reinforcement. The results confirmed the effectiveness of this type of shear reinforcement in improving shear strength and ductility.

2.3.6 Shear strengthening techniques

EI-Salakawy et al. (2003) presented new shear strengthening technique for concrete slab-column connections. The aim of the programme was to test a new method for strengthening existing reinforced concrete slabs for punching shear. The new strengthening technique consists of shear bolts externally installed in holes drilled through the slab thickness. It is found that the presence of shear bolts substantially increased the punching capacity and the ductility of the connections. Elgabry and Ghali (1990) presented rules to design and detail stud-shear reinforcement in accordance with the 1989 ACI Building Code (ACI 318-89). Because of the effectiveness of anchorage, design rules that reduce the amount of shear reinforcement are suggested and applied. Shaaban and Gesund (1994) carried out experimental study to determine whether addition of steel fibers to the concrete mix could significantly increase the punching shear strength of reinforced concrete flat plates. Thirteen slab specimens and their companion cylinder specimens were tested. Test results of this study indicated that the addition of steel fibers to the concrete mix did significantly enhance the punching shear strength of slabs.

Binici and Bayrak (2003) presented a strengthening technique for increasing punching shear resistance in reinforced concrete flat plates using carbon fiber reinforced polymers (CFRPs). This strengthening method employed CFRP strips in the vertical direction as shear reinforcement around the concentrated load area in a specified pattern. The results showed that, by using a sufficient amount of CFRP strips in an efficient configuration, the failure surface can be shifted away from the column. The load carrying capacities of the strengthened reinforced concrete slabs were increased with increasing amount of vertical CFRP reinforcement used in a wider area.

2.3.7 Miscellaneous studies

Broms (2000) presented a design concept that examines the punching failure mode of flat plates, verified by test, and design recommendations are given. The system provided excellent safety against progressive collapse of flat plate buildings, a basic requirement that seems to be overlooked in many current concrete codes. Loo and Chiang (1993) carried out a comparative study on the methods of punching shear strength analysis of reinforced concrete flat plates. It is found that the ACI and the British methods are applicable only to flat plates with torsion strips; the codes also tend to give unsafe predictions for the punching shear strength.

Mitchell and Cook (1984) investigated the slab structures after initial failure in order to determine a means of preventing progressive collapse. Analytical models for predicting the post-failure response of slabs are presented and the predictions are compared with experimental results. These analytical models along with experimental investigation enabled the development of simple design and detailing guidelines for bottom slab reinforcement, which is capable of hanging the slab from the columns after initial failures due to punching shear and flexure. Rangan (1990) presented the background theory and the punching shear design provisions contained in the Australian Standard for Concrete Structures, AS 3600-1988. The correlation of the design equations with test data is also presented. It is believed that the

Australian method could serve as a useful alternative to the ACI Building Code provisions.

2.4 Analytical Investigation

Several investigations have been carried out using various analytical models and theories to evaluate the punching shear strength of flat plates and slabs. These investigations cover beam-strip approach, truss model approach, fracture mechanics, plasticity model, equivalent frame method, and assumed deflection method. Some of these are briefly summarized in the following subsections.

2.4.1 Beam-Strip Approach

Siao (1994) adopted a beam-strip approach to predict the punching shear strength of flat slabs with and without shear reinforcements. Predicted results were compared with existing experimental data previously reported by other researchers. Good agreement was observed. Elstner and Hognestad (1956) utilized the beam-strip approach in their investigation of flat slab punching shear strength. Several beam-strip specimens were tested but reached no useful conclusion, as the specimens failed in flexure.

2.4.2 Truss Model Approach

A truss-model-based design procedure is developed for transversely reinforced slabs by Marti (1990). The truss model approach for shear design of beam is extended to transversely reinforced slabs, and the application of the newly developed design procedures is illustrated for the case of a thick transfer plate in a high-rise building. Alexander and Simmonds (1992) proposed that punching shear failure could be represented by a truss model and that failure is due to the concrete cover failing to contain the out-of-plane component of force between the reinforcement and the concrete compression struts. It is assumed that concrete tensile capacity is related to the square root of the concrete strength. The truss model does not include components of the shear failure mechanism such as aggregate interlock and friction,

dowel action of the longitudinal steel, and shear carried across uncracked concrete. The study led to the conclusion that concrete cover of the top mat reinforcement in slabs of usual span and loading may be as significant to punching shear strength as is the flexural depth of the slab.

2.4.3 Fracture Mechanics

Bazant and Cao (1987) used fracture mechanics, a theory which is based on energy and stability criteria instead of strength criteria to investigate the size effect on punching shear strength. The salient aspect of fracture mechanics is the size effect. The nominal stress at failure of geometrically similar structures decreases as the structure size increases for fracture mechanics. The model used was essentially a modified shear perimeter approach and it was assumed that the shear strength was directly proportional to the concrete strength. It is reported that the larger the slab thickness, the steeper the post-peak decline of the load deflection diagram ; thus, the punching shear behaviour of thin slabs is closer to plasticity, and that of thick slabs is closer to linear elastic fracture mechanics. This independently confirms the applicability of the size-effect law, since this law predicts exactly such kind of behaviour.

2.4.4 Plasticity Model

Salim and Sebastian (2002) presented plasticity model for predicting punching shear strengths of reinforced concrete slabs. The upper-bound theory of plasticity is employed to predict the punching shear failure loads of reinforced concrete slabs without shear reinforcement and without in-plane restraint. A parabolic Mohr failure criterion is adopted for the concrete to ensure that the important variation in angle of friction of the concrete with stress state is represented, with the material assumed to be rigid-perfectly plastic. The problem is treated as three-dimensional axisymmetric. It is found that the predictions correlate well with a range of experimental data for low, normal, and high strength concretes, and for both small-scale and large-scale slabs. A theoretical solution for the punching shear strength of concrete slabs is presented by Bortolotti (1990). By applying the theory of plasticity, the form of the

failure surface generatrix visualizes processes of strain softening by tension and compression in concrete. A comparison with the experimental results in literature shows that the theoretical equations are valid as long as the slabs are rigid enough to prevent displacements of the border of the slab.

If border displacements and rotations are allowed, the theoretical values disagree with the experiment.

2.4.5 Equivalent Frame Method

Equivalent frame method was derived with the assumption that the analysis would be done using the moment distribution method. In the equivalent frame method the structure is divided for analysis, into continuous frames centered on the column lines and extending both longitudinally and transversely. Murray et al. (2003) proposes a modification to the ACI 318-02 equivalent frame method of analysis of reinforced concrete flat plate for exterior panels. Two existing code methods were examined viz, ACI 318-02 and BS 8110. The derivation of the torsional stiffness of the edge strip as proposed by ACI 318-02 is reviewed and a more accurate estimate of this value is proposed based on both theoretical analysis and experimental results. The proposed method leads to a more accurate prediction of the moments in the plate at the column front face, at the panel midspan, and in the edge column. Robertson (1997) applied the effective width and equivalent frame analysis methods to a flat plate test specimen. The theoretical moment distribution and lateral drift show poor agreement with the test specimen results. A modified two-beam analytical model is proposed. The modified model is able to reproduce both the slab moment distribution and lateral drift observed in the test specimen.

2.4.6 Miscellaneous Studies

Aghayere and MacGregor (1990a) developed a method of analysis for determining the load-deflection response of concrete plates simply supported on four edges and subjected to combined action of axial or eccentric in plane loads and transverse loads based on the assumed deflection method. In the assumed deflection method, a

deflection function is assumed for the beam-column throughout the entire load range. A method of analysis is developed based on the assumed deflection method. In this way calculation of the strength of a plate is reduced to a one-degree of freedom problem. Material nonlinearities are taken into account using moment curvature relationships, which include tension-stiffening effects. The results from the analysis are compared to test results from an experimental program carried out by the authors. Good agreement was obtained for square simply supported plates and rectangular plates with an aspect ratio of 1.5.

Loo and Falamaki (1992) presented an analytical procedure for evaluating the punching shear strength of the corner and edge connections of reinforced concrete flat plates with spandrel beams. A comparative study is carried out based on the authors own mode test data and those published by others. The results indicate that the proposed analytical procedure is accurate and reliable. Regan and Jorabi (1988) have shown that analysis using current code provision and making separate calculations of full width shear strength and punching shear are inappropriate. It is proposed that design checks should be based on nominal shear stresses obtained as the sum of stresses arising from two components of load bearing action. The first is a symmetrical spreading of concentrated load and the second is the spanning of the slab carrying the spread load between supports.

2.5 Finite Element Method

In this method, the slab is divided into a number of sub-regions or finite elements, which are generally triangular, rectangular or quadrilateral in shape. They are considered interconnected only at discrete points, called nodes, at the corners of the individual elements.

The main problem in the application of the finite element method to linear elastic slab systems is to obtain a suitable force-displacement relationship between the nodal forces and the corresponding displacements at the nodal degrees of freedom. A further complication, in applying the method to reinforced concrete, is the

derivation of a suitable set of constitutive relations to model the slab behaviour under various loading conditions.

Modeling transverse shear by finite elements is one way of predicting behaviour. In order to mode transverse shear, proper finite element formulations must be used. For plate and shell structures this usually means using either three-dimensional elements or two-dimensional elements to model parts which can be approximated by such models. Three-dimensional elements are powerful and are an excellent choice for modeling details of the structure, but are inefficient for global analysis.

Gonzalez-Vidosa et al. (1988) used existing experimental data for reinforced concrete slabs failing in punching to validate a nonlinear finite element programme for concrete. The programme combines a general-purpose linear finite element analysis system called FINEL with a nonlinear iterative procedure based on the modified Newton-Raphson method and the residual-force concept. The iterative procedure incorporates constitutive laws describing the strength and deformational properties of concrete and steel, as well as criteria for the onset and propagation of the cracking process, which is treated following the smeared-crack approach. The constitutive model is implemented by following a standard stiffness approach. Reinforcing is implemented in the finite element mode by smearing it in isotropic layers. The concrete-steel interaction is governed by the assumption of perfect bond. Isoparametric elements are used to model both concrete and steel. Theoretical predictions showed good agreement with actual ultimate loads, regimes of behaviour, crack patterns, and experimentally available load-deflection curves.
Loo and Guan (1997) presented a nonlinear-layered finite element method capable of analyzing cracking and punching shear failure of reinforced concrete flat plates with spandrel beams or torsion strips. Incorporating a layered approach with transverse shear capabilities, the procedure takes into account the full interaction between cracking and failure analysis. The study is focused on the implementation of a non linear finite element procedure for determining both the deflection and the punching shear strength, at corner and edge-column connections of reinforced concrete flat plates with or without spandrel beams. Cracked concrete is treated as

an orthotropic material using a smeared crack approach. Tension stiffening is included to represent the behaviour of cracked concrete in tension. A strain hardening plasticity approach is employed to model the compressive behaviour of concrete. An eight-node degenerated shell element with biquadratic serendipity shape functions is adopted in conjunction with the layered approach. The model makes use of the transverse shear deformations associated with the Mindlin hypothesis. A postprocessor has been developed to present in graphical form, the crack patterns, finite element mesh and configurations, as well as the deformed shape of the slab. This significantly enhances the presentation of the cracking and failure processes of reinforced concrete flat plates. A comparative study is carried out in an effort to verify the accuracy and reliability of the proposed analytical procedure. Good correlation with the experimental results is observed.

Harmon and Zhangyuan (1989) analyzed transverse shear failures of reinforced concrete pates and shells using layered shell element that has been modified to mode shear behaviour more accurately. Three-dimensional failure criteria are used to predict transverse shear failure. The analytical results are compared with experimental results for beams, plates and shells subjected to concentrated forces. Good agreement between analysis and experiment is obtained for plates with and without shear reinforcement and for shells without reinforcement.

Polak (1998) examined the applicability of the finite element, layered, shell formation in the global analysis of reinforced concrete slabs when subjected to high concentrated transverse loads. A detailed finite element formulations based on the layered, degenerate shell elements is adapted, which can be used for the global analysis of pate-type structures and which accounts for the transverse shear effects. The layered approach, through the rigorous treatment of the states of strain and stress can mode complex behaviour of both thin and thick plates. The nonlinear solution algorithm is based on an iterative, full-load, secant stiffness formulation. The convergence criteria used are based on changes in deformations where displacements and rotations are examined separately. The formulation accounts for nonlinearities due to constitutive behaviour and changing structural geometry. The

results of finite element effective stiffness analyses are compared to both experimental results and the results in the layered analyses. Polak commends that the layered approach is a detailed, versatile and comprehensive approach to model nonlinear behaviour of members subjected to bending. And the effective stiffness approach is simpler and less time consuming. For typical slab systems, the effective stiffness formulations can provide results with accuracy comparable to the accuracy of the layered approach. Polak also checked the sensitivity of the proposed formulation when applied to the analysis of slabs with different reinforcement ratios, boundary conditions, and reinforcement orientations.

A model for predicting punching shear failures at interior slab-column connections was developed by Hueste and Wight (1999) based on experimental results obtained at various universities. This model has been incorporated into a new RC slab element for the nonlinear analysis program, DRAIN-2DM, along with the desired unloading behaviour when a punch occurs. The RC slab element was tested by modeling a four story RC frame building that experienced punching shear damage during the Northridge Earthquake. The observed punching shear failures were successfully post calculated using the RC slab element.

2.6 Slab-Column Connection under Seismic Actions

When exposed to seismic loads, the performance of slab-column frames has often been less than satisfactory. Brittle punching failures of flat slabs have been observed during several earthquakes as documented by AISI (1964) and Mitchell and co-workers (1990 and 1995). This has prompted the design community to establish rather restrictive rules for flat-slab systems in earthquake prone regions. It has also inspired researchers to start extensive experimental work, and to develop new ways to make the connections stronger and more ductile in order to allow more widespread use of flat slab systems in seismic zones.

In the mid-seventies, Hawkins, Mitchell and Hanna (1975) were the first to research the effects of lateral loads. Shortly thereafter, other researchers began to actively

expose a wide range of connections to seismic scenarios. Most of the test specimens contained shear reinforcement as the early studies showed that shear reinforcement not only increases the shear strength but significantly improves the ductility of the connection. To date most experimental work on seismic response of slab-column connections has been conducted on isolated interior specimens and Tests on isolated slab-column connections subjected to reversed-cyclic loading. One of the main objectives of these Research programs has been to identify key parameters and formulate relationships to predict the capacity of slab-column connections under seismic load demands. ASCE-ACI Committee 426 (1974) identified the following key parameters as being most relevant to the performance of the slab-column connections:

1. Concrete strength.
2. Ratio of the column size to the effective depth of the slab.
3. Size effects.
4. Flexural reinforcement ratio.
5. Effect of in-plane (membrane) forces.
6. Shape of the column.
7. Rate of loading.
8. Shear reinforcement.
9. Nature of the loading (i.e., reversed-cyclic versus static).

The experimental programs described a variety of different test configurations. In most cases isolated interior slab-column connections were tested which were intended to represent the negative moment region of slab in the vicinity of the column.

The test specimens were typically square or rectangular in plan, supported along their edges, either on all four sides, or on two opposite sides. Concentric gravity load was then applied through a column cast monolithically with the slab specimen. Cyclic unbalanced moments were most commonly simulated by applying lateral forces to the ends of the columns protruding from either face of the slab. This could be done under load control, in which case the lateral loads applied to the columns ends were equal and opposite to each other, or in displacement control, in which case the displacement of the ends of the columns were equal in magnitude. In

general, displacement control is favoured as it is more representative of the nature of seismic loading. It is also able to capture the descending branch of the moment displacement envelope.

Hawkins, Mitchell, and Hanna (1975) were the first to apply displacement controlled reversed-cyclic unbalanced moments. The primary test variables used in their test series included:

1. Positive and negative reinforcement ratios.
2. Concentration of flexural reinforcement in the vicinity of the column.
3. Amount and configuration of stirrup-type shear reinforcement.

Ghali, Elmasri and Dilger (1976) tested six full-scale isolated specimens, without shear reinforcement, subjected to a constant gravity load and either static or dynamic lateral loads. Pan and Moehle (1989) presented a review of previous tests on slab column connections under reversed-cyclic loading reported in the literature of the day, including four specimens of their own. Cao (1993) and Dilger and Cao (1994) reported on a series of seven isolated interior slab-column connections subjected to reversed-cyclic loading. Brown and Dilger (1994) and Dilger and Brown (1995) reported on the results of a series of test on nine interior slab-column connections. Megally and Ghali (1998) and (2000a) conducted a number of reversed-cyclic tests on both interior and edge isolated slab-column connections. Schreiber and Alexander (2001) tested two full-scale isolated slab-column connections to investigate the effect of adding corrugated steel fibres on the response of slab-column connections exposed to reversed-cyclic lateral loading. Using the same size specimens and testing apparatus as Schreiber and Alexander, Ali and Alexander (2002) tested two connections to investigate the effect of partially debonding the flexural slab reinforcement in the vicinity of the connection. Robertson et al (2002) re-examined the tests of Megally and Ghali (2000a) along with the results of tests on four isolated interior specimens of their own. Megally and Ghali (2000b) assumed effective slab stiffness should be taken from the higher end of the expected range (i.e., one half of the gross uncracked stiffness). Dechka (2001), Brown (2003) and Brown and Dilger (2004) suggested on yield-line theory and eliminates the need to

accurately assess the effective slab stiffness and displacements of the primary lateral load resisting system.

2.7 Punching Shear Prediction Equations

All design codes give provisions for checking punching shear capacity. These are empirical relations based on experimental and analytical results. In general, the punching shear clauses are extensions of the beam shear provisions of codes. Besides, several researchers have put forward their prediction equations based on respective experimental and / or analytical results. Some of these equations and code provisions are summarized in the following subsections.

2.7.1 Regan's equation

Regan (1981) developed an equation to calculate punching shear capacity. Regan's shear perimeter for rectangular columns was a rounded rectangle located 1.25d out from the column; for circular columns, it was the circular perimeter located 1.25d out from the column:

$$V_u = K_a K_{sc} K_s (p \times f'_c)^{\frac{1}{3}} \times d(\sum_c + 7.85d) \qquad (2.1)$$

Where,

V_u= ultimate shear force;

K_a=0.13 for normal density concrete;

K_{sc}=1.15x[4πx column area/(column perimeter)^2]$^{1/2}$;

K_s=size effect term (300/d)$^{1/4}$ (in SI units);

p= steel ratio;

f'_c= concrete strength;

d= effective depth of slab in mm; and

$\sum_c$= perimeter of the column.

2.7.2 Bazant and Cao's equation

Bazant and Cao (1987) were primarily concerned with size effects, but they did propose a formula for punching shear

$$v_u = C(1 + \frac{d}{\lambda_0 d_a})^{-1/2} \quad (2.2)$$

in which

$$\text{constant } C = k_1 f'_t (1 + k_2 \frac{\mathrm{d}}{\mathrm{b}}) \quad (2.3)$$

Where,

v_u = nominal shear stress at failure;

f'_t = direct tensile strength of concrete;

d_a=maximum aggregate size;

λ_0 = empirical parameter, 28.5;

k_1, k_2= empirical constants, (k_1=0.155, k_2=0.35);

b= diameter of punch; and

d=slab thickness.

2.7.3 Gardner's equation

Gardner recommended that the cube root relationship and shear perimeter approach of BS Code be adopted. Hence, it is recommended that a punching shear expression of the following form be adopted

$$\mathrm{v_c} = 27.32[(p \times f'_c)]^{1/3} \text{ x } [(15.75/d)]^{1/4} \text{ (in U.S.units)} \quad (2.4)$$

Where,

$\mathrm{v_c}$ = shear strength in psi;

d = effective slab depth in inch;

p = steel ratio; and

f'_c = cylinder strength in psi.

$$v_c = 0.99[(px f'_c)]^{1/3} \times [(400/d)]^{1/4} \quad \text{(in S.I. units)} \tag{2.5}$$

Where,

v_c = shear strength in MPa;

d = effective slab depth in mm;

p = steel ratio; and

f'_c = cylinder strength in MPa.

The shear perimeter should be rectangular at a distance 1.5 times the effective slab depth outside the column.

2.7.4 Code provision equations

For the design of flat plates, flat slabs and column footings punching shear strength of concrete in the vicinity of columns, concentrated loads or reaction is one of the design criterion which governs the design. Thus, the critical shear section for this type of shear should be located so as the perimeter of critical section is a minimum, but need not approach closer than a certain distance from edge or corners of columns, concentrated load or reaction areas. Different Code provisions provide the location of this critical section differently. But for all the Codes, when this is done, the shear strength is taken almost independent of the column size, slab depth, span-to-depth ratio and edge restraint.

2.7.4.1 ACI 318, 2008 code provisions

According to ACI 318 (2008) code, the critical section for shear in slabs subjected to bending in two directions follow the perimeter (b_0) located at a distance *d/2* from the periphery of the concentrated load. It further assumes that the shear capacity of the concrete is proportional to the square root of the concrete strength. According to this Code, for non-prestressed slabs and footing, nominal punching shear strength

provided by concrete (V_c in pounds or Newton) shall be smallest of the following three equations;

In F.P.S. Unit:

$$V_c = (2 + 4/\beta_c)\sqrt{f'_c}b_0 d \quad (2.6)$$

$$V_c = (2 + \alpha_s d/b_0)\sqrt{f'_c}b_0 d \quad (2.7)$$

$$V_c = 4\sqrt{f'_c}b_0 d \quad (2.8)$$

In S.I. Unit:

$$V_c = (1 + 2/\beta_c)\sqrt{f'_c}b_0 d/6 \quad (2.9)$$

$$V_c = (1 + 0.5\alpha_s d/b_0)\sqrt{f'_c}b_0 d/6 \quad (2.10)$$

$$V_c = 0.33\sqrt{f'_c}b_0 d \quad (2.11)$$

Here,

β_c= ratio of long side to short side of concentrated load or reaction area;

f'_c= uniaxial cylinder (compressive) strength of concrete in MPa or psi;

b_0 = perimeter of critical section of slab or footing at a distance of *d/2* away from the column faces in inch or mm;

d = effective depth (Distance from extreme compression fiber to the centroid of longitudinal tension reinforcement) in inch or mm; and

α_s= 40 for interior column, 30 for edge column, 20 for corner column.

2.7.4.2 British (BS 8110, 1985) code provisions

The punching shear requirements of the current British Standard BS 8110: (1985) are very similar to those proposed by Regan. According to BS 8110: (1985) Code the critical shear perimeter is taken as a rectangle located at a distance of 1.5*d* from the edge of column regardless of whether the columns are rectangular or circular in section and punching shear strength of concrete is given by the following equation;

$$V_p = 0.79\sqrt[3]{100\rho}\ \sqrt[3]{f_{cu}/25}\ \sqrt[4]{400/d}\{4(c + 3d\}d \quad (2.12)$$

Where,

ρ ≤ 3.0 percent, 400/d ≥ 1.0 and f_{cu} ≤40 (MPa);

V_p= punching shear strength in Newton (N);

ρ = Reinforcement ratio in percentage;

f_{cu} = uniaxial cube (compressive) strength of concrete in MPa;

c = width of column or side length of loaded area in mm; and

d = effective depth in mm.

2.7.4.3 Canadian (CAN3-A23.3-M84, 1984) code provisions

According to CAN3-A23.3-M84 (1984) Code, the punching shear strength is evaluated at the critical section which assumed to be located at a distance d/2 from the periphery of the concentrated load. The punching shear strength provided by the concrete is given by the following equation;

$$V_p = 0.4\sqrt{f'_c}\ b_0 d \quad \text{(In S.I. unit)} \tag{2.13}$$

Where,

V_p = Punching shear strength provided by concrete in Newton (N);

f'_c = Uniaxial cylinder (compressive) strength of concrete in MPa;

b_0 = Perimeter of critical section of slab or footing in mm; and

d = Effective depth in mm.

2.7.4.4 European (CEB-FIP, 1978) code provisions

According to CEB-FIP (1978) Code, the critical section for punching shear follows the perimeter (b_0) located at a distance d/2 from the periphery of the concentrated load. The punching shear strength provided by the concrete is given by the following equation;

$$V_p = \nu_c b_0 d \tag{2.14}$$

Where,

V_p = Punching shear strength provided by concrete in Newton (N);

b_0= Perimeter of critical section of slab or footing in mm;

d = Effective depth in mm;

ν_c= Concrete Shear strength in MPa given by:

$\nu_c = 1.6\tau_{rd}k(1 + \rho/2)$

Here,

$\tau_{rd} = 0.075(f'_c)^{2/3}$;

f'_c = Ultimate cylinder strength of concrete in MPa;

$k = (1.6 - d/1000) \geq 1.0$; and

$\rho \leq 0.8$ percent.

2.7.4.5 Bangladesh (BNBC, 2006) code provisions

According to this Code, for non-prestressed slabs and footing, the critical section for shear in slabs subjected to bending in two directions follow the perimeter (b_0) located at a distance *d*/2 from the periphery of the concentrated load. According to this Code, for non-prestressed slabs and footing, nominal punching shear strength provided by concrete (V_c in Newton) shall be smallest of the following three equations;

$$V_c = (0.17(1 + 2/\beta_c)\sqrt{f'_c}b_0 d) \quad (2.15)$$

$$V_c = (0.17(1 + \alpha_s d/b_0)\sqrt{f'_c}b_0 d) \quad (2.16)$$

$$V_c = 0.33\sqrt{f'_c}b_0 d \quad (2.17)$$

Here,

β_c= ratio of long side to short side of concentrated load or reaction area;

f'_c= uniaxial cylinder (compressive) strength of concrete in MPa;

b_0 = perimeter of critical section of slab or footing at a distance of *d/2* out from the column faces in mm;

d = effective depth in mm; and

α_s = 20 for interior column, 15 for edge column, 10 for corner column.

2.8 Remark

Punching shear failure mechanism of flat plate structure has been discussed in this chapter. Some existing literatures on slab-column connection of flat plate structure based on experimental investigation, analytical methods, numerical models and various codes of practice are also thoroughly reviewed. Provisions of punching shear strength of different codes has been discussed. It has been found that BNBC (2006) adopted ACI Code with minor modification.

Chapter 3

FINITE ELEMENT MODELING

3.1 General

With the advent of sophisticated numerical tools for analysis like the finite element method (FEM), it has become possible to model the complex behaviour of reinforced concrete plates. The actual work regarding the finite element modeling of reinforced concrete plate has been described in this chapter. Representation of various physical model with the finite elements, properties assignment to them, representation of various physical phenomenon etc. have been discussed in relation to the package software used in this study.

3.2 Finite Element Packages

A number of good finite element analysis computer packages are available in the field of civil engineering. They vary in degree of complexity, usability and versatility. Some of such packages are:

- ABAQUS
- ADINA
- ANSYS
- DIANA
- FEMSKI
- MARC
- Micro Feap
- SAP 90
- STAAD
- STRAND

A few of these programs are intended for a special type of structure. For example Micro Feap P1 is developed for the analysis of plane frames and truss while Micro Feap P2 is for the analysis of slab and grid system. Of these, the package ABAQUS has been used in this study for its relative ease of use, detailed documentation, flexibility and vastness of its capabilities.

3.3 An Overview of ABAQUS

Abaqus is a suite of powerful engineering simulation programs, based on the finite element method, which can solve problems ranging from relatively simple linear analyses to the most challenging nonlinear simulations. Abaqus contains an extensive library of elements that can model virtually any geometry. It has an equally extensive list of material models that can simulate the behaviour of most typical engineering materials including metals, rubber, polymers, composites, reinforced concrete, crushable and resilient foams, and geotechnical materials such as soils and rock. Designed as a general-purpose simulation tool, Abaqus can be used to study more than just structural (stress/displacement) problems. It can simulate problems in such diverse areas as heat transfer, mass diffusion, thermal management of electrical components (coupled thermal-electrical analyses), acoustics, soil mechanics (coupled pore fluid-stress analyses), and piezoelectric analysis.

Abaqus offers a wide range of capabilities for simulation of linear and nonlinear applications. Problems with multiple components are modeled by associating the geometry defining each component with the appropriate material models and specifying component interactions. In a nonlinear analysis Abaqus automatically chooses appropriate load increments and convergence tolerances and continually adjusts them during the analysis to ensure that an accurate solution is obtained efficiently.

Abaqus consists of two main analysis products—Abaqus/Standard and Abaqus/Explicit. Abaqus/CAE is the complete Abaqus environment that includes capabilities for creating Abaqus models, interactively submitting and monitoring Abaqus jobs, and evaluating results. Abaqus/Viewer is a subset of Abaqus/CAE that includes just the postprocessing functionality.

Abaqus/Standard:

Abaqus/Standard is a general-purpose analysis product that can solve a wide range of linear and nonlinear problems involving the static, dynamic, thermal, and electrical response of components. Abaqus/Standard solves a system of equations implicitly at each solution "increment."

Abaqus/Explicit:

Abaqus/Explicit is a special-purpose analysis product that uses an explicit dynamic finite element formulation. It is suitable for modeling brief, transient dynamic events, such as impact and blast problems, and is also very efficient for highly nonlinear problems involving changing contact conditions, such as forming simulations. Abaqus/Explicit marches a solution forward through time in small time increments without solving a coupled system of equations at each increment (or even forming a global stiffness matrix).

Abaqus/CAE:

Abaqus/CAE (Complete Abaqus Environment) is an interactive, graphical environment for Abaqus. It allows models to be created quickly and easily by producing or importing the geometry of the structure to be analyzed and decomposing the geometry into meshable regions. Physical and material properties can be assigned to the geometry, together with loads and boundary conditions. Abaqus/CAE contains very powerful options to mesh the geometry and to verify the resulting analysis model. Once the model is complete, Abaqus/CAE can submit, monitor, and control the analysis jobs. The Visualization module can then be used to interpret the results.

Abaqus/Viewer:

Abaqus/Viewer is a subset of Abaqus/CAE that contains only the postprocessing capabilities of the Visualization module.

3.4 Modeling of Reinforced Concrete Plate

Reinforced concrete plate, speaking in very common sense, is a mass of hardened concrete with steel reinforcement embedded within it. This arrangement when in use acts as a single material with the steel providing adequate tensile capacity to concrete, which has high compression capacity. However, the interaction between the concrete mass and the steel reinforcement is not very simple, when subjected to various loading conditions. Complicated physical phenomenon such as bond slip, anchorage failure etc comes into play at different condition. Hence the whole of reinforced concrete may not be treated as a single material during FEM analysis and may not be modeled as a unique composite material.

In nonlinear modelling of reinforced concrete an appropriate material model is usually the most critical factor for successful and accurate analysis. Many constitutive models based on plasticity and nonlinear elasticity has been proposed. The modelling of reinforced concrete, as outlined in this thesis, used separate materials and elements for the concrete and steel reinforcement. Concrete is modeled by three-dimensional eight node solid elements while the reinforcing steel is modeled by two node truss elements. The separate treatment in the element level ensures better approximtion of the actual condition. The inherent assumption is that there is full displacement compatibility between the rinforcement and the concrete and that no bond slippage occurs and perfect bond between mterials is assumed. The nonlinear behaviour of reinforced concrete (RC) structural systems is very complex. Thus, in order to more accurately simulate them, there is a need for the development of efficient sophisticated elements that can be incorporated in a nonlinear finite element framework. The nonliner effect due to the cracking and crushing of concrete and the yielding of steel reinforcement has been included. The concrete crcking is modeled by damage plasticity model, in the sense that it would provide concrete tension and compression damage. An incremental finite element technique is used which simulates the nonlinear load-deflction behaiour of reinforced concrete structure.

3.4.1 Element types adopted

In general, element types are used for the simulation of the punching failure three.

- symmetric Rotational(2-D) continuum element.
- Spatial(3-D) continuum elements.
- Shell elements.

The advantage of2-D elements is that rotational symmetric problem can be small number of elements and therefore a minimum numerical simulated with a effort. However slabs with orthogonal reinforcement which are generally found in practical applications as well as punching with moment transfer or punching at edge delled usingand corner columns can not be mo2-D elements.

In contrast, 3-D elements offer high flexibility and accuracy in the modelling of reinforced concrete structures and generally lead to the most realistics results. On the other hand, using3-D elements the pre and post processing of theFE mesh becomes more difficult, and the numerical effort is highit is more expensive in terms of analysis time.As a result , the application of3-D elements is up to now limited to smaller structures.

on of punching to allow for the Shell elements were applied for the simulati application of the FEM to large structures because of the relatively small number of degrees of freedom per node with these elements. However, shell elements require a of the elements and transformation of the strains perpendicular to the plane, therefore, lead to less accurate results compare to a continuum analysis.

In this study, Spatial(3-D) continuum elements has been used for representing the concrete element to get more realistic results, which is an eight- node solid element and defined by isotropic material properties. The solid element has eight nodes with three degrees of freedom at each node viz translation in the node x, y and z directions. The element is capable of plastic deformation, cracking in three orthogonal directions and crushing. The most important aspect of this element is the

treatment of nonlinear material properties. In ABAQUS 6.7 (2007), there are different types of mesh available i.e., free, structured, sweep etc. Free and sweep mesh is irregular triangular and hexahedron in shape and it has no restrictions in terms of specified pattern. Compared to a free and sweep mesh a structured mesh is regular hexahedron shape and also have a restriction to form a specified pattern. Therefore, the geometry of the model should be fairly regular for volume or structured mesh. So, structured mesh has been selected to mesh of all slabs in this present study, as this type of mesh is most suitable for solid continuum element. The geometry, node locations and the coordinate system for this element are shown in Fig. 3.1.

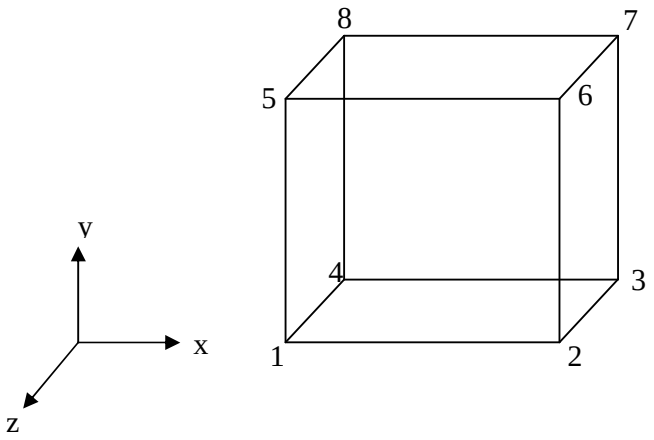

Figure 3.1 Eight-node solid element

The steel for the finite element models is assumed as an elastic-perfectly plastic material and identical in tension and compression. The internal reinforceement is modeled using three dimentional truss element. Two nodes are required for this element. The element is also capable of plastic deformation. The geometry and node locations for this element type are shown in Fig. 3.2.

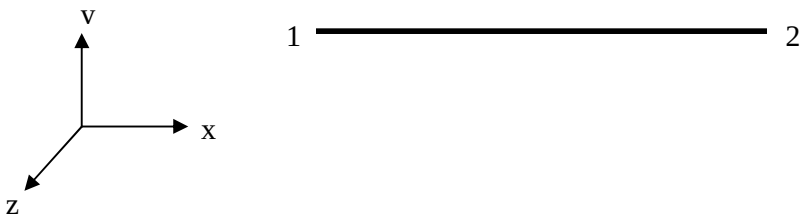

Figure 3.2 Two-node truss element

The embedded element technique is used to specify that an element or group of elements is embedded in “host” elements. The embedded element technique can be used to model rebar reinforcement. Abaqus searches for the geometric relationships between nodes of the embedded elements and the host elements. If a node of an embedded element lies within a host element, the translational degrees of freedom at the node are eliminated and the node becomes an “embedded node”. The translational degrees of freedom of the embedded node are constrained to the interpolated values of the corresponding degrees of freedom of the host element. However, the host element can have only translational degrees of freedom and the number of translational degrees of freedom at a node on the embeded element must be identical to the number of translational degrees of freedom at a node on the host element.

3.4.2 Material properties

An understanding of the materials characteristics and behaviour under load is fundamental to understanding the performance of structural concrete. Performance of a structure under load depends to a large degree on the stress-strain relationship of the material from which it is made, under the type of stress to which the material is subjected in the structure. In ABAQUS, depending on the application, material properties may be:

- Linear or nonlinear
- Isotropic, orthotropic, or anisotropic
- Constant temperature or temperature-dependent.

Reinforced concrete structures are made up of two materials with different characteristics, namely, concrete and steel. Steel can be considered a homogeneous material and its material properties are generally well defined. Concrete is, on the other hand, a heterogeneous material made up of cement, mortar and aggregates. Its mechanical properties scatter more widely and cannot be defined easily. For the

convenience of analysis and design, however, concrete is often considered a homogeneous material in the macroscopic sense.

The nonlinear response is caused by two major effects, namely, cracking of concrete in tension or crushing of concrete in compression and yielding of the reinforcement. Nonlinearities also arise from the interaction of the constituents of reinforced concrete, such as bond-slip between reinforcing steel and surrounding concrete, aggregate interlock at a crack and dowel action of the reinforcing steel crossing a crack. The time-dependent effects of creep, shrinkage and temperature variation also contribute to the nonlinear behaviour. Furthermore, the stress-strain relation of concrete is not only nonlinear, but is different in tension than in compression and the mechanical properties are dependent on concrete age at loading and on environmental conditions, such as ambient temperature and humidity. The material properties of concrete and steel are also strain-rate dependent to a different extent.

Because of these differences in short- and long-term behaviour of the constituent materials, a general purpose model of the short- and long-term response of RC members and structures should be based on separate material models for reinforcing steel and concrete, which are then combined along with models of the interaction between the two constituents to describe the behaviour of the composite reinforced concrete material. This is the approach adopted in this study. The assumptions made in the description of material behaviour are summarized below:

- The stiffness of concrete and reinforcing steel is formulated separately. The results are then superimposed to obtain the element stiffness;
- The damage plasticity model is adopted in the description of the behaviour of concrete;
- Cracking in more than one direction is represented by a system of orthogonal cracks;
- The crack direction changes with load history;
- The reinforcing steel is assumed to carry stress along its axis only and the effect of dowel action of reinforcement is neglected;

To determine the element stiffness and resisting force, the material model must provide stresses and material moduli. This section presents the concrete and reinforcing steel material models that are selected in this study. Material properties for the constituent model are described in the following subsection.

3.4.2.1 Concrete

Development of a material model for the behaviour of concrete is not a straightforward task. Concrete is a quasi-brittle material and has different behaviour in compression and tension. The tensile strength of concrete is typically 8 to 15% of the compressive strength [Shah, et al. (1995)]. The equivalent uniaxial model is selected for concrete. This model uses the concept of the Poisson's effect to determine the equivalent strain in a given direction. The increase in strain in one direction increases the equivalent strain in another direction. To adopt the equivalent uniaxial model, the uniaxial stress-strain relationship for concrete is required. The relation used in the present analysis is shown in Fig. 3.3.

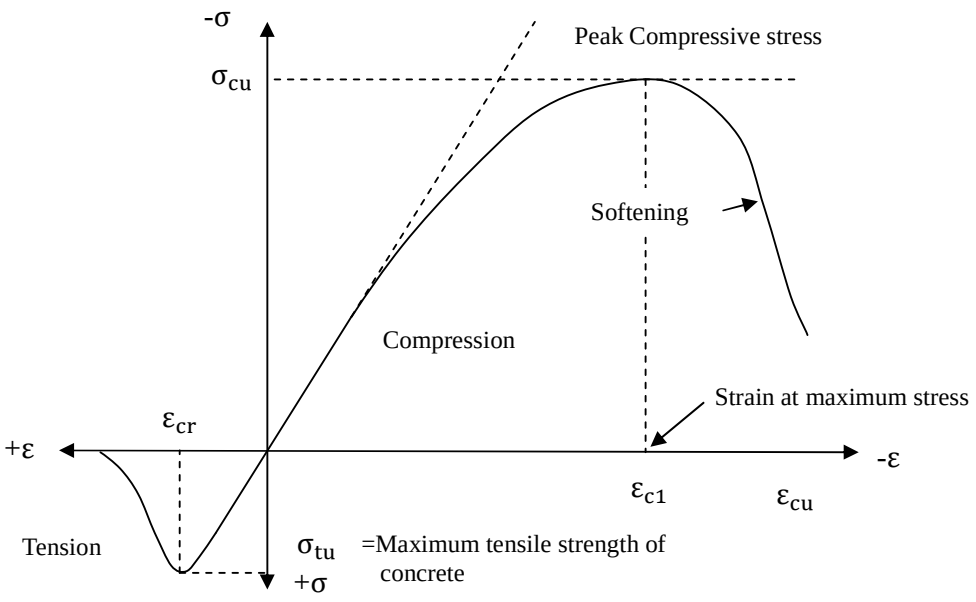

Figure 3.3 Typical uniaxial compressive and tensile stress-strain curves for concrete [Bangash (1989)]

In compression, the stress-strain curve for concrete is linearly elastic up to about 40 percent of the maximum compressive strength. Above this point, the stress increases nonlinearly up to the maximum compressive strength. Beyond the maximum compressive strength σ_{cu}, the curve descends into a softening region, and eventually crushing failure occurs at an ultimate strain of ε_{cu}. In tension, the stress-strain curve for concrete is approximately linearly elastic up to the maximum tensile strength. After this point, the concrete cracks and the strength decreases gradually to zero [Bangash (1989)].

Concrete exhibits a large number of microcracks, especially, at the interface between coarser aggregates and mortar, even before subjected to any load. The presence of these microcracks has a great effect on the mechanical behaviour of concrete, since their propagation during loading contributes to the nonlinear behaviour at low stress levels and causes volume expansion near failure. Many of these microcracks are caused by segregation, shrinkage or thermal expansion of the mortar. Some microcracks may develop during loading because of the difference in stiffness between aggregates and mortar. Since the aggregate-mortar interface has a significantly lower tensile strength than mortar, it constitutes the weakest link in the composite system. This is the primary reason for the low tensile strength of concrete.

The response of a structure under load depends to a large extent on the stress-strain relation of the constituent materials and the magnitude of stress. Since concrete is used mostly in compression, the stress-strain relation in compression is of primary interest. Such a relation can be obtained from cylinder tests with a height to diameter ratio of 2 or from strain measurements in beams.

For concrete, ABAQUS require input data for material properties as follows:

Elastic modulus (E_c)
Ultimate uniaxial compressive strength (f'_c)
Ultimate tensile strength (modulus of rupture), (f_r)
Poisson's ratio (ν).

The modulus of elasticity (E_c in psi units), i.e., the slope of the initial straight portion of the stress-strain curve, is seen to be larger the higher the strength of the concrete [Nilson (1997)]. For normal sand and stone concretes, E_c is computed with reasonable accuracy from the empirical equation found in the ACI Code:

$$E_c = 57500\sqrt{f'_c} \tag{3.1}$$

For compressive strengths in the range from 6000 to 12000 psi, the ACI Code equation overestimates E_c for both normal weight and lightweight material by as much as 20 percent [Nilson (1997)]. Numerical expression, Equation 3.2 [Nilson (1997)] is used for normal density concretes with f'_c in the range of 3000 to 12000 psi:

$$E_c = (40000\sqrt{f'_c} + 1000000)(\frac{w_c}{145})^{1.5} \tag{3.2}$$

Where w_c is the unit weight of the hardened concrete in pcf.

Value of ultimate uniaxial compressive strength (f'_c) is obtained from cylinder tests with a height to diameter ratio of 2.

Modulus of rupture (f_r) is calculated by Equation 3.3 & 3.4 (ACI 318-99):

$$f_r = 7.5\sqrt{f'_c} \ (f'_c \text{ in psi unit}) \tag{3.3}$$

$$f_r = 0.33\sqrt{f'_c} \ (f'_c \text{ in MPa unit}) \tag{3.4}$$

At stresses lower than about $0.7f'_c$, Poisson's ratio for concrete fall within the limits of 0.15 to 0.20 [Nilson (1997)]. In this study Poisson's ratio for concrete is assumed to be 0.17.

According to Winkler et al. 2007, the stress-strain relation behaviour of concrete under uniaxial compressive loading can be divided into three domains. As shown in Figure 3.4, the first section represents the linear-elastic branch, which can be formulated as a linear-elastic function of the secant modulus of elasticity E_c :

$$\sigma_c = E_c . \varepsilon_c \tag{3.5}$$

Where,

σ_c = stress at any strain ε_c

Figure 3.4 shows the typical compressive uniaxial stress-strain relationship that was used in this study. The curve starts at zero stress and strain. Point no. 1, at $0.40 f'_c$, is calculated for the stress-strain relationship of the concrete in the linear range (Equation 3.5).

Equation 3.6 describes the ascending branch of the uniaxial stress-strain relation for a compression loading up to the peak load f'_c at the corresponding strain level ε_{c1}.

$$\sigma_c = \frac{E_{ci} \cdot \frac{\varepsilon_c}{f'_c} - \left(\frac{\varepsilon_c}{\varepsilon_{c1}}\right)^2}{1 + \left(E_{ci} \cdot \frac{\varepsilon_{c1}}{f'_c} - 2\right) \cdot \frac{\varepsilon_c}{\varepsilon_{c1}}} \cdot f'_c \tag{3.6}$$

According to this, the modified parameter E_{ci} corresponds to the modulus of elasticity in Equation (3.6)(CEB-FIP, 1993; Mark, 2006) and can be calculated from:

$$E_{ci} = \frac{2}{3.E_c} \cdot \left(\frac{f'_c}{\varepsilon_{c1}}\right)^2 - \frac{4}{3} \cdot \frac{f'_c}{\varepsilon_{c1}} + \frac{5}{3} \cdot E_c \tag{3.7}$$

Beyond peak compressive stress in Fig. 3.4 represents the post-peak branch and is described by Equation (3.8).

$$\sigma_c = \left(\frac{2+\gamma_c \cdot f'_c \cdot \varepsilon_{c1}}{2 \cdot f'_c} - \gamma_c \cdot \varepsilon_c + \frac{\gamma_c \cdot \varepsilon_c^2}{2 \cdot \varepsilon_{c1}}\right)^{-1} \tag{3.8}$$

The post-peak behaviour depends on the decent function γ_c:

$$\gamma_c = \frac{\pi^2 \cdot f'_c \cdot \varepsilon_{c1}}{2.\left[g_{cl} - \frac{f'_c}{2}(\varepsilon_{c1} \cdot (1 - b_c) + \frac{b_c \cdot f'_c}{E_c})\right]^2} > 0 \tag{3.10}$$

Basing on the assumption that the constant crushing energy G_{cl} (Polling, 2000) is a material property. The best approximation was found using a crushing energy of G_{cl}=19.0kN/m. Equation (3.11) considers its dependency on the geometry of the tested or simulated specimen (Vonk,1993;Van Mier,1984) to almost eliminate mesh dependencies of the simulation results:

$$g_{cl} = \frac{G_{cl}}{l_c} \tag{3.11}$$

Here in l_c represents the characteristics length of the simulated or tested specimen.

The description of the stress-strain relation for tensile loading is divided into two sections. Up to the maximum concrete tension strength, the linear part is calculated from:

$$f_r = E_c . \varepsilon_{cr} \tag{3.12}$$

The descent branch of the stress-strain relation of concrete loaded in uniaxial tension can be derived from a stress-crack opening relation (Equation 3.13) according to (Hordijk, 1992), basing on the fictitious crack model of (Hillerborg, 1983).

$$\frac{\sigma_t(w)}{f_r} = \left(1 + \left(c_1 . \frac{w}{w_c}\right)^3\right) . e^{-c_2 \frac{w}{w_c}} - \frac{w}{w_c} . (1 + c_1^3) . e^{-c_2} \tag{3.13}$$

The free parameters could be experimentally determined to c_1=3 and c_2=6.93 (Hordijk, 1992). Damage parameters according to (Polling, 2000) b_c=0.7, b_t=0.1. Maximum crack opening according to(Hordijk, 1992) w_c=180μm.

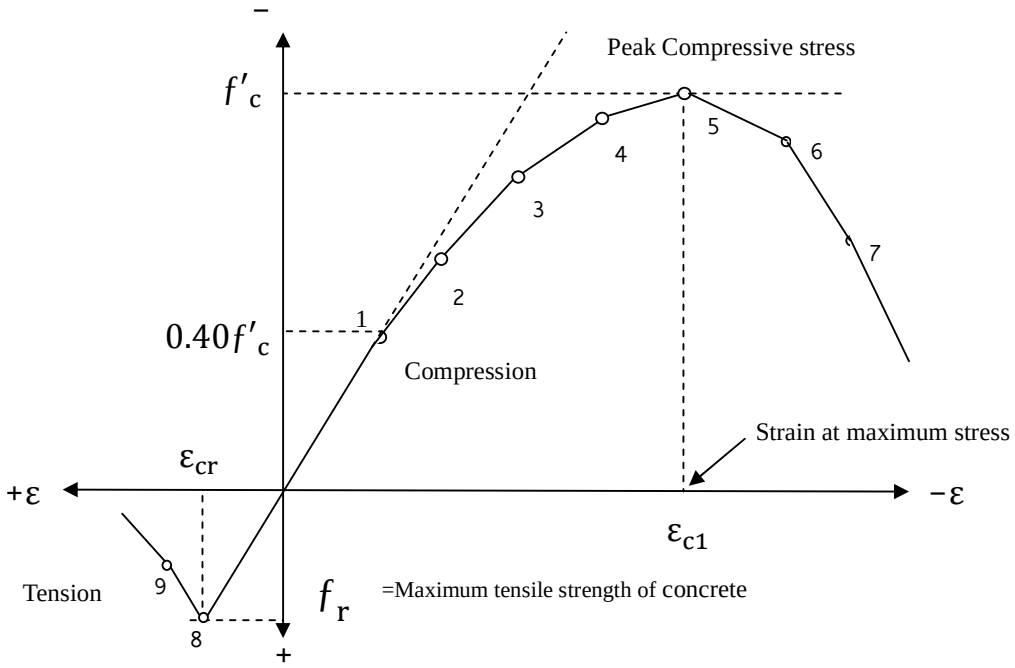

Figure 3.4 Concrete stress-strain curve

3.4.2.2 Steel reinforcement

Reinforcement in concrete structures is typically provided by means of rebars, which are one-dimensional rods that can be defined singly or embedded in oriented surfaces. Rebars are typically used with metal plasticity models to describe the behaviour of the rebar material and are superposed on a mesh of standard element types used to model the concrete. In this study, the steel for the finite element model is assumed as an elastic-perfectly plastic material and identical in tension and compression. The properties, i.e., elastic modulus and yield stress, for the steel reinforcement used in this study follow the design material properties used for the experimental investigation. Since the steel reinforcement is modeled as a one-dimensional element, only a one-dimensional stress-strain relation for steel is required. Figure 3.5 shows the typical uniaxial stress-strain relation for reinforcement

used in the analysis. As can be seen from this figure, it is linear elastic up to the steel yield stress f_y. The stress is then assumed to be constant with increasing steel strain. The stress-strain relation in compression is assumed to be the same as the one in tension. Poisson's ratio of 0.3 was assumed for steel reinforcement.

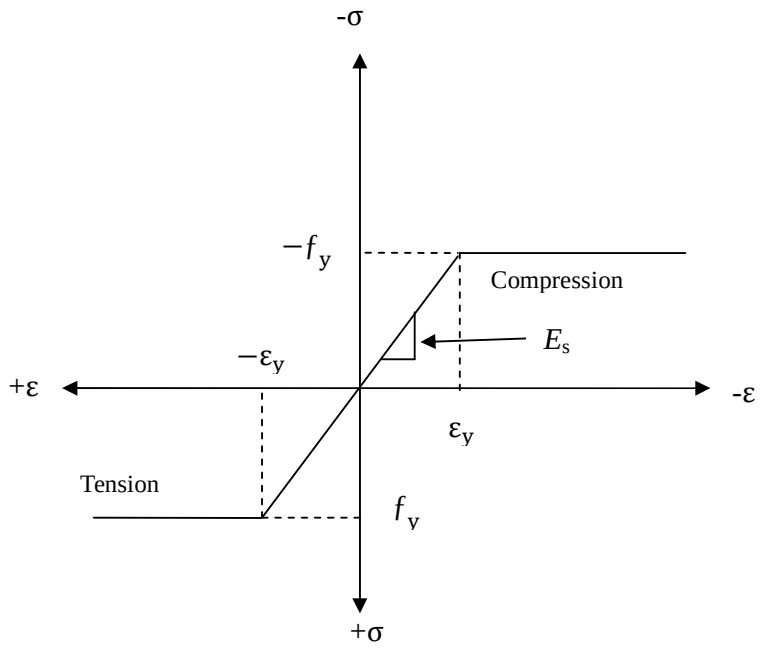

Figure 3.5 Idealised stress-strain curve for steel reinforcement

3.4.3 Failure criteria for concrete

The mechanical behaviour of RC structures is very complex. It is characterized by material nonlinearity. The element includes concrete damaged plasticity model based on the assumption of isotropic damaged elasticity in combination with isotropic tensile and compressive plasticity to represent the inelastic behaviour of concrete and is designed for applications in which the concrete is subjected to arbitrary loading conditions. Depending on the load intensity, the degree of nonlinearity may be significant. The model takes into consideration the degradation of the elastic stiffness induced by plastic straining both in tension and compression. It also accounts for stiffness recovery effects.

The model is a continuum, plasticity-based, damage model for concrete. It assumes that the main two failure mechanisms are tensile cracking and compressive crushing

of the concrete material. The evolution of the yield (or failure) surface is controlled by two hardening variables of tensile and compressive equivalent plastic strains, which linked to failure mechanisms under tension and compression loading, respectively. The model assumes that the uniaxial tensile and compressive response of concrete is characterized by damaged plasticity. Under uniaxial tension the stress-strain response follows a linear elastic relationship until the value of the failure stress is reached. The failure stress corresponds to the onset of micro-cracking in the concrete material. Beyond the failure stress the formation of micro-cracks is represented macroscopically with a softening stress-strain response, which induces strain localization in the concrete structure. Under uniaxial compression the response is linear until the value of initial yield. In the plastic regime the response is typically characterized by stress hardening followed by strain softening beyond the ultimate stress. This representation, although somewhat simplified, captures the main features of the response of concrete. The model assumed that the uniaxial stress-strain curves can be converted into stress versus plastic-strain curves. When the concrete specimen is unloaded from any point on the strain softening branch of the stress-strain curves, the unloading response is weakened: the elastic stiffness of the material appears to be damaged (or degraded). The degradation of the elastic stiffness is characterized by two damage variables (Concrete tension and compression damage variables), which are assumed to be functions of the plastic strains. The damage variables can take values from zero, representing the undamaged material, to one, which represents total loss of strength. In this model the damage variables are treated as non-decreasing material point quantities. Another term “Stiffness recovery” is an important aspect of the mechanical response of concrete. The experimental observation in most quasi-brittle materials, including concrete, is that the compressive stiffness is recovered upon crack closure as the load changes from tension to compression. On the other hand, the tensile stiffness is not recovered as the load changes from compression to tension once crushing micro-cracks have developed.

The model is capable of predicting failure for concrete materials. The two input strength parameters i.e., ultimate uniaxial tensile and compressive strengths are required to define a failure surface for concrete. Consequently, a criterion for failure

of concrete due to a multiaxial stress state can be calculated [William and Warnke (1975)]. In multiaxial stress states these observations are generalized through the concept of surfaces of failure and flow in stress space. These surfaces are fitted to experimental data. The failure surfaces of concrete due to biaxial stress state [Kupfer (1973)] used as shown in Fig. 3.6.

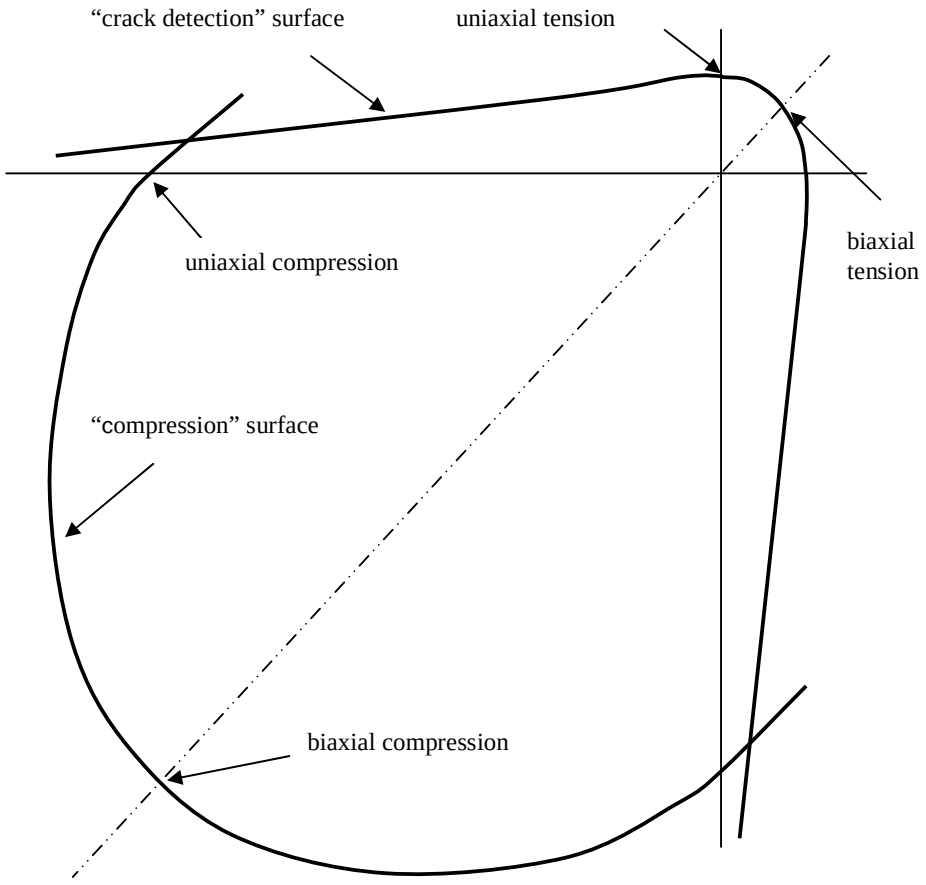

Figure 3.6 Yield and failure surfaces in plane stress

Failure surface can specify failure ratios to define the shape of the failure surface. Four failure ratios can be specified:

- The ratio of the ultimate biaxial compressive stress to the ultimate uniaxial compressive stress.
- The absolute value of the ratio of the uniaxial tensile stress at failure to the ultimate uniaxial compressive stress.
- The ratio of the magnitude of a principal component of plastic strain at ultimate stress in biaxial compression to the plastic strain at ultimate stress in uniaxial compression.
- The ratio of the tensile principal stress at cracking, in plane stress, when the other principal stress is at the ultimate compressive value, to the tensile cracking stress under uniaxial tension.

3.5 Damage Plasticity Theories

Most materials of engineering interest initially respond elastically. Elastic behaviour means that the deformation is fully recoverable: when the load is removed, the specimen returns to its original shape. If the load exceeds some limit (the "yield load"), the deformation is no longer fully recoverable. Some part of the deformation will remain when the load is removed. Plasticity theories model the material's mechanical response as it undergoes such non-recoverable deformation in a ductile fashion. The theories have been developed most intensively for metals, but they are also applied to soils, concrete, rock, ice, crushable foam, and so on. These materials behave in very different ways.

Most materials that exhibit ductile behaviour (large inelastic strains) yield at stress levels that are orders of magnitude less than the elastic modulus of the material, which implies that the relevant stress and strain measures are "true" stress (Cauchy stress) and logarithmic strain. Material data for all of these models should, therefore, be given in these measures.

If there have nominal stress-strain data for a uniaxial test and the material is isotropic, a simple conversion to true stress and logarithmic plastic strain is

$$\sigma_{true} = \sigma_{nom}(1 + \varepsilon_{nom}) \tag{3.14}$$

$$\varepsilon_{true} = \ln(1 + \varepsilon_{nom}) \quad (3.15)$$

Where,

σ_{true} = True stress

σ_{nom} = Nominal stress

ε_{true} = True strain

ε_{nom} = Nominal strain

The classical metal plasticity model in Abaqus defines the post-yield behaviour for most metals. Abaqus approximates the smooth stress-strain behaviour of the material with a series of straight lines joining the given data points. Any number of points can be used to approximate the actual material behaviour; therefore, it is possible to use a very close approximation of the actual material behaviour. The plastic data define the true yield stress of the material as a function of true plastic strain. The first piece of data given defines the initial yield stress of the material and, therefore, should have a plastic strain value of zero.

The strains provided in material test data used to define the plastic behaviour are not likely to be the plastic strains in the material. Instead, they will probably be the total strains in the material. It must decompose these total strain values into the elastic and plastic strain components. The plastic strain is obtained by subtracting the elastic strain, defined as the value of true stress divided by the Young's modulus, from the value of total strain as shown in Fig. 3.7.
This relationship is written as:

$$\varepsilon^{pl} = \varepsilon^{t} - \varepsilon^{el} = \varepsilon^{t} - \sigma_{true}/E \quad (3.16)$$

Where,

ε^{pl} = True plastic strain

ε^{t} = True total strain

ε^{el} = True elastic strain

E = Modulus of elasticity

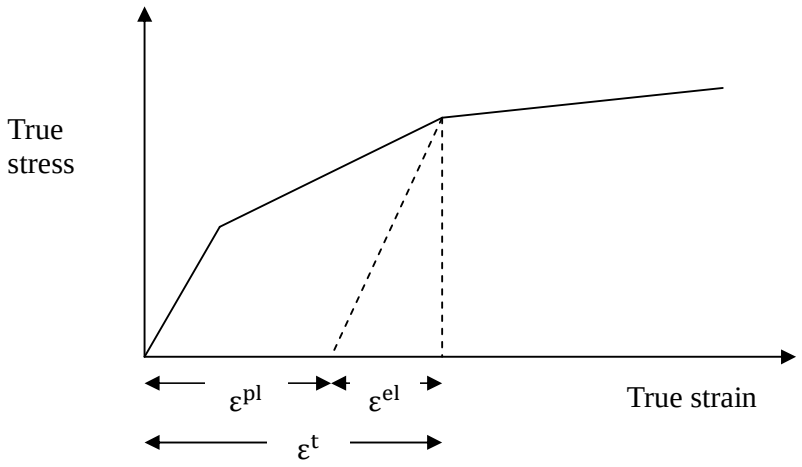

Figure 3.7 Decomposition of the total strain into elastic and plastic components

The concrete damaged plasticity model in Abaqus provides a general capability for modeling concrete and other quasi-brittle materials in all types of structures (beams, trusses, shells, and solids). It can be used for plain concrete, even though it is intended primarily for the analysis of reinforced concrete structures and can be used with rebar to model concrete reinforcement. The degradation of the elastic stiffness is shown in Fig. 3.8 as characterized by damage variables d and also can represent by two damage variables under tensile loading d_t and compressive loading d_c, which are assumed to be functions of the plastic strains. Equations 3.17 and 3.18 represent the damage variables. The damage variables can take values from zero, representing the undamaged material, to one, which represents total loss of strength.

$$d_c = 1 - \frac{\sigma_c . {E_c}^{-1}}{\varepsilon_c^{pl} . \left(\frac{1}{b_c} - 1\right) + \sigma_c . {E_c}^{-1}} \tag{3.17}$$

$$d_t = 1 - \frac{\sigma_t . {E_c}^{-1}}{\varepsilon_t^{pl} . \left(\frac{1}{b_t} - 1\right) + \sigma_t . {E_c}^{-1}} \tag{3.18}$$

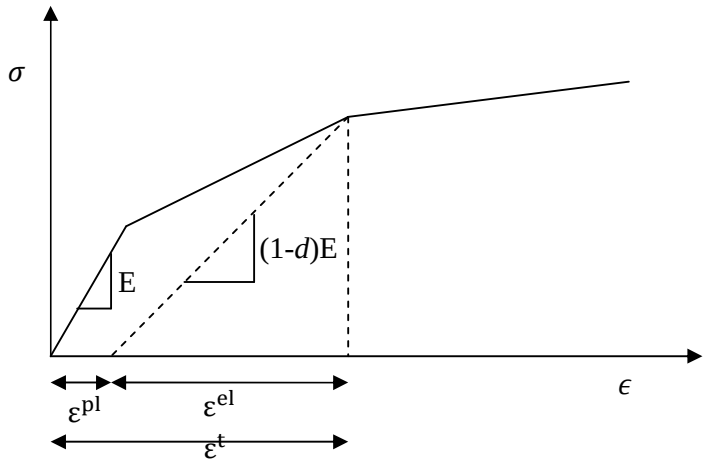

Figure 3.8 Degradation of the elastic stiffness as characterized by damage variables

3.6 Nonlinear Solution Strategies

For reinforced concrete structures, cracking and crushing in concrete through the depth as well as yielding of reinforcing steel are the major sources of material nonlinearity. Cracking results in the permanent loss of both tensile stiffness and the tensile strength in a direction normal to the crack, but the stiffness and strength characteristics in other direction may remain unaltered. In case of crushing, the concrete is simply assumed to loss its entire rigidity and strength in all directions.The effects of some numerical parameters are studied in order to establish the stability of the overall solution process and as a basic guide for subsequent analytical problems.

A nonlinear structural problem is one in which the structure's stiffness changes as it deforms. All physical structures are nonlinear. Linear analysis is a convenient approximation that is often adequate for design purposes. It is obviously inadequate for many structural simulations. A solution strategy uses the well-known Newton-Raphson iterative technique is obtained to solve the nonlinear problems. In a nonlinear analysis the solution cannot be calculated by solving a single system of equations, as would be done in a linear problem. Instead, the solution is found by

applying the specified loads gradually and incrementally working toward the final solution. Therefore, it breaks the simulation into a number of load increments and finds the approximate equilibrium configuration at the end of each load increment. It often takes several iterations to determine an acceptable solution to a given load increment. The sum of all of the incremental responses is the approximate solution for the nonlinear analysis. Thus, by using Abaqus software it combines incremental and iterative procedures for solving nonlinear problems.

During a step time period is assigned for the analysis. This is necessary for cross-references to the amplitude options, which can be used to determine the variation of loads and other externally prescribed parameters during a step. An increment is part of a step. In nonlinear analyses the total load applied in a step is broken into smaller increments so that the nonlinear solution path can be followed. Abaqus software uses Newton's method to solve the nonlinear equilibrium equations. The solution usually is obtained as a series of increments, with iterations to obtain equilibrium within each increment. Increments must sometimes be kept small to ensure correct modeling. Most commonly the choice of increment size is a matter of computational efficiency: if the increments are too large, more iterations will be required. Furthermore, Newton's method has a finite radius of convergence; too large an increment can prevent any solution from being obtained because the initial state is too far away from the equilibrium state that is being sought—it is outside the radius of convergence. Thus, there is an algorithmic restriction on the increment size. At the end of each increment the structure is in (approximate) equilibrium and results are available for writing to the output database, restart, data, or results files. An iteration is an attempt at finding an equilibrium solution in an increment when solving with an implicit method. If the model is not in equilibrium at the end of the iteration, it again tries another iteration. With every iteration the solution obtains should be closer to equilibrium; sometimes it may need many iterations to obtain an equilibrium solution. When an equilibrium solution has been obtained, the increment is complete. Results can be requested only at the end of an increment.

3.6.1 Equilibrium iterations and convergence in Abaqus/Standard

The nonlinear response of a structure to a small load increment ΔP is shown in Fig. 3.9. It uses the structure's initial stiffness, K_0,which is based on its configuration at u_0 and ΔP to calculate a displacement correction c_a for the structure. Using the structure's configuration is updated to u_a. It forms a new stiffness K_a for the structure based on its updated configuration u_a. It also calculates I_a in this updated configuration. The difference between the total applied load P and I_a can now be calculated as R_a=P-I_a. Where R_a is force residual for the iteration. If R_a is zero at every degree of freedom in the model, point a in Fig. 3.9 would lie on the load-deflection curve, and the structure would be in equilibrium. In a nonlinear problem it is almost impossible to have R_a equal zero, so it compares to a tolerance value. If R_a is less than this force residual tolerance, it accepts the structure's updated configuration as the equilibrium solution. By default, this tolerance value is set to 0.5% of an average force in the structure, averaged over time. Abaqus/Standard automatically calculates this spatially and time-averaged force throughout the simulation. If R_a is less than the current tolerance value P and I_a are in equilibrium and u_a is a valid equilibrium configuration for the structure under the applied load. However, before it accepts the solution, it also checks that the displacement correction, c_a ,is small relative to the total incremental displacement, $\Delta u_a = u_a - u_0$.If c_a is greater than 1% of the incremental displacement, it performs another iteration. Both convergence checks must be satisfied before a solution is said to have converged for that load increment. If the solution from iteration is not converged, it performs another iteration to try to bring the internal and external forces into balance.

This second iteration uses the stiffness K_a calculated at the end of the previous iteration together with R_a to determine another displacement correction c_b that brings the system closer to equilibrium (point b in Fig. 3.9). It calculates a new force residual R_b using the internal forces from the structure's new configuration u_b. Again, the largest force residual at any degree of freedom R_b is compared against the force residual tolerance, and the displacement correction for the second iteration c_b

is compared to the increment of displacement $\Delta u_b = u_b - u_0$. If necessary, it performs further iterations. For each iteration in a nonlinear analysis it forms the model's stiffness matrix and solves a system of equations. This means that each iteration is equivalent, in computational cost, to conducting a complete linear analysis. It should now be clear that the computational expense of a nonlinear analysis in Abaqus/Standard can be many times greater than for a linear one. It is possible with Abaqus to save results at each converged increment. Thus, the amount of output data available from a nonlinear simulation is many times that available from a linear analysis of the same geometry.

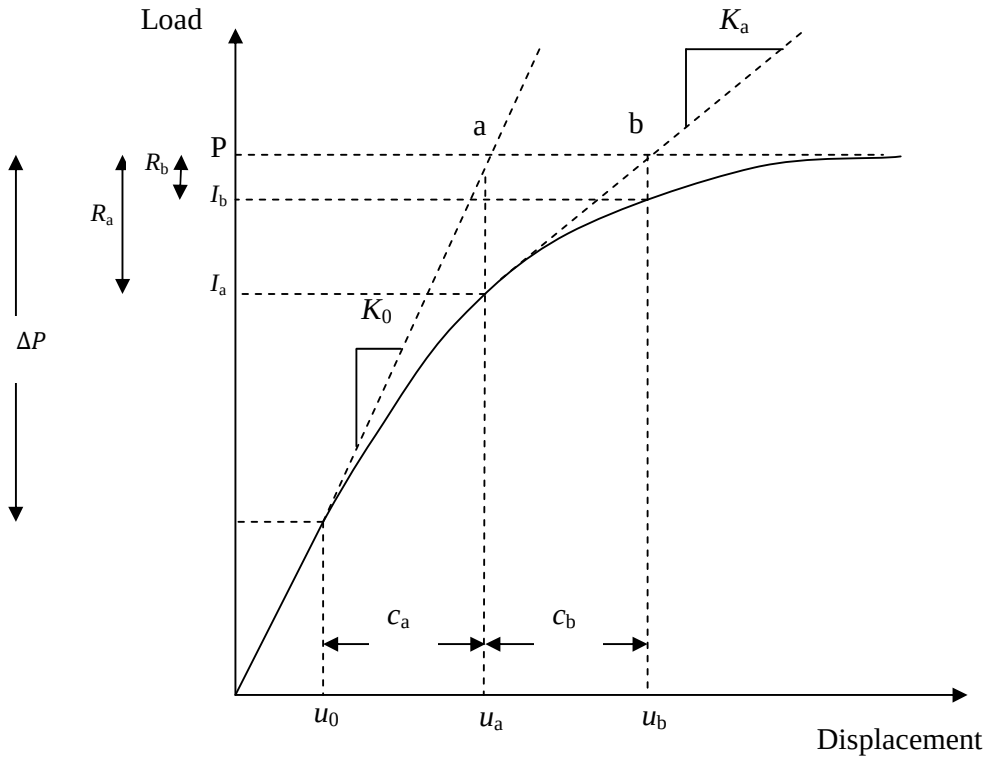

Figure 3.9 Iteration in an increment by using Newton-Raphson iterative technique

Abaqus/Standard automatically adjusts the size of the load increments so that it solves nonlinear problems easily and efficiently. It only needs to suggest the size of the first increment in each step of the simulation. Thereafter, Abaqus/Standard

automatically adjusts the size of the increments. The number of iterations needed to find a converged solution for a load increment will vary depending on the degree of nonlinearity in the system. By default, if the solution has not converged within 16 iterations or if the solution appears to diverge, Abaqus/Standard abandons the increment and starts again with the increment size set to 25% of its previous value. An attempt is then made at finding a converged solution with this smaller load increment. If the increment still fails to converge, Abaqus/Standard reduces the increment size again. By default, Abaqus/Standard allows a maximum of five cutbacks of increment size in an increment before stopping the analysis. If the increment converges in fewer than five iterations, this indicates that the solution is being found fairly easily. Therefore, Abaqus/Standard automatically increases the increment size by 50% if two consecutive increments require fewer than five iterations to obtain a converged solution.

3.6.2 Equilibrium time increment in Abaqus/Explicit

The explicit dynamics procedure performs a large number of small time increments efficiently. An explicit central-difference time integration rule is used; each increment is relatively inexpensive (compared to the direct-integration dynamic analysis procedure available in Abaqus/Standard) because there is no solution for a set of simultaneous equations. The explicit central-difference operator satisfies the dynamic equilibrium equations at the beginning of the increment, t; the accelerations calculated at time t are used to advance the velocity solution to time $t + \Delta t/2$ and the displacement solution to time $t + \Delta t$.

The time increment used in an analysis must be smaller than the stability limit of the central-difference operator. Failure to use a small enough time increment will result in an unstable solution. When the solution becomes unstable, the time history response of solution variables such as displacements will usually oscillate with increasing amplitudes. The total energy balance will also change significantly. If the model contains only on a material type, the initial time increment is directly proportional to the size of the smallest element in the mesh. If the mesh contains

uniform size elements but contains multiple material descriptions, the element with the highest wave speed will determine the initial time increment. In nonlinear problems—those with large deformations and/or nonlinear material response—the highest frequency of the model will continually change, which consequently changes the stability limit. Abaqus/Explicit has two strategies for time incrementation control: fully automatic time incrementation (where the code accounts for changes in the stability limit) and fixed time incrementation.

The default time incrementation scheme in Abaqus/Explicit is fully automatic and requires no user intervention. Two types of estimates are used to determine the stability limit: element by element and global. An analysis always starts by using the element-by-element estimation method and may switch to the global estimation method under certain circumstances.

3.6.3 Advantages of the Abaqus/Explicit method

The use of small increments (dictated by the stability limit) is advantageous because it allows the solution to proceed without iterations and without requiring tangent stiffness matrices to be formed. It also simplifies the treatment of contact. The explicit dynamics procedure is ideally suited for analyzing high-speed dynamic events, but many of the advantages of the explicit procedure also apply to the analysis of slower (quasi-static) processes. A good example is sheet metal forming, where contact dominates the solution and local instabilities may form due to wrinkling of the sheet. The results in an explicit dynamics analysis are not automatically checked for accuracy as they are in Abaqus/Standard (Abaqus/Standard uses the half-step residual). In most cases this is not of concern because the stability condition imposes a small time increment such that the solution changes only slightly in any one time increment, which simplifies the incremental calculations. While the analysis may take an extremely large number of increments, each increment is relatively inexpensive, often resulting in an economical solution. It is not uncommon for Abaqus/Explicit to take over 10^5 increments for an analysis. The method is, therefore, computationally attractive for problems where the total

dynamic response time that must be modeled is only a few orders of magnitude longer than the stability limit; for example, wave propagation studies or some “event and response” applications.

3.7 Remark

Considering all the factors discussed above a reinforced concrete plate can be successfully modeled for nonlinear finite element analysis to predict behaviour of slab-column joint. Concrete and reinforcing steel are represented by separate elements and material models which are combined together with a model of the interaction between reinforcing steel and concrete element that share the same node. The material behaviour of concrete is described by considering failure criteria of concrete. The element includes concrete damaged plasticity model to represent the inelastic behaviour of concrete. On the other hand, reinforcing steel behaves as an elastic-perfectly plastic material. For nonlinear analysis of reinforced concrete plate, there are two solution strategies (Implicit method and explicit method) available. Explicit method requires a small time increment size that depends solely on the highest natural frequencies of the model and is independent of the type and duration of loading. The use of small increments is advantageous because it allows the solution to process without iterations and without requiring tangent stiffness matrices to be formed. On the other hand, implicit method depends on increment size that generally determined from accuracy and convergence considerations. Though a global set of equations must be solved in each increment, the cost per increment of an implicit method is far greater than that of an explicit method. However, in case of material degradation like concrete cracking model and ductile failure model often lead to severe convergence difficulties in implicit analysis programs. By knowing these characteristics Abaqus-Explicit procedure is appropriate for the present study.

Chapter 4

VALIDATION OF NONLINEAR FINITE ELEMENT MODELING OF FLAT PLATE SLABS

4.1 General

With the advent of sophisticated numerical tools like FEM for structural analysis, it has become possible to model the complex behaviour of punching shear failure in reinforced concrete structures. ABAQUS 6.7 (2007), a commercial FE package is used in the current study to model slab-column joint of RC flat plate and study the behaviour of the connection. The modeling work regarding the finite element analysis of reinforced concrete plate has been described in Chapter 3. In this chapter, punching failure experiments are simulated using the numerical model. The purpose of these simulations is to examine the capabilities and limitations of the numerical model to mimic failure behaviour in reinforced concrete structures.

Fourteen real RC slabs are modeled with nonlinear FE package ABAQUS 6.7 (2007) and the results of this numerical analysis are compared with the experimental results or other numerical results available from different literature for validation. A discussion of the failure phenomenon is presented by adding to the description of all these numerical results. Developments of cracks and concrete damage due to different stresses, their pattern and load versus deflection curves have been studied in the subsequent sections. Sensitivity analysis for the selection of correct size of mesh is also presented.

4.2 FE Modeling of Slab-Column Connection

Before numerical analysis some input data for failure criteria developed by Kupfer (1973) with five parameters are discussed. The application of loads, the damage value and the mesh sensitivity analysis are also discussed in the subsequent section.

4.2.1 Input data

Failure criteria for concrete in tension and compression was developed by Kupfer (1973) with five parameters have used in this analyses. These parameters are given in the following Table 4.1.

Table 4.1 Parameters used for failure criteria

Parameter	Denotation
$\psi = 30^0$	Dilatational angle according to Lee (1998)
$fb_0/ fc_0 = 1.16$	Ratio of biaxial to uniaxial compressive strength according to Kupfer (1973)
K = 0.67	Second stress invariant ratio according to Lubliner et al. (1989)
e = 0	Default value for Eccentricity in ABAQUS 6.7 (2007) [no eccentricity regularization is performed]
μ = 0	Default value for Viscosity parameter in ABAQUS 6.7 (2007) [no viscoplastic regularization is performed]

4.2.2 Application of loads and boundary conditions

In most of the cases, vertical load has been gradually increased on numerical model to develop early tensile crack and finally punching shear failure occurs. Afterwards, a slab is also subjected to both gravity and lateral loads to observe the slab-column connection behaviour. In real situation, the vertical loads come from slab and reactions are provided by column. But in this numerical analysis to simulate the model with experiment, the loads have been applied from bottom of the column and boundary conditions have been applied on cutting face of slab which is different from real situation. All vertical and horizontal loads are applied in the same manner during FE analyses. Loads are applied in terms of displacement control criteria and numerical behaviour also has been observed after slab-column connection failure.

4.2.3. Concrete damage value

The degradation of the elastic stiffness is characterized by two damage variables d_t and d_c which are assumed to be functions of the plastic strain as discussed in Chapter 3. The damage variables can take values from zero, representing the undamaged material, to one, which represents total loss of strength. According to Cicekli et al. (2007), the following graph between strain and uniaxial tensile or compression damage have represented in Fig. 4.1. It can be noted from Fig. 4.1a that the maximum tensile damage is about 0.88 which corresponds to a strain of 0.6×10^{-3}, whereas Fig. 4.1b shows a maximum compressive damage of 0.62 at a strain of 5×10^{-3}. In this research work Fig. 4.2 shows complete load-deflection response of a square slab (A-1a plate) for varying tensile damage values. The damage value ranged from 60% to 98%. It appears that numerical solutions are sensitive during the check on tensile damage value. It is observed that in a nonlinear analysis, above 88% tensile damage may cause numerical instability of concrete and the analysis will not be sufficiently accurate. Therefore, the choice of the damage properties is important since, generally, excessive damage may have a critical effect on the rate of convergence. So from the above discussion, in this present study it is recommended to avoid using values of the damage variables above 0.62, which corresponds to a 62% reduction of the stiffness in case of compression damage and the damage variables above 0.88, which corresponds to a 88% reduction of the stiffness in case of tensile damage.

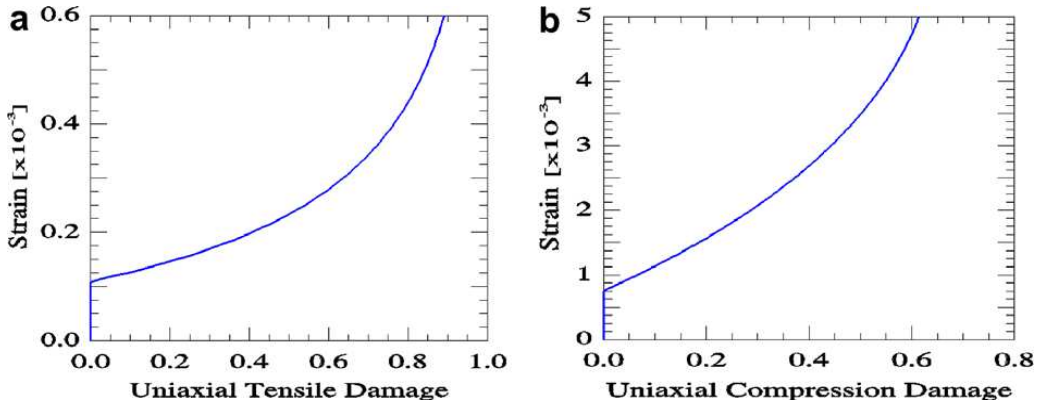

Figure 4.1 Uniaxial tensile and compression damage value with corresponding strain value [adapted from Cicekli et al. (2007)]

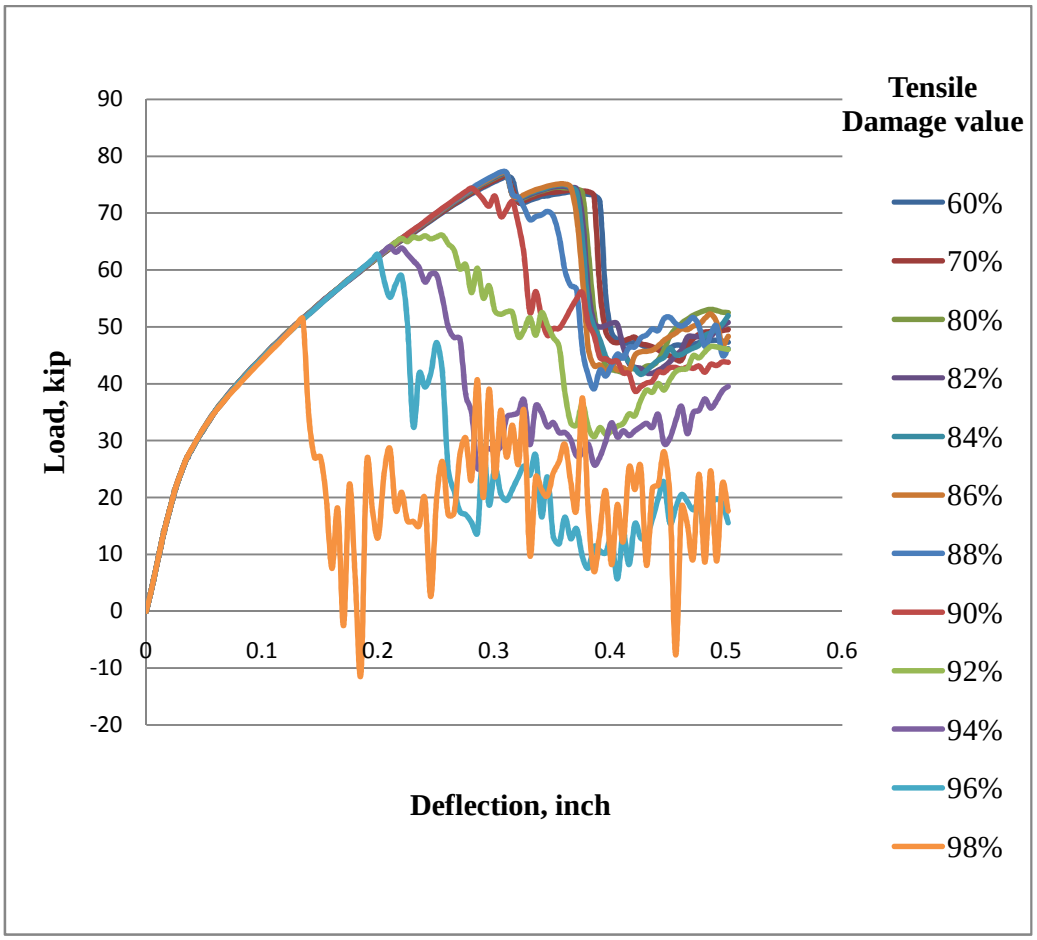

Figure 4.2 Load-deflection response of a square slab (A-1a plate) for varying uniaxial tensile damage value

4.2.4 Mesh sensitivity analysis

At the beginning of FE model development, a reasonable mesh and a convergence study are needed to obtain a reliable solution. In other word, the structure is divided into a number of small elements and after loading, stress and strain are calculated at the integration points of these small elements (Bathe, 1996). An important step in finite element modeling is the selection of the mesh density. A convergence of results is obtained when an adequate number of elements are used in a model. This is practically achieved when an increase in the mesh density has a negligible effect on the results (Adams and Askenazi, 1998). In this present study, a sensitivity analysis is carried out to determine the suitable size of mesh which can give an acceptable result to save CPU time. The structured mesh has been selected to mesh

of all slabs which are most suitable for solid continuum element as discussed in Chapter 3. Figure 4.3 shows ultimate load capacity of a square slab (A-1a plate) for varying mesh size i.e., number of elements. The mesh size ranged between 2.75in x 2.75in x 1in to 5in x 5in x 1in. It appears that numerical solutions are sensitive during mesh sensitivity analysis and it is also observed that in a nonlinear analysis, however, too fine a mesh may cause numerical instability and if the mesh is too coarse, the analysis will not be sufficiently accurate. Therefore, in this study, 3in x 3in x 1in mesh size is a reasonable one to give acceptable result for FE analysis and also save CPU time.

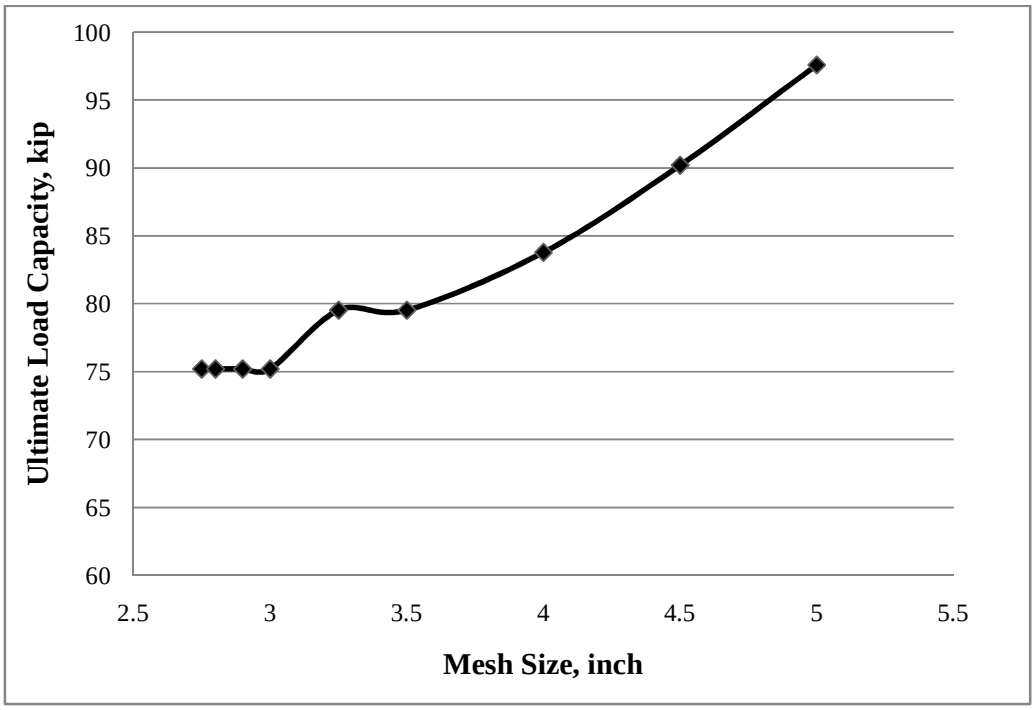

Figure 4.3 Ultimate load capacity of a square slab (A-1a plate) for varying mesh size

4.3 Description of Different Slabs Used in FE Modeling of Slab-Column Joint

To carry out finite element analysis in order to predict the behaviour of any structure, it is essential to verify the developed model against some well-established theoretical solutions or experimental results to ensure that the developed model is tracing the actual response closely. A number of RC slabs are selected from the recognized literatures and journals for modeling, analyses and their validation with the experimental results or other numerical results. Five RC slabs (A-1a, A-7b, A-7, B-14 and B-16) tested by Elstner and Hognestad (1956), four RC slabs (G-1, G-2, G-3, and G-4) tested by Graf (1938), three RC circular slabs (IB15a, IC15a and IA15a) tested by Kinnunen and Nylander (1960), one RC slab tested by Jofreit and McNeice (1971) and one RC slab (YL-L1) tested by Tan and Teng (2005) are numerically modeled by using FE method. The material properties, dimensions, type of mesh, boundary conditions and applied loads (The vertical and lateral loads in these slabs are applied with appropriate load steps) on these models are described and graphically presented. Finally stress distribution, cracking/crushing pattern, concrete damage and slab central deflection are compared with available experimental results/numerical analyses for validation. Few missing data adopted for this analysis (which are not available) are assumed with a reasonable value.

4.3.1 FE modeling of RC flat plate (Elstner and Hognestad)

Elstner and Hognestad (1956) investigated extensively the behaviour of reinforced concrete slabs. Contrary to most of the tests performed at that time, they investigated the strength of relatively thin slabs. They tested a full-size plate with dimensions 70in x70in x6in square slabs supported at the edges and the slabs were restrained in the vertical direction over supports. In the experiment, the column stub dimension used for loading was 10in x10in and loaded up to failure. A typical section of the test slab is shown in Fig. 4.4. The influence of the percentage of flexural reinforcement was illustrated among all slabs. It was observed that slabs with a high percentage of reinforcement failed in a brittle way whereas slabs with a low reinforcement percentage failed in a ductile manner. In this experimental

investigation, they also observed the influence of the concrete strength on the slab behaviour. For slab made of low compressive strength concrete, it was not possible to observe any yielding of the reinforcement because the punching failure occurs first.

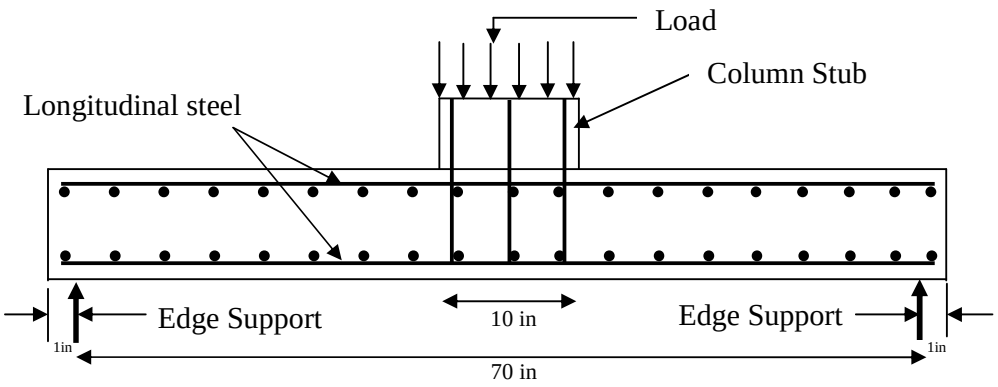

Figure 4.4 A test slab section of Elstner and Hognestad (1956)

Five real RC slabs tested by Elstner and Hognestad (1956) are taken as reference for numerical modeling. The summary of the material properties used in the finite element modeling is shown in Table 4.2. Other parameters of the test slabs and the corresponding FE model plates are shown in Table 4.3. It is to be noted that the ratio of the longitudinal reinforcement is applicable for the entire slab.

Table 4.2 Material properties used

Plate No.	E_c (ksi)	E_s (ksi)	f'_c (psi)	f_r (psi)	f_y (ksi)	ν_c	ν_s	Longitudinal Reinforcement		Shear Reinforcement A_v sq in
								Tension Reinforcement ρ percent	Compression Reinforcement ρ percent	
A-1a	2597	$29x10^3$	2040	339	48.20	0.17	0.3	1.15	0.56	----
A-7b	3659	$29x10^3$	4050	477	46.60	0.17	0.3	2.47	1.15	----
A-7	3659	$29x10^3$	4050	477	46.60	0.17	0.3	2.47	1.15	----
B-14	4922	$29x10^3$	7330	642	47.20	0.17	0.3	3.00	----	----
B-16	4922	$29x10^3$	7330	642	47.20	0.17	0.3	3.00	----	1.60

Table 4.3 Details of slab dimension

Plate No.	Plate Dimension (in)		Column Stub Dimension (in)	h (in)	d (in)		Support Condition
	Test	FE			Test	FE	
A-1a	72x72x6	70x70x6	10x10	6.00	4.63	5	Symmetrical Support on four edges
A-7b	72x72x6	70x70x6	10x10	6.00	4.50	5	do
A-7	72x72x6	70x70x6	10x10	6.00	4.50	5	Symmetrical Support on two opposite edges
B-14	72x72x6	70x70x6	10x10	6.00	4.50	5	Symmetrical Support on four edges
B-16	72x72x6	70x70x6	10x10	6.00	4.50	5	do

In the FE model, the boundary condition of U2=0 along the supports is used to simulate the test condition and the loading pattern are shown in Figs. 4.5 and 4.6.

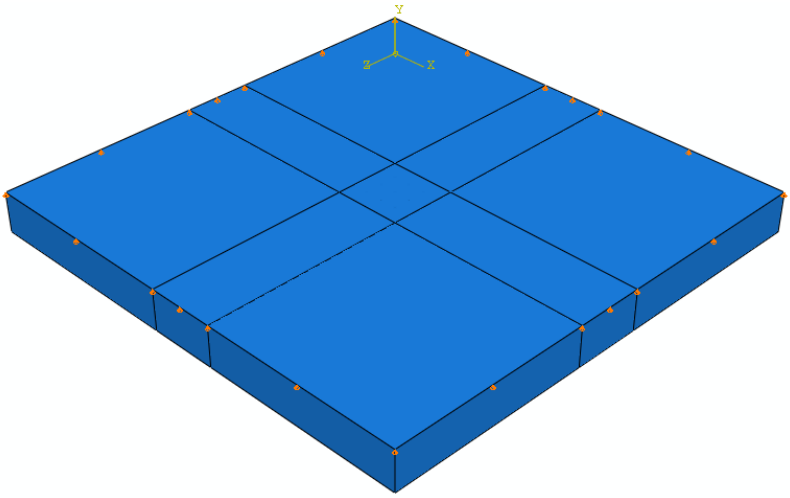

Figure 4.5 Typical finite element model of the plate with boundary condition

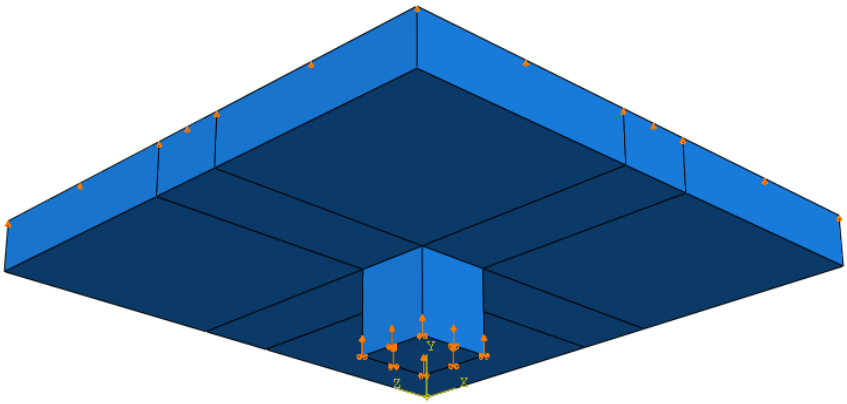

Figure 4.6 Typical finite element model of the plate with loading pattern

Typical concrete mesh, reinforcement for tension and compression reinforcement and shear reinforcement for B-16 slab are shown in Figs. 4.7 to 4.9.

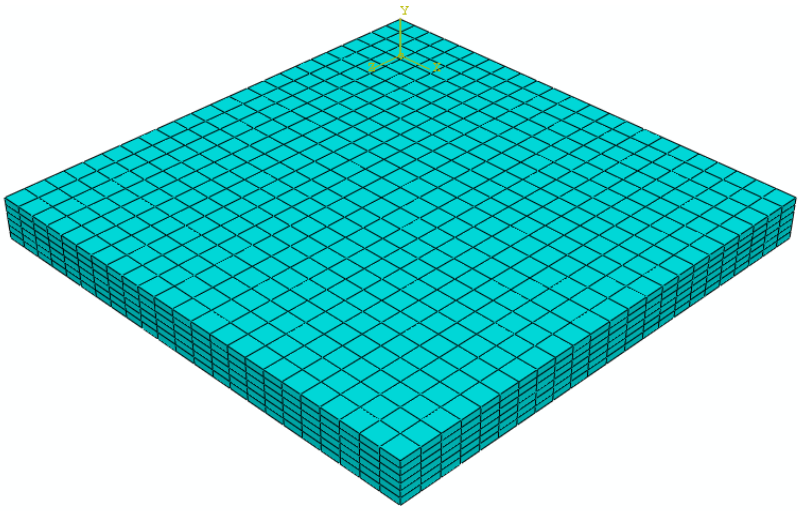

Figure 4.7 Typical finite element model of concrete mesh

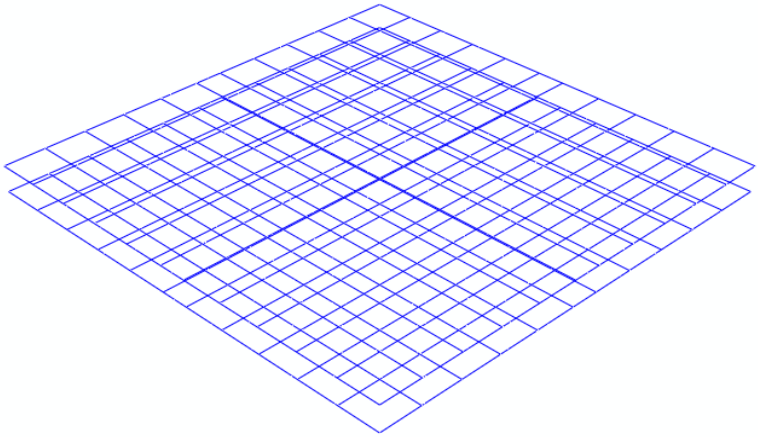

Figure 4.8 Typical tension and compression reinforcement for A-1a, A-7b and A-7 slabs

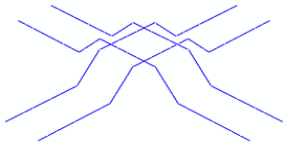

Figure 4.9 Typical bent bar reinforcement for B-16 slab

With the start of the loading process both concrete and steel behave in a linear and elastic manner so that no cracking or yielding is observed. When the first crack arises which corresponds to the cracking load, a small jump with a sudden loss of stiffness is observed. With this first crack flexural response appears. This crack is also known as tangential crack located on the top surface (tension side) along the circumference of the column as shown in Figs. 4.10 and 4.11. Under increasing load, radial cracks begin to form at the perimeter of the column and spread out toward the extremity of the slab as shown in Figs. 4.12 and 4.13 and the nonlinear response of the finite element model is consistent with the test data. Once the first tangential crack is a stress free crack, the behaviour of the slab changes and shear resistance is mobilized. This shear behaviour is characterized by inclined cracks across the slab thickness. The shear resistance is not only influenced by the concrete strength but also by the shear reinforcement and the dowel action. Slab B-16 can sustain more load than slab B-14 as both slabs have same material properties and dimensions except shear reinforcement. These existing inclined cracks open and sudden coalescence into a single inclined crack which is the punching crack occurs as shown in Figs. 4.14 and 4.15. Some concrete are fully damaged due to tension on the top surface of the slab along the circumference of the column. The post-punching failure phenomenon also presented in Fig. 4.16 when the slab is separated into two parts connected by reinforcement and the steel being yielded as shown in Fig. 4.17.

The load versus deflection curves are shown in Figs. 4.18 to 4.22. In a quantitative sense, there are difference in the load-deflection behaviour between present FE analysis (FE) and experimental results (EXPT). It is observed that for plate A-1a, A-7b, A-7, B-14 and B-16 the punching loads obtained numerically (75.2 kip, 126 kip, 120 kip, 181 kip and 198 kip) are higher than the experimental failure loads (67.5 kip, 107 kip, 84 kip, 130 kip and 170 kip) as it represents 11.4%, 17.7%, 42.8%, 39.2% and 16.5% higher than experimental failure loads respectively. At the maximum load for plate A-1a and A-7b, the numerical vertical displacements are 0.33 in and 0.31 in representing around 89.2% and 96.9% of the experimental one respectively and for plate A-7, B-14 and B-16, the numerical vertical displacements

are 0.45 in, 0.39 in and 0.45 in representing around 36.4%, 11.4% and 7.14% higher than experimental one respectively. However, the cracking pattern and failure phenomenon of FE model is in good agreement with the experimental results.

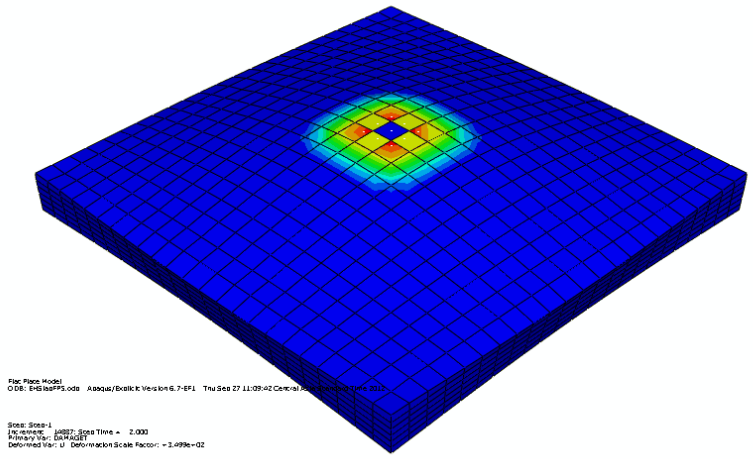

Figure 4.10 First crack arises through slab at 18.1 kip cracking load and initial tensile damage of concrete

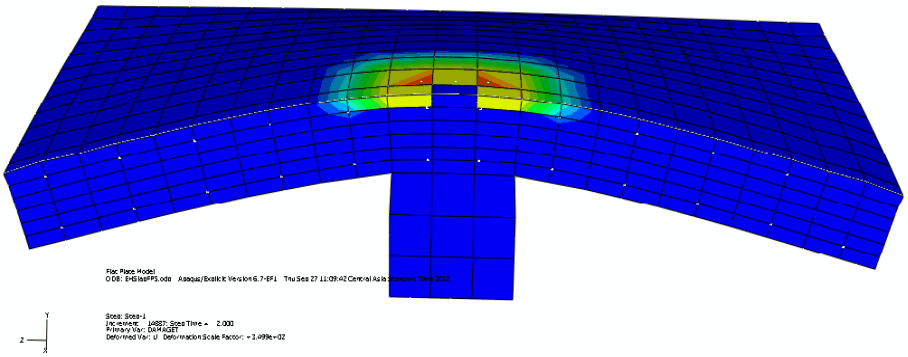

Figure 4.11 First crack starts through top surface at 18.1 kip cracking load and initial tensile damage of concrete on half slab

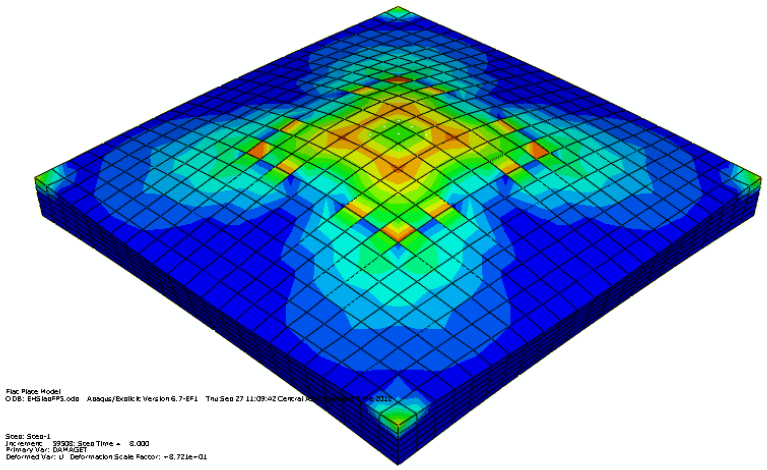

Figure 4.12 Radial crack pattern at the perimeter of the column and tensile damage of concrete at 41.33 kip load

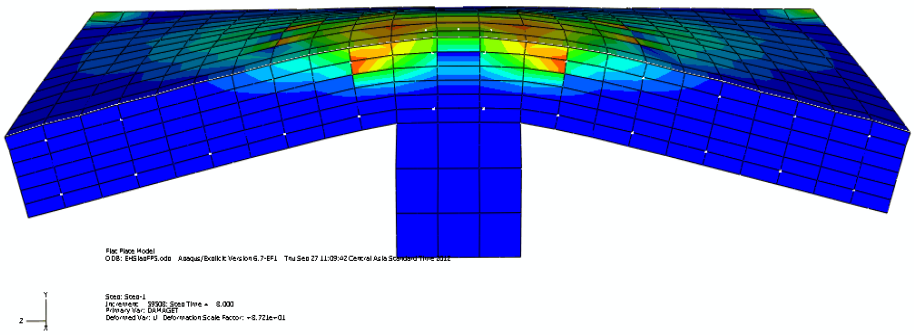

Figure 4.13 Radial crack spread out with forming pyramid shape and tensile damage of concrete at 41.33 kip load on half slab

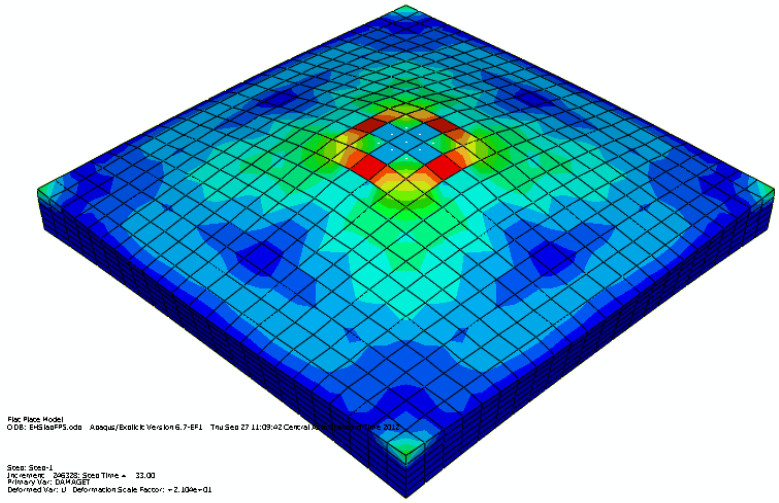

Figure 4.14 Total tensile damage of concrete on top surface of slab and punching failure at 75.18 kip load

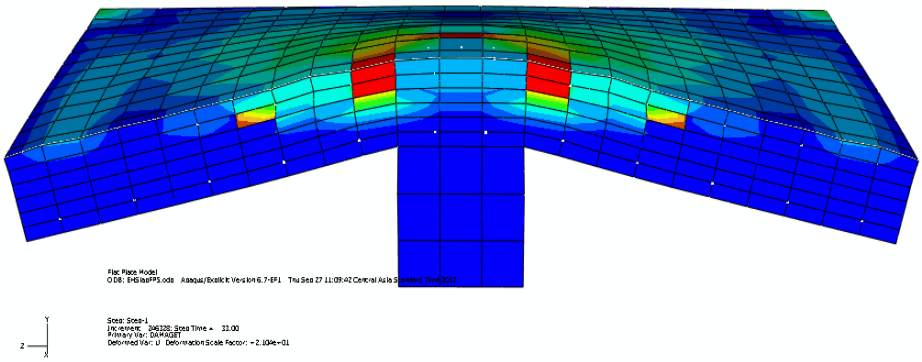

Figure 4.15 Total tensile damage of concrete on top surface of half slab and punching failure with a pyramid shape at 75.18 kip load

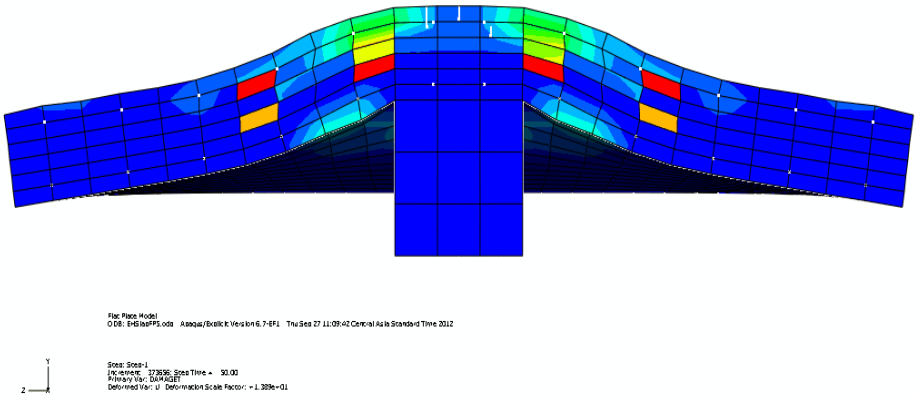

Figure 4.16 Post-punching failure phenomenon of half slab

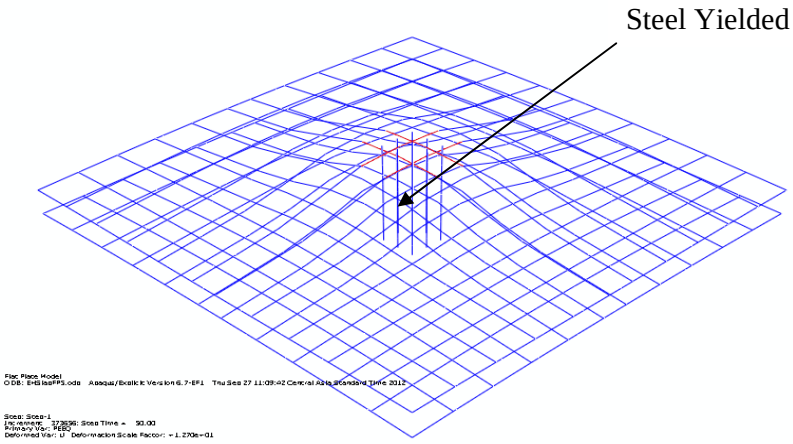

Figure 4.17 Steel yielded during post-punching failure

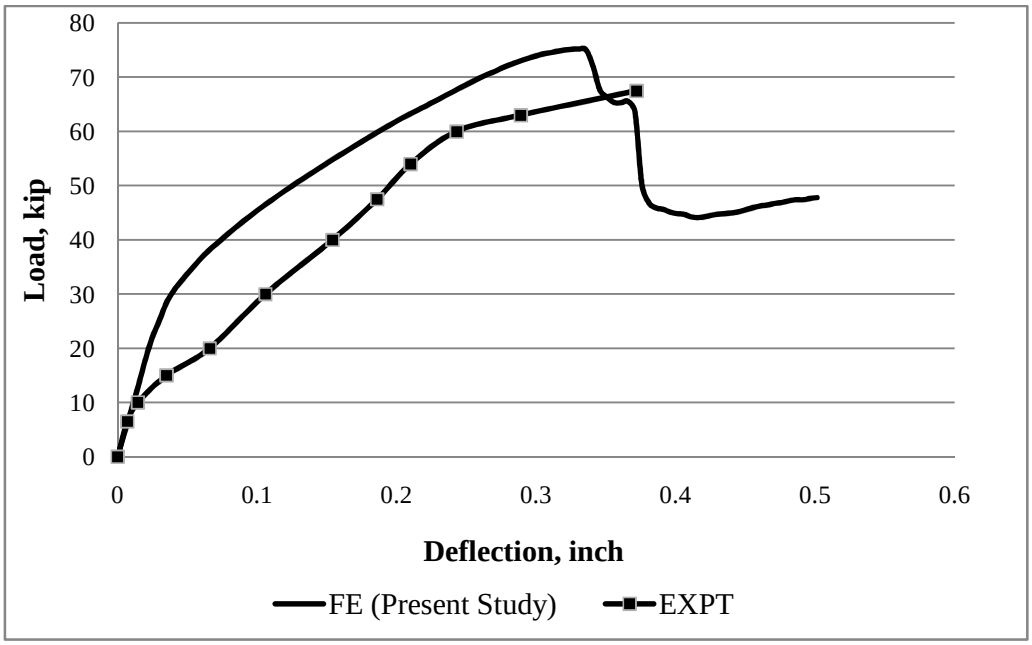

Figure 4.18 Comparative load-deflection responses for A-1a

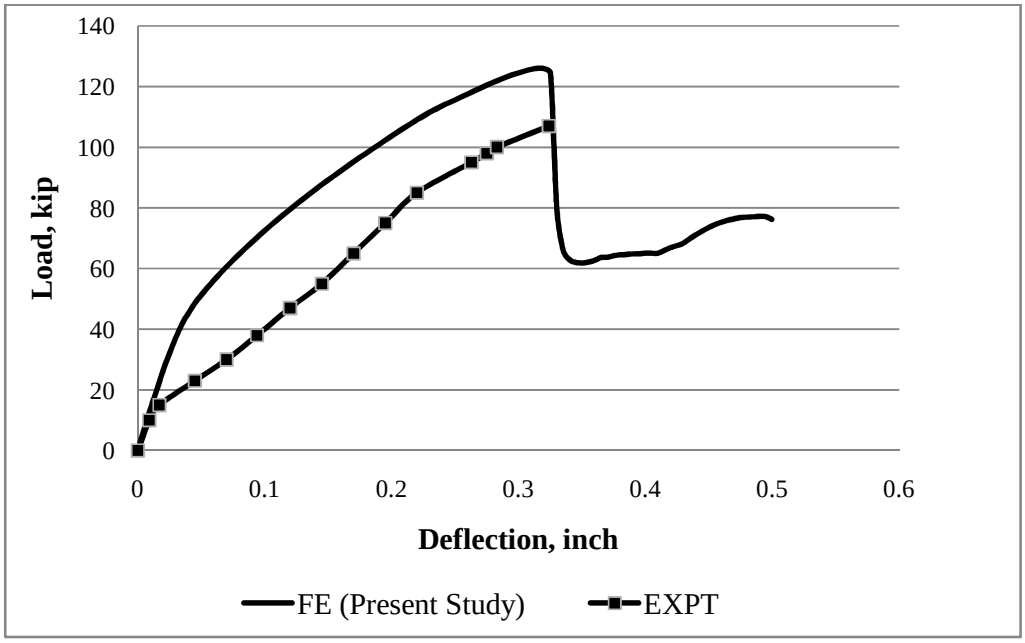

Figure 4.19 Comparative load-deflection responses for A-7b

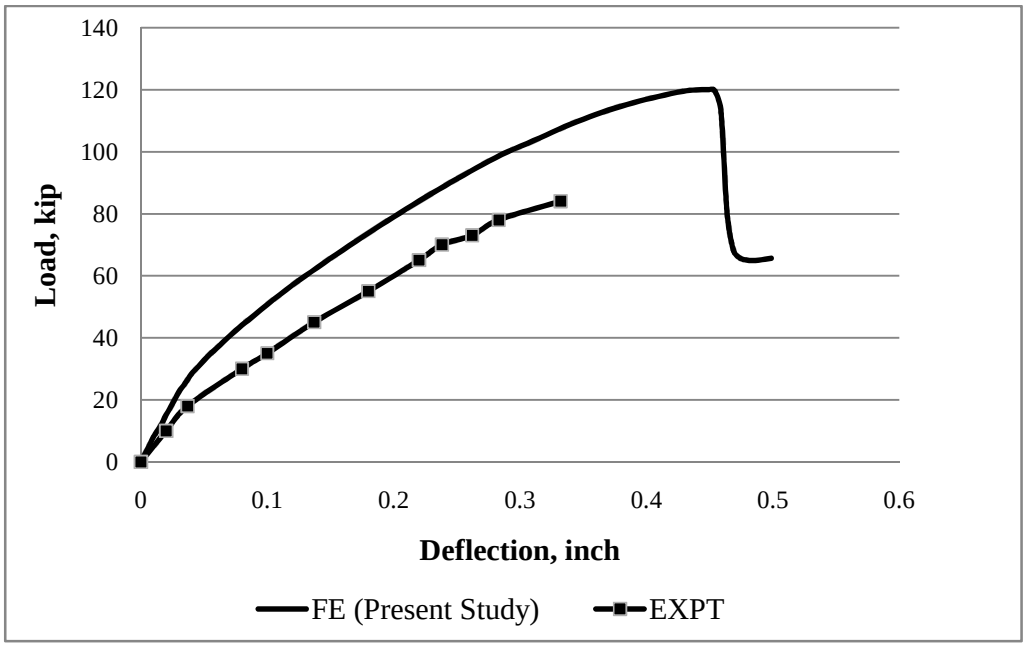

Figure 4.20 Comparative load-deflection responses for A-7

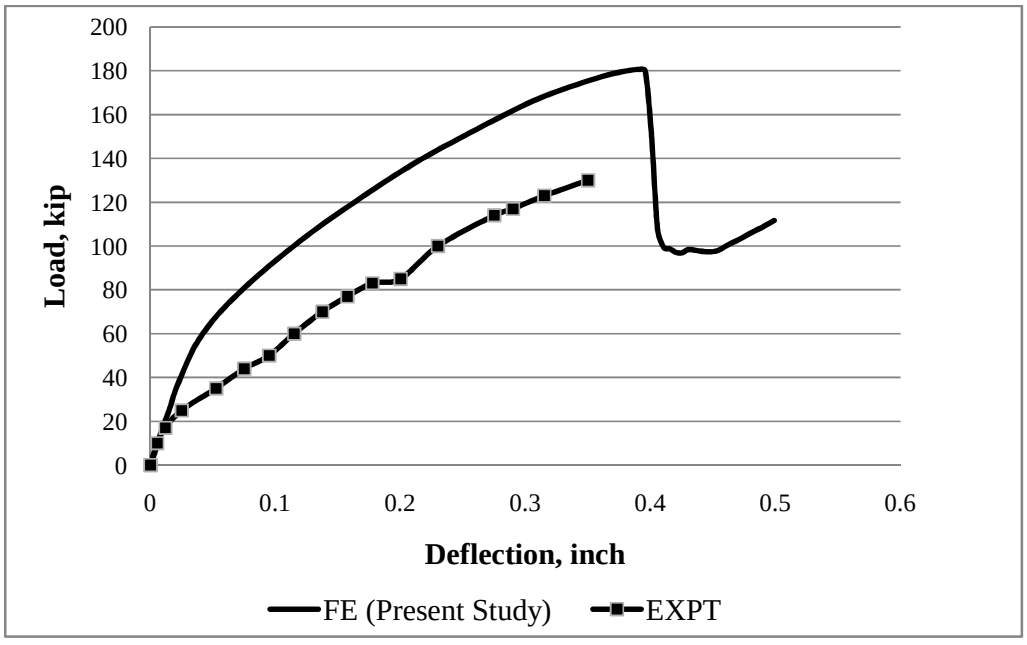

Figure 4.21 Comparative load-deflection responses for B-14

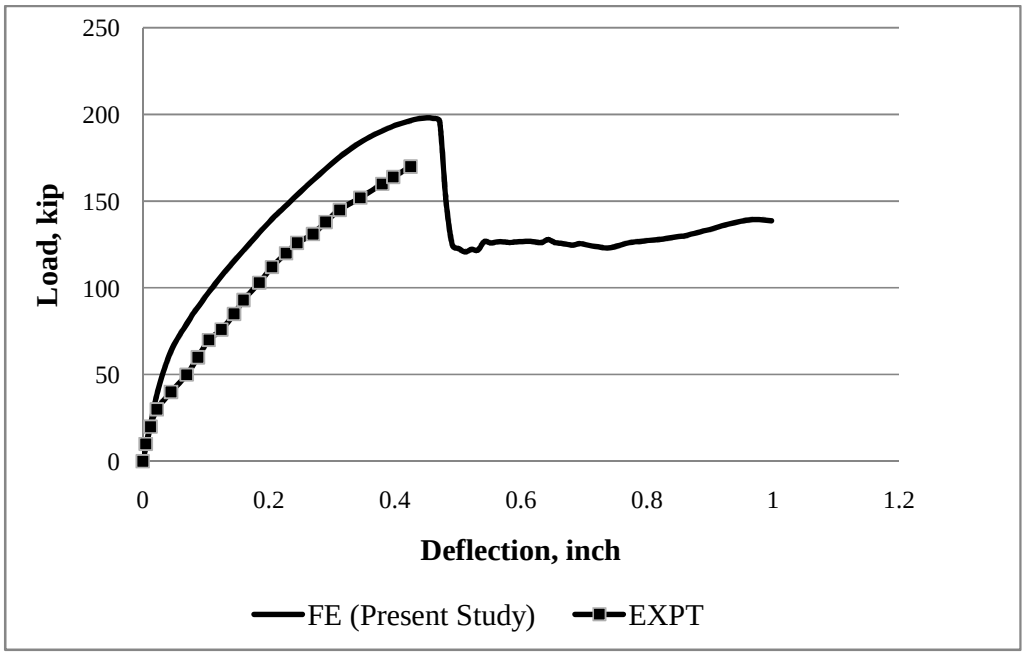

Figure 4.22 Comparative load-deflection responses for B-16

4.3.2 FE modeling of RC flat plate (Graf)

Graf (1938) investigated the strength of thick reinforced concrete slabs submitted to concentrated loading. To illustrate by an example, four slabs 11.81 inch and 19.7 inch thick and 66.93 inch square, composed of straight or bent reinforcement as shown in Figs. 4.23 and 4.24 are considered. All slabs supported at the edges and the slabs were restrained in three directions over supports. The vertical load applied through column. It was reported that punching failure was characterized by a distinctive cracking sequence. The first crack appeared at the bottom (tension side) of the slab along the perimeter of the column. With the increase of the load number of crack was expended through the slab thickness. At the outermost part of the slab, only radial cracks were observed. The punching failure took place suddenly at the load called the punching load. The punching crack across the slab thickness for slabs with straight reinforcement was depicted along the direction of the reinforcement and was characterized by an inclination which varies from 31^{o} to 53^{o}. This inclination was increased with increasing slab thickness, as for the thin slab, the punching crack had a lower inclination than for the thick one. The type of

reinforcement also influenced the shape of the punching crack. For slabs with straight reinforcement, one punching crack which was practically linear was observed whereas for slabs with bent reinforcement the punching crack was curved and various opened shear cracks were observed. For slabs with straight reinforcement, prior to failure, no crack could be seen on the top (compression side) of the slab, whereas for slabs with bent reinforcement, the punching crack at the top (compression side) of the slab could be observed.

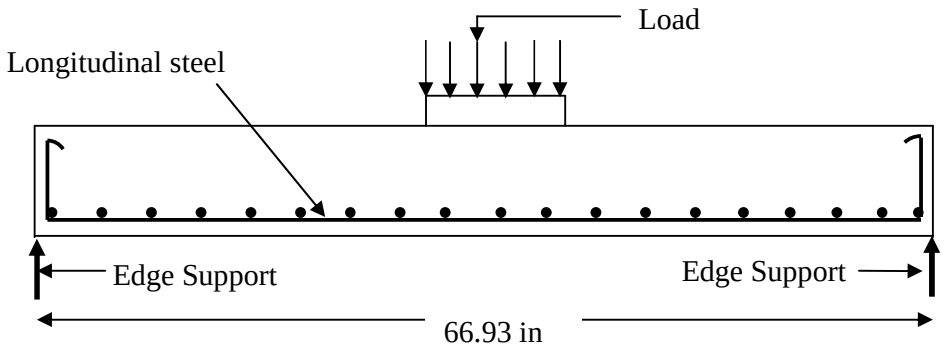

Figure 4.23 Setup of slab section with straight reinforcement and 11.81 inch or 19.7 inch thick; (Graf 1938)

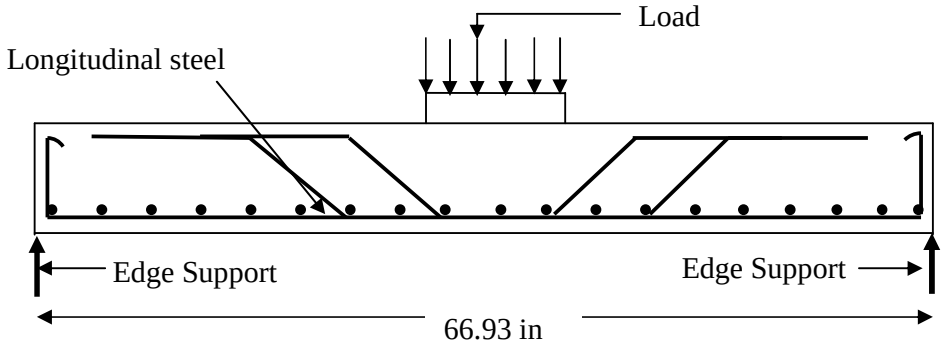

Figure 4.24 Setup of slab section with bent reinforcement and 11.81 inch or 19.7 inch thick; (Graf 1938)

Four real RC slabs tested by Graf (1938) are taken as reference for numerical modeling. The summary of the material properties used in the finite element modeling is shown in Table 4.4. Other parameters of the test slabs and the corresponding FE model plates are shown in Table 4.5. It is to be noted that the ratio of the longitudinal reinforcement is applicable for the entire slab.

Table 4.4 Material properties used

Plate No.	E_c (ksi)	E_s (ksi)	f'_c (psi)	f_r (psi)	f_y (ksi)	ν_c	ν_s	Longitudinal Reinforcement		Shear Reinforcement A_v sq in
								Tension Reinforcement ρ percent	Compression Reinforcement ρ percent	
G-1	2512.531	$29x10^3$	1943	323.3	39.9	0.2	0.3	0.91	----	----
G-2	2512.531	$29x10^3$	1943	323.3	39.9	0.2	0.3	0.91	----	----
G-3	2512.531	$29x10^3$	1943	323.3	39.9	0.2	0.3	0.91	----	7.81
G-4	2512.531	$29x10^3$	1943	323.3	39.9	0.2	0.3	0.91	----	13.44

Table 4.5 Details of slab dimension

Plate No.	Plate Dimension (in)	Column Stub Dimension (in)	h (in)	d (in)	Support Condition
G-1	66.93x66.93x11.81	14.96x14.96	11.81	10.63	Symmetrical Pin Support on four edges
G-2	66.93x66.93x19.7	14.96x14.96	19.7	18.5	Symmetrical Pin Support on four edges
G-3	66.93x66.93x11.81	14.96x14.96	11.81	10.63	Symmetrical Pin Support on four edges
G-4	66.93x66.93x19.7	14.96x14.96	19.7	18.5	Symmetrical Pin Support on four edges

Typical concrete mesh, reinforcement for tension and including tension and shear reinforcement for G-3 and G-4 slab are shown in Figs. 4.25 to 4.27.

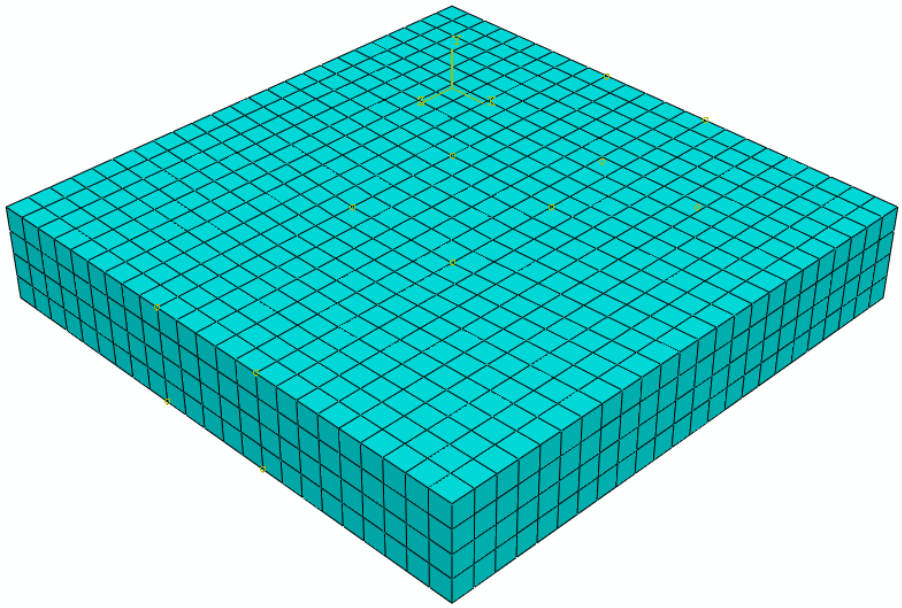

Figure 4.25 Typical finite element model of concrete mesh

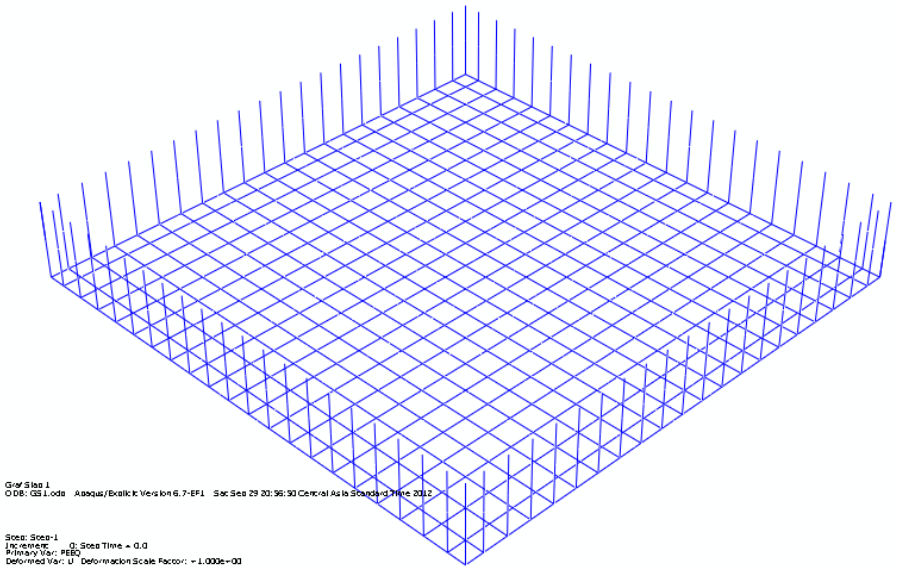

Figure 4.26 Typical tension reinforcement for G-1 and G-2 slabs

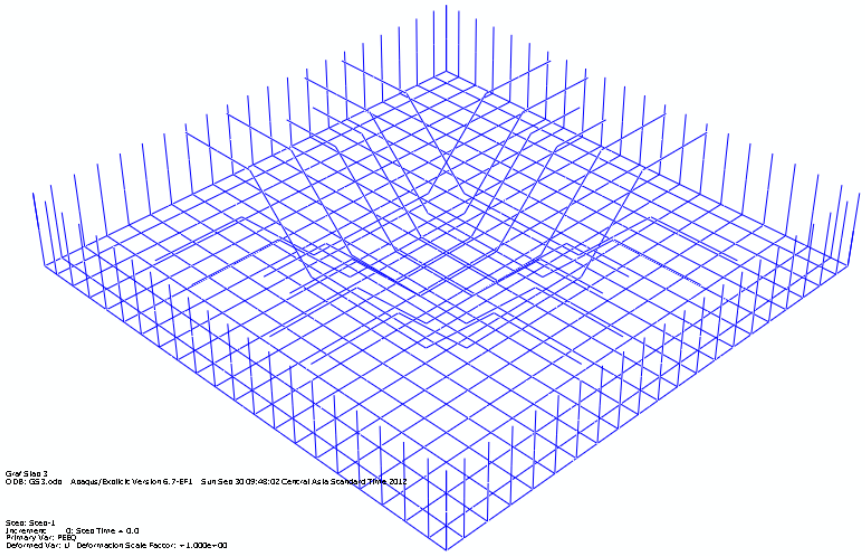

Figure 4.27 Typical tension and bent bar reinforcement for G-3 and G-4 slabs

With the start of the loading process same phenomenon has observed in finite element analyses as Elstner and Hognestad slab art. It was reported that punching failure was characterized by a distinctive cracking sequence and concrete damage and the punching failure took place suddenly at the load called the punching load. The punching crack has a lower inclination in case of thin slab than for the thick one. It is also observed that the type of reinforcement also influenced the shape of the punching crack. The load-deflection curves of these four slabs are presented in Figs. 4.28 to 4.31. Slab G-1 and G-2 which are made of straight reinforcement but different thickness behave in a similar way even though slab G-2 is much stiffer than slab G-1 and there are also some difference in the load-deflection behaviour between present FE analysis (FE) and experimental results (EXPT). The same analogy is valid for slabs with bent reinforcement. Slab with bent bar can sustain larger deflection and higher load. The shape of the bars influences the slab response. It is observed that for plate G-1, G-2 and G-4 the punching loads obtained numerically (289 kip, 619 kip and 793 kip) are higher than the experimental failure loads (265 kip, 366 kip and 675 kip) as it represents 9.06%, 69.1% and 17.5% higher than experimental failure loads respectively and for plate G-3 the punching load obtained numerically (336 kip) is lower than the experimental failure load (394 kip) as it represents 85.3% of the experimental failure load. At the maximum load for plate G-

1, G-3 and G-4, the numerical vertical displacements are 0.06 in, 0.08 in and 0.08 in representing around 75%, 36.4% and 66.7% of the experimental one respectively and for plate G-2, the numerical vertical displacement is 0.05 in representing around 66.7% higher than experimental one. However, the cracking pattern and failure phenomenon of FE model is in good agreement with the experimental results.

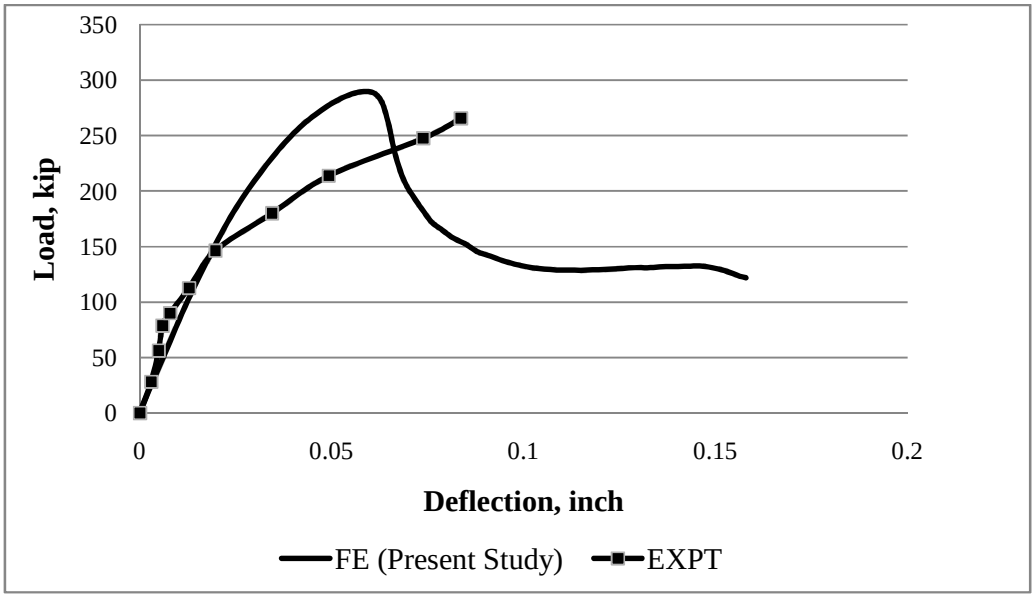

Figure 4.28 Comparative load-deflection responses for G-1

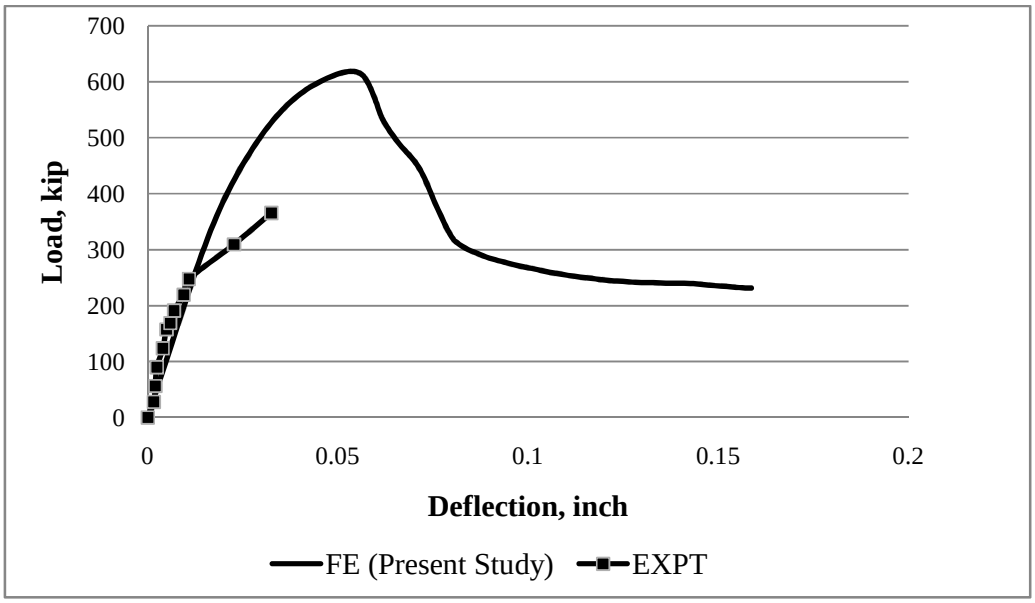

Figure 4.29 Comparative load-deflection responses for G-2

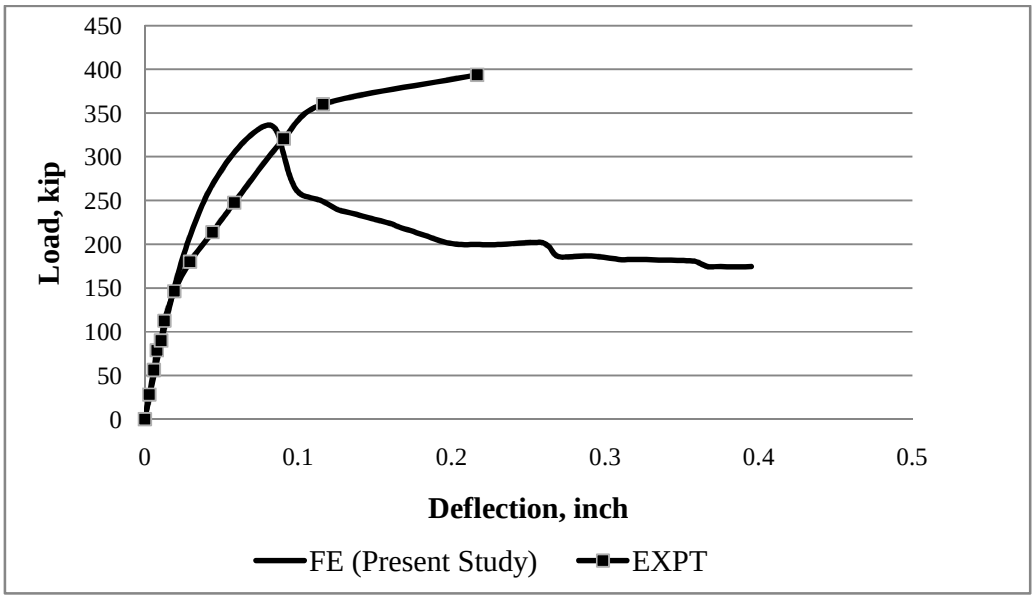

Figure 4.30 Comparative load-deflection responses for G-3

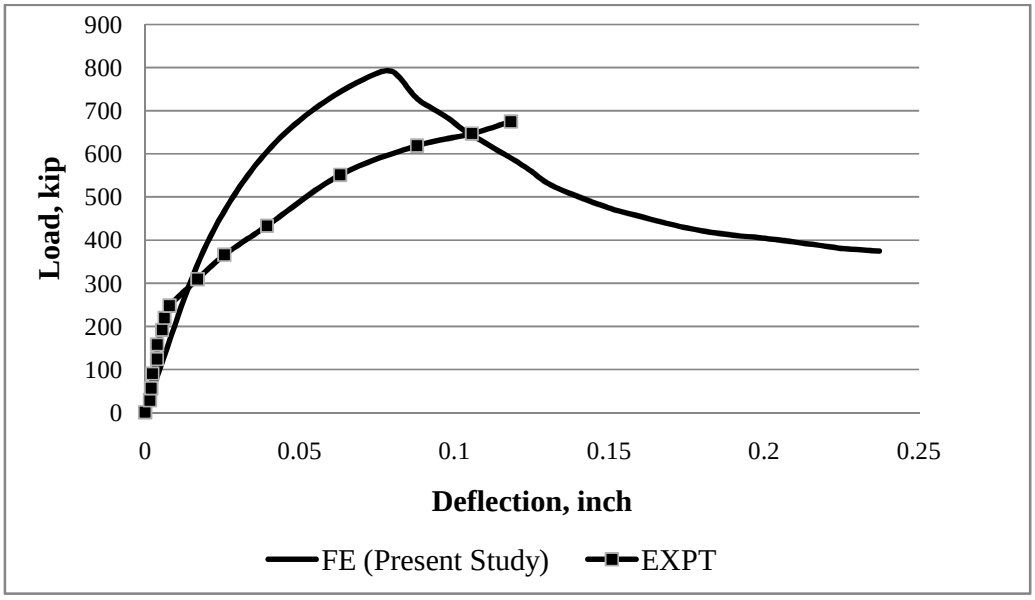

Figure 4.31 Comparative load-deflection responses for G-4

4.3.3 FE modeling of RC flat plate (Kinnunen and Nylander)

Three circular slabs tested by Kinnunen and Nylander (1960) were simulated because they cover different types of reinforcement with the same geometry allowing to preserve the finite element mesh. The first slab to be simulated was the slab made of ring reinforcement only. This slab was already analyzed numerically by Andra (1982). The second slab to be analyzed is made of ring and radial reinforcement. This slab was already analyzed numerically by Loseth et al. (1982). The last simulation was investigated the behaviour of slab made of orthogonal reinforcement. The last slab was already analyzed numerically by Kinnunen (1963). Kinnunen and Nylander tested circular 5.9 inch thick slabs, 72.44 inch in diameter supported along the circumference and loaded on a column stub 5.9 inch in diameter at the center by mean of a hydraulic jack and transferred to the floor. In the experiment, the concrete was made with standard portal cement, water-cement ratio of 0.7 and aggregate from 0.005 inch to 1.26 inch. The influence of the arrangement of the reinforcement was demonstrated with all slabs. The overall behaviour of all slabs was similar except for little differences. The shape of the punching crack

through the slab thickness was observed that the punching crack was more inclined for the slab with ring reinforcement than for the slab with orthogonal reinforcement. In slab with ring reinforcement the tangential and the radial cracks could be clearly distinguished, whereas in the slab with orthogonal reinforcement, the crack pattern did not follow the radial and tangential geometry but was more like a net, especially inside the punching cone.

Three real RC circular slabs tested by Kinnunen and Nylander (1960) are taken as reference for numerical modeling. The summary of the material properties used in the finite element modeling is shown in Table 4.6. Other parameters of the test slabs and the corresponding FE model plates are shown in Table 4.7. It is to be noted that the ratio of the longitudinal reinforcement is applicable for the entire slab.

Table 4.6 Material properties used

Plate No.	E_c (ksi)	E_s (ksi)	f'_c (psi)	f_r (psi)	f_y (ksi)	ν_c	ν_s	Longitudinal Reinforcement	
								Tension Reinforcement type	Tension Rebar
IA15a	3625	$30.4x10^3$	4074.5	435	65.25	0.2	0.3	Orthogonal	φ 4
IB15a	3625	$30.4x10^3$	3625	435	65.25	0.2	0.3	Ring	φ 4
IC15a	3625	$30.4x10^3$	4176	449.5	65.25	0.2	0.3	Ring & Radial	φ 4

Table 4.7 Details of slab dimension

Plate No.	Plate Diameter (in)		Column Stub Diameter (in)	h (in)	d (in)	Support Condition
	Test	FE				
IA15a	72.44	67.32	5.9	5.9	5.12	Symmetrical Support on circular edge
IB15a	72.44	67.32	5.9	5.9	5.12	Symmetrical Support on circular edge
IC15a	72.44	67.32	5.9	5.9	5.12	Symmetrical Support on circular edge

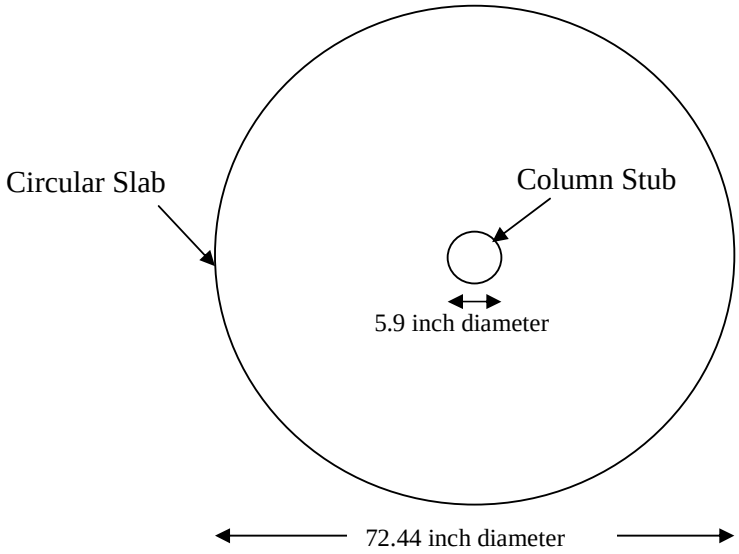

Figure 4.32 Plan view of 5.9 inch thick circular slab; (Kinnunen and Nylander 1960)

In the FE model, one fourth of the slab is plotted. The geometry of these slabs is shown in Fig. 4.33. The boundary condition of U3=0 along the supports is used to simulate the test condition and the loading pattern are also shown in Fig. 4.33.

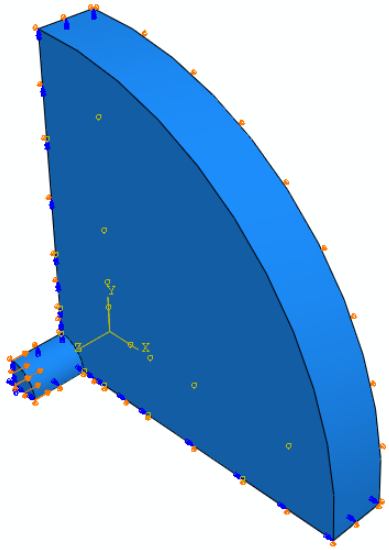

Figure 4.33 Typical finite element model of one-forth slab with boundary condition and loading pattern

Typical concrete mesh, reinforcement for ring, ring & radial and orthogonal reinforcement mat are shown in Figs. 4.34 to 4.37.

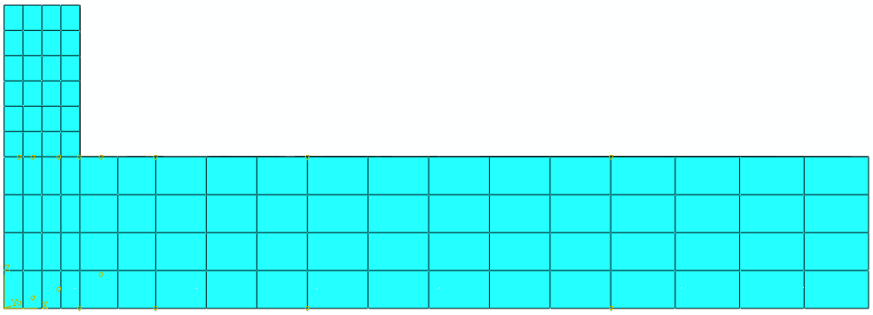

Figure 4.34 Typical finite element model of concrete mesh

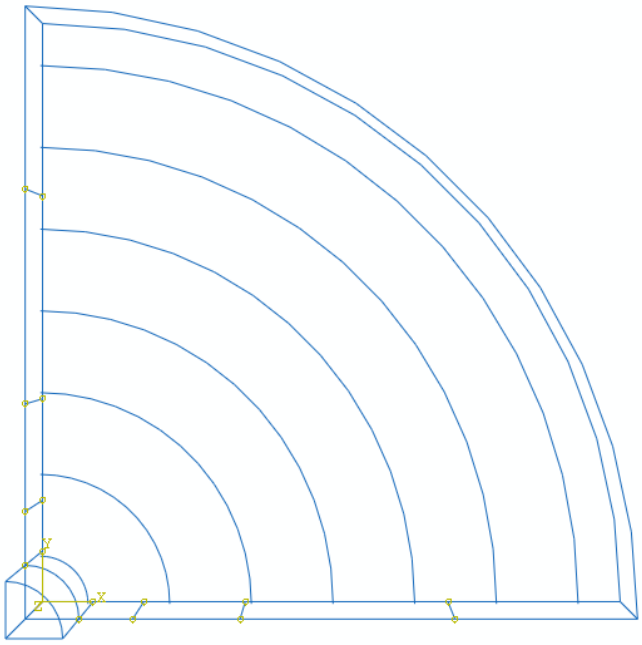

Figure 4.35 Overview of one-forth slab (IB15a) with ring reinforcement

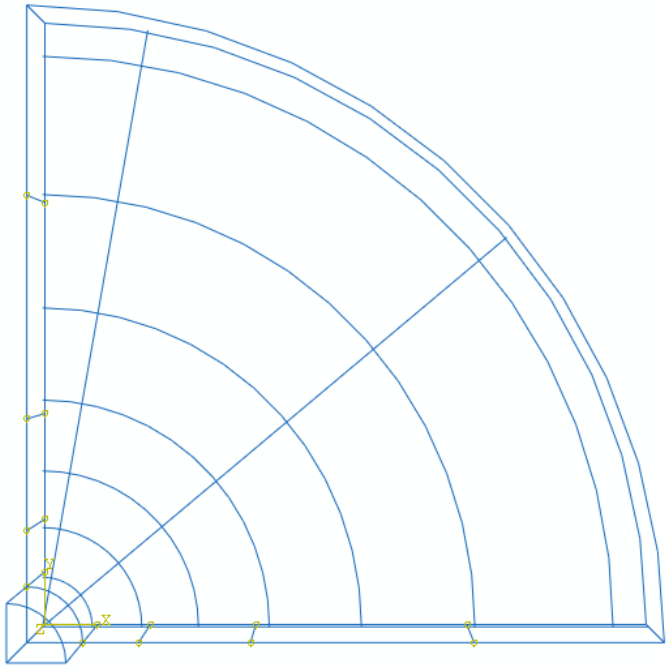

Figure 4.36 Overview of one-forth slab (IC15a) with ring and radial reinforcement

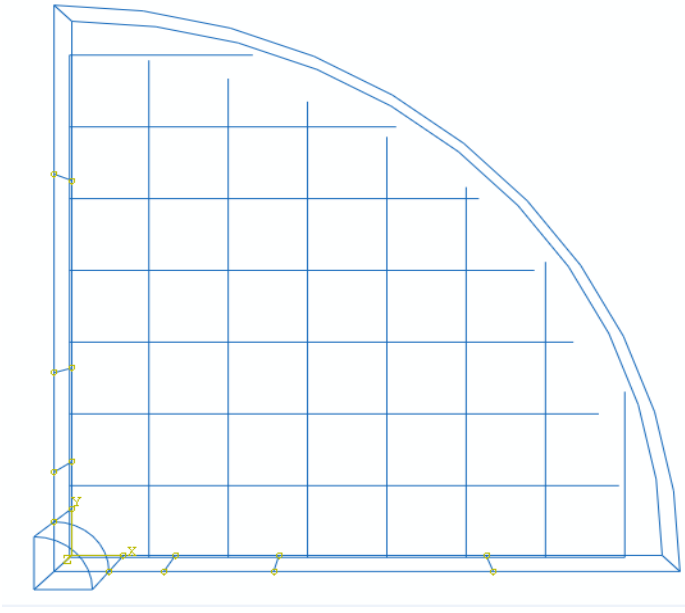

Figure 4.37 Overview of one-forth slab (IA15a) with orthogonal reinforcement

With the start of the loading process same phenomenon also has observed in finite element analyses as Elstner and Hognestad and Graf slab art. The shape of the punching crack through the slab thickness for slab with orthogonal, ring and ring & radial reinforcement are shown in Figs. 4.38 to 4.40 respectively. It is observed that the punching crack is more inclined for the slab with ring reinforcement than for the slab with orthogonal and ring & radial reinforcement. The type of reinforcement is not the only difference among these slabs as the percentage of reinforcement is not similar. Therefore, the inclination of the punching crack is influenced by the type and the percentage of reinforcement.

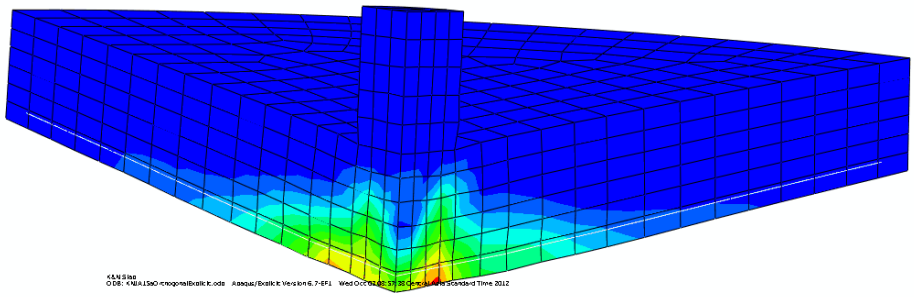

Figure 4.38 Tensile damage of concrete on bottom surface of one-forth slab (IA15a) and punching failure with a pyramid shape at 51.7 kip load

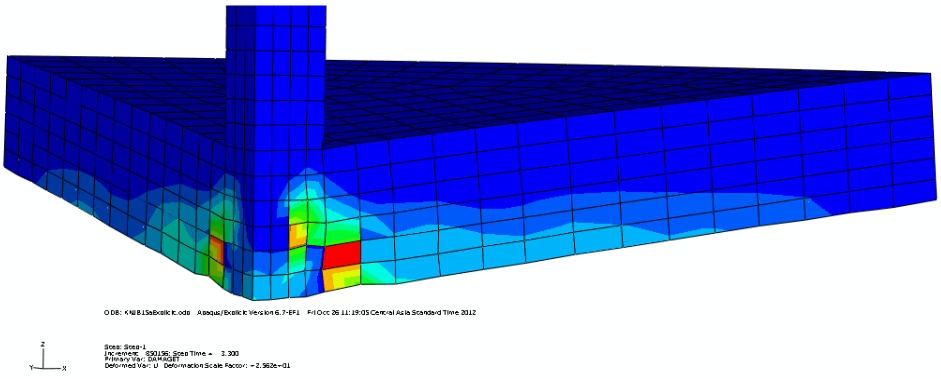

Figure 4.39 Tensile damage of concrete on bottom surface of one-forth slab (IB15a) and punching failure with a pyramid shape at 44.1 kip load

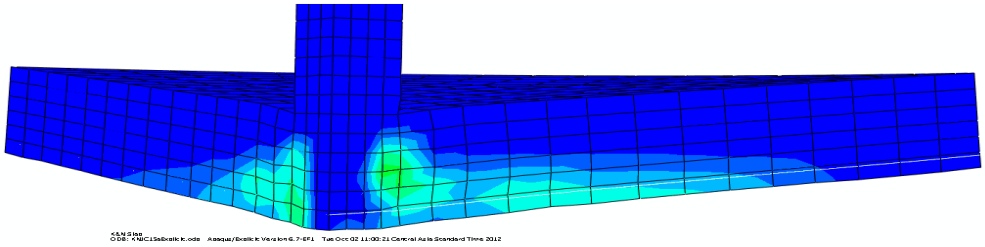

Figure 4.40 Tensile damage of concrete on bottom surface of one-forth slab (IC15a) and punching failure with a pyramid shape at 53.7 kip load

The load-deflection curves of these three slabs are presented in Figs. 4.41 to 4.43. All the curves exhibit a linear elastic behaviour at the initial stage. After some time with the increase of load, it is followed a gradual development of non-linear response. There are also some difference in the load-deflection behaviour between present FE analysis (FE) and experimental results (EXPT). It is observed that for plate IC15a the punching load obtained numerically (53.7 kip) is higher than the experimental failure load (45.9 kip) as it represents 17% higher than experimental failure load and for plate IA15a and IB15a the punching loads obtained numerically (51.7 kip and 44.1kip) are lower than the mean experimental failure loads (59.5 kip and 44.5 kip) as it represents 86.9% and 99% of the mean experimental failure loads respectively. At the maximum load for plate IA15a, IB15a and IC15a, the numerical vertical displacements are 0.14 in, 0.13 in and 0.15 in representing around 35%, 42.6% and 55.5% of the mean experimental one respectively. However, the present FE analysis (FE) and the previous FE analysis by Kinnunen (1963), Andra (1982) and Loseth et al (1982) have shown very close results at every stages of load history of slab up to failure. It is observed that for plate IA15a, IB15a and IC15a, the punching loads from present FE analysis (51.7 kip, 44.1 kip and 53.7 kip) are very close with other numerical analysis as specified above (49.5 kip, 45 kip and 48.4 kip) respectively and the vertical displacements from present FE analysis (0.14 in, 0.13 in and 0.15 in) are also very close with other numerical analysis as specified above (0.13 in, 0.13 in and 0.18 in) respectively.

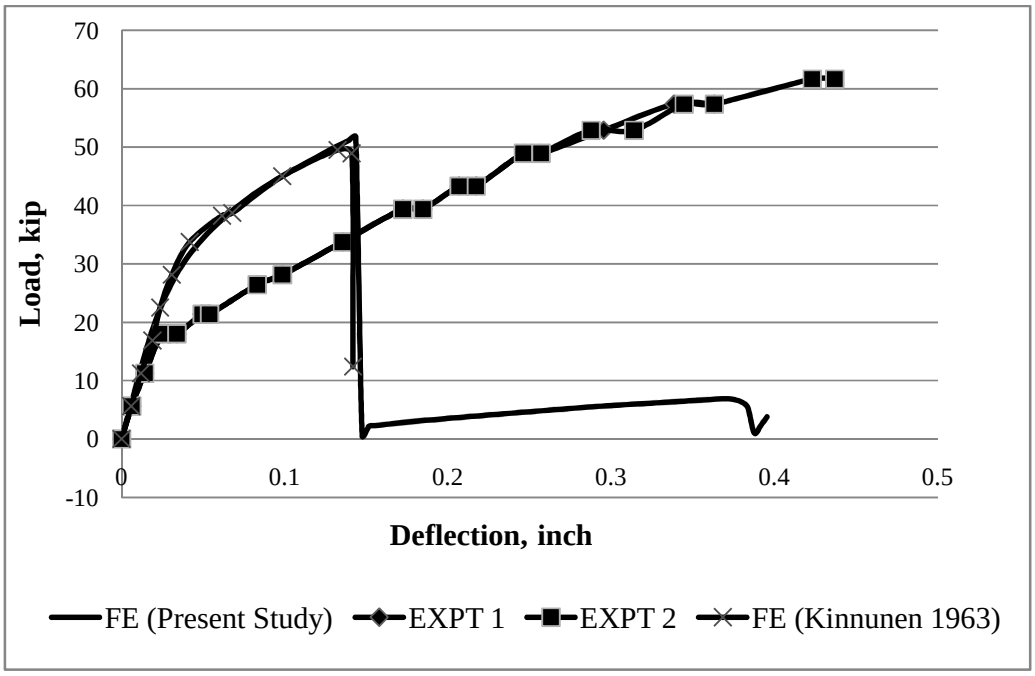

Figure 4.41 Comparative load-deflection responses for IA15a

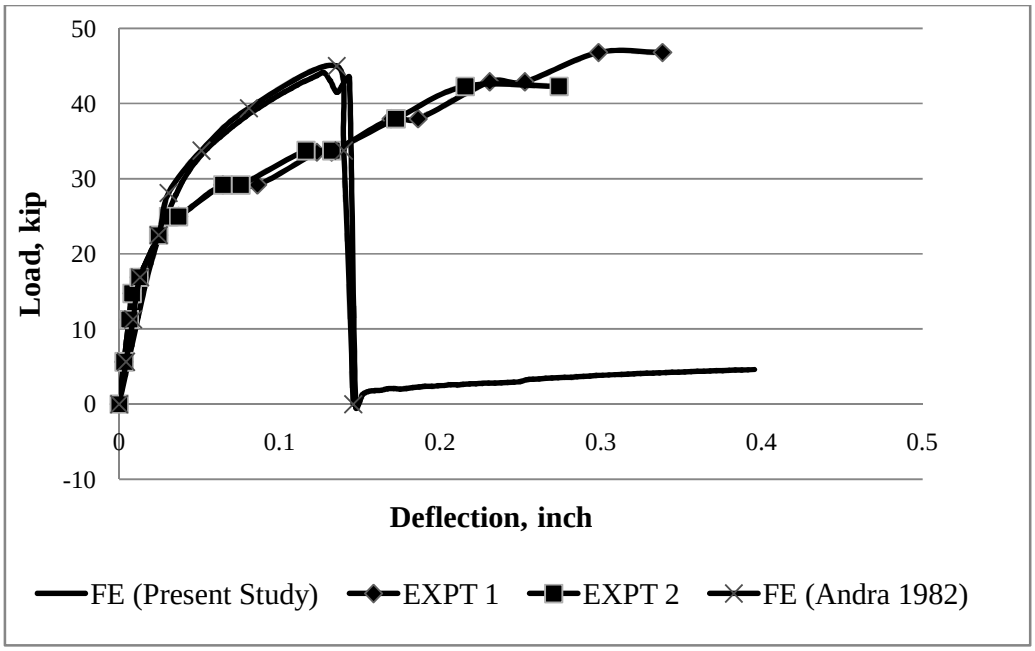

Figure 4.42 Comparative load-deflection responses for IB15a

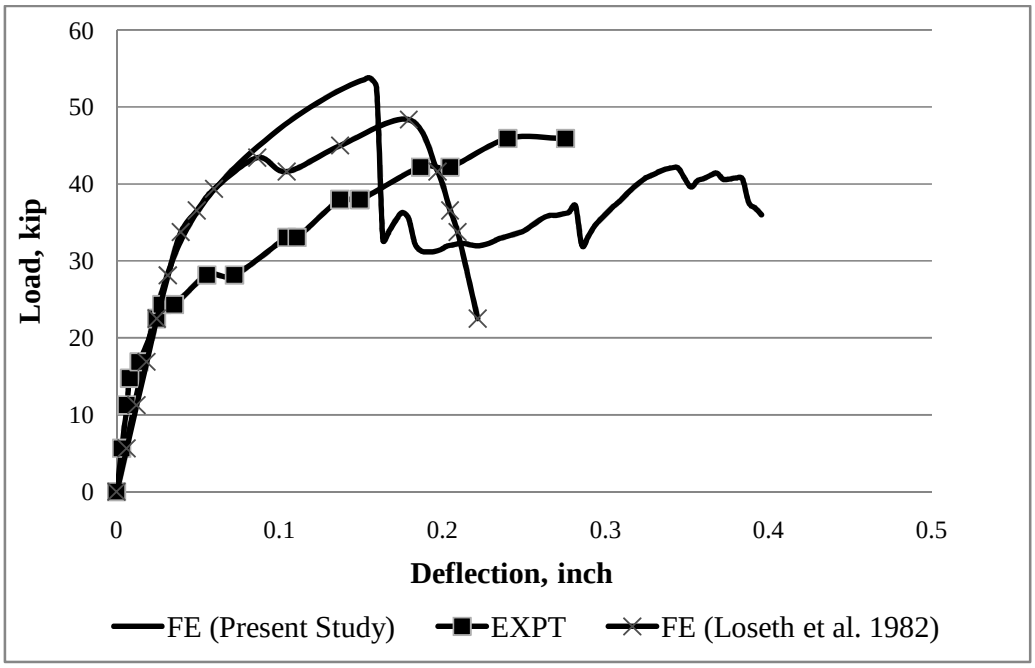

Figure 4.43 Comparative load-deflection responses for IC15a

4.3.4 FE modeling of RC flat plate (Jofreit and McNeice)

A set of specimen tested by Jofreit and McNeice (1971) Consisted of corner-supported slabs subjected to a point load applied at the centre. The Jofreit and McNeice slab was one often used as a benchmark for calibrating nonlinear analyses. The corner supported two-way slab was 36in x 36in square and 1.73 inch thick and reinforced with an orthogonal direction. The purpose of the test was to gauge service load deflections and thus was not loaded to ultimate. This slab was already analyzed numerically by using a full nonlinear shell analysis (RASP program). The program was developed by Seracino (1995).

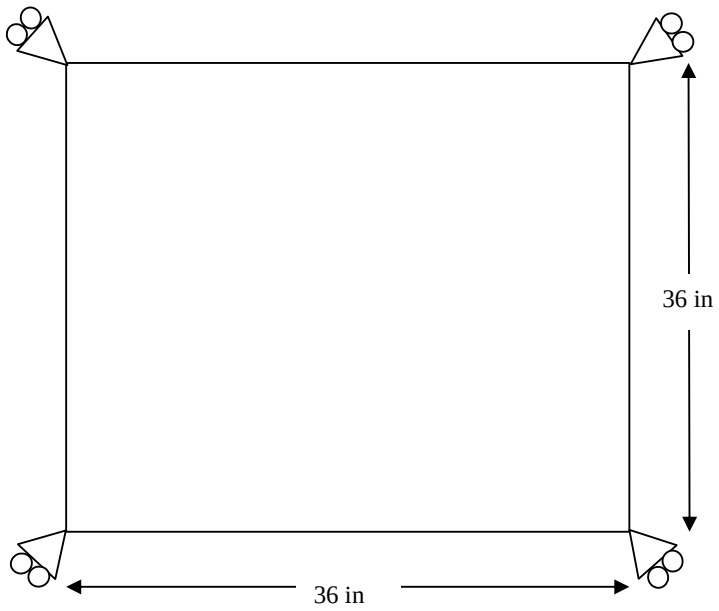

Figure 4.44 Plan view of 1.73 inch thick slab; (Jofreit and McNeice 1971)

One real RC slab tested by Jofreit and McNeice (1971) is taken as reference for numerical modeling. The summary of the material properties used in the finite element modeling is shown in Table 4.8. Other parameters of the test slabs and the corresponding FE model plates are shown in Table 4.9. It is to be noted that the ratio of the longitudinal reinforcement is applicable for the entire slab.

Table 4.8 Material properties used

E_c (ksi)	E_s (ksi)	f'_c (psi)	f_r (psi)	f_y (ksi)	ν_c	ν_s	Longitudinal Reinforcement	
							Tension Reinforcement ρ percent	Compression Reinforcement ρ percent
4147	$29x10^3$	5495.5	549.55	58	0.15	0.3	0.85	----

Table 4.9 Details of slab dimension

Plate Dimension (in)	Column Stub Dimension (in)	h (in)	d (in)	Support Condition
36x36x1.73	4.53x4.53	1.73	1.3	Pin support on one corner and roller support on rest of three corners of the slab

Typical concrete mesh and tension reinforcement are shown in Figs. 4.45 and 4.46.

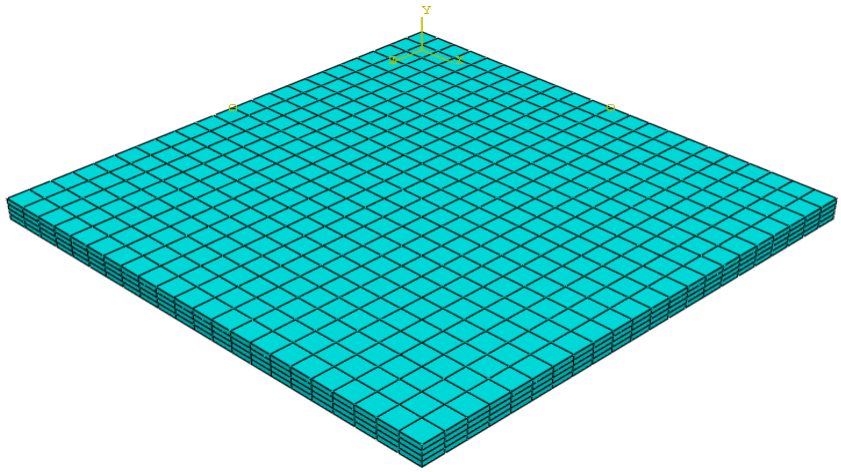

Figure 4.45 Typical finite element model of concrete mesh

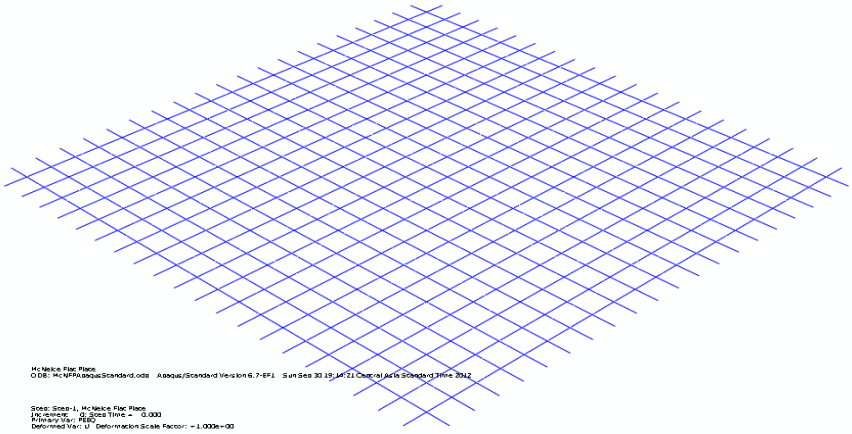

Figure 4.46 Typical tension reinforcement

The purpose of the numerical analysis is to gauge service load deflections. The load-deflection curve of this slab is presented in Fig. 4.47. It is observed that all the curves exhibit a linear elastic behaviour at the initial stage. After some time with the increase of load, it is followed a gradual development of non-linear response and have some difference in the load-deflection behaviour between present FE analysis (FE) and experimental results (EXPT) or other numerical results (RASP program) as specified above. The present FE analysis (FE), experimental results (EXPT) and other numerical results (RASP program) have represented the loads up to 2.25 kip,

3.15 kip and 3.15 kip respectively and the vertical displacements for the above mentioned loads are 0.22 in, 0.38 in and 0.31 in respectively.

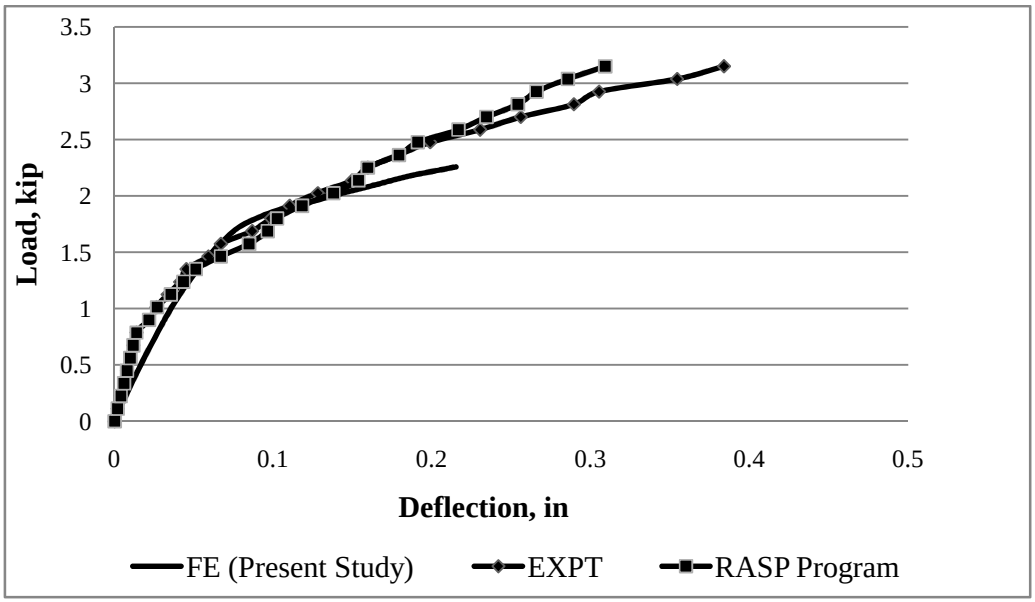

Figure 4.47 Comparative load-deflection responses

4.3.5 FE Modeling of RC Flat Plate (Tan and Teng)

Tan and Teng (2005) investigated the effects of uniaxial and biaxial loading and the use of stud shear reinforcement, on the performance of the connections for rectangular column with aspect ratio of 5. A series of tests were conducted on interior slab-rectangular column connections by the desired level of gravity loading and then performing lateral loadings on the specimens until failure. The actual test specimens would represent a 75% scale down of the portion of the floor plan to be modeled as shown in Fig. 4.48. This would work out to the specimens having dimensions of 177.2 inch by 137.8 inch and column size of 35.4 inch by 7.1 inch and a slab thickness of 5.9 inch. The overall height of the specimen was 7.4 ft and was assumed to terminate at the column mid-height in an actual prototype building. This was because the column mid height represented the lines of contra flexure in the column during lateral loadings. In addition, the size of each specimen was determined such that the stresses near the connections would be relatively unaffected

by the boundary conditions near the slab edge. Since the panel centerlines in an actual building would only move horizontally under lateral loading (with very little relative deflections), the slab boundaries were assumed to be on rollers. A schematic diagram showing the boundary and support conditions for the single column test specimens are shown in Fig. 4.49. The roller supports were simulated by means of edge link supports with steel rocker simulating the pin support. Throughout the course of the experiment, more flexural cracks were formed and propagated towards the slab edges as the load increased. Cracks in the tangential direction crossing the cracks in the radial direction were also observed.

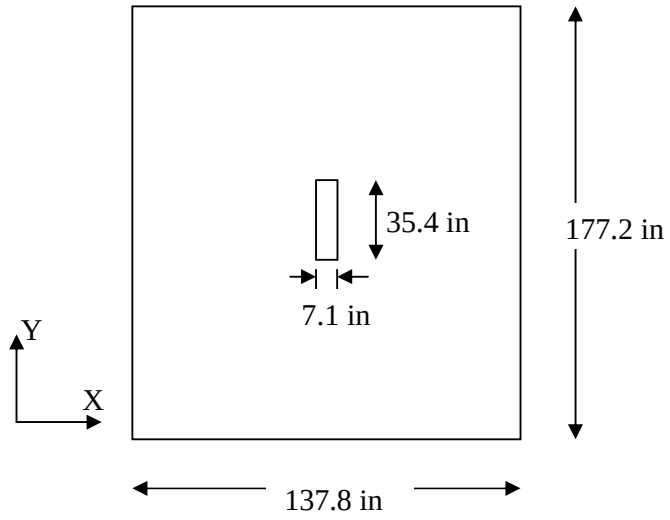

Figure 4.48 Plan view of 5.9 inch thick slab; (Tan and Teng)

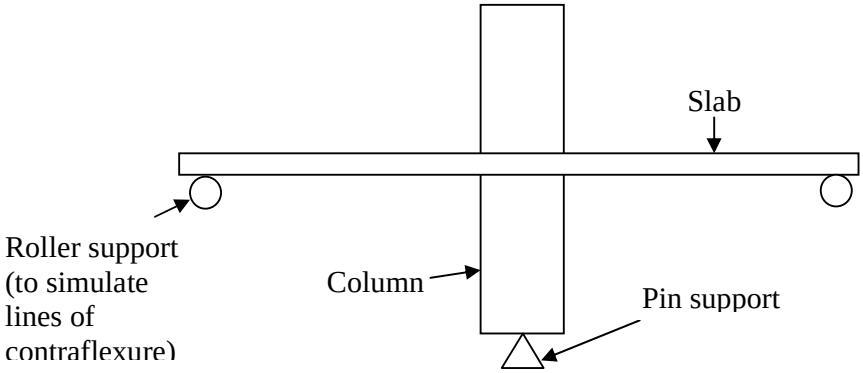

Figure 4.49 Schematic diagram of single column specimen

One real RC slab (YL-L1) tested by Tan and Teng (2005) is taken as reference for numerical modeling. The summary of the material properties used in the finite element modeling is shown in Table 4.10. Other parameters of the test slabs and the corresponding FE model plates are shown in Table 4.11.

Table 4.10 Material properties used

E_c (ksi)	E_s (ksi)	f'_c (psi)	f_r (psi)	f_y (ksi)	ν_c	ν_s	Longitudinal Reinforcement		Column Longitudinal Reinforcement ρ percent
							Top Reinforcement ρ percent in regions of c+3h	Bottom Reinforcement ρ percent	
3625	$30.45x10^3$	5800	507.5	75.4 for no.3 bar 76.85 for no.4 and no.6 bar	0.2	0.3	1.2	0.4	2.5

Table 4.11 Details of slab dimension

Plate Dimension (in)	Column stub Dimension (in)	Column Height (ft)	h (in)	d (in)	Support Condition
177.2x137.8x5.9	35.4x7.1	7.4	5.9	4.8	Roller supports on each corner of the slab and pin support at the bottom of the column

In the FE model, the boundary condition along the supports is used to simulate the test condition and the loading pattern are shown in Fig. 4.50. The slab is preloaded with gravity load and uniaxial lateral load in the X-direction (along the week column axis) is increased until slab-column connection failure. The gravity loading case corresponded to the slab being loaded with a 15.66 psf of live load in addition to the 20.88 psf super-imposed dead load and self-weight of the slab. The gravity shear ratio, V_g/V_0 would be 0.17. The term V_g is the shear force transferred at the slab column connection due to gravity loads and is calculated using tributary area, while V_0 is the punching shear strength of the connection in the absence of moment transfer. Lateral loading procedures are displacement based and the drift ratio parameter is used. Drift ratio is defined as the relative displacement between the top and bottom of the column divided by the column height.

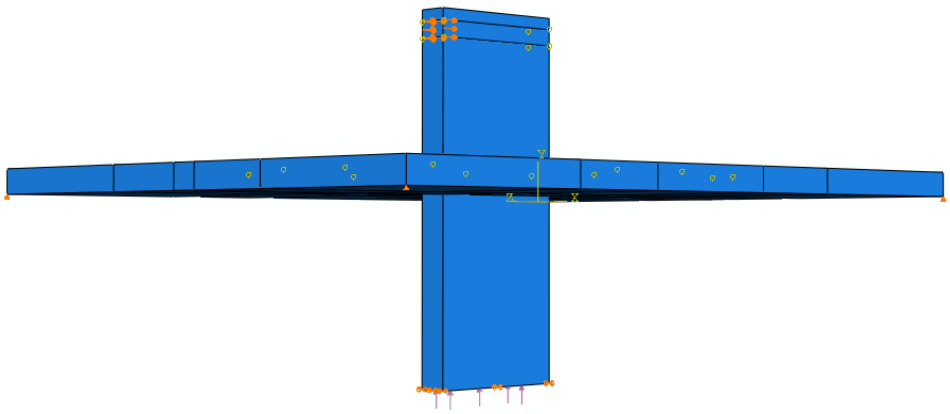

Figure 4.50 Typical finite element model of the plate with boundary condition and loading pattern

Typical concrete mesh, top (tension) and bottom (compression) reinforcement are shown in Figs. 4.51 to 4.53 respectively. Figure 4.54 includes top, bottom and column reinforcement, all in one figure. The slab is reinforced with top (tension) flexural reinforcement ratio of 1.2% in regions of c+3h across the column width where c is the width of column transverse to the direction of the lateral loading and h is the overall depth of the slab. The c+3h width is used as specified in ACI 318 (2008) to prevent flexural failure due to transfer of unbalanced moments by flexural

stresses. In addition, at least two bottom (compression) bars have passed through the column continuously to prevent total collapse of the specimen during punching shear failure. The column is reinforced with steel ratio of 2.5%, aligning with the “strong column and weak beam” concept in design.

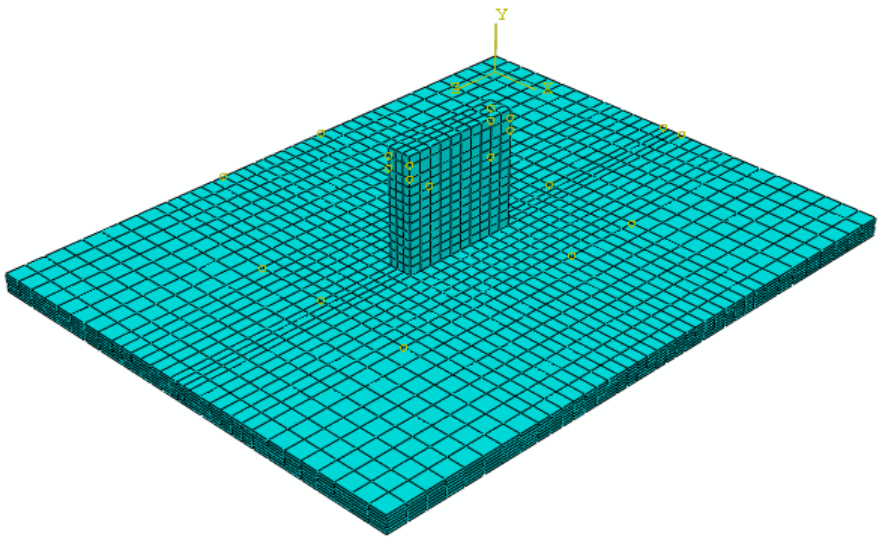

Figure 4.51 Typical finite element model of concrete mesh

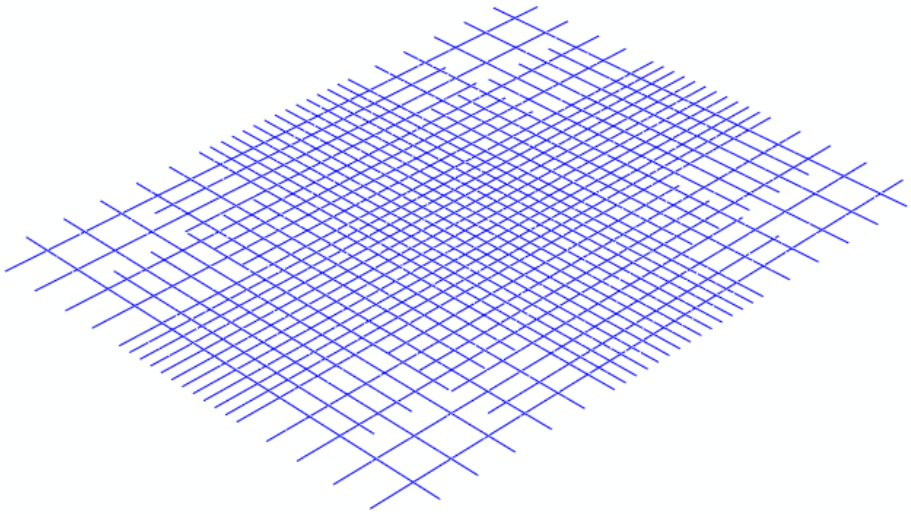

Figure 4.52 Typical top bar reinforcement for YL-L1 slabs

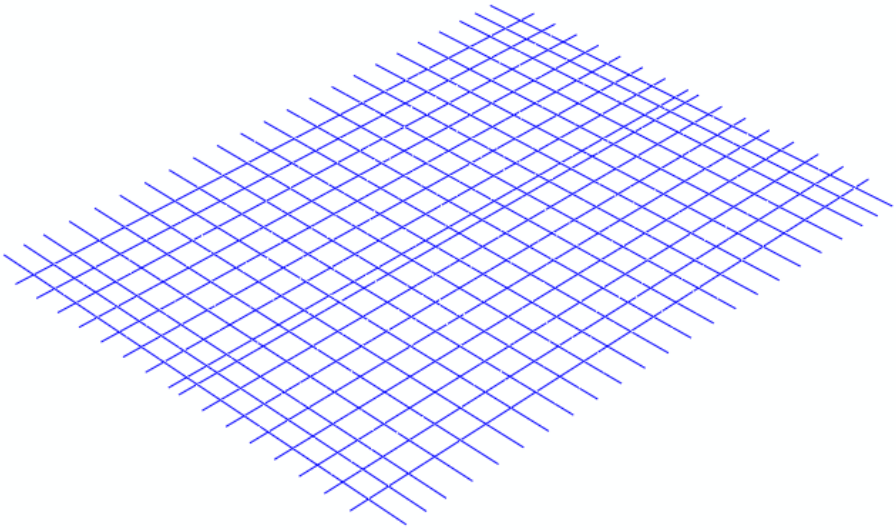

Figure 4.53 Typical bottom bar reinforcement for YL-L1 slabs

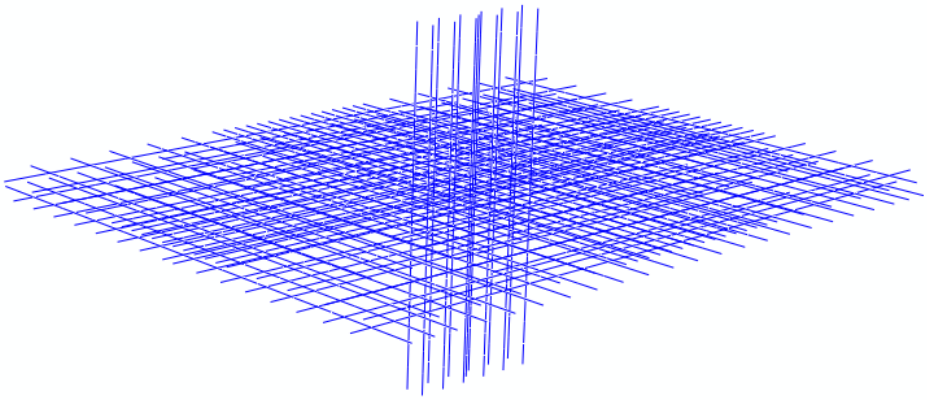

Figure 4.54 Typical top, bottom and column stub reinforcement for YL-L1 slabs

The purpose of the numerical analysis is to gauge the RC slab-column connection behaviour subjected to both gravity and lateral loads. Due to gravity shear and drift ratio 7.5% in column weak directions, the Mises stresses, tension damage and compression damage on slab-column connection are shown in Figs. 4.55 to 4.57 respectively.

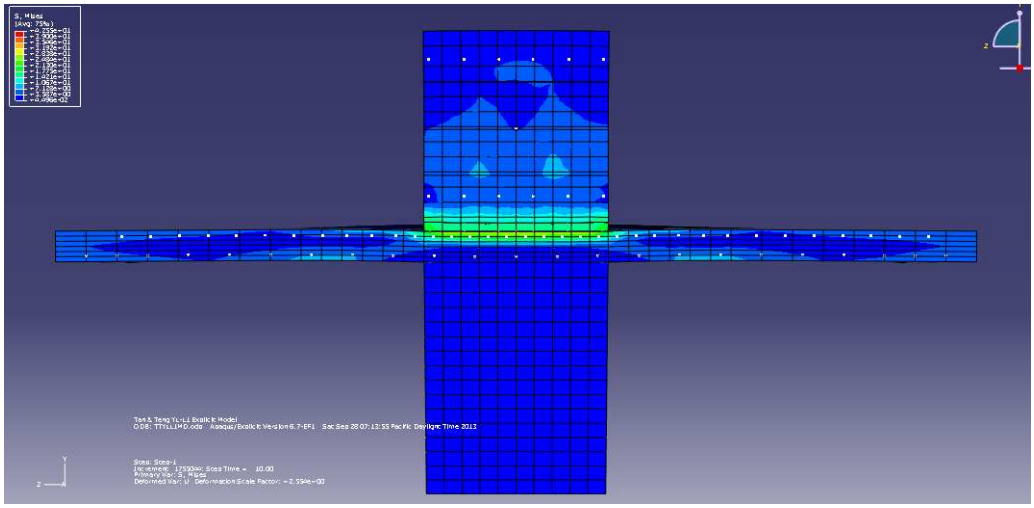

Figure 4.55 Mises stress distributions through slab-column connection of half slab YL-L1

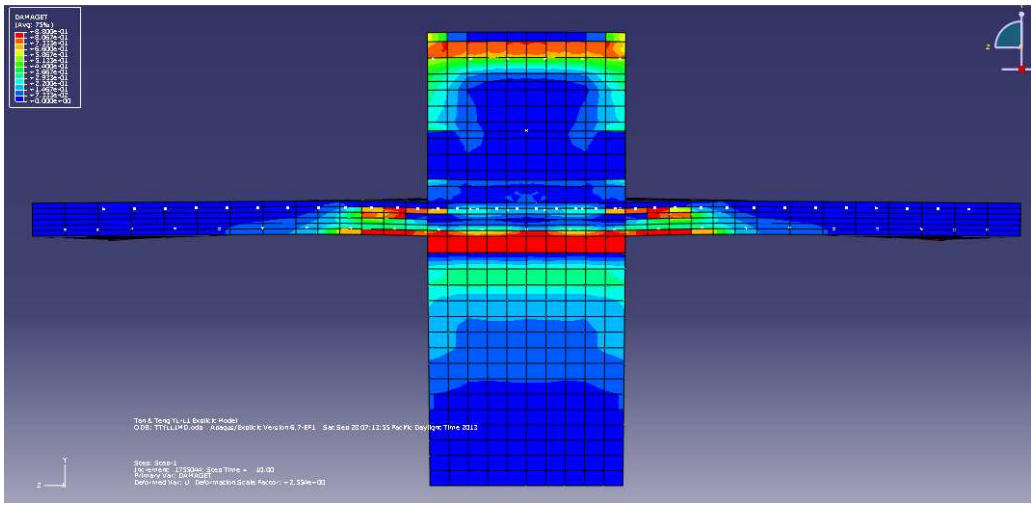

Figure 4.56 Tension damage on slab-column connection of half slab YL-L1

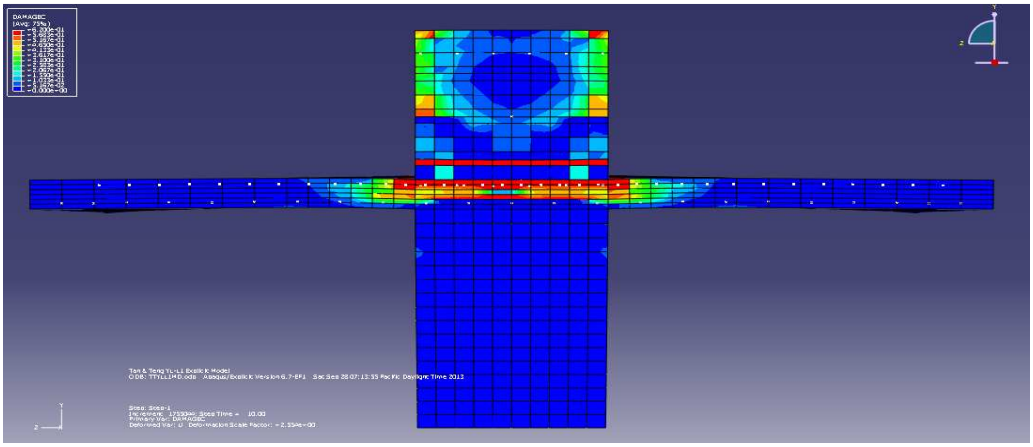

Figure 4.57 Compression damage on slab-column connection of half slab YL-L1

From the above all these figures it could be noted that, in case of flat plate slab-column connection behaviour is critical as it transfer combined gravity and lateral loads. So it is important to understand the slab-column connection including punching shear behaviour at critical section of flat plates. The horizontal force-drift ratio curves of this slab are presented in Fig. 4.58 and there are also some difference in the horizontal force-drift ratio behaviour between present FE analysis (FE) and experimental result (EXPT). It is observed that for plate YL-L1 the maximum horizontal force obtained numerically (24.4 kip) is higher than the experimental maximum horizontal force (14.6 kip) as it represents 67.1% higher than experimental force and at this maximum horizontal force the numerical drift ratio(%) is 4.83% representing around 21.7% higher than experimental one.

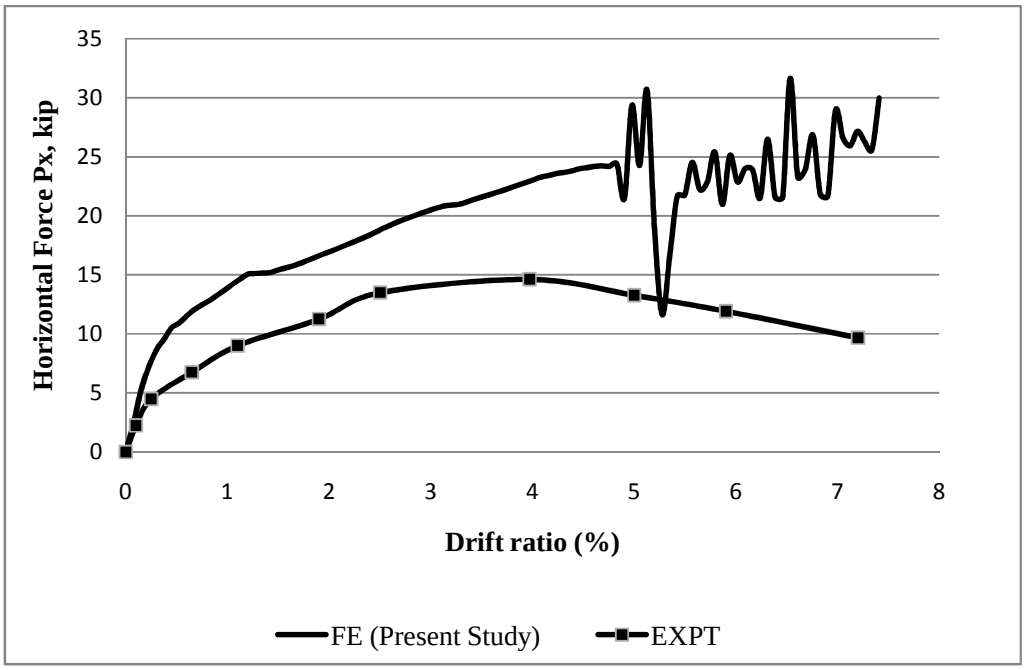

Figure 4.58 Comparative horizontal force (P_x)-drift ratio curves for YL-L1

4.4 Remark

All slabs specified above are modeled numerically by using Abaqus-Explicit approach. During these analyses, it is observed that with the increase of vertical loads, slab tends to punch around the column perimeter and it forms a truncated pyramid shape. At this stage, concrete tensile damage has increased significantly on convex side of deflected slab. A coalescence of inclined crack has clearly observed in the triaxial condition of the modeling. In these analysis, it is also observed that the stress variation, concrete damage through slab-column connection due to both gravity and lateral loads. However, lateral load also enhance the punching shear failure.

The general behaviour of the finite element model like cracking pattern and tensile or compressive damage of concrete due to applied load, development of stresses and the load-deflection graph at centre of plate are represented a good agreement with

the test data. In a quantitative sense, there are some differences in the load-deflection behaviour between the used FE models and experimental results or other numerical results. Finite element results show slightly higher stiffness than the experimental results. This may be due to non-availability of some data used in the FE modeling. However, the effects of bond slip (between concrete and reinforcement), dowel action, micro cracks developed through the slab and aggregate interlock were absent in the finite element modeling. The correlation of experimental and numerical data also depends on the assignment of accurate and appropriate linear and nonlinear material properties.

Finally, from all these discussion it would seem that these numerical models can be used with confidence in this research work regarding behaviour of slab-column connection of RC flat plate.

Chapter 5

INFLUENCE OF MATERIAL AND GEOMETRIC PARAMETERS ON PUNCHING SHEAR STRENGTH

5.1 General

In Chapter 4 the developed model was verified against test results to ensure that the model is tracing the actual response closely to ensure the acceptability of the obtained results. This chapter is dedicated to a thorough parametric study to identify the effects of material and geometric parameters on the punching shear capacity of flat plates. The general idea of parametric study for a number of independent parameters embodies the fact that at a single instance only one variable should be allowed to vary while all other parameters are fixed at some initial value. If two or more parameters were allowed to vary at the same time it would cause confusion in the results of the parametric study and their interpretation. Another point that is worth mentioning is the range of different variables, as the parameters were varied one at a time it is expected that they remain within certain bounds. This is due to the fact that exceptionally large or small values, which are not likely to occur in real-life problems, would cause wastage of computational effort. Hence investigation at hand specifies a fixed range for all the variables within which the actual work of parametric study is carried out. Investigation conducted in this chapter leads to a recommendation on the choice of structure parameters and also suggests a modification on punching shear equation according to ACI 318 (2008) code provision to enhance the punching shear strength.

5.2 Material Parameters

Reinforced concrete plate, speaking in a very common sense, is a mass of hardened concrete with steel reinforcement embedded within it. Material details of concrete like cement, aggregate, water-cement ratio etc would not be included in FE analysis like experimental research. Material parameters mainly concrete cylinder strength, flexural reinforcement ratio, yield strength of steel and effect of compression

reinforcement are considered. For this parametric study a basic slab of Elstner and Hognestad (1956) has considered as discussed in Fig. 4.4 of Chapter 4 to model for numerical analysis. The referred slab is 70 inches square, supported along the edges, and loaded with a central load uniformly distributed over an area of 10in × 10in and applied through a column stub. The thickness of the slabs is 6 inches. The orthogonal longitudinal reinforcement is provided in the tension and compression zone. The distance from the centroid of the tension reinforcement to the compression face of slab has taken 5 inches as effective depth though it varied slightly for the test slabs.

5.2.1 Concrete strength

Concrete strengths varying from 2000 psi to 5000 psi with increment of 500 psi were analyzed without reinforcement and with tension reinforcement percentages of 0.5, 1, 1.25, 1.5, 1.75, 2 and 2.5. Figure 5.1 shows the load-deflection response with varying concrete compressive strength for reinforcement ratio of 1.5% as discussed above. From figure it shows that the slope of load-deflection curve gradually increases with increase in concrete compressive strength. Variation of the ultimate loads for these slabs with variation in concrete compressive strength is graphically shown in Fig. 5.2. Ultimate loads on 2000 psi, 3000 psi, 4000 psi and 5000 psi of concrete strength for different reinforcement ratio as discussed above and for ACI code equation are given in Table 5.1. The variation of ultimate loads with concrete compressive strength f'_c and $\sqrt{f'_c}$ can be measured by calculating the ratio of ultimate loads from 2000 psi to 3000 psi, 3000 psi to 4000 psi and 4000 psi to 5000 psi of concrete strength for different reinforcement ratio. Table 5.2 describes the values for different ratio of ultimate loads with the increase of concrete compressive strength under different reinforcement ratio. From Table 5.2, it is evident that shear capacity is proportional to $\sqrt{f'_c}$ rather than f'_c. The increasing rate of ultimate loads is different for different reinforcement ratio. The rate of increase of ultimate loads are 22.2%, 15.3%, 18.2%, 23.2%, 24.4%, 24.3%, 25.1% and 25.3% for reinforcement ratio 0%, 0.5%, 1%, 1.25%, 1.5%, 1.75%, 2% and 2.5% respectively under concrete compressive strength from 2000 psi to 3000 psi. Similarly, the rate

of increase of ultimate loads are 15.7%, 14.7%, 13%, 14%, 17.2%, 19%, 17.5% and 18.7% for reinforcement ratio 0%, 0.5%, 1%, 1.25%, 1.5%, 1.75%, 2% and 2.5% respectively under concrete compressive strength from 3000 psi to 4000 psi and 11.9%, 10.4%, 8.22%, 8.5%, 9.6%, 12.6%, 14.9% and 13.4% for reinforcement ratio 0%, 0.5%, 1%, 1.25%, 1.5%, 1.75%, 2% and 2.5% respectively under concrete compressive strength from 4000 psi to 5000 psi. It is seen that increase in ultimate load is more prominent with lower strength concrete compared to higher strength concrete. The load-carrying capacity of the plates increased with the addition of steel reinforcement, changing significantly as the reinforcement ratio increased from 0.5 to 2.5 percent. From plain concrete to 1 percent reinforcement load-carrying capacity has increased rapidly whereas from 1.25 to 2.5 percent that has increased gradually. Hence it may be concluded that concrete compressive strength have significant effect on increasing the ultimate load capacity for particular reinforcement ratio. Figure 5.2 also compares the predictions using the ACI code (ACI 318-08) expressions to investigating the influence of concrete compressive strength. It is seen that ACI code prediction without considering flexural reinforcement effect is more or less similar with ultimate load capacity having tension reinforcement ratio 0.5%. After that by increasing tension reinforcement ratio, ultimate load capacity has increased than ACI code prediction.

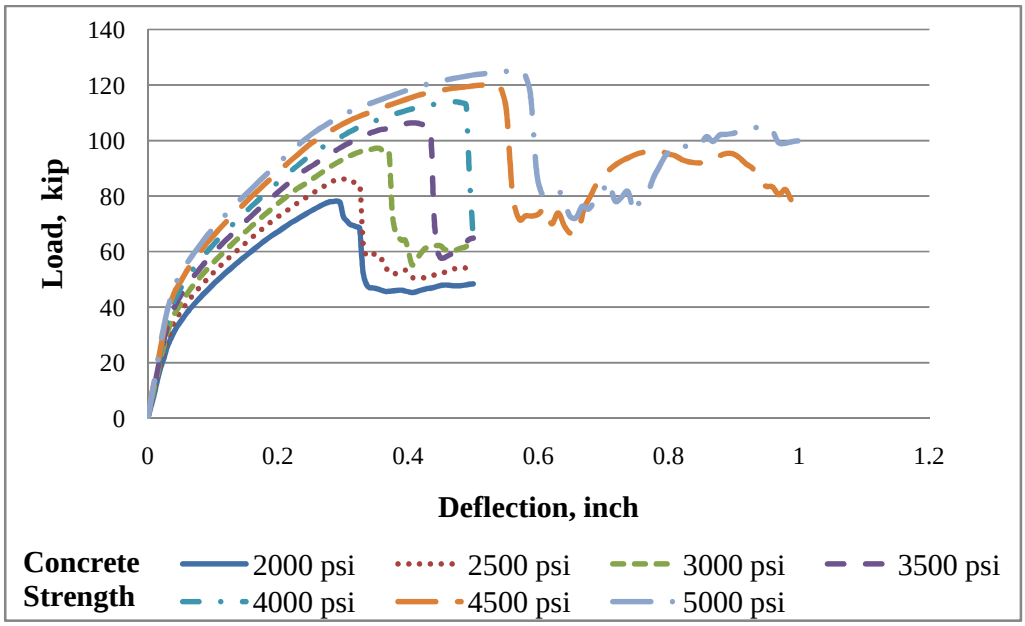

Figure 5.1 Load-deflection responses with varying concrete compressive strength for reinforcement ratio of 1.5%

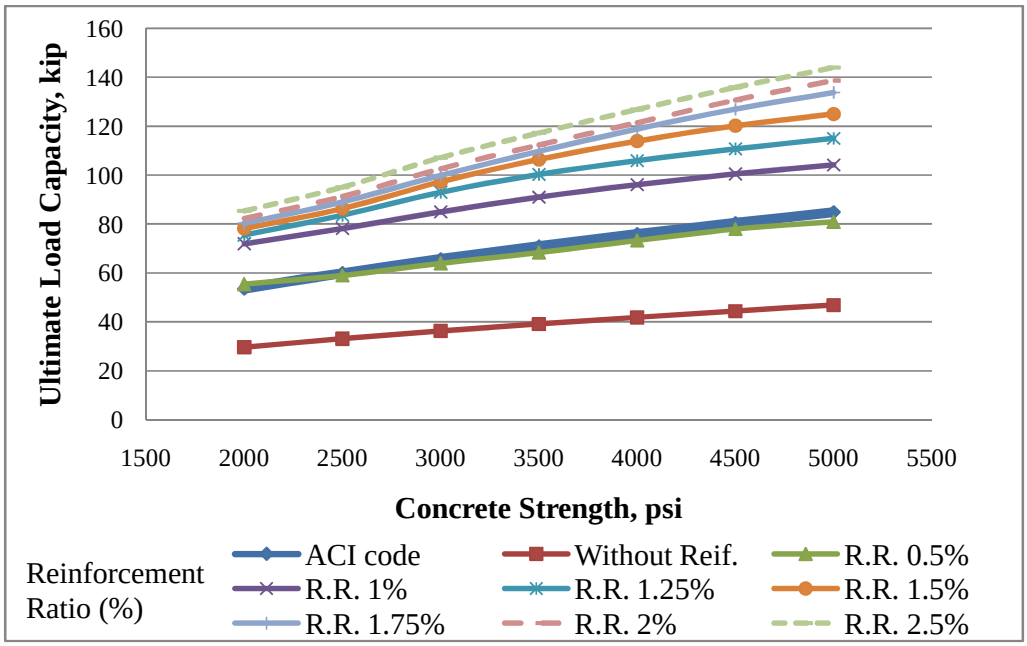

Figure 5.2 Variation of ultimate load capacity with varying compressive strength of concrete for different reinforcement ratio

Table 5.1 Ultimate loads for different reinforcement ratio and for ACI code equation

Concrete compressive strength (f'_c), psi	Ultimate load capacity, kip								
	ACI code eq^n	Finite element result							
		W.R.	R.R. 0.5 %	R.R. 1%	R.R. 1.25%	R.R. 1.5 %	R.R. 1.75 %	R.R. 2%	R.R. 2.5 %
2000	53.7	29.7	55.4	71.9	75.5	78.2	80.4	82.3	85.4
3000	65.7	36.3	63.9	85	93	97.3	100	103	107
4000	75.9	42	73.3	96.1	106	114	119	121	127
5000	84.8	47	80.9	104	115	125	134	139	144

Table 5.2 Ratio of ultimate loads

Concrete compressive strength (f'_c), psi	Ratio of ultimate loads									
	f'_c ratio	ACI code eq^n or $\sqrt{f'_c}$ ratio	Finite element result							
			W.R.	R.R. 0.5 %	R.R. 1%	R.R. 1.25%	R.R. 1.5 %	R.R. 1.75 %	R.R. 2%	R.R. 2.5 %
From 2000 to 3000	1.5	1.22	1.22	1.15	1.18	1.23	1.24	1.24	1.25	1.25
From 3000 to 4000	1.33	1.15	1.16	1.15	1.13	1.14	1.17	1.19	1.17	1.19
From 4000 to 5000	1.25	1.12	1.12	1.1	1.1	1.1	1.1	1.13	1.15	1.13

5.2.2 Flexural reinforcement ratio

This effect is already highlighted in Sec. 5.2.1 and in Figs. 5.1 to 5.2 where the variation of ultimate load with respect to change in the compressive strength and percentage of flexural reinforcement are illustrated. In plain concrete slab and slab with lower percentage of reinforcement have failed in flexure. On the other hand, slabs with higher percentage of reinforcement have failed in punching shear. However, ultimate load capacity is increased significantly by increasing percentage of flexural reinforcement. Figure 5.2 also compares the predictions using the ACI code (ACI 318-08) expressions to investigating the influence of flexural reinforcement ratio. However, ACI code has totally ignored the effect of flexural reinforcement. Figure 5.3 also shows the influence of flexural reinforcement ratio on ultimate load capacity for varying concrete compressive strength. From figure it is clear that with increasing the percentage of reinforcement, the value of the punching load is increased. The change in behaviour with the change in the reinforcement ratio was particularly noticeable for higher values of compressive strength. It can be observed that after a similar initial elastic response, the behaviour of the slabs varies tremendously depending on the percentage of reinforcement. The rate of increase of ultimate loads are 41.1%, 46%, 52.3%, 55%, 55.5%, 53.8% and 54.5% for concrete compressive strength 2000 psi, 2500 psi, 3000 psi, 3500 psi, 4000 psi, 4500 psi and 5000 psi respectively under reinforcement ratio from 0.5% to 1.5%. Similarly, the rate of increase of ultimate loads are 9.2%, 10.2%, 10%, 10.4%, 11.4%, 13.3% and 15.2% for concrete compressive strength 2000 psi, 2500 psi, 3000 psi, 3500 psi, 4000 psi, 4500 psi and 5000 psi respectively under reinforcement ratio from 1.5% to 2.5%. It is seen that increase in ultimate load is more prominent with lower percentage of reinforcement compared to higher percentage of reinforcement. Therefore it must be concluded that the amount of flexural reinforcement has a significant influence on the punching capacity of slab-column connection.

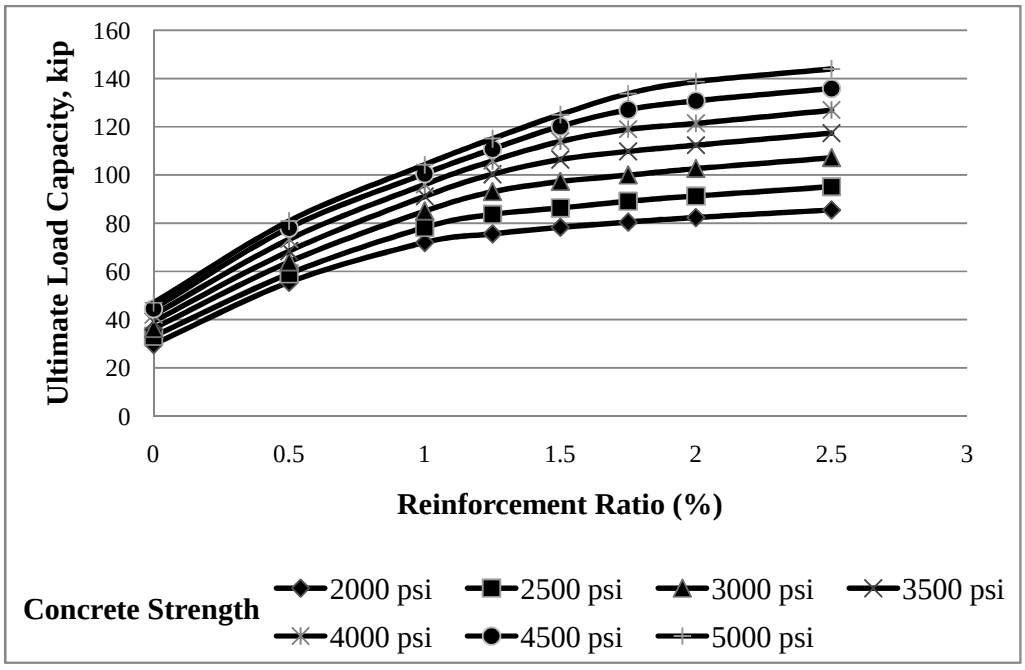

Figure 5.3 Variation of ultimate load capacity with varying reinforcement ratio for different compressive strength of concrete

5.2.3 Yield strength

To study the effect of yield strength of steel on the punching shear, same basic flat plate FE model was taken with tension reinforcement ratio 1.5% and concrete compressive strength 2000psi, 3000psi, 3500psi and 4000psi. Yield strength was varied from 40ksi to 75ksi (40, 45, 50, 60, 70, 72.5 and 75ksi). Figure 5.4 represents the variation of ultimate strength due to change in yield strength of the steel. For concrete strength of 2000psi same load carrying capacity has observed with the increase of yield strength of steel. However, for concrete strength of 3000psi, 3500psi and 4000psi ultimate strength is increased with the increase of yield strength of steel at initial stage due to yielding of steel. But for same condition, the rate of increase in ultimate load is very low for yield strength greater than 50ksi. From Fig. 5.4, one strong conclusion on the influence of the yield strength of the flexural reinforcement on the punching capacity of slab-column connection can be drawn. Only the ratio of the flexural reinforcement would affect the shear capacity and which is independent of its yield strength. Therefore, the punching load is not

influenced by the yield strength of the flexural reinforcement if the slab does not experience yielding.

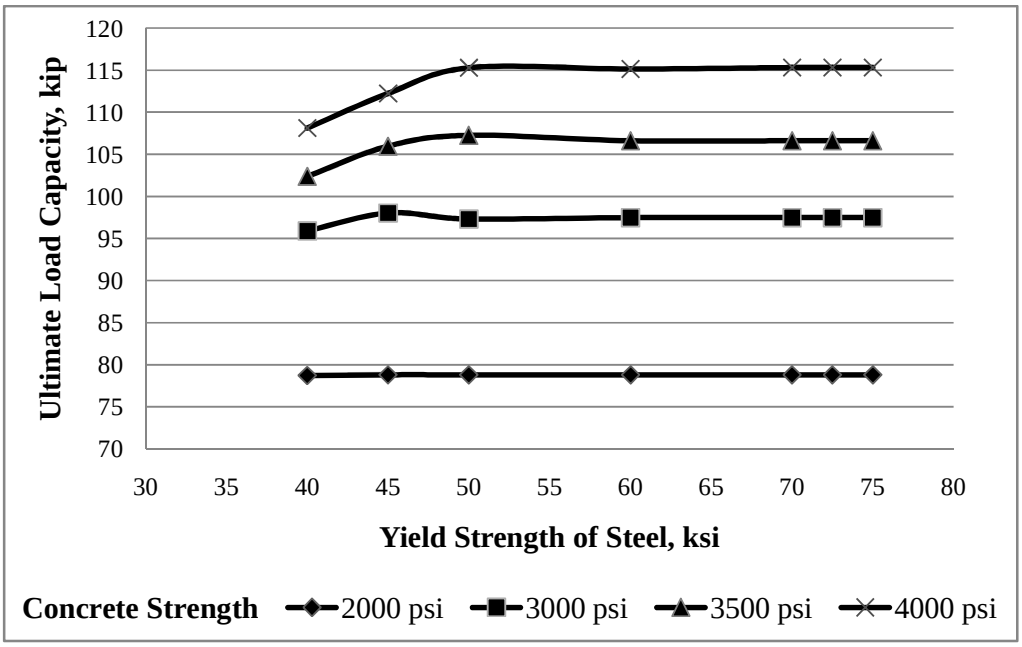

Figure 5.4 Variation of ultimate load capacity due to change in yield strength of reinforcement

5.2.4 Effect of compression reinforcement

Flexural reinforcement for both tension and compression face was considered. Parametric study was conducted observe the effect of tension and compression reinforcement on model slab A-1a, A-7b and A-7 of Elstner and Hognestad (1956). Load-deflection response of these slabs is shown in Figs. 5.5 to 5.7. From these figures, it can be seen that the influence of compression reinforcement on the ultimate load carrying capacity is not so significant. There also have no significant change in stiffness and ductility as seen from result. However, a research work has conducted by Mitchell et al. (1984) to prevent progressive collapse where flat plate slab must be capable of providing post-failure resistance in the presence of punching shear failures and severe distress around the columns. A noticeable difference was found in post-failure resistance of slab-column connections having with and without compression reinforcement. After shear failure have occurred the tension

reinforcement rips-out of the top surface of the slab and becomes ineffective in carrying the load. Therefore, slab-column connection without compression reinforcement has negligible post punching shear resistance which would result in the collapse of the slab. In contrast with compression reinforcement did not rip-out of the slab and thus provide some post-punching shear resistance. So, the role of both tension and compression reinforcement in hanging up the slab is significant. But in this research work there is a limitation to model post-failure effect having with and without compression reinforcement based on above discussed journal. To observe such failure criteria or post-punching failure phenomenon, the slab should be model considering geometric nonlinearity. Whereas in this research work the effect of geometric nonlinearity is fully absent.

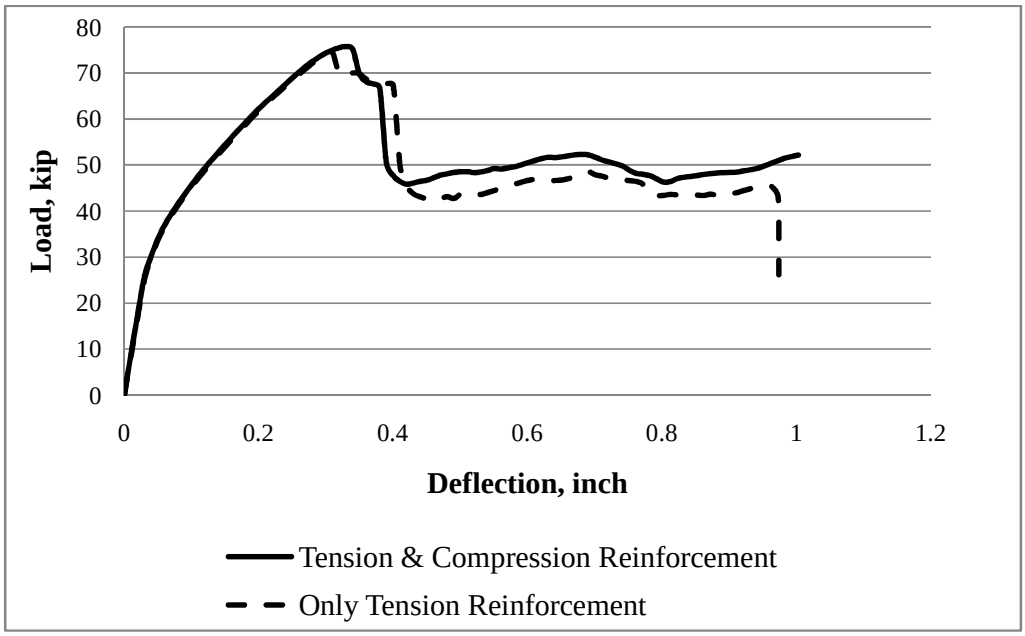

Figure 5.5 Influence of flexural reinforcement on load-deflection response for model slab A-1a

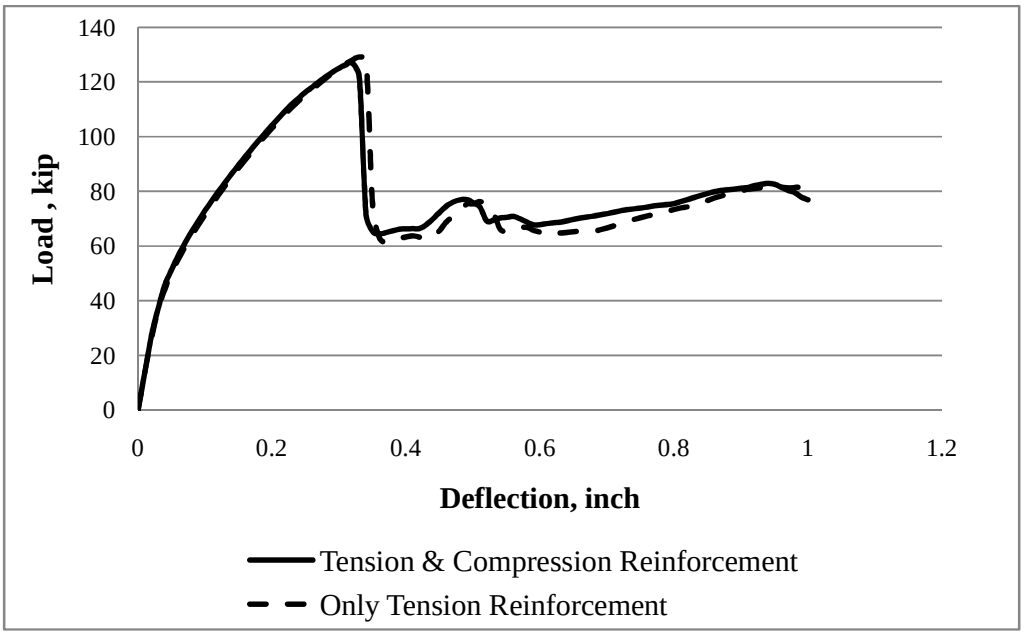

Figure 5.6 Influence of flexural reinforcement on load-deflection response for model slab A-7b

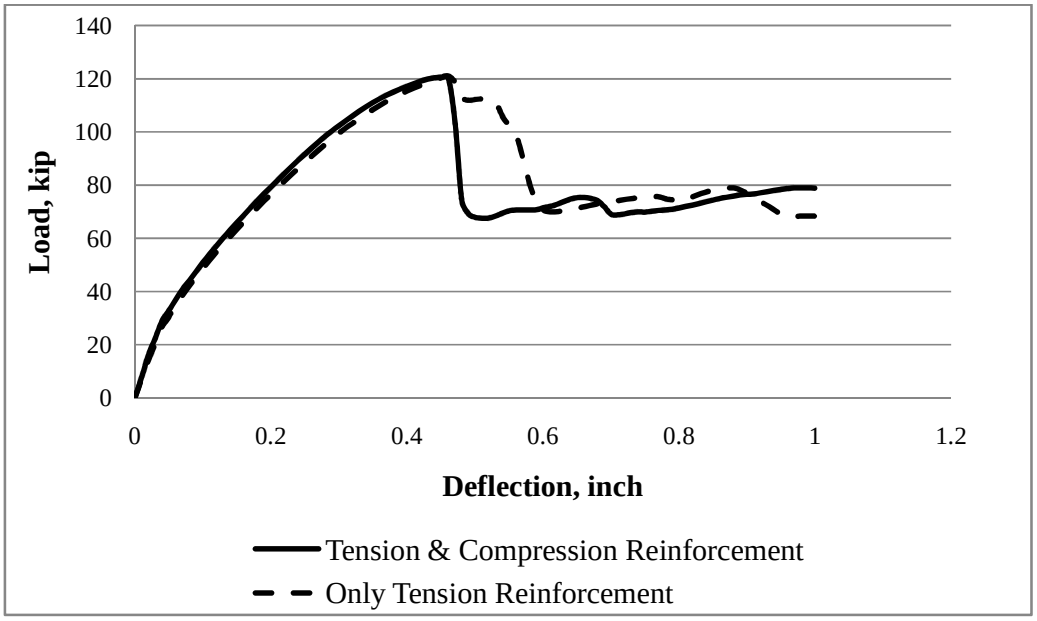

Figure 5.7 Influence of flexural reinforcement on load-deflection response for model slab A-7

5.3 Geometric Parameters

In the geometric parameters mainly the size effect like span-depth ratio, the column size that is the load or the concentrated reaction area or the support and boundary condition is considered. Same basic flat plate FE model were 70 inch square on supports in planer dimension while the plate thickness, column or loading area and boundary conditions were varied. A suitable material property was chosen for the study of geometric parameters.

5.3.1 Plate thickness (span-depth ratio)

Different span-depth ratios were achieved by varying plate thickness of the model. The thickness varied from 3 in to 12 in with span-depth ratio varies from 23.33 to 5.83. For this, the amount of flexural reinforcement has kept as a fixed value and reinforcement ratio has varied with varying plate thickness. Concrete compressive strength 3500 psi and steel yield stress 60 ksi were chosen. Figure 5.8 shows that the thicker the slabs, the higher the punching shear strength. At lower slab thickness, flexure governs the failure and behaves as a ductile slab. On the other hand at higher slab thickness, shear governs the failure and abrupt failure occurs. The increasing rate of ultimate loads is different for different plate thickness. The rate of increase of ultimate loads are 62.7%, 56.4%, 35.8%, 32.5%, 24.9%, 22.4%, 17.9%, 14.9% and 11.2% for plate thickness from 3 in to 4 in, 4 in to 5 in, 5 in to 6 in, 6 in to 7 in, 7 in to 8 in, 8 in to 9 in, 9 in to 10 in, 10 in to 11 in and 11 in to 12 in respectively. It is seen that increase in ultimate load is more prominent with lower slab thickness compared to higher slab thickness and it decrease with the increase of slab thickness. Figure 5.9 shows the variation of unit shear stress due to change in plate thickness where the straight line represents $4\sqrt{f'_c}$ value. Figure 5.10 shows the plot of ultimate load capacity vs. span-depth ratio that can be divided into two zones. First zone, a flatter slope of the curve having span-depth ratio above 14 indicates ductile zone where flexure governs the failure and next zone, a steeper slope of the curve having span-depth ratio from 14 to 5.83 indicates abrupt zone where shear governs the failure. The strength increase with small span-depth ratios may be due to the development of compression struts forming a tied-arch mechanism similar to that

observed in deep beams and the interaction of in-plane compressive forces resulting from friction at the support. Similar behaviour was reported by Lovrovich and McLean (1990). They have observed for the test series with circular slabs. The specimen strengths increased as span-depth ratios decreased from 6 to 2. There was some evidence of the formation of compression struts between the point of application of the load and the support as the specimens approached failure. Thus, a tied-arch mechanism similar to that observed in deep beams is developed. Additionally, in-plane compressive forces resulting from friction between the slab and the supports may have interacted with the arch mechanism. This interaction may have also contributed to the increased strengths observed in the specimens with small span-depth ratios. Therefore, it appears that the thickness is an important factor affecting the punching load capacity of a reinforced concrete flat plate with slightly varying response in different zones.

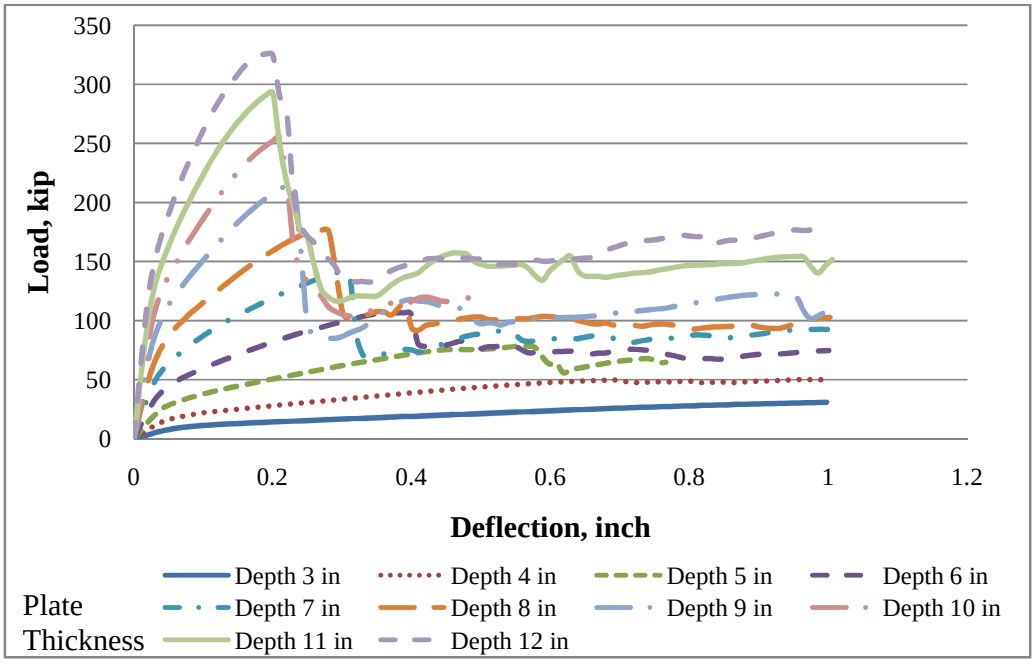

Figure 5.8 Load-deflection response with varying plate thickness

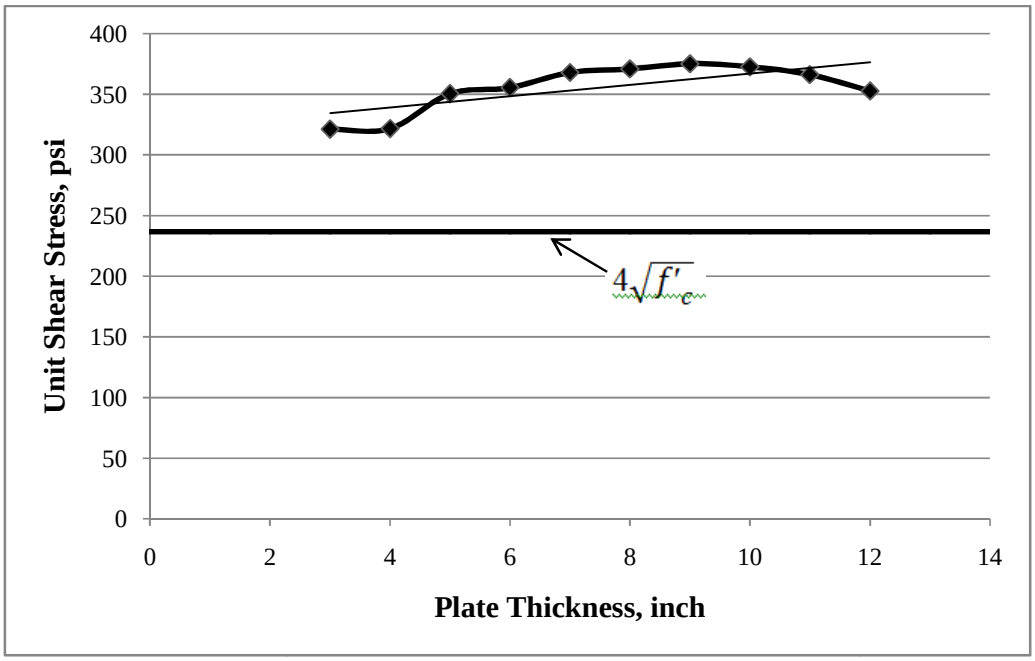

Figure 5.9 Variation of unit shear stress due to change in plate thickness

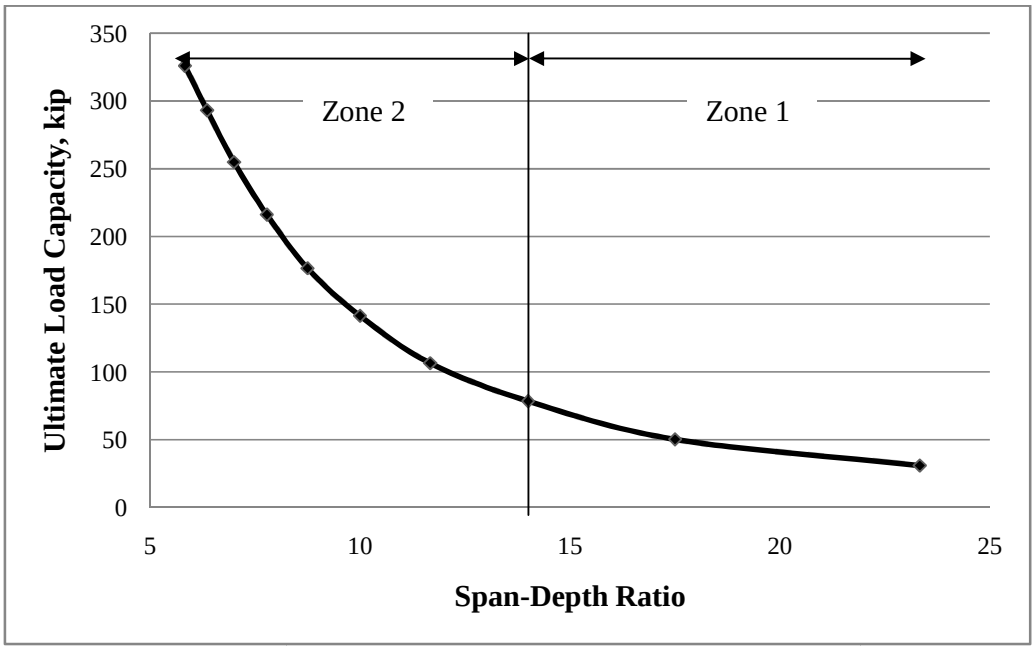

Figure 5.10 Influence of span-depth ratio on ultimate load capacity

5.3.2 Column size

To study the effect of column size on punching shear capacity 10, 12, 15, 18, 20, 25 and 30 inch square size column and 10in × 20in, 10in × 30in, 10in × 40in and 10in × 50in rectangular size column was used while all other parameters were constant. For this, reinforcement ratio 1.5%, concrete compressive strength 3500 psi, steel yield stress 60 ksi and plate thickness 6 inch were chosen.

Figures 5.11 and 5.13 represent the load-deflection curves for varying square column size and rectangular column size respectively. As would be expected, the increase in square column size and longer side for rectangular column increased the slab stiffness and there by increased the slopes of the load-deflection curves. Figure 5.12 shows the variation of ultimate load with varying square column size. Ultimate loads on 10, 12, 15, 18, 20, 25 and 30 inch of square column are 107 kip, 121 kip, 134 kip, 149 kip, 163 kip, 179 kip and 187 kip respectively. The increasing rate of ultimate loads is different for different square column. The rate of increase of ultimate loads are 13.1%, 10.7%, 11.2%, 9.4%, 9.8% and 4.5% for column size from 10 inch to 12 inch, 12 inch to 15 inch, 15 inch to 18 inch, 18 inch to 20 inch, 20 inch to 25 inch and 25 inch to 30 inch respectively. From 10 inch square column to 25 inch square column, the rate of increase of ultimate loads are decreasing uniformly, whereas from 25 inch square column to 30 inch square column, the rate of increase of ultimate load is decrease rapidly. From this investigation it is seen that increase in ultimate load is more prominent with smaller column size compared to larger column size. Again, the rate of increase of ultimate load is 52.3% for column size from 10 inch to 20 inch. So, it is also observed that by doubling the square column size, ultimate load is increased over 50%. Basically in this case the punching perimeter increase is 67%. Again Fig. 5.14 also shows the variation of ultimate load by increasing longer side of rectangular column. Ultimate loads on 10in × 20in, 10in × 30in, 10in × 40in and 10in × 50in of rectangular size column are 127 kip, 130 kip, 134 kip and 140 kip respectively. The rate of increase of ultimate loads are 18.7%, 2.4%, 3.1% and 4.5% for column size from 10in × 10in to 10in × 20in, 10in × 20in to 10in × 30in, 10in × 30in to 10in × 40in and 10in ×40in

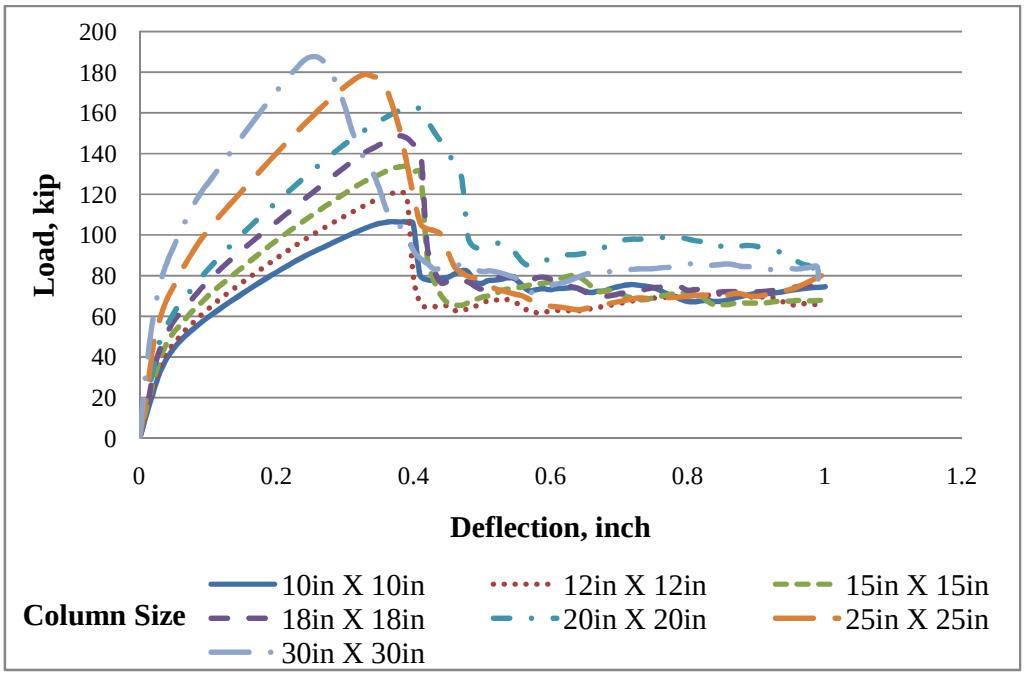

Figure 5.11 Load-deflection responses for different column size

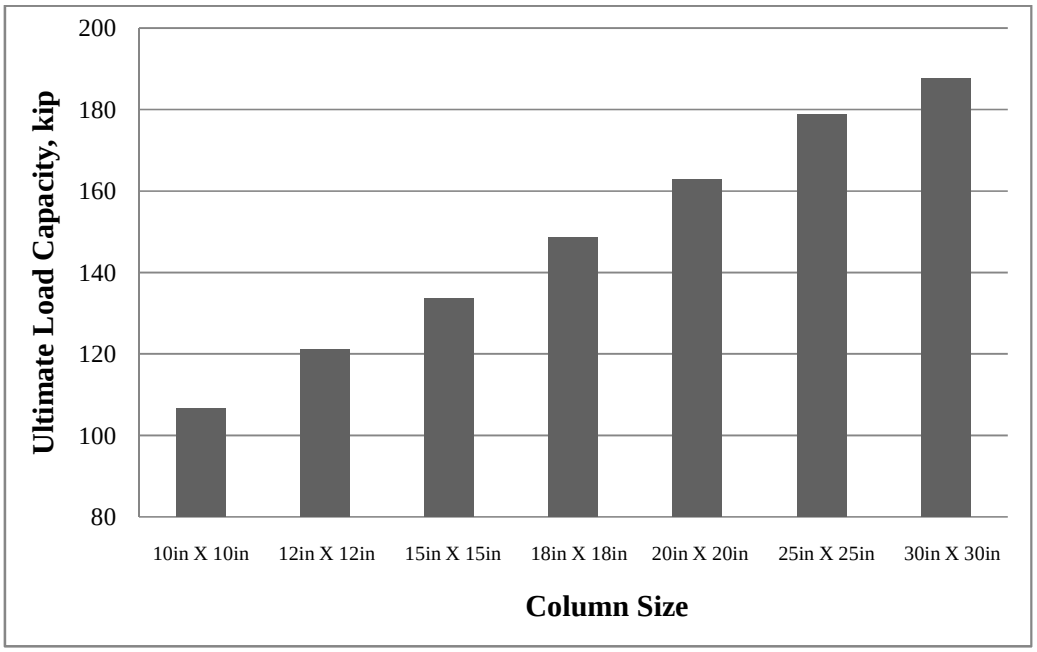

Figure 5.12 Variation of ultimate load capacity due to change in column size

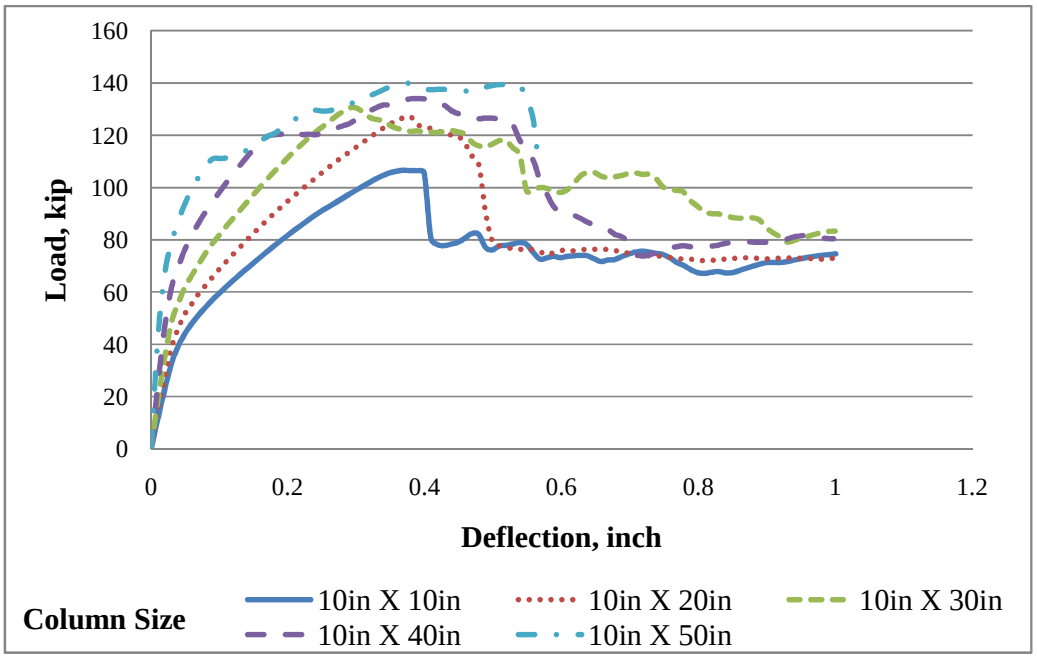

Figure 5.13 Load-deflection responses for different column size

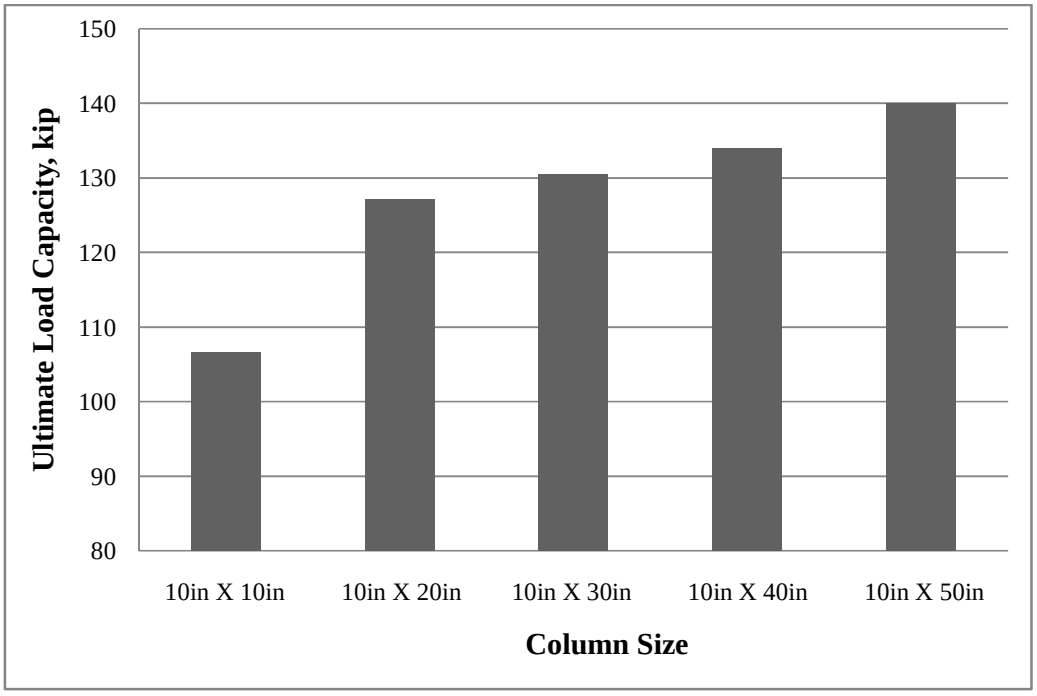

Figure 5.14 Variation of ultimate load capacity due to change in column size

to 10in × 50in respectively. From 10in × 10in column to 10in × 20in column, the rate of increase of ultimate loads is very high compare to the rate of increase of ultimate loads from 10in × 20in to 10in × 50in. The increasing rate of ultimate loads is very low by increasing longer side of rectangular column. Again, the rate of increase of ultimate loads is 21.6% for 20 inch square column size in place of 10in × 40in rectangular column size. It may be concluded that the square column with same cross sectional area of a rectangular column yield higher punching strength.

5.3.3 Support condition

To study the effect of edge condition, three slabs of model plates were square (70″ x 70″) and loaded with a central load uniformly distributed over an area of 10″ x 10″ and applied through a column stub. For this, reinforcement ratio 1.5%, concrete compressive strength 3500 psi, steel yield stress 60 ksi and plate thickness 6 inch were chosen. The orthogonal longitudinal reinforcement was provided in the tension and compression zone. Three different support conditions were applied: symmetrical support on four edges, symmetrical support on two opposite edges and symmetrical support on four corners. Corresponding load-deflection response is plotted in Fig. 5.15. From figure it must be concluded that different boundary condition has different influence on the punching capacity of slab-column connection. Therefore, boundary condition is an important part of the model slab to get realistic result.

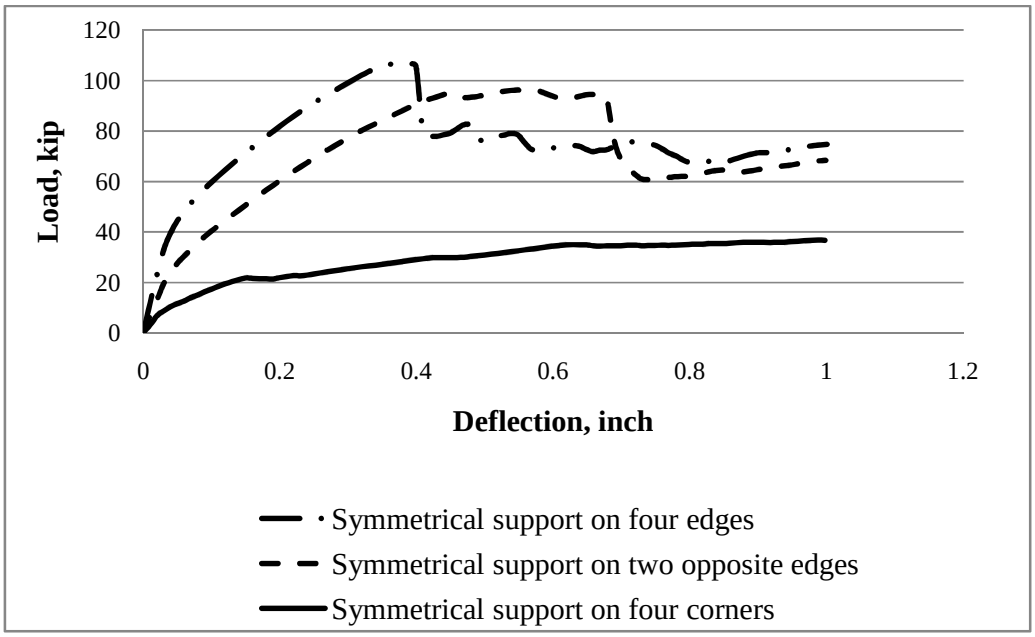

Figure 5.15 Load-deflection responses for different edge condition of the plate

5.4 Punching Shear Prediction Equation

For the design of flat plate structure, punching shear strength of concrete in the vicinity of columns is one of the design criterions which often govern the design. Thus, the critical shear section for this type of shear should be located. Different building code provisions provide the location of this critical section differently. But for all the codes, when this is done, the shear strength is taken almost independent of the edge condition, reinforcement ratio and span-depth ratio. There are scopes of modification within the method. The purpose of the parametric study is to identify these scopes of modifications and propose changes. Efforts are then made to check the performance of the suggested proposition.

In Chapter 2, various code provisions along with few individual researchers' prediction equations are presented. Among all code predictions the critical shear perimeter is taken as a rectangle located at a distance of 1.5d from the edge of column by British Code (BS 8110, 1985), but for all other codes this perimeter is taken at d/2 from the column face. It is to be noted that BNBC (2006) adopted ACI

Code with minor modification. As such all the succeeding discussions are mainly related to ACI Code.

5.5 ACI 318-08 Code Provision

Provisions in ACI 318 (2008) are based on the assumption that the punching shear failure surface will develop at an angle of 45 degree. The permissible nominal shear stresses in the concrete are empirically derived based on a critical section located at half the effective depth of the slab away from the perimeter of the load. The ACI equation for predicting punching shear mentioned in Chapter 2. As can be seen, ACI building code does not recognize the effect of restraining action at the support when treating punching shear in reinforced concrete slabs. The expression for nominal punching shear stress does not include terms considering the ratio of main steel, yield strength of steel, column size effect and the slab depth. Effects of span-depth ratio are not addressed in the current punching shear provisions. Analysis performed in parametric study reveals that reinforcement ratio and span-depth ratio has a significant influence on punching shear strength.

5.6 Comparison of Numerical Results with ACI 318-08 Code Provision

Some of the analytical results (Present FE analysis) getting from parametric study is compared with predicted nominal punching shear values according to ACI 318-08 code for slabs. Figures 5.16 to 5.21 are described the ratio of FE shear to nominal shear according to ACI 318-08 code.

It is observed from the figures that most of the cases ACI 318-08 code prediction are conservative, giving an underestimate results. In Figs. 5.16 and 5.17 represent ACI predicted values about 20 to 70 percent lower than the FE results considering reinforcement ratio from 1% to 2.5% respectively. This is because, it can be seen from Fig. 5.6 that for a particular compressive strength with all other parameters left constant ultimate strength increases with increase in reinforcement ratio. But this effect cannot be accommodated in the ACI 318-08 code provision. However, one exception is found in Figs. 5.16 and 5.17 whereas slab sections without

reinforcement and 0.5% reinforcement, ACI 318-08 code represents an overestimate results with FE shear values. This is because of ACI 318-08 code were not intended for preventing connection failure dominated by flexure. This equation should not be used to estimate gravity load-carrying capacity of slab-column connection with relatively low tensile reinforcement ratio.

It is also observed that for a particular reinforcement ratio the increase in ratio of FE shear to nominal shear with increase in compressive strength is very low. This is because; the progressive rate of increase in shear strength is more or less same in case of FE shear and nominal shear strength.

Figure 5.18 also represents some conservative results considering ACI 318-08 code having different yield strength with all other parameters constant. Here, all results are containing more or less same ratio which represent that there have no significant change of ultimate strength due to change of yield strength of steel. However, ACI predicted values are about 50 percent lower than the FE results and particularly this difference is due to underestimate of reinforcement ratio by ACI 318-08 code provision.

In Fig. 5.19 considering tensile reinforcement index ρf_y which is the product of reinforcement ratio and steel yield strength also represents more or less same behaviour as discussed in Fig. 5.17 for variation of the ratio between FE shear to nominal shear according to ACI 318-08 code provision with varying reinforcement ratio for different compressive strength of concrete. Though for a particular compressive strength the increase in ratio of FE shear to nominal shear with increase in yield strength of steel is very low and for same condition the increase in same ratio with increase in reinforcement ratio is significant. That is why; the progressive rate of increase in FE shear to nominal shear ratio is more or less same with Fig. 5.17.

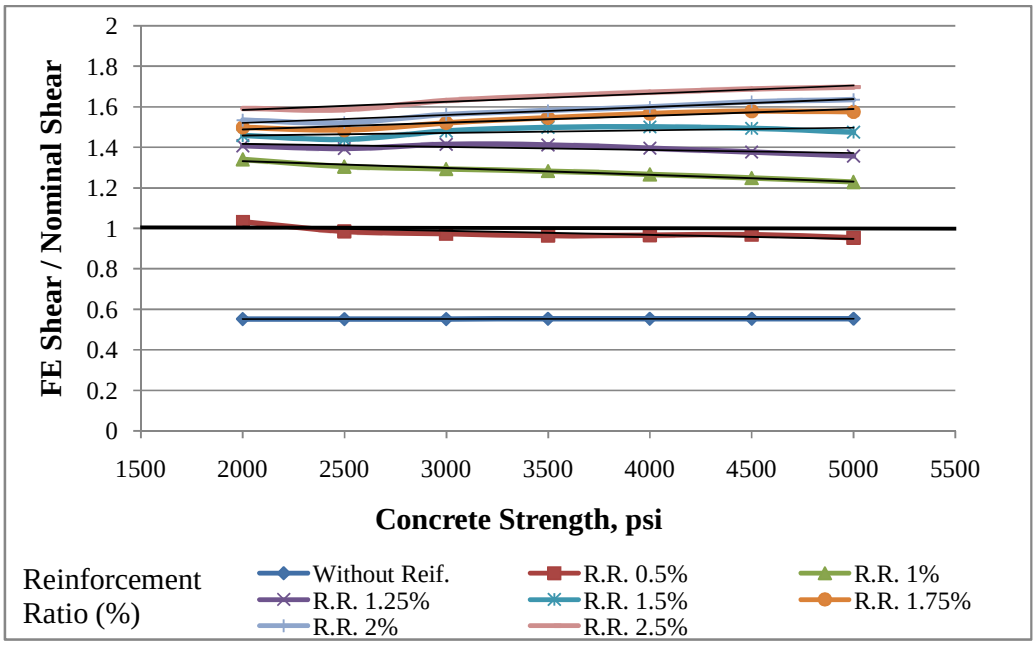

Figure 5.16 Variation of the ratio between FE shear to nominal shear according to ACI 318-08 code provision with varying compressive strength of concrete for different reinforcement ratio

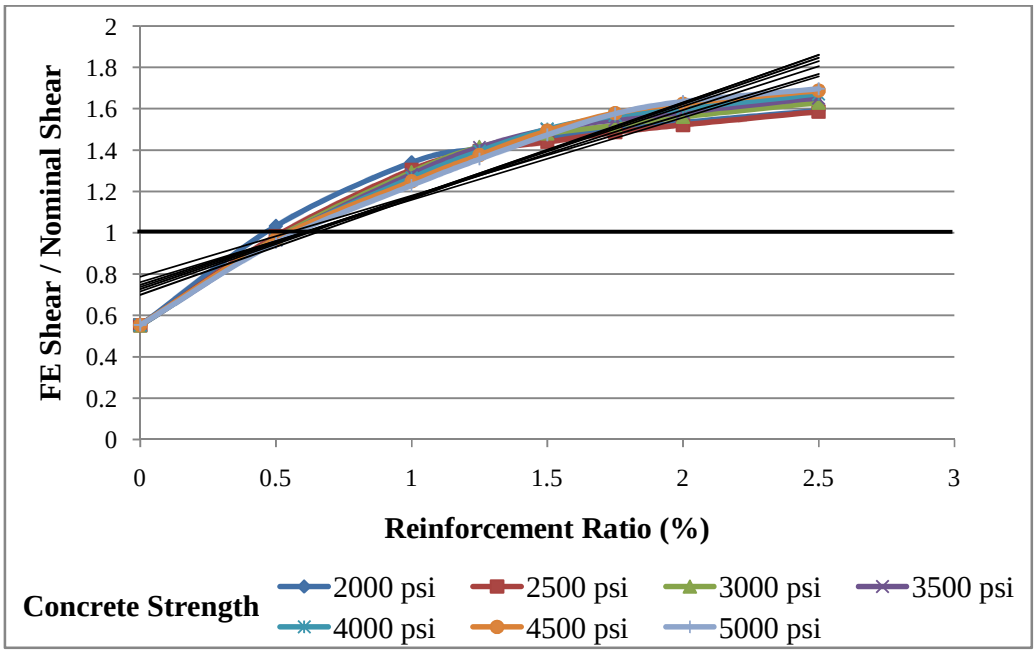

Figure 5.17 Variation of the ratio between FE shear to nominal shear according to ACI 318-08 code provision with varying reinforcement ratio for different compressive strength of concrete

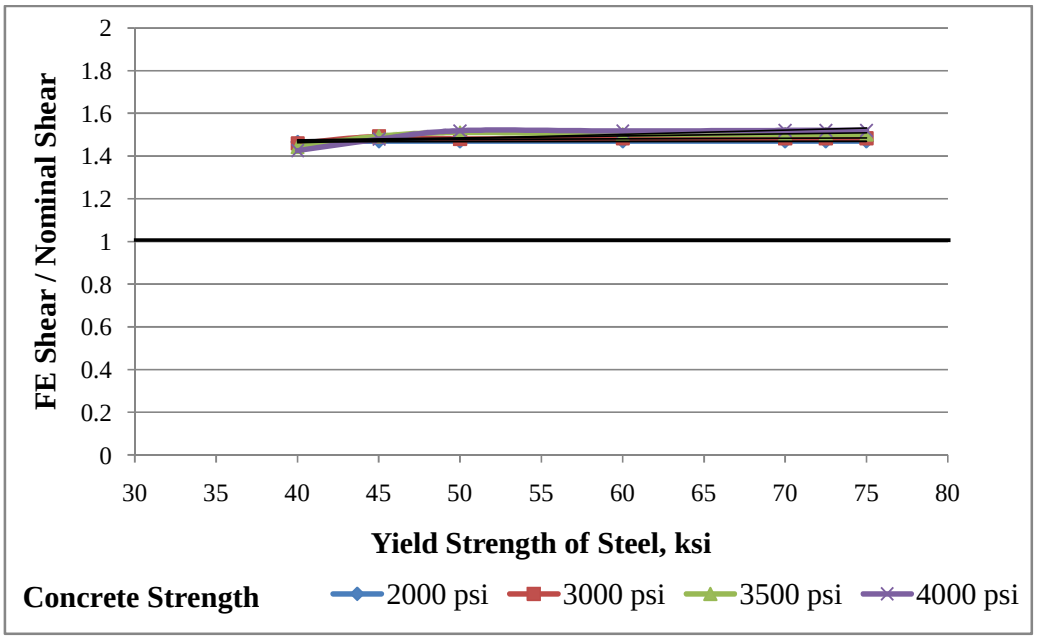

Figure 5.18 Variation of the ratio between FE shear to nominal shear according to ACI 318-08 code provision with varying yield strength of reinforcement for different compressive strength of concrete

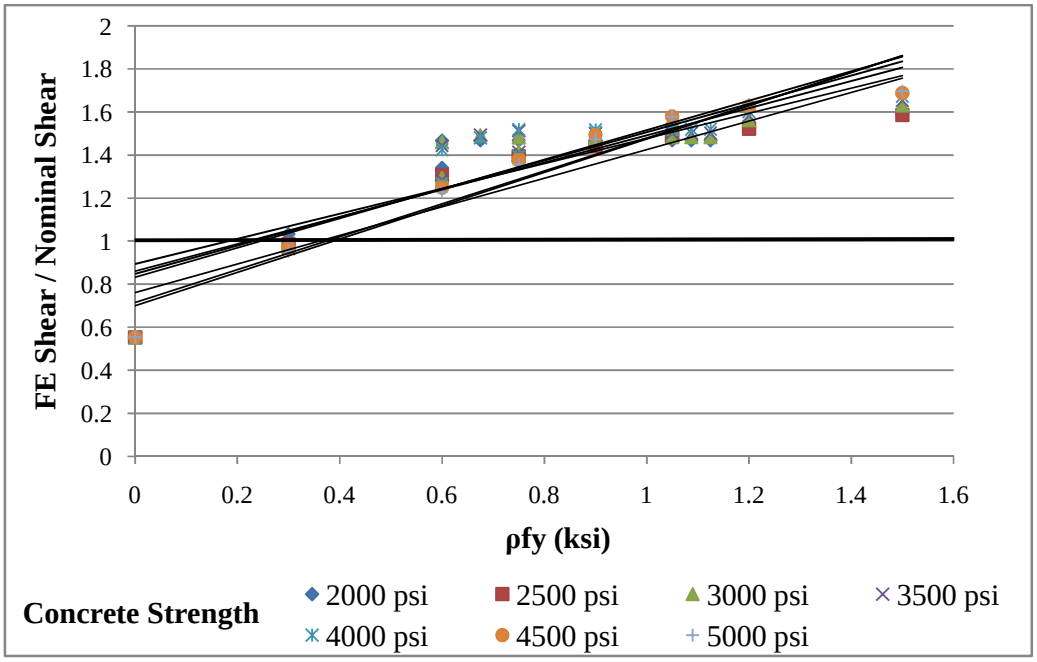

Figure 5.19 Variation of the ratio between FE shear to nominal shear according to ACI 318-08 code provision with varying reinforcement index for different compressive strength of concrete

In Fig. 5.20 represents ACI predicted values about 35 to 60 percent lower than the FE results considering plate thickness from 3 inch to 9 inch respectively. That is conservative results by ACI 318-08 code provision. With the increase of slab thickness than 9 inch plate thickness, the ratio between FE shear and nominal shear has decreased. Therefore, this effect should be accommodated in the ACI 318-08 code provision.

In Fig. 5.21, whereas column size is varying represents conservative results by ACI 318-08 code provision and also represents same behaviour as discussed above for slab thickness. With increasing column size, ACI 318-08 code provision will represent unconservative results. So, to calculate the punching capacity by using ACI 318-08 code provision having large column size is no longer valid. This is because of absence of column size effect in ACI 318-08 code provision.

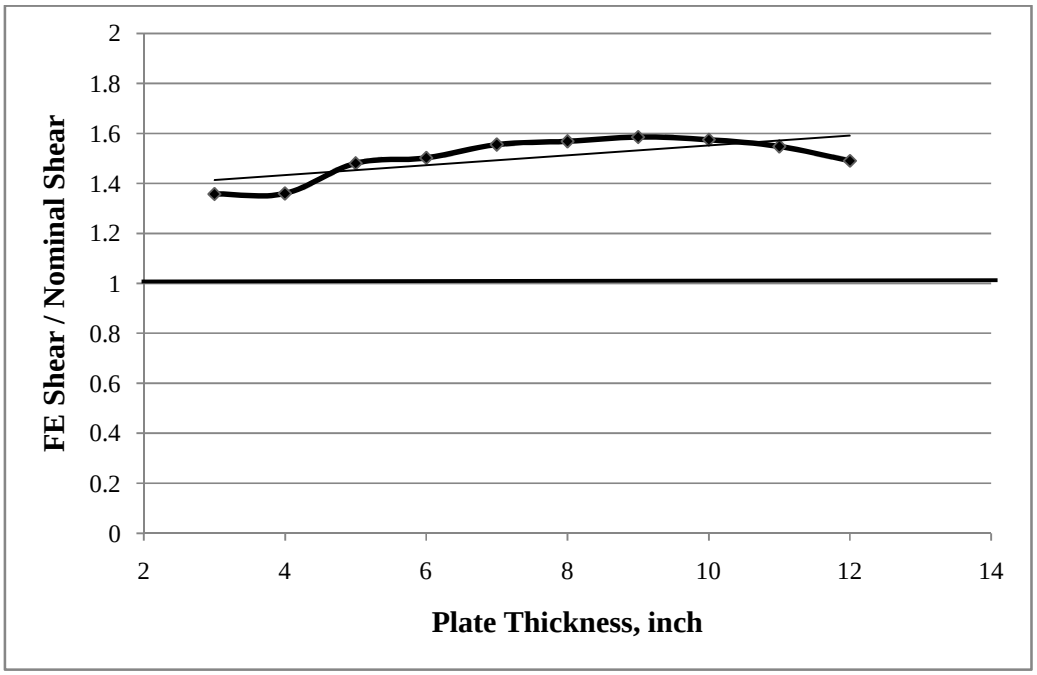

Figure 5.20 Variation of the ratio between FE shear to nominal shear according to ACI 318-08 code provision with varying plate thickness

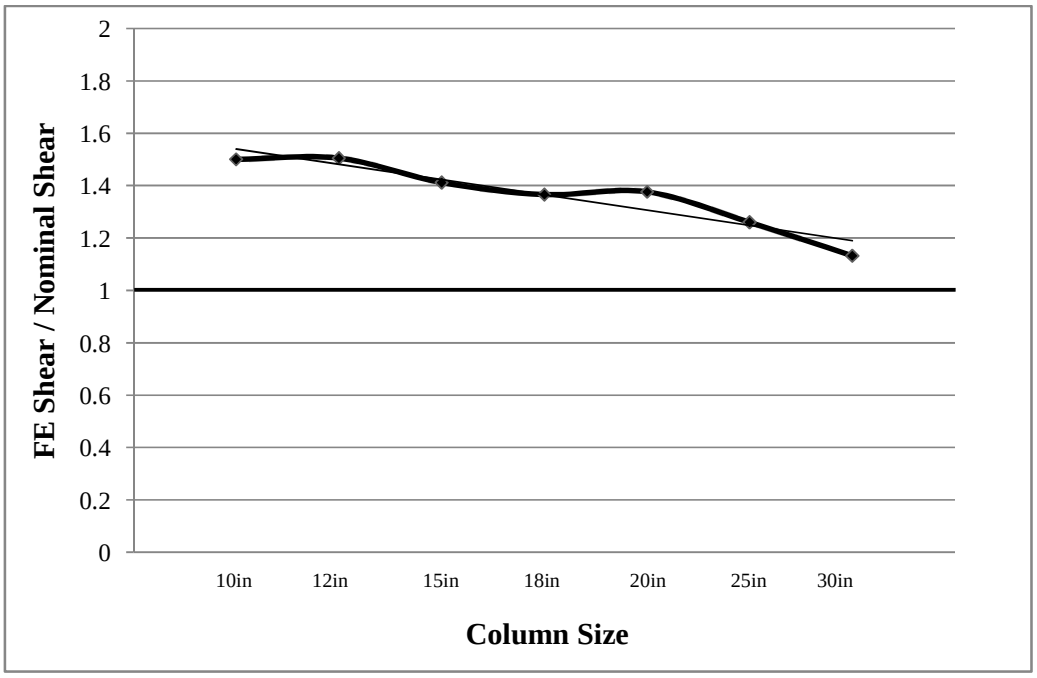

Figure 5.21 Variation of the ratio between FE shear to nominal shear according to ACI 318-08 code provision with varying column size

From 98 parametric study (Present FE analysis) results, the FE shear strength is plotted in Fig. 5.22 against the nominal strength estimated based on ACI 318-08 code provision. It is observed that most of the cases ACI 318-08 code prediction are conservative, giving an underestimate results. Only some models having no reinforcement and a low tensile reinforcement index ρf_y equal to or less than 0.3 ksi represents overestimate results of shear capacity by ACI 318-08 code provision. From Fig. 5.22 it is also evident that nominal shear strength values according to ACI 318-08 code are scattered to FE shear strength values.

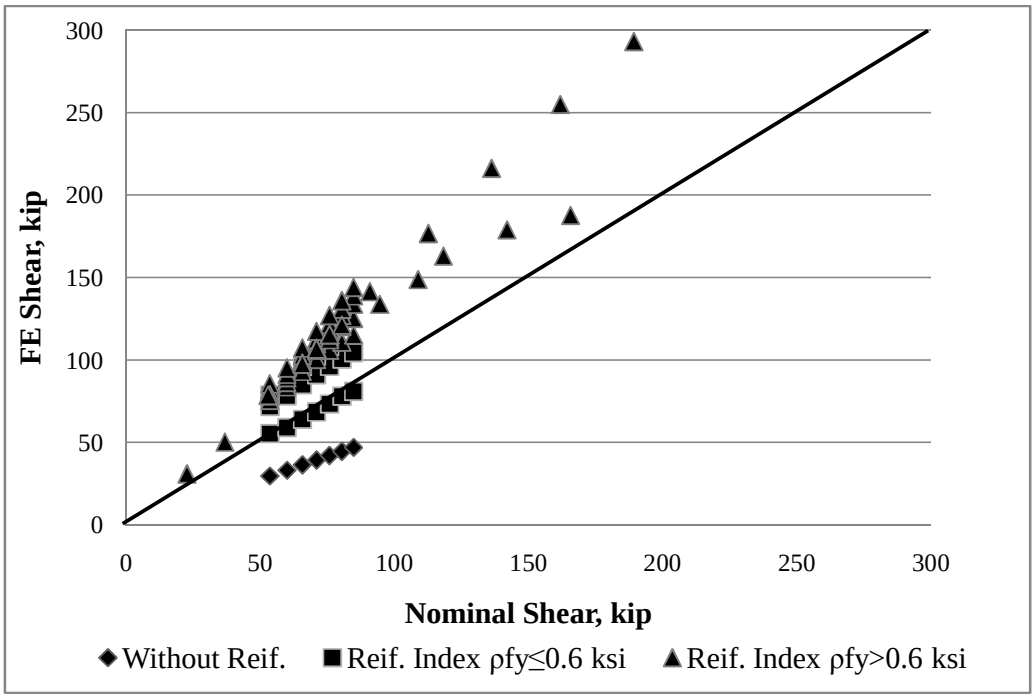

Figure 5.22 Comparisons of FE shear strength and nominal shear strength according to ACI 318-08 code provision

5.7 Scope of Modification

From the above discussion, it is evident that to eliminate the problem of underestimation or overestimation of punching strength by ACI 318 (2008) Code, a modification is required to attain a level of accuracy that can reasonably be compared with finite element solution. This study, therefore, identifies that the code provisions may be reviewed taking into consideration the influence of the following:

- Influence of reinforcement ratio (flexural).
- Influence of yield strength of steel (flexural).
- Effects of span-depth ratio on punching shear strength
- Influence of column size
- Influence of edge restraint.

5.8 Tian Equation to Modify the ACI 318-08 Code Equation

A research work has already been conducted by Tian et al. (2008). Considerable experimental research has been carried out on slab-column connections of reinforced concrete flat plate structures subjected to concentrated gravity load. The research reported herein focuses on strength evaluation of interior connections with square columns. Relevant tests satisfying the following conditions were collected to form the basis of the study :1) connections were constructed with normal weight concrete; 2) slab flexural reinforcement strength as measure by ρf_y was less than 8 MPa (1200psi); 3) no shear reinforcement was used; and 4) slab thickness was at least 75mm (3 in). According to analyses of available test data, the effects of several variables on connection behaviour were individually studied and a modified equation using function of concrete strength, slab reinforcement ratio, steel yield strength and the ratio of column size to slab effective depth were formulated for calculating connection shear strength.

An empirical solution was developed using an approach similar to that adopted by Zsutty (1968) and Zsutty (1971) for predicting beam shear strength. The effects of slab size and boundary condition on shear strength were not considered due to lack of test data for connections supported on square columns. The connection shear strength was assumed to take the following general form

$$V_n = q \,.\, (f_{ct})^{\alpha} \,.\, (\rho f_y)^{\beta} \,.\, A_c \,.\, y(c/d) \tag{5.1}$$

Where f_{ct} is the concrete tensile strength; $A_c = 4d(c + 2s)$ is the area of a critical section located at a distance s from the column faces; and y is the dimensionless function of c/d. Assuming f_{ct} is related to $\sqrt{f'_c}$ and the equation was rewritten as

$$V_n = k \,.\, (f'_c)^{\alpha/2} \,.\, (\rho f_y)^{\beta} \,.\, A_c \,.\, y(c/d) \tag{5.2}$$

The parameters k, α, β, s and the expression of y were determined from analyses of the test results. Test data of specimens with top bars evenly distributed in two

orthogonal directions of the slab were used to generate equation for punching shear strength.

The effect of a single variable on connection shear capacity was examined by eliminating the influence of others. For example, when investigating the influence of concrete strength, the specimens with similar flexural reinforcement ratio and strength, column size and slab effective depth but with different concrete strength formed a data group. The average ratio of measured shear strength to calculated shear strength for each group was calculated. Then for each specimen, the deviation of the prediction from the average of the corresponding group was defined. Finally, the average deviation for all tests used in the analysis was calculated. The average deviation was minimized by adjusting the value of α and β and repeating all steps. It was found that the contribution of concrete strength and slab flexural reinforcement is best described by assuming the punching strength to be proportional to $(f'_c)^{0.25}$ and $(\rho f_y)^{0.5}$ (α = β = 1/2). Similar procedure applied to 10 groups of test data (49 specimens) to determine an appropriate critical section location. It was found that, if $s \leq 2d$, the deviation was insensitive to s. Therefore, $s = 0.5d$, the same value as used in ACI 318-08, was adopted. Based on a regression analysis, the effect of c/d on the connection strength expressed. Based on data analyses described previously, the shear capacity of a slab-column connection was derived as

$$V_n = 0.65\xi A_c(\rho f_y\sqrt{f'_c})^{\frac{1}{2}} \quad \text{(in SI units)} \tag{5.3}$$

$$V_n = 2.3\xi A_c(\rho f_y\sqrt{f'_c})^{\frac{1}{2}} \quad \text{(in customary units)} \tag{5.4}$$

Where,

$$A_c = 4d(c+d)$$

$$\xi = \sqrt{\frac{d}{c}}$$

It should be noted that the comparison of shear capacity estimated by using modified equation with the measured strength from experiment were very close. It was also suggested that 95% of the test results were expected to exceed the strength defined by modified equation by considering a reduction factor 0.83 to the right-hand side of these equations to derive a characteristic strength.

In this study, same modified equation suggested by Tian et al. (2008) has considered and compares the ultimate loads obtained from present FE analysis with the modified equation to confirm the acceptability of the modified equation.

5.9 Comparison of Numerical Results with Tian Equation

Again the analytical results (Present FE analysis) are compared with predicted nominal punching shear values according to Tian equation for slabs. Figures 5.23 to 5.28 are described the ratio of FE shear to nominal shear according to Tian equation.

It is observed from the figures that most of the cases, nominal shear results according to Tian equation are very close to FE results (Present study). In Figs. 5.23 and 5.24 represent a small amount of overestimate results for lower concrete strength having higher reinforcement ratio and slightly underestimate results for higher concrete strength having lower reinforcement ratio. Similarly in Fig. 5.25 also represents a small amount of overestimate results for lower concrete strength having higher yield strength of steel and slightly underestimate results for higher concrete strength having lower steel yield strength. Now after a meticulous investigation from Figs. 5.23 to 5.26 it is evident that a slab section having 3500 psi concrete strength with tensile reinforcement ratio 1.5% and 60 ksi yield strength represents an exact result on punching shear capacity by using Tian equation. However, a reduction factor can be used to get more or less exact capacity in case of overestimate results. In Fig. 5.27 represents overestimate result for very small slab thickness and close results for slab thickness from 5 inch to 11 inch. In Fig. 5.28 also represents some underestimate results for nominal shear based on Tian equation.

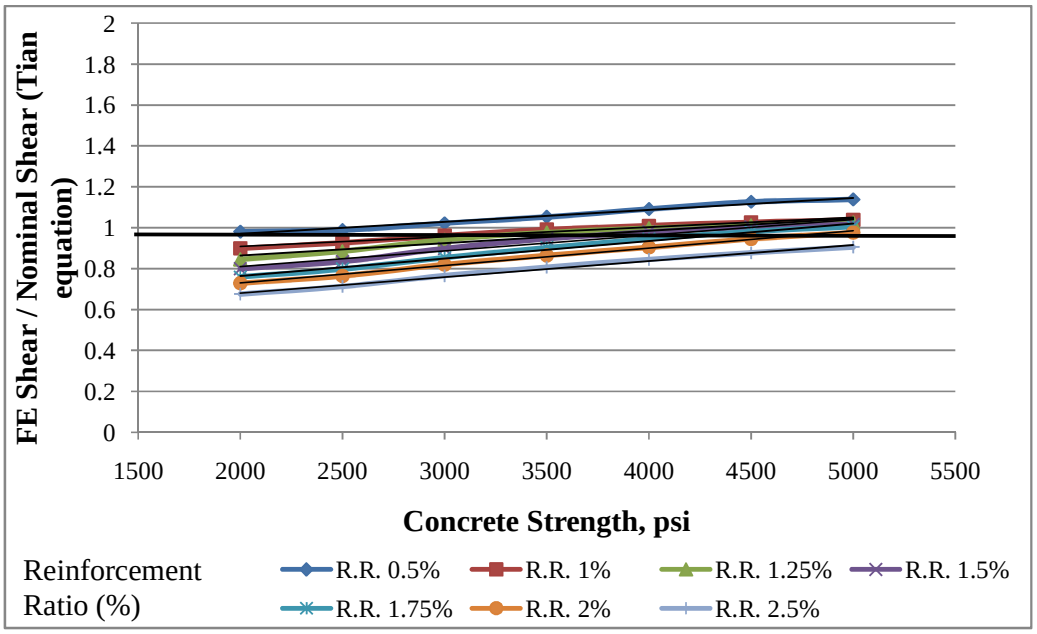

Figure 5.23 Variation of the ratio between FE shear to nominal shear according to Tian equation with varying compressive strength of concrete for different reinforcement ratio

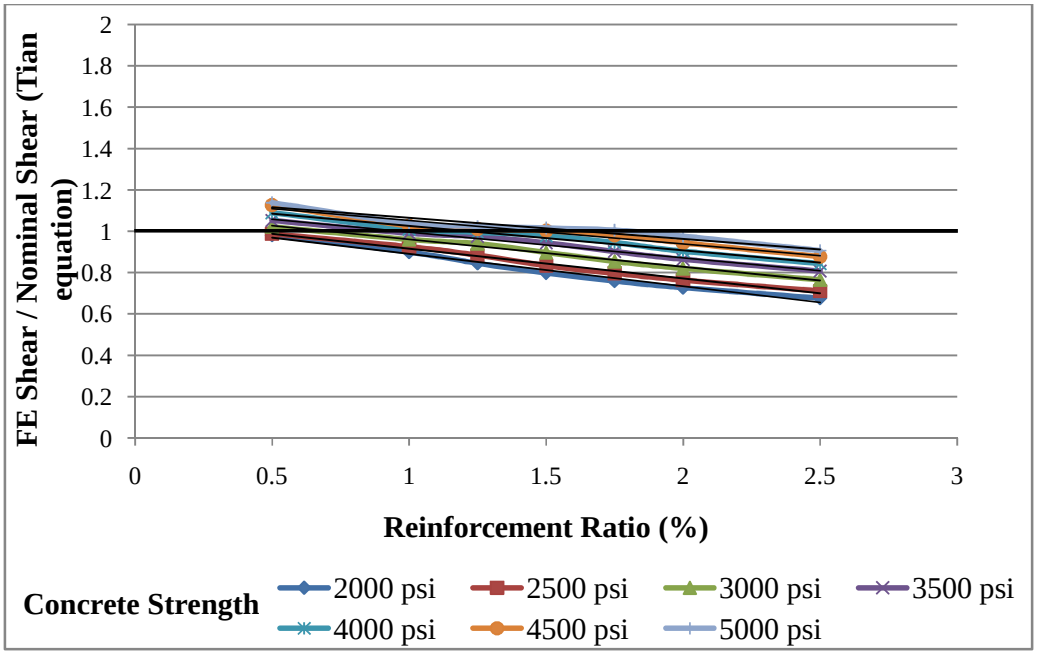

Figure 5.24 Variation of the ratio between FE shear to nominal shear according to Tian equation with varying reinforcement ratio for different compressive strength of concrete

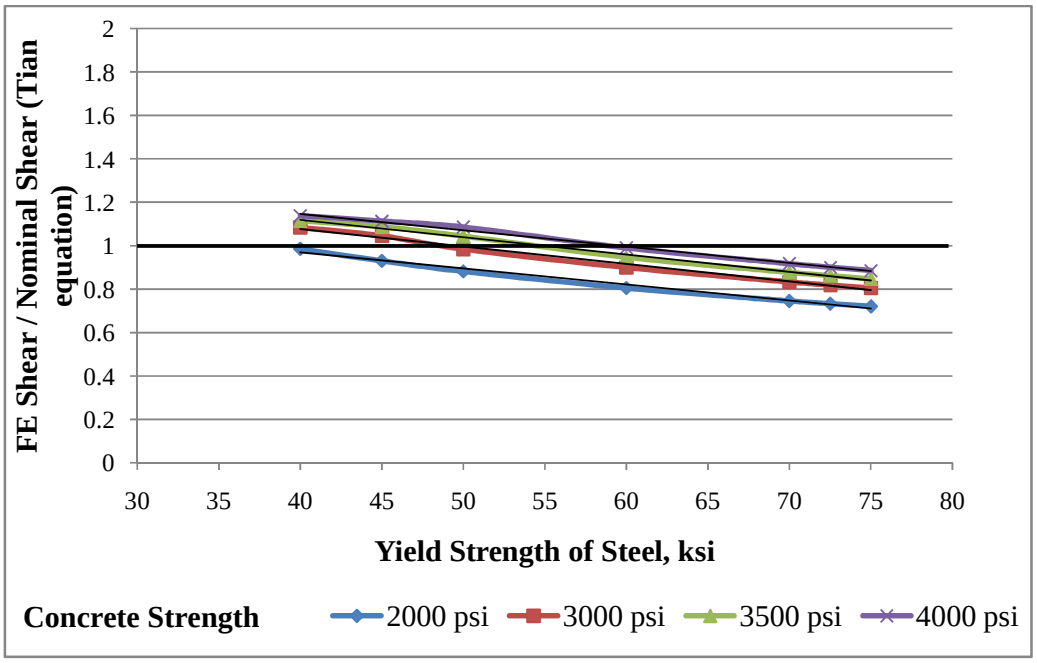

Figure 5.25 Variation of the ratio between FE shear to nominal shear according to Tian equation with varying yield strength of reinforcement for different compressive strength of concrete

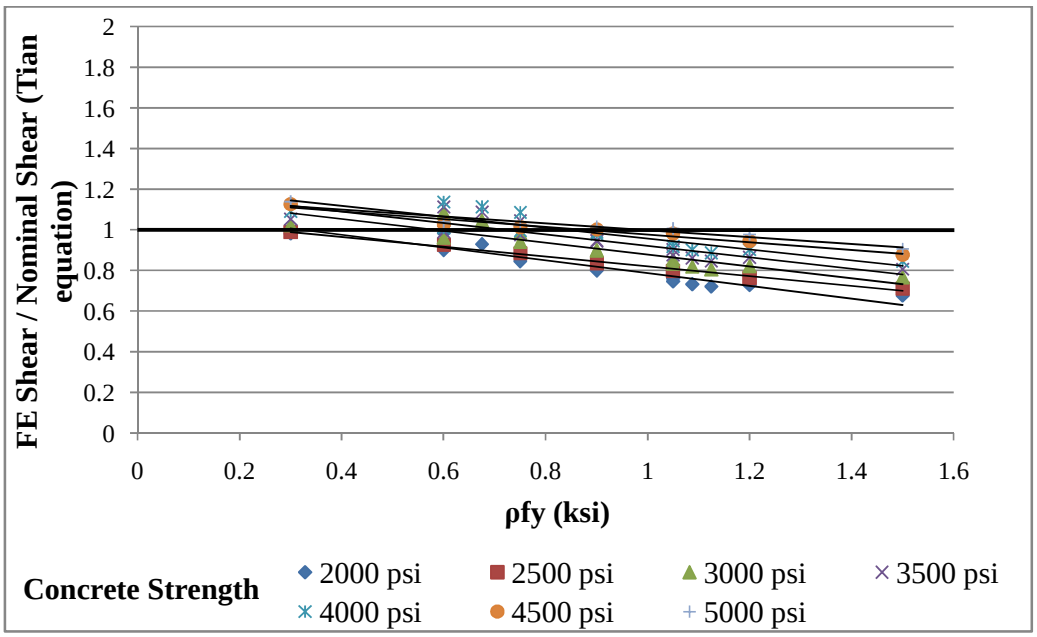

Figure 5.26 Variation of the ratio between FE shear to nominal shear according to Tian equation with varying reinforcement index for different compressive strength of concrete

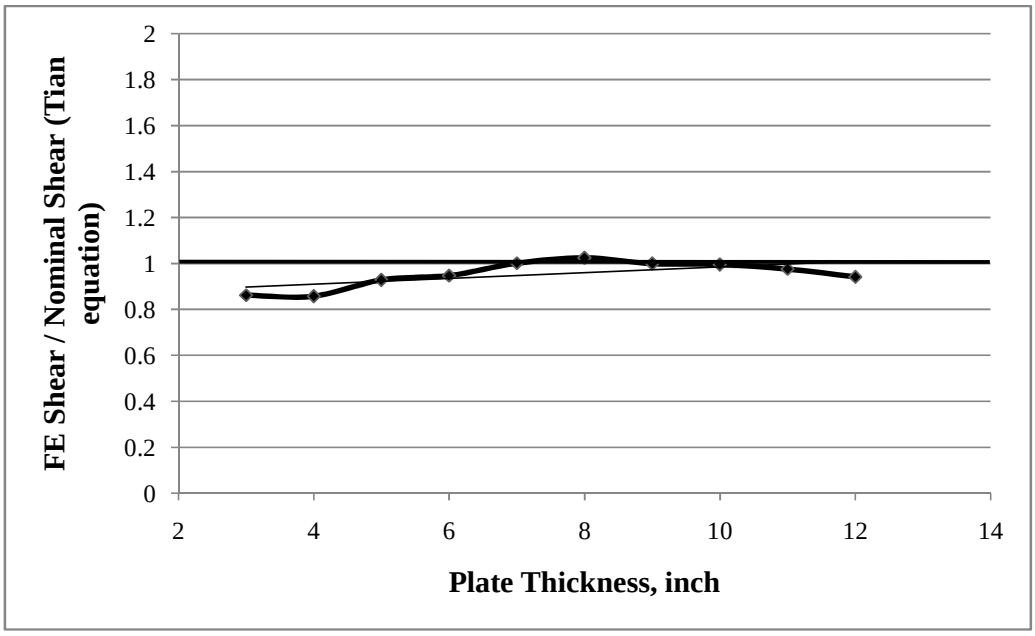

Figure 5.27 Variation of the ratio between FE shear to nominal shear according to Tian equation with varying plate thickness

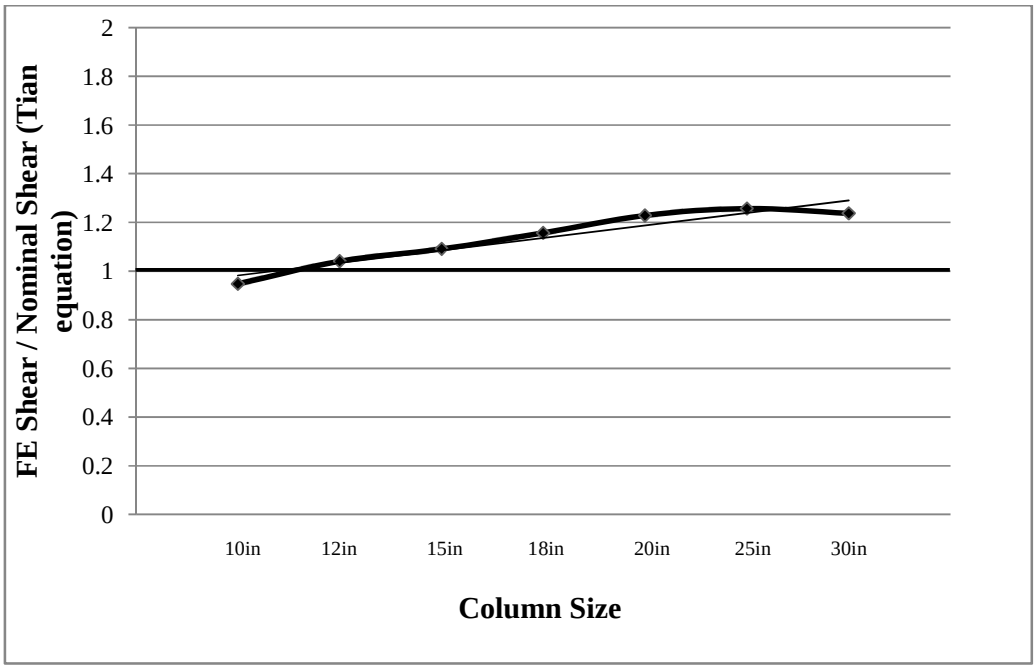

Figure 5.28 Variation of the ratio between FE shear to nominal shear according to Tian equation with varying column size

Again from 91 parametric study (Present FE analysis) results, the FE shear strength is plotted in Fig. 5.29 against the nominal strength estimated based on Tian equation. It is observed that most of the cases nominal shear according to Tian equation are very close to FE results (Present study) as the scatter is reduced.

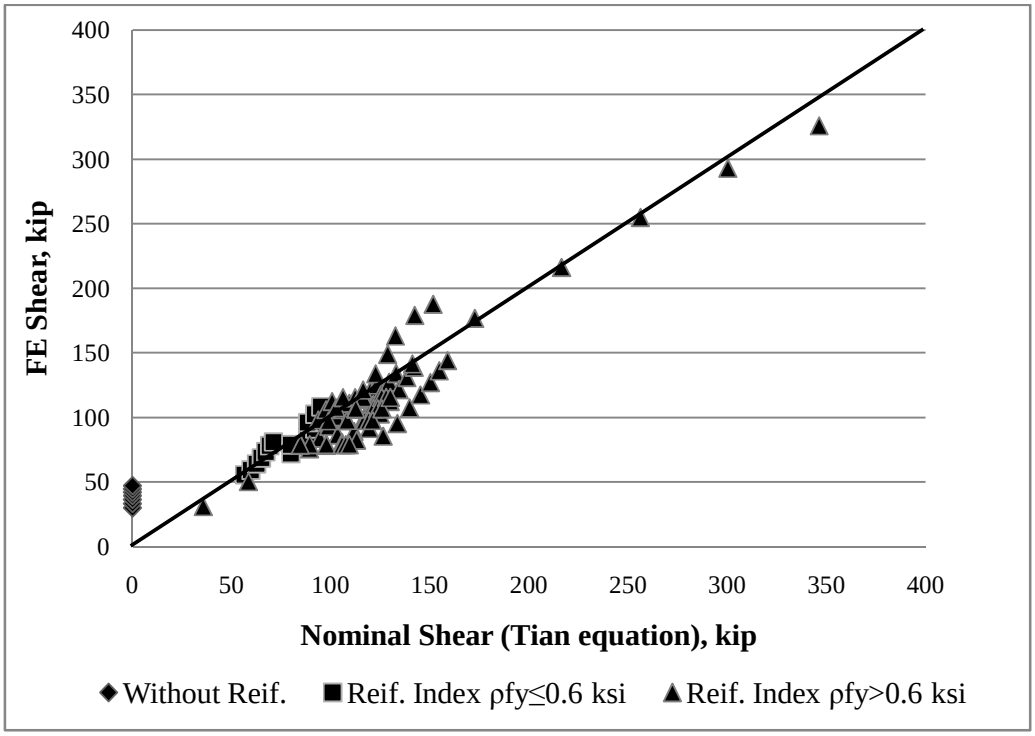

Figure 5.29 Comparisons of FE shear strength and nominal shear strength according to Tian equation

According to Tian et al. (2008), if 95% of the test results are expected to exceed the strength defined by Tian equation, a reduction factor of 0.83 should be applied to derive a characteristic strength. So, the FE shear strength is plotted in Fig. 5.30 against the design strength estimated based on Tian equation. However, from the present FE analysis about 18% FE results have not exceed the strength defined by Tian equation with reduction factor 0.83. So, a trial and error process have applied to get appropriate reduction factor for design strength and again the FE shear strength is plotted in Fig. 5.31 against the design strength estimated based on Tian equation having reduction factor of 0.73. This final value for reduction factor of 0.73 is

decided depending on proximity of about 95% FE results exceed the strength defined by Tian equation.

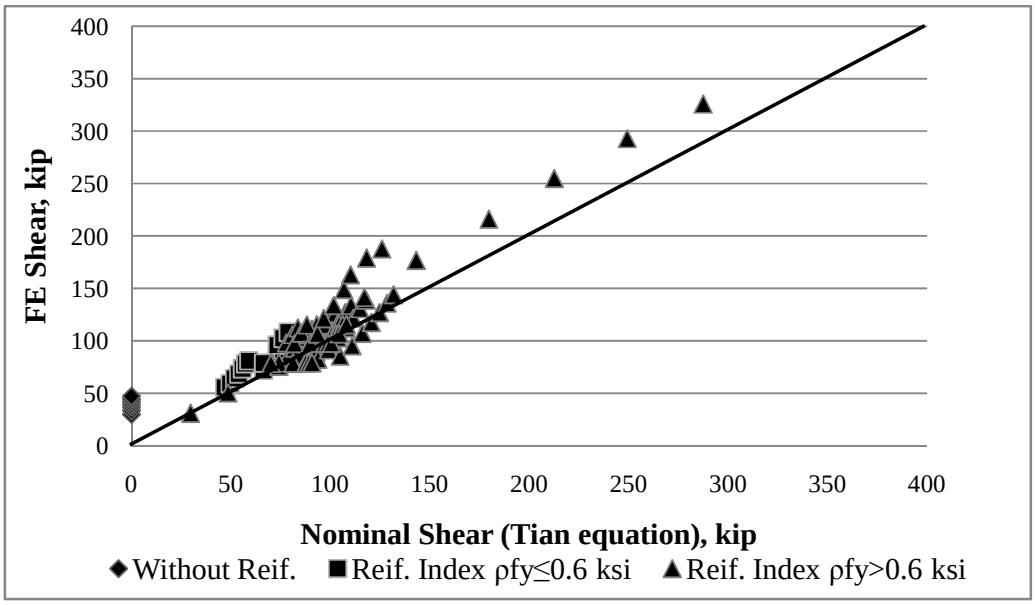

Figure 5.30 Comparisons of FE shear strength and nominal shear strength according to Tian equation with reduction factor 0.83

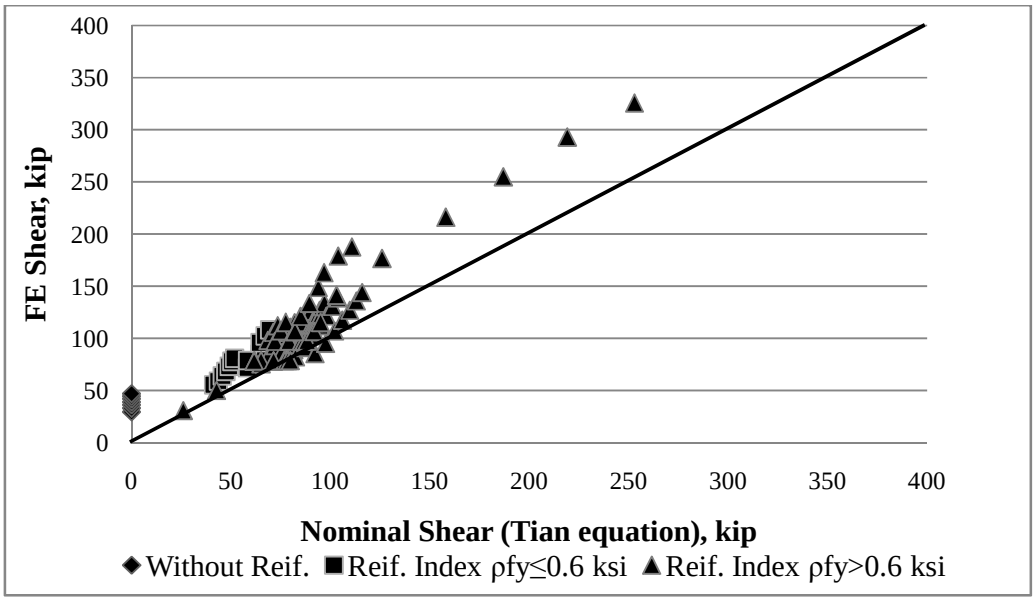

Figure 5.31 Comparisons of FE shear strength and nominal shear strength according to Tian equation with reduction factor 0.73

5.10 Proposed Modified Equation for Rectangular Column

The research work conducted by Tian et al. (2008) has carried out on slab-column connections of reinforced concrete flat plate structures subjected to concentrated gravity load to focuses on strength evaluation of interior connections with square columns. In this section, a modified equation has proposed which is more or less same as suggested by Tian et al. (2008) with have some minor modification by using rectangular column and compares the ultimate loads obtained from present FE analysis with the proposed modified equation to check the acceptability of the proposed modified equation. The minor modification by using rectangular column is only for column aspect ratio. The average dimension of rectangular column have used to calculate the value for A_c and $\sqrt{\frac{d}{c}}$ and a coefficient γ also has introduced in the proposed modified equation. The proposed modified equation is given below:

$$V_n = 0.65\gamma\xi A_c(\rho f_y\sqrt{f'_c})^{\frac{1}{2}} \quad \text{(in SI units)} \tag{5.5}$$

$$V_n = 2.3\gamma\xi A_c(\rho f_y\sqrt{f'_c})^{\frac{1}{2}} \quad \text{(in customary units)} \tag{5.6}$$

Where,

$$A_c = 4d(c+d)$$

$$\xi = \sqrt{\frac{d}{c}}$$

$$c = (c_1 + c_2)/2$$

$$\gamma = \{(2+\frac{4}{\beta_c})/4\} \quad \text{if, } \beta_c \geq 2$$

$$\gamma = 1 \quad \text{if, } \beta_c < 2$$

Here, β_c is the ratio of long to short sides of the column. The value of suggested shear strength coefficient is decrease with the increase of β_c. By considering only this modification for large rectangular column, the shear strength predicted by proposed modified equation has been found to be safe. Figures 5.33 and 5.34 are plotted the ratio of FE shear to nominal shear according to ACI 318-08 code

provision and the ratio of FE shear to nominal shear according to proposed modified equation respectively. In Fig. 5.33, whereas column size is varying represents conservative results by using ACI 318-08 code provision. On the other hand, Fig. 5.34 represents slightly overestimate result with column aspect ratio less than two and by increasing column aspect ratio the nominal shear based on proposed modified equation represents safe results. The analytical results (Present FE analysis) are plotted with predicted nominal punching shear values according to ACI 318-08 code provision and predicted nominal punching shear values according to proposed modified equation for slabs. The FE shear strength is plotted in Fig. 5.35 against the nominal strength estimated based on ACI 318-08 code provision. It is observed that nominal shear strength values according to ACI 318-08 code are scattered to FE shear strength values. Again, the FE shear strength is plotted in Fig. 5.36 against the nominal strength estimated based on proposed modified equation. It is observed from the figure that the nominal shear according to proposed modified equation is close to FE results (Present study) as the scatter is reduced. However, there have some overestimate results with column aspect ratio less than two and that need to adjust by using a reduction factor 0.73.

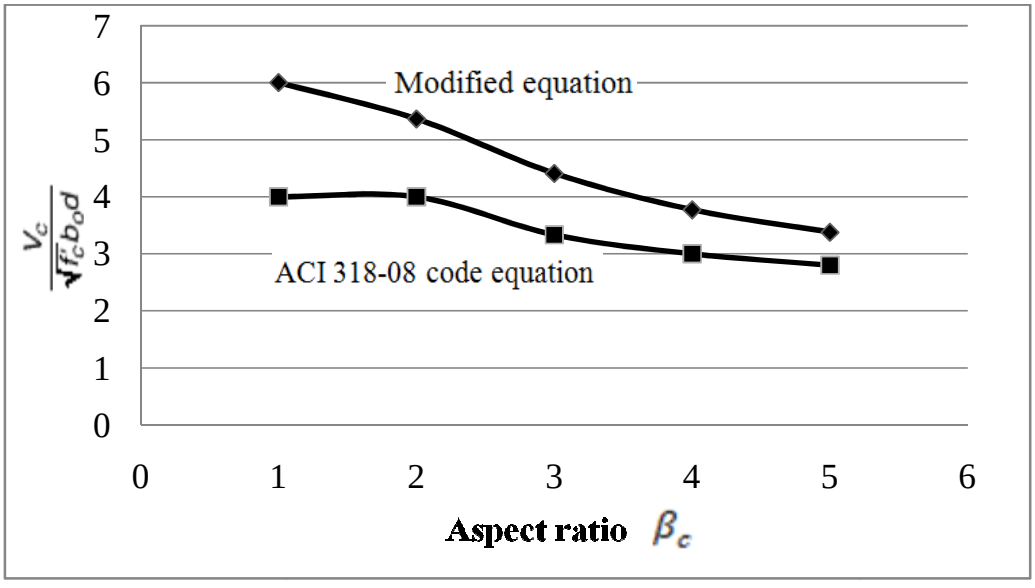

Figure 5.32 Variation of shear strength coefficient $\frac{V_c}{\sqrt{f'_c}b_0 d}$ with varying aspect ratio

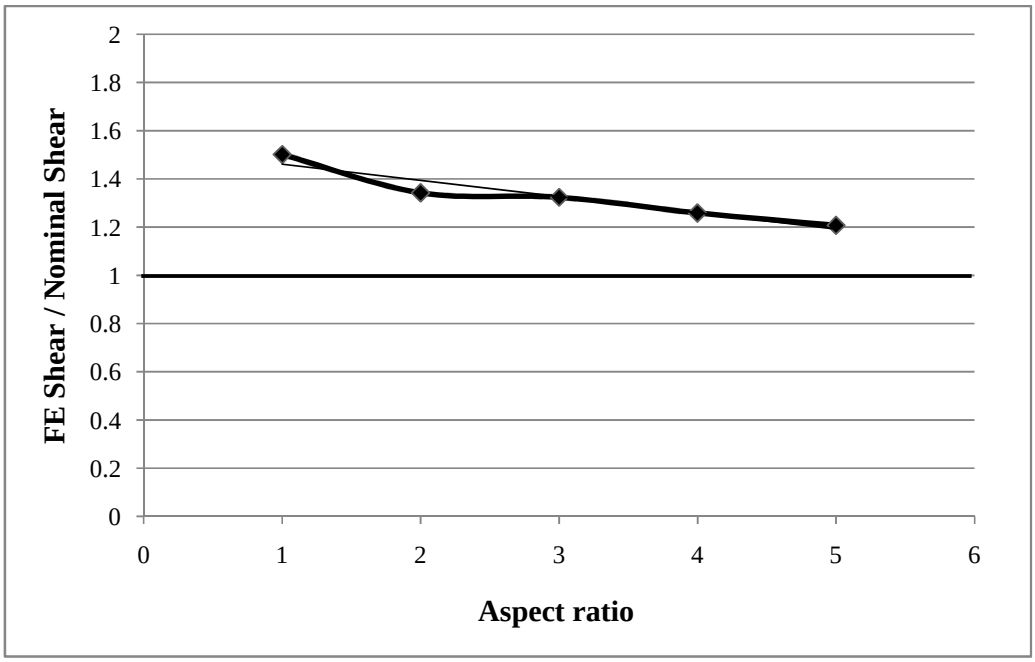

Figure 5.33 Variation of the ratio between FE shear to nominal shear according to ACI 318-08 code provision with varying aspect ratio

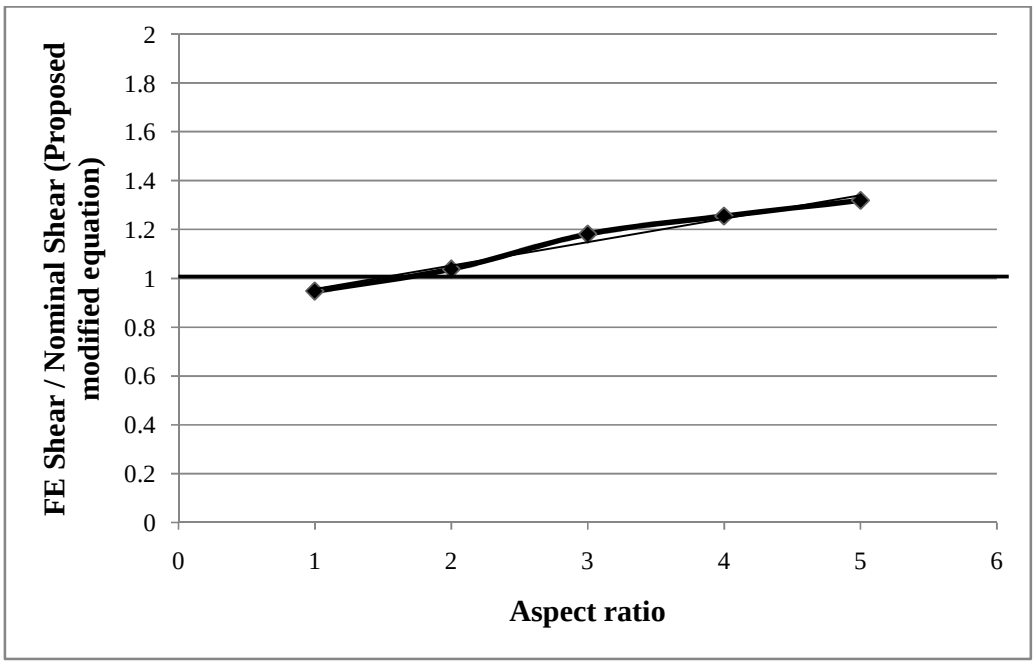

Figure 5.34 Variation of the ratio between FE shear to nominal shear according to proposed modified equation with varying aspect ratio

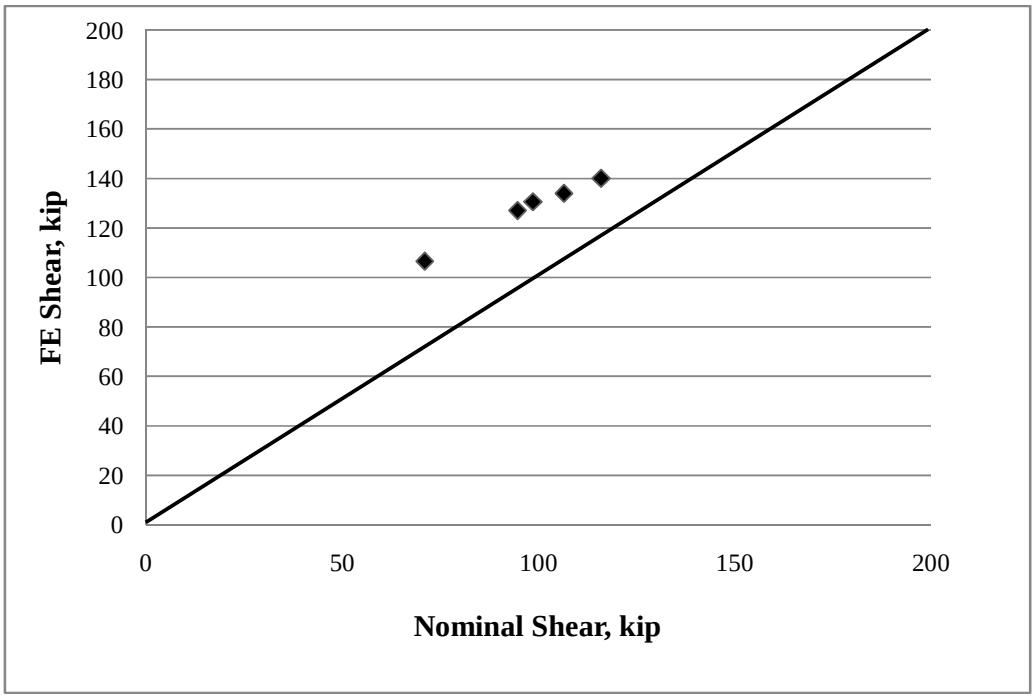

Figure 5.35 Comparisons of FE shear strength and nominal shear strength according to ACI 318-08 code provision

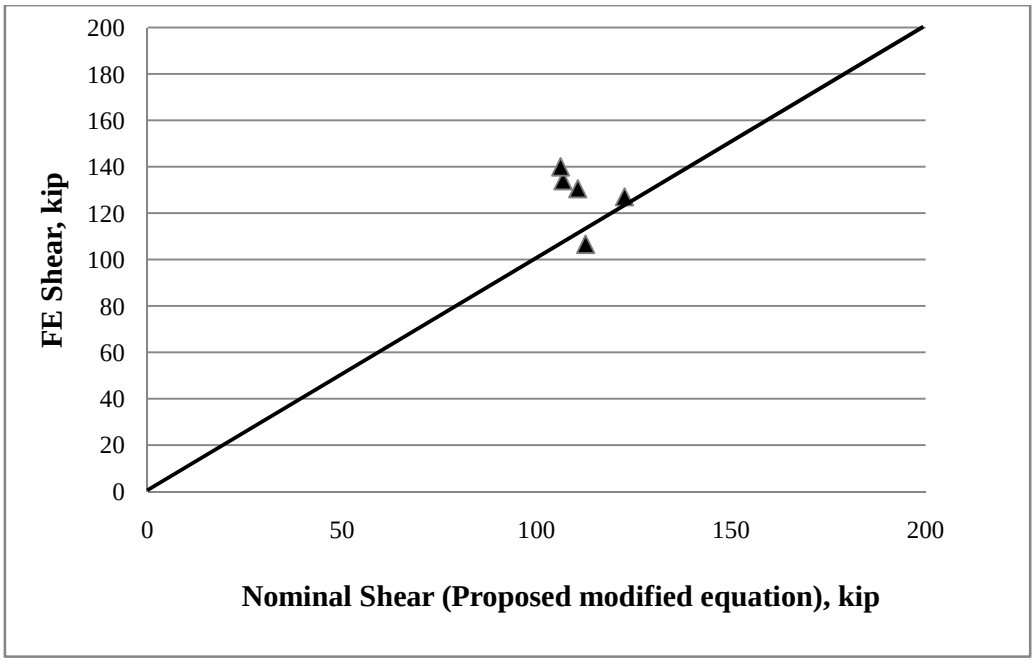

Figure 5.36 Comparisons of FE shear strength and nominal shear strength according to proposed modified equation

The proposed modified equation with considering reduction factor 0.73 to the right-hand side of these equations to derive a characteristic strength is given below:

$$V_n = 0.47\gamma\xi A_c(\rho f_y\sqrt{f'_c})^{\frac{1}{2}} \quad \text{(in SI units)} \qquad (5.5)$$

$$V_n = 1.7\gamma\xi A_c(\rho f_y\sqrt{f'_c})^{\frac{1}{2}} \quad \text{(in customary units)} \qquad (5.6)$$

Where,

$A_c = 4d(c+d)$

$\xi = \sqrt{\frac{d}{c}}$

$c = (c_1 + c_2)/2$

$\gamma = \{(2+\frac{4}{\beta_c})/4\}$ if, $\beta_c \geq 2$

$\gamma = 1$ if, $\beta_c < 2$

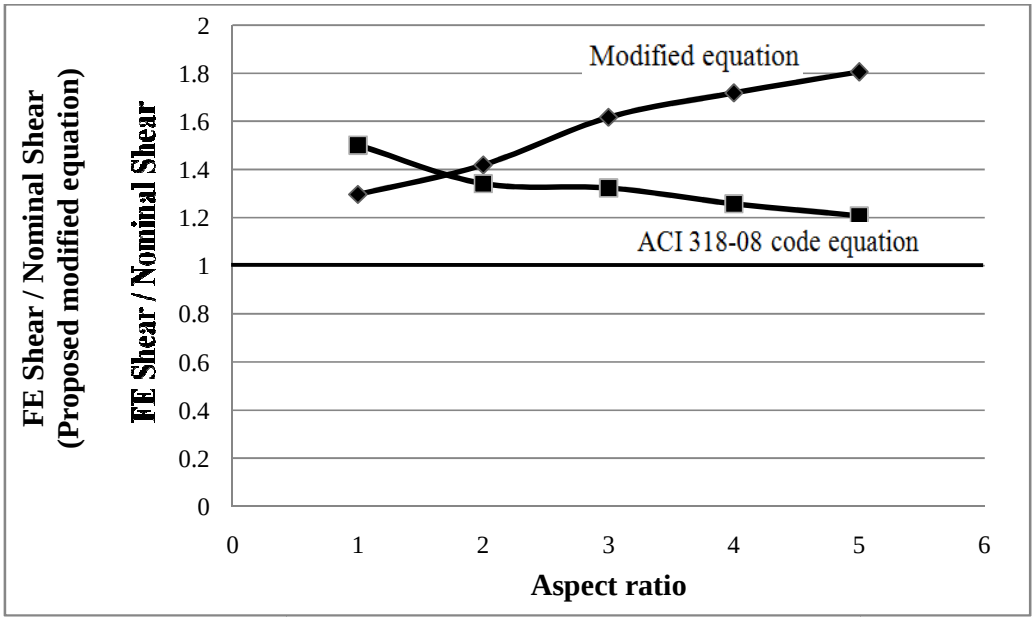

Figure 5.37 Variation of the ratio between FE shear to nominal shear according to ACI 318-08 code provision and proposed modified equation con--sidering reduction factor 0.73 with varying aspect ratio

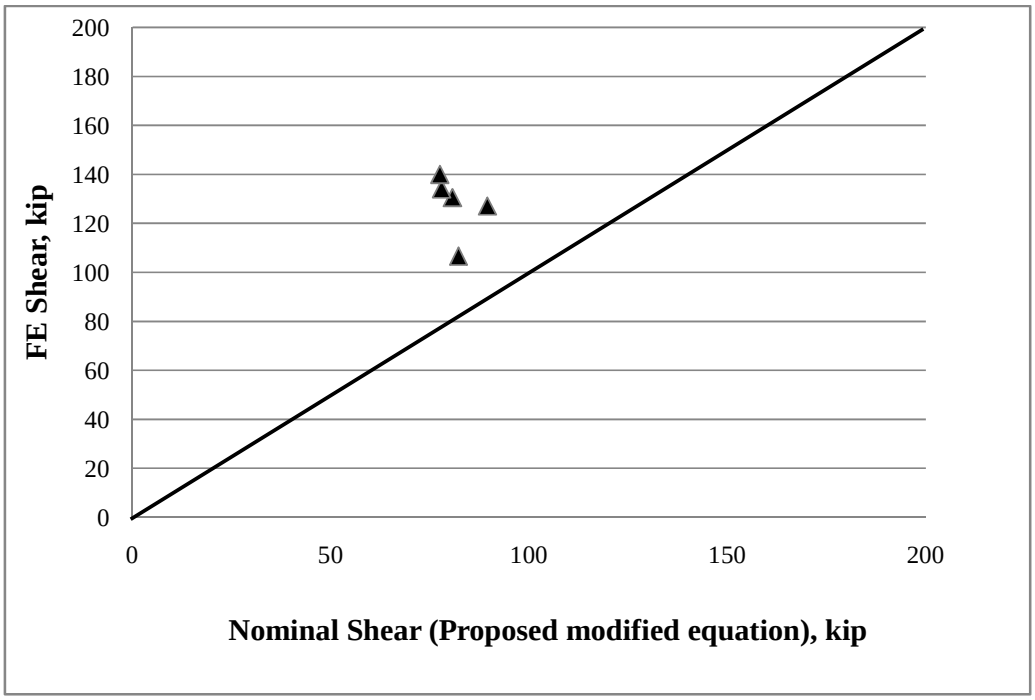

Figure 5.38 Comparisons of FE shear strength and nominal shear strength according to proposed modified equation with reduction factor 0.73

5.11 Remark

Numerical modeling of slab-column joint of RC flat plate by using 'ABAQUS' software based on nonlinear finite element method was used to investigate the influence of several factors on the behaviour of plate subjected to gravity load. The factors studied regarding material properties and geometric properties. Concrete compressive strength, the amount of longitudinal reinforcement, yield stress of steel, effect of compression reinforcement, the slab thickness, column dimensions and boundary conditions for the plates analyzed as part of this parametric study. The results of the analysis represent the general behaviour of slab-column joint at every stages of load history of slab up to failure. The concrete compressive strength, longitudinal reinforcement ratio, slab thickness and column dimensions increases punching shear capacity in a certain level.

The increase in ultimate load is more prominent with lower strength concrete compared to higher strength concrete for different steel ratios. From analysis, it is found that shear strength is proportional to $\sqrt{f'_c}$ which is similar with ACI 318 (2008) code equation and shear strength according to ACI 318-08 code equation is more or less similar with ultimate load capacity having tension reinforcement ratio 0.5% and by increasing tension reinforcement ratio, ultimate load capacity has increased than ACI code prediction. It is also found that from plain concrete to 1 percent reinforcement ratio slab load-carrying capacity has increased rapidly whereas from 1.25 to 2.5 percent that has increased gradually. Therefore, the increase in ultimate load is more prominent with lower percentage of reinforcement compared to higher percentage of reinforcement. Punching load is not influenced by the yield strength of the flexural reinforcement if the slab does not experience yielding and the effect of compression reinforcement on the ultimate load carrying capacity is not so significant.

For slab thickness it is found that the thicker the slabs, the higher the punching shear strength. From analysis, it is also found that the increase in ultimate load is more prominent with lower slab thickness compared to higher slab thickness and it decreases with the increase of slab thickness. The behaviour was different for different span-depth ratio. At lower slab thickness or span-depth ratio above 14 indicates ductile zone where flexure governs the failure. On the other hand at higher slab thickness or span-depth ratio from 14 to 5.83 indicates abrupt zone where shear governs the failure. The increase in square column size and the longer side for rectangular column have increased the stiffness on slab-column joint and ultimate load carrying capacity. The increase in ultimate load is more prominent with smaller size square column compared to larger size square column and the increasing rate of ultimate loads is very low by increasing longer side for rectangular column. It is observed that by doubling the square column size, ultimate load is increased over 50%, where the punching perimeter is increased 67% and the increase of ultimate loads is 21.6% for 20 inch square column size in place of 10in × 40in rectangular column size which means that the square column with same cross sectional area of a rectangular column yield higher punching strength. Similarly different boundary

condition has different influence on the punching capacity of slab-column connection. Therefore, boundary condition also is an important part of the model slab to get realistic result.

In case of punching shear design; ACI 318-08 code provision is more conservative. ACI 318-08 design equation underestimates the results to predict punching shear capacity. A modified equation as suggested by Tian et al. (2008) to predict punching shear capacity has been investigated. It is observed that the present study finds good correlation between FE results and those obtained by suggested equation. It is found that the contributions of concrete strength is best described by assuming connection punching capacity to be proportional to $(f'_c)^{0.25}$ instead of $\sqrt{f'_c}$ and strength of slab tensile reinforcement and c/d significantly affect the connection strength, as suggested by Tian. The suggested equation to predict punching shear capacity appears to be safe with reduction factor of 0.73. A modified equation has been proposed in the current work which is similar as suggested by Tian et al. (2008) with some minor modification to predict punching shear capacity for rectangular column. A satisfactory and safe result has come by using the proposed modified equation with reduction factor of 0.73 for rectangular column. However, still there are scopes to review the modified equation by taking into consideration the influence of the effects of edge restraint on punching shear strength.

The Tian equation and the proposed modified equation are based on numerical model where the effects of bond slip between concrete and reinforcement, dowel action and aggregate interlock were not considered. On the other hand, ACI 318-08 code equation is derived using experimental results where the above mentioned behaviours are included and this equation has been proved to be safe in practice. Therefore more intensive research works both experimental and numerical, need to be performed on the above discussed behaviour to derive a more logical punching shear formula to predict the actual punching capacity.

Chapter 6

BEHAVIOUR OF SLAB-COLUMN CONNECTIONS UNDER SEISMIC LOAD

6.1 General

In Chapter 5 the parametric study was done to identify the effects of different parameters on punching shear strength of flat plates under gravity loads. However, Flat plate structural behaviour is very critical under lateral load consists of the inertial force that results from the shaking of its foundation by a seismic disturbance. The inertial force which produces a significant unbalanced moment at slab-column connection would enhance punching shear failure. Therefore, by knowing the importance of seismic load this chapter is dedicated to study the behaviour of slab-column connection under both gravity and lateral loads. Under earthquake (lateral) loading the behaviour of a flat-plate structure is similar to that of moment resisting frame, that is, its lateral resistance depends on the flexural stiffness of the components and their connection. Therefore, the influence of this action must therefore be considered from the very beginning of the design process. The structure must be designed to resist the gravitational and lateral forces, both permanent and transient. In this chapter based on design criteria according to ACI 318 (2008) code provision, four different full scale slabs have been modeled under various combination of gravity and lateral loading according to BNBC (2006) and discuss the model behaviour at slab-column connection.

A better lateral load carrying system such as shear wall have discussed on flat plate high-rise building structure to resist most efficiently the various combinations of gravity and lateral loading. This shear wall is applied on structural system to improve resistance by increasing strength and stiffness. A safety provision have also been checked for design under direct design method by using shear wall on flat plate high-rise building structure at seismic Zone-2 and Zone-3 according to BNBC (2006).

Finally, recheck the percentage of moment which plays on column strip and middle strip as specified by direct design method under gravity load and also the percentage of moment transfer through column strip and effective width due to lateral load and suggest possible modification on percentage if required.

6.2 Numerical Modeling of Interior Slab-Column Connections

For structures in regions of high seismic risk or for structures assigned to high seismic performance is very critical. In case of high-rise building structure having flat plate slab system of large span length is affected by lateral load due to earthquake action to an extent that they play an important role in the structural design. The design criteria based on direct design method of slab-column connections of flat plate slab system, the intermediate moment resisting frames of flat plate structure according to ACI 318-08 code provisions and also having a drop panel that resist seismic forces have been discussed. For this, a typical interior slab-column connection of a fourteen storied commercial building was considered having 26.5 ft square slab, supported on a column of area 42″ × 42″ as shown in Fig. 6.1. The thickness of the slabs is 10 inches by ensuring that punching shear failure has not occurred according to ACI 318-08 and BNBC (2006) code provision. In this modeling the dead load with self weight is 200 psf and the live load is 80 psf as it is a commercial building. The load combination and seismic zone have considered according to BNBC (2006) code provision. Zone-2 has selected to analyze the lateral loads as the above mentioned commercial building is considered at Dhaka city. For this interior flat plate slab-column connection, concrete compressive strength and steel yield strength have considered 3500 psi and 60 ksi respectively. Based on above mentioned concept and design specification, a numerical model have generated for the following condition:

i. Model-1 which is based on direct design method considering only gravity load.

ii. Model-2 which is also based on direct design method considering only gravity load and fifty percent of column strip reinforcement have passed through effective width (c+3h).

iii. Model-3 is for slab-column connections of intermediate moment resisting frames.

iv. Model-4 is for slab-column connections with drop panel.

The limitation of modeling has also been discussed in this section.

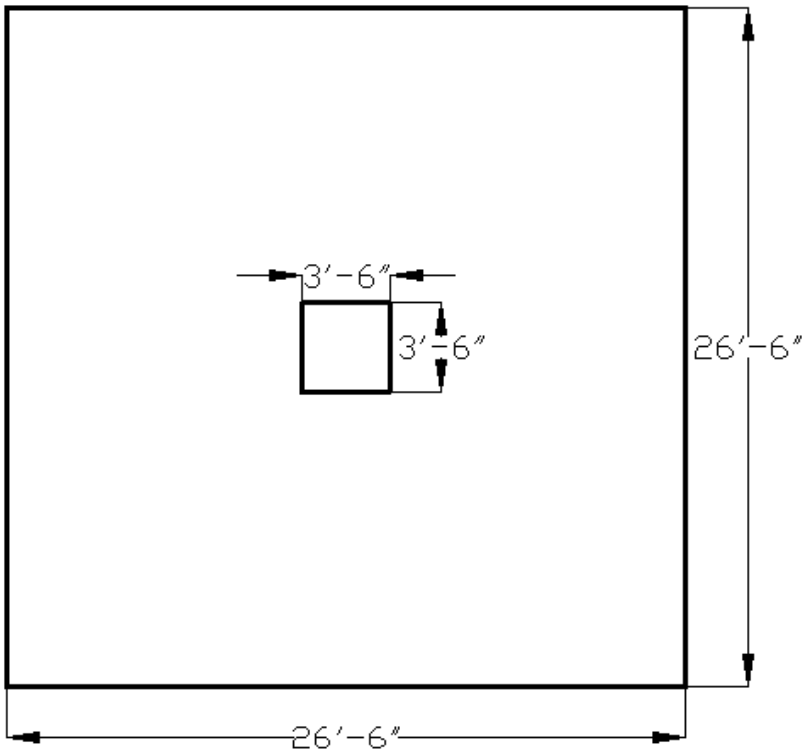

Figure 6.1 Plan view of interior panel of flat plate slab system

Finally an overview of the ACI 318-08 code provisions for moment transfer to column are summarized that presents the background information on the existing provisions to calculate the lateral load stiffness of two-way slab structures in accordance with requirements. It is also described how to utilize the provisions of Sec. 11.11.7 for shear resulting from moment transfer to column, Sec. 13.5.3 for

reinforcement requirements for moment transfer to column and moment distribution between slab and column and Sec. 21.3.6 for intermediate moment frames consisting of two-way slabs without beams.

6.2.1 Slab-column connections designed only for gravity load (Model-1)

The modeling of reinforcement detailing for slab-column connections is designed only for gravity load based on direct design method (empirical design). The direct design method consists of a set of rules for distributing moments to slab sections to satisfy safety requirements and most serviceability requirements simultaneously. This method is considerably simple to determine the distribution of total span moment at column strip and middle strip without the need for computation of equivalent column stiffness.

Based on direct design method, the total factored static moment in a span, for a strip bounded laterally by the centerline of the panel on each side of the centerline of supports shall be determined for load combinations according to BNBC (2006) as given in Eq. (6.1) is 729 kip-ft. All calculations are given in *Appendix A*. Distribute this total factored static moment to negative and positive sections and also these negative and positive factored moments to the column and middle strips based on specified percentage. The portion of negative and positive factored moments not resisted by column strips shall be proportionately assigned to corresponding half middle strips.

$$U = 1.4\,DL + 1.7\,LL \tag{6.1}$$

According to ACI 318-08 code provisions for interior panel, the percentages are as follows:

Negative factored moment ..... 65% of total factored static moment
Positive factored moment..... 35% of total factored static moment
Column strip negative moment..... 75% of negative factored moment
Middle strip negative moment..... 25% of negative factored moment

Column strip positive moment..... 60% of positive factored moment
Middle strip positive moment..... 40% of positive factored moment

Considering the above mentioned percentage, the column strip negative moment is 355 kip-ft. By this moment the required cross-sectional area of reinforcement in longitudinal direction is 9.4 in^2 and in transverse direction is 10.2 in^2. Similarly, for column strip positive moment, middle strip negative moment and middle strip positive moment is 153 kip-ft, 118 kip-ft and 102 kip-ft respectively and also by all these moments the required cross-sectional areas of reinforcement in longitudinal direction are 4 in^2, 3.08 in^2 and 2.86 in^2 respectively and in transverse direction are 4.2 in^2, 3.3 in^2 and 2.86 in^2 respectively. Development length of reinforcement has considered in accordance with ACI 318-08 code requirements as it describes the Sec. 13.3.8 for minimum extension of reinforcement. Based on these reinforcement detailing and also considering the dimensions and material properties as discuss in Sec. 6.2, a model has been prepared by using 'Abaqus' software.

6.2.2 Slab-column connections designed only for gravity load considering effective width (Model-2)

The modeling of reinforcement detailing for slab-column connections is also designed only for gravity load based on direct design method (empirical design) with have some minor modification. The calculation of total factored static moment and the distribution of this calculated moment to negative and positive sections and also to the column and middle strips is same as Sec. 6.2.1. The amount of reinforcement calculation for column strip and middle strip is also same as Sec. 6.2.1. In case of reinforcement detailing a minor modification has conducted. About fifty percent of column strip reinforcement has passed through effective slab width (c+3h) between lines that are one and one-half slab (1.5*h*) outside opposite faces of the column. Development length of reinforcement is also same as Sec. 6.2.1. Considering above mentioned modification, another model has been prepared by using 'Abaqus' software.

6.2.3 Slab-column connections of intermediate moment resisting frames (Model-3)

When both gravity and lateral forces cause transfer of moment between slab and column, a fraction of the unbalanced moment given by $\gamma_f M_u$ shall be considered to be transferred by flexure within an effective slab width between lines that are one and one-half slab ($1.5h$) outside opposite faces of the column, where M_u is the factored unbalanced moment to be transferred.

$$\gamma_f = \frac{1}{1+(\frac{2}{3})\sqrt{b_1/b_2}} \tag{6.2}$$

Where,

$b_1 =$ The width of the critical section for shear measured in the direction of the span for which the moments are determined

$b_2 =$ The width of the critical section for shear measured in the direction perpendicular to b_1.

The fraction of unbalanced moment $\gamma_v M_u$ not transferred by flexure shall be transferred by eccentricity of shear about the centroid of the critical section. The shear stress resulting from moment transfer by eccentricity of shear shall be assumed to vary linearly about the centroid of the critical sections.

$$\gamma_v = 1 - \gamma_f \tag{6.3}$$

Though the model slab is square and b_1/b_2 value is 1. That is why; the fraction of the moment transferred by flexure is 60 percent of the total unbalanced moment which can be calculated by using the Eq. (6.2).

According to ACI 318-08 code provision Sec. 13.5.3.3, the value of γ_f may be modified if certain conditions are met: For interior supports, the unbalanced moment transferred by flexure is permitted to be increased up to 25 percent provided that the factored shear (excluding the shear caused by the moment transfer) at the interior

supports does not exceed 40 percent of the shear strength φV_c. However, in this model the ratio between the factored shear and the shear strength φV_c is 0.97. Therefore, the unbalanced moment transferred by flexure is not permitted to be increased up to 25 percent in this model. When the factored shear for a slab-column connection is large, the slab-column joint cannot always develop all of the reinforcement provided in the effective width. The modifications for interior slab-column connections in accordance with ACI 318-08 code provisions as it describes the Sec. 13.5.3.3 are permitted only when the reinforcement (within the effective width) required developing the unbalanced moment $\gamma_f M_u$ does not exceed $0.375\rho_b$ or has a net tensile strain ϵ_t not less than 0.010.

The use of Eq. (6.2) without the modification permitted in Sec. 13.5.3.3 in accordance with ACI 318-08 code provisions will generally indicate overstress conditions on the joint. The provisions are intended to improve ductile behaviour of the slab-column joint. When a reversal of moments occurs at opposite faces of an interior support, both top and bottom reinforcement should be concentrated within the effective width. A ratio of top to bottom reinforcement of approximately 2 has been observed to be appropriate.

According to ACI 318-08 code provision Sec. 21.3.6, intermediate moment frames two-way slabs without beams forming a part of the seismic-force-resisting system. Factored slab moment at support including earthquake effects, ***E***, shall be determined for load combinations according to BNBC (2006) as given in Eq. (6.4) and Eq. (6.5) to calculate top and bottom reinforcement at the vicinity of the support.

$$\mathrm{U} = 0.75\,[\,1.4\,\mathrm{DL} + 1.7\,\mathrm{LL} + 1.7\,(1.1\,\mathrm{E})] \tag{6.4}$$

$$\mathrm{U} = 0.9\,\mathrm{DL} + 1.3\,(1.1\,\mathrm{E}) \tag{6.5}$$

An equivalent frame analysis can be used based on equivalent static force method to calculate seismic forces ***E***. By using Eq. (6.4), a reversal of moments occurs at opposite faces of an interior support. One side of the slab of the supporting column unbalanced negative moment is 758 kip-ft and other side of the slab of the

supporting column unbalanced positive moment is 223 kip-ft. All calculations are given in *Appendix A.* Similarly, by using Eq. (6.5), unbalanced negative moment is 655 kip-ft and unbalanced positive moment is 344 kip-ft. After a comparison of all negative and positive moments for both sides of slab, it is decided that 758 kip-ft negative moment and 344 kip-ft positive moment are maximum for model the reinforcement detailing. Reinforcement provided to resist unbalanced moment M_{slab} at both side of slab shall be placed within the column strip. Considering negative moment (758 kip-ft) the required cross-sectional area of reinforcement in longitudinal direction is 23 in^2 and in transverse direction is 25 in^2. Similarly considering positive moment (344 kip-ft), the required cross-sectional area of reinforcement both in longitudinal direction and in transverse direction is 10 in^2.

The moment M_{slab} refers, for the above mentioned design load combination with $\boldsymbol{E}$ acting in one horizontal direction, to that portion of the factored slab moment that is balanced by the supporting members at a joint. It is not necessarily equal to the total design moment at support for a load combination including earthquake effect. In accordance with ACI 318-08 code provision Sec. 13.5.3.2, only a fraction of the moment M_{slab} is assigned to the slab effective width and reinforcement placed within the effective width not less than one-half of the reinforcement in the column strip at support shall be proportioned to resist $\gamma_f M_{slab}$. Based on the fraction of the moment transferred by flexure is 60 percent of the total unbalanced moment, a similar reversal of moments occurs at opposite faces of an interior support.

Considering above mentioned percentage of unbalanced moment and again by using Eq. (6.4), one side of the slab of the supporting column unbalanced negative moment is 416 kip-ft and other side of the slab of the supporting column unbalanced positive moment is 172 kip-ft. Similarly, by using Eq. (6.5), unbalanced negative moment is 371 kip-ft and unbalanced positive moment is 229 kip-ft. After a comparison of all negative and positive moments for both sides of slab, it is decided that 416 kip-ft negative moment and 229 kip-ft positive moment are maximum for model the reinforcement detailing. Considering negative moment (416 kip-ft), the required cross-sectional area of reinforcement in longitudinal direction is 13 in^2

which is not less than $0.375\rho_b$ and has a net tensile strain 0.0033 which is not more than 0.010 and in transverse direction is 15 in^2 which is also not less than $0.375\rho_b$ and has a net tensile strain 0.0022 which is also not more than 0.010. Similarly considering positive moment (229 kip-ft), the required cross-sectional area of reinforcement both in longitudinal direction and in transverse direction is 7 in^2 which is not less than $0.375\rho_b$ and has a net tensile strain 0.0087 which is not more than 0.010. Therefore, the modifications for interior slab-column connections in accordance with ACI 318-08 code provisions as it describes the Sec. 13.5.3.3 are not permitted.

Due to the above specified condition within the effective width it generally indicates overstress conditions on the joint and requires more depth to provide necessary reinforcement to resist unbalanced moment. However, without increasing the depth of slab the model has been prepared by using 'Abaqus' software. Some other reinforcement detailing (Seismic detailing) according to ACI 318-08 code provision Sec. 21.3.6 provided that reinforcement not less than one-quarter of the top reinforcement at the support in the column strip shall be continuous throughout the span and continuous bottom reinforcement in the column strip shall be not less than one-third of the top reinforcement at the support in the column strip and also not less than one-half of all bottom middle strip reinforcement and all bottom column strip reinforcement at midspan shall be continuous.

6.2.4 Slab-column connections with drop panel (Model-4)

When high shear forces are being transferred at a slab-column connection, the slab shear strength can be increased locally by using a drop panel to locally increase the thickness of the slab. The term drop panel stems from the requirement to 'drop' the form-work around the column to increase the cast-in-place thickness of the slab. The ACI Code Section 13.2.5 requires that to control deflections and to reduce the amount of negative moment reinforcement over a column, the total thickness of the slab and drop panel to be at least 1.25 times the thickness of the slab adjacent to the drop panel and not greater than one-quarter the distance from the edge of drop panel

to the face of column and this drop panel should extend in each direction from the centerline of support a distance not less than one-sixth the span length measured from center-to-center of supports in that direction.

In this model the slab thickness is 10 in and span length is 318 in. Therefore, the total thickness of the slab and drop panel is considered 14 in and the drop panel have extend in each direction from the centerline of support is 79.5 in which is more than one-sixth the span length. All calculations are given in *Appendix A*. Two critical sections have considered for checking the punching shear failure according to ACI 318-08 code provision. A drop panel gives additional depth at the column, thereby increasing the area of the critical shear perimeter which provides more strength to resist punching shear failure. In similar way, by using drop panel, it stiffens the slab in the region of highest moments and hence reduces the deflection.

Same factored slab moment at support including earthquake effects, ***E***, as specified in Sec. 6.2.3 shall be determined for load combinations according to BNBC (2006) as given in Eq. (6.4) and Eq. (6.5) to calculate top and bottom reinforcement at the vicinity of the support. Reinforcement provided to resist unbalanced moment M_{slab} at both side of slab shall be placed within the column strip. Considering negative moment (758 kip-ft) same as Sec. 6.2.3, the required cross-sectional area of reinforcement in longitudinal direction is 14 in^2 and in transverse direction is 14.6 in^2. Similarly considering positive moment (344 kip-ft), same as Sec. 6.2.3, the required cross-sectional area of reinforcement in longitudinal direction is 6.2 $in^2$and in transverse direction is 6.4 in^2.

According to ACI 318-08 code provision Sec. 13.5.3.2, only a fraction of the moment M_{slab} is assigned to the slab effective width and reinforcement placed within the effective width not less than one-half of the reinforcement in the column strip at support shall be proportioned to resist $\gamma_f M_{slab}$. Again considering negative moment (416 kip-ft) within the effective width same as Sec. 6.2.3, the required cross-sectional area of reinforcement in longitudinal direction is 7.8 in^2 which is less than $0.375\rho_b$ and has a net tensile strain 0.0122 which is more than 0.010 and in

transverse direction is 8.2 in^2 which is also less than $0.375\rho_b$ and has a net tensile strain 0.0108 which is also more than 0.010. Similarly considering positive moment (229 kip-ft) within the effective width same as Sec. 6.2.3, the required cross-sectional area of reinforcement in longitudinal direction is 4.2 in^2 which is less than $0.375\rho_b$ and has a net tensile strain 0.025 which is more than 0.010 and in transverse direction is 4.4 in^2 which is also less than $0.375\rho_b$ and has a net tensile strain 0.0228 which is also more than 0.010. Therefore, the modifications for interior slab-column connections in accordance with ACI 318-08 code provisions as it describes the Sec. 13.5.3.3 are permitted. Some other reinforcement detailing (Seismic detailing) according to ACI 318-08 code provision Sec. 21.3.6 have provided throughout the slab.

6.2.5 FE model and limitation

The continuous simple supports (Restrained in vertical direction) along all four peripheral lines of the slab in the numerical model are approximately 1/2 of the span length apart from the column, having a full scale interior slab-column connection subjected to either only gravity loading (by applying compression on the column for simulating the gravity loads) or lateral loading. Under gravity loading a zero rotational restrained have applied at mid-span to get maximum positive moment by restrained in horizontal direction along the four peripheral lines of the slab in the numerical model. On the other hand, under lateral loading at mid-span there have zero moment with maximum rotation.

In a real structure, inflection points for combined gravity and lateral loading would differ from those under gravity loading or lateral loading only. Under combined gravity and lateral loading the inflection point is neither at mid-span as under lateral loading nor at one-tenth of the total span measured from supporting end as under gravity loading. With the increase of gravity and lateral loading the inflection point would change its position. If the model slab is subjected to subsequent lateral loads, with gravity loads applied first and sustained having the boundary conditions for combined gravity and lateral loading are identical with the boundary conditions for

gravity loading or lateral loading only, there are several unrealistic features that could have directly affected the numerical results. The horizontal resultant forces due to both gravity and lateral loading at the slab edges perpendicular to the gravity loading direction would have been larger in the numerical model than those in the real structure, which in turn would have produced larger one way shear forces around the bottom column than the top column. Also, slab moments generated in the slab-column interfaces due to both gravity and lateral loading would differ in the numerical model slab than those in the real structure. In short, the magnitude of direct shear or unbalanced moment occurring at the slab-column interfaces depends on the locations of inflection points.

However, in the numerical model it is not possible to change different boundary conditions in different places over the total loading period and the supports would not devised to simulate inflection points under combined gravity and lateral loading. Therefore, in this study two individual boundary conditions are modeled separately to simulate the inflection point under gravity loading or lateral loading only.

6.3 Performance Analysis under Gravity and Lateral Loads

After complete to model four slabs having different reinforcement detailing as specified in Sec. 6.2.1, 6.2.2, 6.2.3 and 6.2.4, the analysis part have completed by applying only gravity and lateral loads. The gravity and lateral loads and boundary conditions are discussed in Sec. 6.2.5 whereas the gravity loads have applied by applying compression on the column and the lateral loads have applied at halfway of top and bottom columns from slab as like shear forces at inflection point of column at mid height.

Under gravity load the load-deflection diagram of four different model slabs are given in Fig. 6.2. From figure it is clear that Model-4 with drop panel can take more loads than other three models. Under 368 kip load at bottom of the column as simulating 537 psf load on slab, first yielding of tensile steel at the vicinity of the column have occurred on Model-1 with a central deflection of 1.03 in and concrete

tensile damage of 49.8% as shown in Fig. 6.3. Under same load on Model-2, Model-3 and Model-4, there have no yielding of steel. The central deflection of Model-2, Model-3 and Model-4 is 1.03 in, 0.73 in and 0.26 in respectively and the concrete tensile damage is 48.8%, 32.2% and 8.2% as shown in Figs. 6.4, 6.5 and 6.6 respectively. From Fig. 6.2 it is found that Model-2 behaviour is more or less same with Model-1 as Model-2 flexural reinforcement amount is same with Model-1 and Model-3 behaviour is very close to Model-1 as Model-3 is not fully maintain the ACI 318-08 code provisions and it is in overstress conditions on the slab-column joint. Under 373 kip load at bottom of the column as simulating 545 psf load on slab, first yielding of tensile steel at the vicinity of the column have occurred on Model-2 with a central deflection of 1.06 in and concrete tensile damage of 49.6% which is very close to Model-1. In Model-1, it can take maximum 420 kip load at bottom of the column as simulating 614 psf load on slab with a central deflection of 1.55 in and have full concrete tensile damage at the vicinity of the column before punching shear failure have occurred. Similarly in Model-2, it can take maximum 423 kip load at bottom of the column as simulating 618 psf load on slab with a central deflection of 1.56 in and have full concrete tensile damage at the vicinity of the column before punching shear failure have occurred which is also very close to Model-1.

Similarly, Under 473 kip load at bottom of the column as simulating 691 psf load on slab, first yielding of compressive steel at the vicinity of the column have occurred on Model-3 with a central deflection of 1.13 in and concrete tensile damage of 48.6%. Under same load on Model-4, there have no yielding of steel. The central deflection and concrete tensile damage is 0.38 in and 16.5% respectively. In Model-3, it can take maximum 519 kip load at bottom of the column as simulating 758 psf load on slab with a central deflection of 1.34 in and have 58.6% concrete tensile damage at the vicinity of the column before punching shear failure have occurred.

Similarly, Under 823 kip load at bottom of the column as simulating 1203 psf load on slab, first yielding of tensile steel at the vicinity of the column have occurred on Model-4 with a central deflection of 0.95 in and concrete tensile damage of 64%. In

Model-4, it can take maximum 870 kip load at bottom of the column as simulating 1271 psf load on slab with a central deflection of 1.09 in and have 76.1% concrete tensile damage at the vicinity of the column before punching shear failure have occurred.

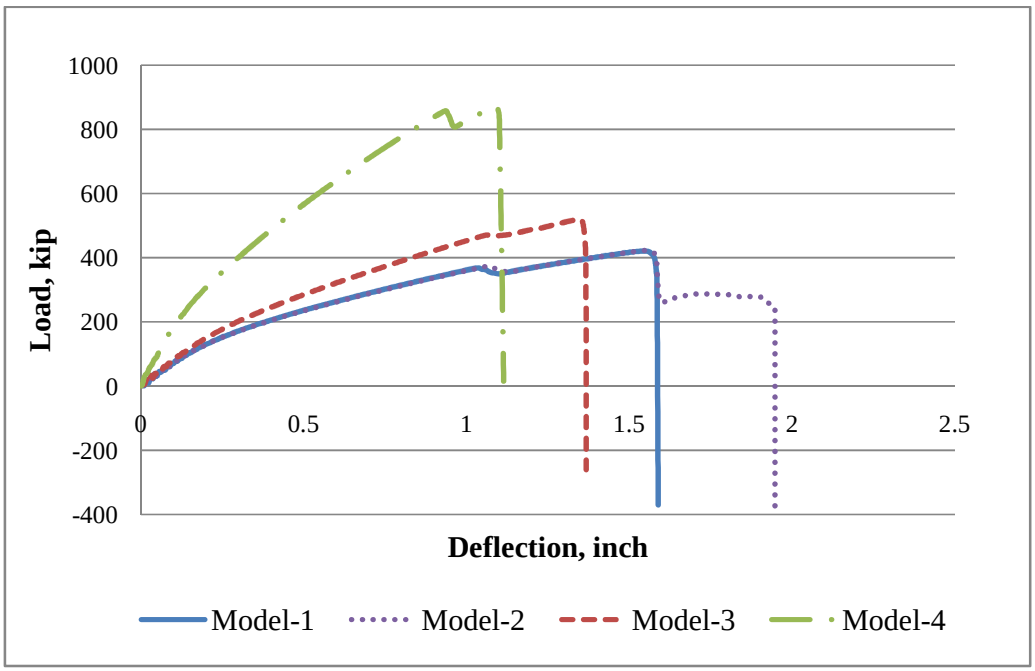

Figure 6.2 Load-deflection responses under gravity load of four model slabs

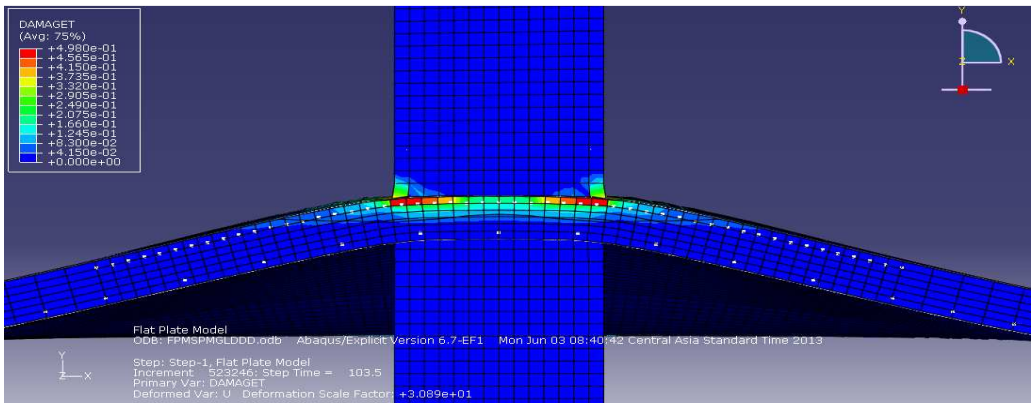

Figure 6.3 Radial crack spread out with pyramid shape and 49.8% tensile damage of concrete at 368 kip load on half slab of model-1

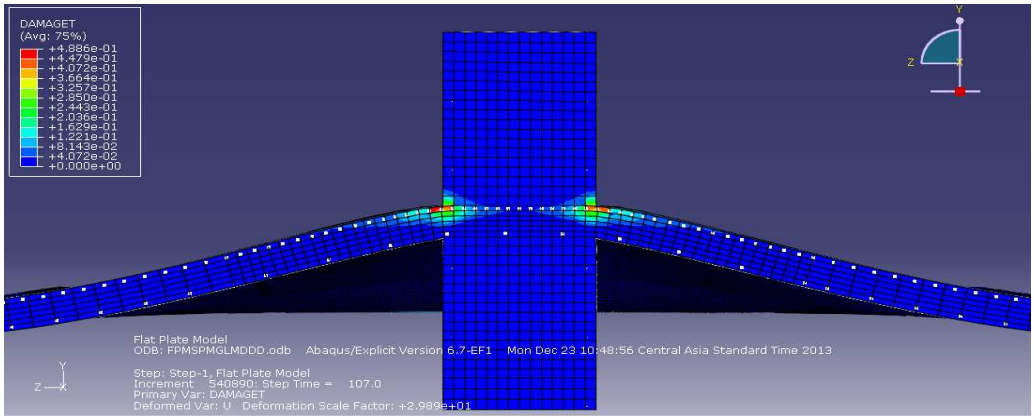

Figure 6.4 Radial crack spread out with pyramid shape and 48.8% tensile damage of concrete at 368 kip load on half slab of model-2

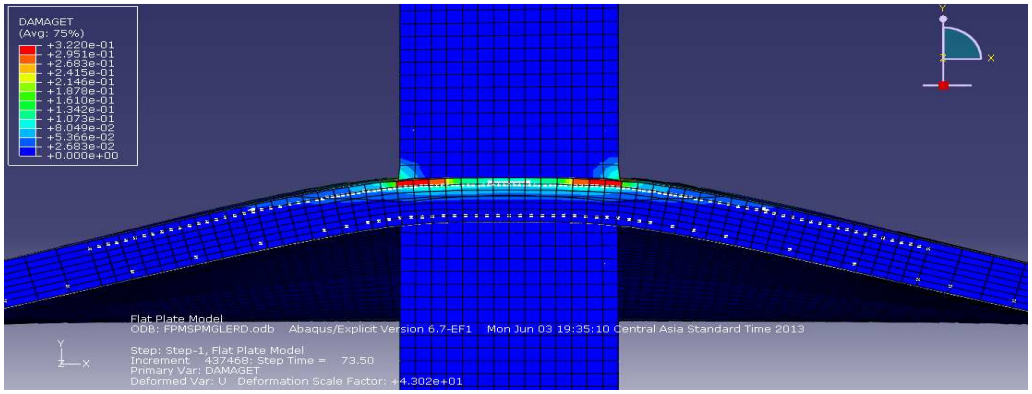

Figure 6.5 Radial crack spread out with pyramid shape and 32.2% tensile damage of concrete at 368 kip load on half slab of model-3

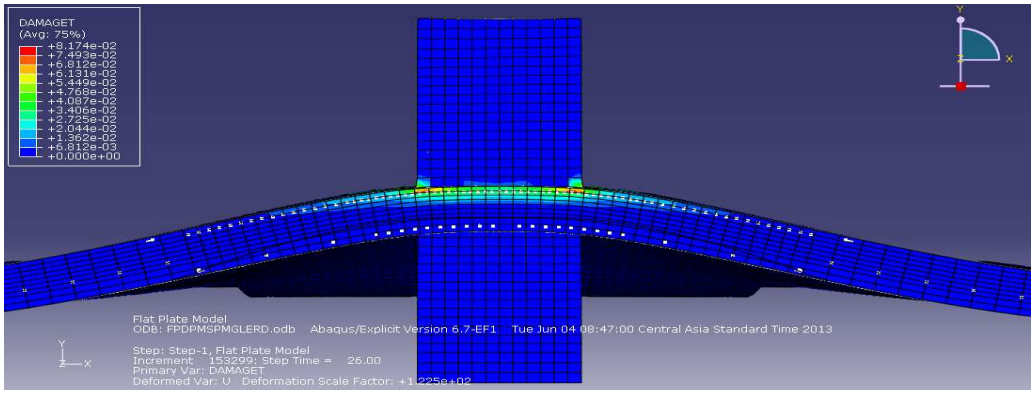

Figure 6.6 Radial crack spread out with pyramid shape and 8.2% tensile damage of concrete at 368 kip load on half slab of model-4

Under lateral load the load-deflection diagram and unbalanced moment-drift ratio diagram of four different model slabs are given in Figs. 6.7 and 6.8 respectively. According to Smith et al. (1991), under lateral load the design drift index limits that have been used in different countries range from 0.001 to 0.005. To put this in perspective, a maximum horizontal top deflection of 0.12 in to 0.6 in would be allowed over a story height of 10 ft. Under 86.7 kip lateral load at halfway of top and bottom columns from slab as like shear forces at inflection point of column at mid height or 867 kip-ft unbalanced moment at slab-column joint, first yielding of steel on bottom tensile side at the vicinity of the column have occurred on Model-1 and Model-2 with a top lateral deflection of 0.50 in and 0.49 in and drift ratio of 0.42% and 0.41% respectively which is within the limiting drift ratio and having concrete tensile damage of 53% and 50% respectively at the bottom tensile side of slab. Under same lateral load and unbalanced moment on Model-3 and Model-4, there have no yielding of steel. The top lateral deflection and drift ratio of Model-3 is 0.34 in and 0.29% respectively and for Model-4 is 0.13 in and 0.11% respectively where in both case the drift ratio is within the limiting drift ratio. The concrete tensile damage for Model-3 and Model-4 is 21% and 5.3% at the bottom tensile side of slab respectively. From Figs. 6.7 and 6.8 it is found that Model-2 behaviour is more or less same with Model-1 as Model-2 flexural reinforcement amount is same with Model-1 and Model-3 behaviour is very close to Model-1 as Model-3 is not fully maintain the ACI 318-08 code provisions and it is in overstress conditions on the slab-column joint. In Model-1, it can take maximum 128.5 kip lateral load or 1285 kip-ft unbalanced moment with a top lateral deflection of 2.21 in and drift ratio of 1.85% which is beyond the limiting drift ratio and have full concrete tensile damage at both top and bottom tensile side of slab before punching shear failure have occurred. Similarly in Model-2, it can take maximum 130 kip lateral load or 1300 kip-ft unbalanced moment with a top lateral deflection of 2.03 in and drift ratio of 1.69% which is beyond the limiting drift ratio and have full concrete tensile damage at both top and bottom tensile side of slab before punching shear failure have occurred which is very close to Model-1.

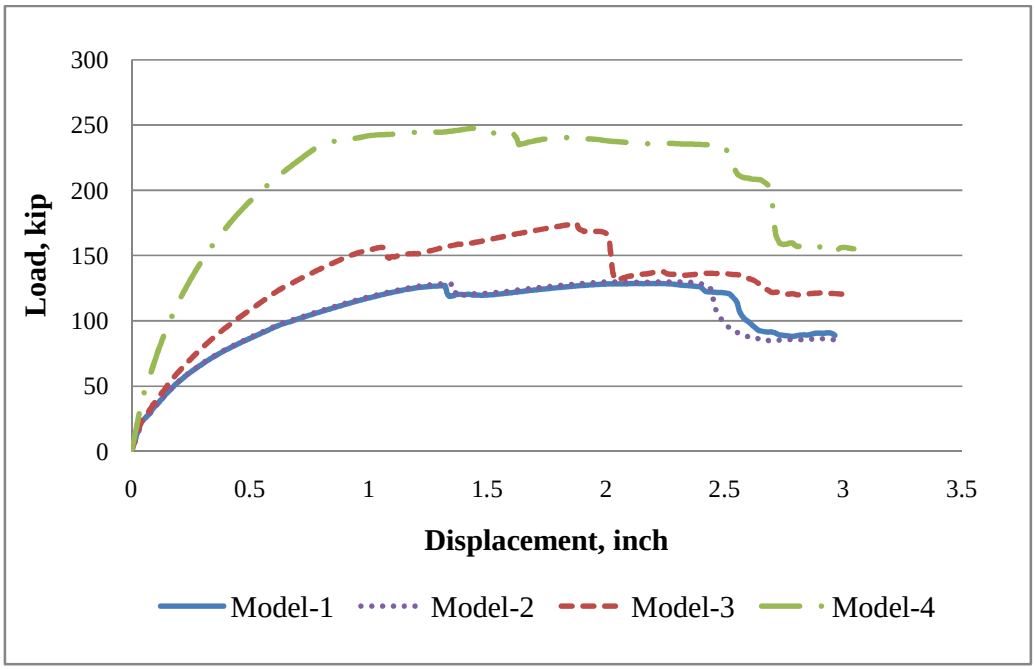

Figure 6.7 Load-displacement responses under lateral load of four model slabs

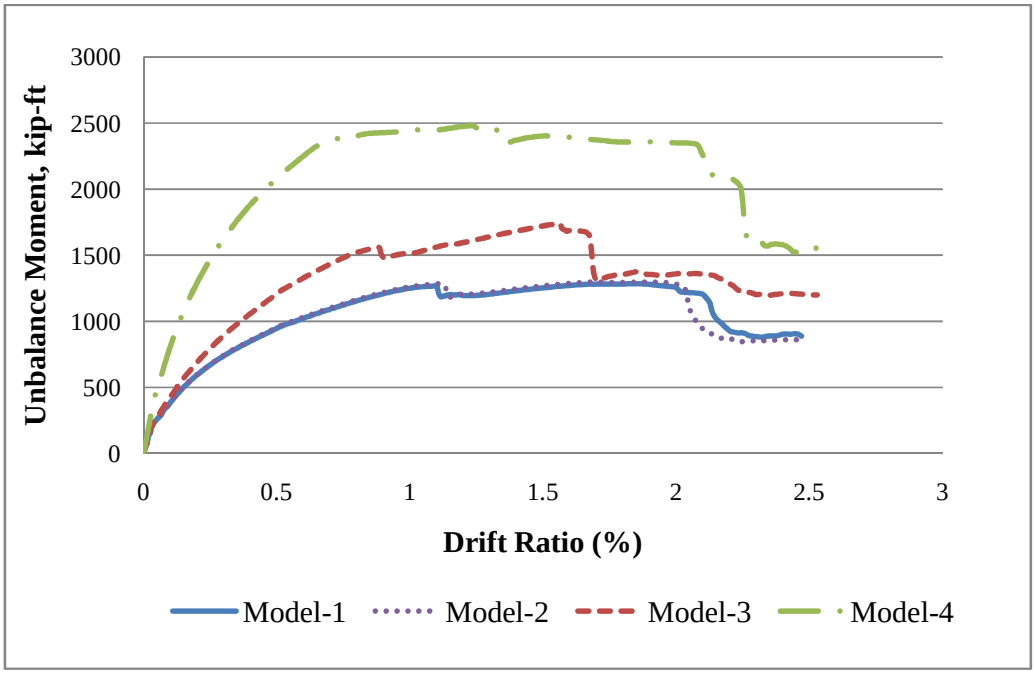

Figure 6.8 Unbalanced moment-drift ratio diagram under lateral load of four model slabs

Similarly, Under 151.3 kip lateral load or 1513 kip-ft unbalanced moment, first yielding of steel on bottom tensile side at the vicinity of the column have occurred on Model-3 with a top lateral deflection of 1.19 in and drift ratio of 0.99% which is beyond the limiting drift ratio and having concrete tensile damage of 62% at both top and bottom tensile sides of slab. Under same lateral load and unbalanced moment on Model-4, there have no yielding of steel. The top lateral deflection and drift ratio of Model-4 is 0.31 in and 0.26% respectively where the drift ratio is within the limiting drift ratio. The concrete tensile damage for Model-4 is 19.5% at the bottom tensile side of slab. In Model-3, it can take maximum 174.1 kip lateral load or 1741 kip-ft unbalanced moment with a top lateral deflection of 1.87 in and drift ratio of 1.56% which is again beyond the limiting drift ratio and have full concrete tensile damage at both top and bottom tensile sides of slab before punching shear failure have occurred.

Similarly, Under 206.9 kip lateral load or 2069 kip-ft unbalanced moment, first yielding of steel on bottom tensile side at the vicinity of the column have occurred on Model-4 with a top lateral deflection of 0.59 in and drift ratio of 0.49% which is within the limiting drift ratio and having concrete tensile damage of 33% at both top and bottom tensile sides of slab. In Model-4, it can take maximum 248.1 kip lateral load or 2481 kip-ft unbalanced moment with a top lateral deflection of 1.47 in and drift ratio of 1.23% which is beyond the limiting drift ratio and have full concrete tensile damage at the bottom tensile side of slab before punching shear failure have occurred.

From Figs. 6.2 to 6.8 and from the above analysis on both gravity and lateral loads it is evident that Model-4 having seismic detailing with drop panel have more strength and can take more gravity loads and lateral loads or unbalanced moment and it can also sustain more drift than the other three models.

6.4 Elastic Analysis of Flat-Plate Structures under Combined Gravity and Lateral Loads

In case of high-rise building structure up to fourteenth storey having flat plate slab system of large span length is affected by lateral load due to seismic load. For such type of flat plate structures in regions of high seismic risk, the design considering only gravity load based on direct design method is safe and efficient up to which floor level have discussed in this section. Better lateral load carrying system such as shear wall is discussed on flat plate high-rise building structure to resist most efficiently the various combinations of gravity and lateral loading. Computer software 'ETABS' have used for equivalent frame analysis based on elasticity under same geometric property and material property as discussed in Sec. 6.2. Finally investigate the results from analysis considering seismic Zone-2 and Zone-3 according to BNBC (2006) for seismic response and recheck the percentage of moment for column strip and middle strip under gravity and lateral loads.

6.4.1 Flat-plate structure behave as a moment resisting frame under combined gravity and lateral loads

Flat plate structures whereas the columns are cast integrally with the floor slabs behave similar to moment resisting frames under horizontal loading. The lateral deflections of the structure are a result of simple double curvature bending of the columns and a more complex three-dimensional form of double bending in the slab. The response of the structure can be studied by considering each bay-width replaced by an equivalent frame bent. The slab is replaced for the analysis by an equivalent beam with the same double bending stiffness as shown in Fig. 6.9. The horizontal stiffness of such a frame is governed mainly by the bending resistance of the slab-column connections. The accumulated horizontal shear above any story of a frame is resisted by shear in the columns of that story. The shear causes the story-height columns to bend in double curvature with points of contraflexure at approximately mid-story-height levels. The moments applied to joint from the columns above and below the slab are resisted by the slab both sides, which also bend in double

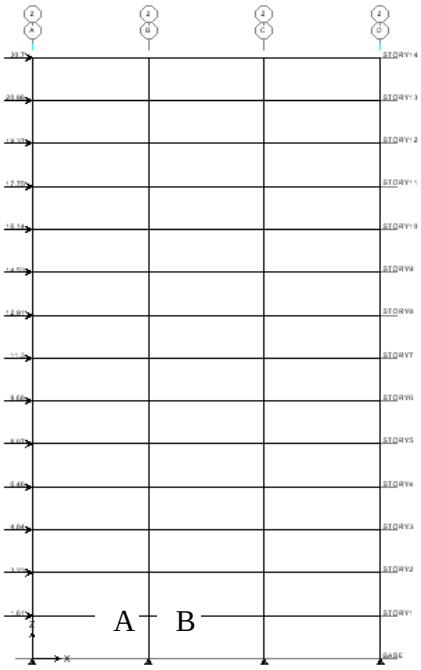

Figure 6.9 Flat plate structure similar to moment resisting frame under horizontal loading

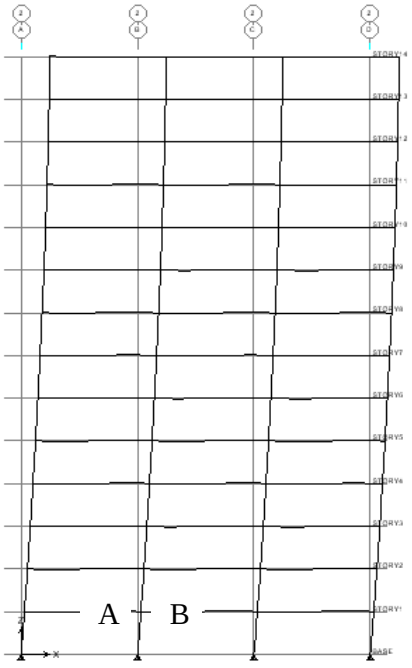

Figure 6.10 Overall deflected shape of moment resisting frame

curvature, with points of contraflexure at approximately midspan. These deformations of the columns and slabs allow racking of the frame and horizontal deflection in each story. The overall deflected shape of a moment resisting frame due to racking has a shear configuration with concavity in upward direction, a maximum inclination near the base and a minimum inclination at the top of the structure as shown in Fig. 6.10.

Based on direct design method, flat plate slab system with interior panel considering same geometry as discussed in Sec. 6.2 column strip negative moment is 355 kip-ft due to only gravity loads considering load combination of Equation (6.1). However, due to combined gravity and lateral loads considering load combinations of Equation (6.4) and Equation (6.5) more negative unbalanced moments and positive unbalanced moments have come at slab-column joint respectively. In Fig. 6.9, side 'A' and side 'B' have specified at bottom storey level of an interior panel slab-column connection whereas the unbalanced moments have compared because of maximum moment will come at bottom storey level due to lateral loads. The unbalanced moment due to only gravity loads and combined gravity and lateral loads at side 'A' and side 'B' of bottom storey level considering up to fourteen storied building is given in Table 6.1. In Table 6.1, up to which storey level is safe among all thirteen buildings up to fourteen stories for design by using direct design method of flat plate structures can be decided easily by making a comparison in between two unbalanced moments at bottom storey level due to only gravity loads and combined gravity and lateral loads.

Table 6.1 Unbalanced moments due to only gravity loads and combined gravity and lateral loads at side 'A' and side 'B' of bottom storey level

Storey	Unbalanced Moment (kip-ft) at Bottom Storey Level of Side 'A'			Unbalanced Moment (kip-ft) at Bottom Storey Level of Side 'B'		
	Due to Only Gravity Loads	Due to Combined Gravity and Lateral Loads	Remarks	Due to Only Gravity Loads	Due to Combined Gravity and Lateral Loads	Remarks
Two Storied Building	-355	-384	Not safe	-355	-150	Safe
Three Storied Building	-355	-426	Not safe	-355	+6.76	Not safe
Four Storied Building	-355	-467	Not safe	-355	+49	Not safe
Five Storied Building	-355	-507	Not safe	-355	+89.5	Not safe
Six Storied Building	-355	-545	Not safe	-355	+127	Not safe
Seven Storied Building	-355	-579	Not safe	-355	+162	Not safe
Eight Storied Building	-355	-610	Not safe	-355	+194	Not safe
Nine Storied Building	-355	-639	Not safe	-355	+223	Not safe
Ten Storied Building	-355	-666	Not safe	-355	+251	Not safe
Eleven Storied Building	-355	-691	Not safe	-355	+276	Not safe
Twelve Storied Building	-355	-715	Not safe	-355	+300	Not safe
Thirteen Storied Building	-355	-737	Not safe	-355	+323	Not safe
Fourteen Storied Building	-355	-758	Not safe	-355	+344	Not safe

6.4.2 Flat-plate structure with shear wall

A shear wall structure is considered to be one whose resistance to horizontal loading is provided entirely by shear walls and floors acting as horizontal diaphragms transmit lateral loads equally to the shear walls. The walls may be part of a service core or a stairwell, or they may serve as partitions between accommodations as shown in Fig. 6.9. They are usually continuous down to the base to which they are rigidly attached to form vertical cantilevers. Their high inplane stiffness and strength makes them well suited for carrying gravity loading simultaneously. The distribution of lateral forces to the shear walls is a function of the geometrical arrangement of the resisting wall systems. It is usual to locate the walls on plan so that they attract an amount of gravity loading sufficient to suppress the maximum tensile bending stresses in the wall caused by lateral loading. If the resultant of the lateral forces acts through the centroid of a building's relative stiffness, only translational reaction will be generated. The most obvious case is the symmetrical pure shear wall building. In a moment resisting frame with shear wall, the shear may be assumed to be resisted completely by the core as a first approximation. This is because its stiffness is so much greater than the lateral stiffness of the frame. On the other hand, if the shear wall arrangement is asymmetrical, the resultant lateral force does not act through the centroid of the building's stiffness. Rotation of the shear walls in addition to translation will be generated. The distribution of the stresses is dependent on the shape of the shear wall system.

The lateral rigidity is greatly improved to resist lateral forces by using not only the shear wall but also for combined shear wall and rigid frame system. The total deflection of the interacting shear wall and rigid frame systems is obtained by superimposing the individual modes of deformation as shown in Fig. 6.12. In case of moment resisting frame, the slope of the deformation is greatest at the base of the structure where the maximum shear is acting. On the other hand in case of shear wall, the slope of the deflection is greatest at the top of the building, indicating that in this region, the shear wall system contributes the least stiffness. However, the interaction of frame and shear wall is obtained by superimposing the separate

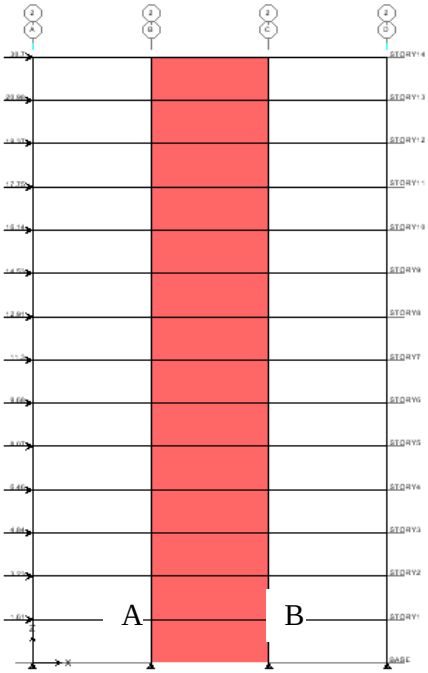

Figure 6.11 Flat plate structure similar to moment resisting frame with shear wall under horizontal loading

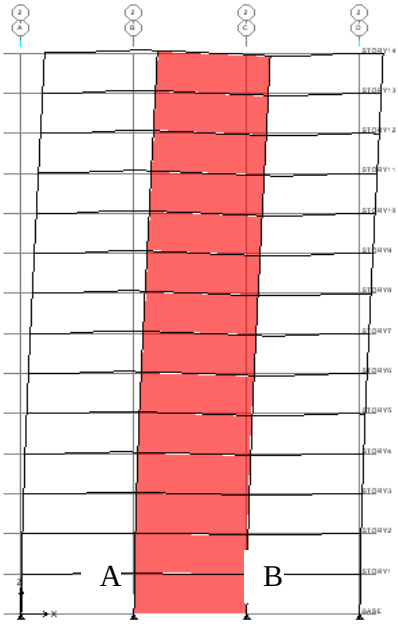

Figure 6.12 Overall deflected shape of moment resisting frame with shear wall

deflection modes resulting in a flat-S-curve. Because of the different deflection characteristics of shear wall and frame, the shear wall is pulled back by the frame in the upper portion of the building, and pushed forward in the lower.

Same as Sec. 6.4.1 based on direct design method, flat plate slab system with interior panel considering same geometry as discussed in Sec. 6.2 column strip negative moment is 355 kip-ft due to only gravity loads considering load combination of Equation (6.1). However, by using shear wall with flat plate structure subjected to combined gravity and lateral loads considering load combinations of Equation (6.4) and Equation (6.5) a very few unbalanced moments have come at slab-column joint. In Fig. 6.11, side 'A' and side 'B' have specified again at bottom storey level of an interior panel slab-column connection whereas the unbalanced moments have compared. The unbalanced moment due to only gravity loads and combined gravity and lateral loads at side 'A' and side 'B' of bottom storey level considering up to fourteen storied building is given in Table 6.2. After investigate the results from Table 6.2, it can be decided that by using shear wall in a flat plate structures can minimize the unbalanced moments at bottom storey level for up to fourteen storied building and can design the building safely by using direct design method of flat plate structures under combined gravity and lateral loads.

From the above discussion it is evident that shear wall is stiffer than moment resisting frame. That is why, maximum amount of unbalanced moment have transferred through shear wall and minimum amount of unbalanced moment have transferred through slab-column joint. From various observations on flat plate structure with shear wall by different researchers, an approximate percentage of moment has decided to transfer through shear wall and slab-column joint. About 80% unbalanced moment have transferred through shear wall and rest 20% have transferred through slab-column joint. Considering same geometry and material properties as discussed in Sec. 6.2, a fourteen storied flat plate structure having shear wall is analyzed by using 'ETABS' software under combined gravity and lateral loads considering seismic Zone-2 and Zone-3 according to BNBC 2006 for seismic response. All calculations are given in *Appendix B*. Comparing the moment at

interior slab-column joint from the above discussed analysis considering combined gravity and lateral loads with the moment at same joint considering only gravity load based on direct design method, a satisfactory and safe result have come at seismic Zone-2. From analysis, the maximum moment considering load combination as given in Eq. (6.4) and Eq. (6.5) is 350 kip-ft and 240 kip-ft respectively. The moment capacity for only gravity load based on direct design method is 355 kip-ft and which is more than the result from Eq. (6.4) and Eq. (6.5). That is why, the flat plate structure having shear wall can design only for gravity load based on direct design method at seismic Zone-2 without having any risk. However, the unbalanced moment due to combined gravity and lateral loads at seismic Zone-3 has exceeded the moment from direct design method considering only gravity load. From analysis, the maximum moment considering load combination as given in Eq. (6.4) and Eq. (6.5) is 405 kip-ft and 295 kip-ft respectively. The moment capacity for only gravity load based on direct design method is 355 kip-ft and which is less than the result from Eq. (6.4). So, the direct design method cannot be used in case of fourteen storied flat plate building having large span at seismic Zone-3 which is most vulnerable for seismic action in Bangladesh even though there have the shear wall structure.

Table 6.2 Unbalanced moments due to only gravity loads and combined gravity and lateral loads at side 'A' and side 'B' of bottom storey level

Storey	Unbalanced Moment (kip-ft) at Bottom Storey Level of Side 'A'			Unbalanced Moment (kip-ft) at Bottom Storey Level of Side 'B'		
	Due to Only Gravity Loads	Due to Combined Gravity and Lateral Loads	Remarks	Due to Only Gravity Loads	Due to Combined Gravity and Lateral Loads	Remarks
Two Storied Building	-355	-269	Safe	-355	-265	Safe
Three Storied Building	-355	-270	Safe	-355	-263	Safe
Four Storied Building	-355	-271	Safe	-355	-262	Safe
Five Storied Building	-355	-273	Safe	-355	-261	Safe
Six Storied Building	-355	-274	Safe	-355	-259	Safe
Seven Storied Building	-355	-275	Safe	-355	-258	Safe
Eight Storied Building	-355	-277	Safe	-355	-257	Safe
Nine Storied Building	-355	-278	Safe	-355	-255	Safe
Ten Storied Building	-355	-279	Safe	-355	-254	Safe
Eleven Storied Building	-355	-281	Safe	-355	-252	Safe
Twelve Storied Building	-355	-282	Safe	-355	-251	Safe
Thirteen Storied Building	-355	-283	Safe	-355	-250	Safe
Fourteen Storied Building	-355	-285	Safe	-355	-248	Safe

6.4.3 Percentage of moment transfer through different strip of flat-plate slab system under gravity and lateral loads

As discussed in Sec. 6.2.1 regarding the percentages of moment due to gravity load transfer through different strip of flat-plate slab system based on direct design method, an analysis has done in this section by using 'ETABS' software to check the percentage of moment transfer through column strip and middle strip and also recheck the amount of total moments due to lateral load have transferred through column strip and effective width.

A graphical representation of moments under gravity load is given below:

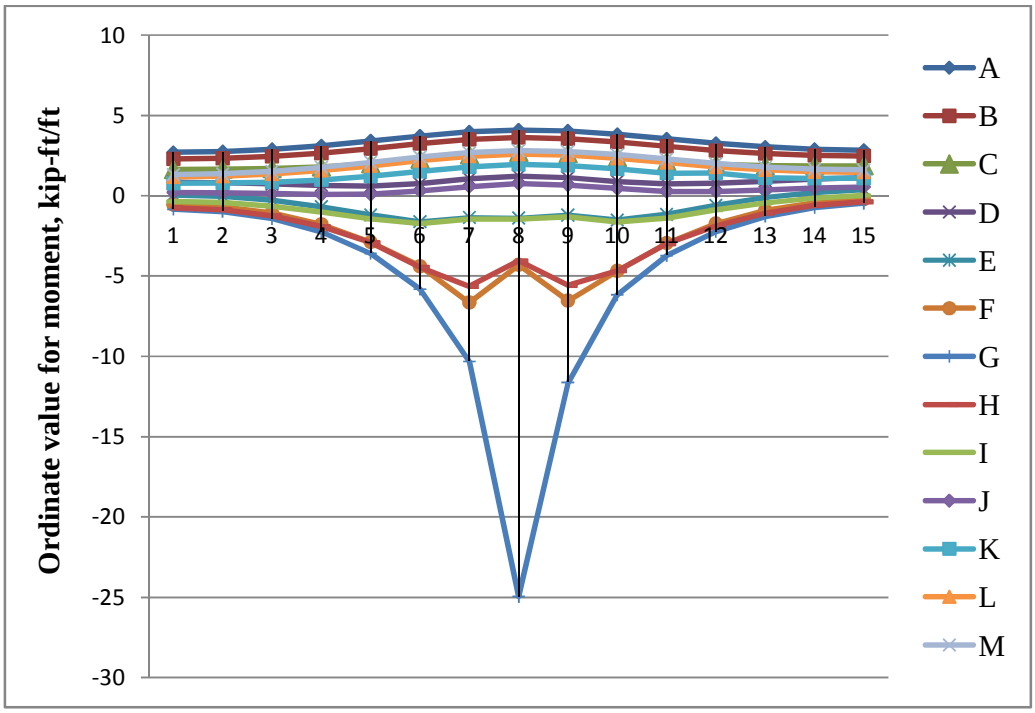

Figure 6.13 Ordinate value for moment in kip-ft/ft under gravity load along the interior panel of flat plate structure

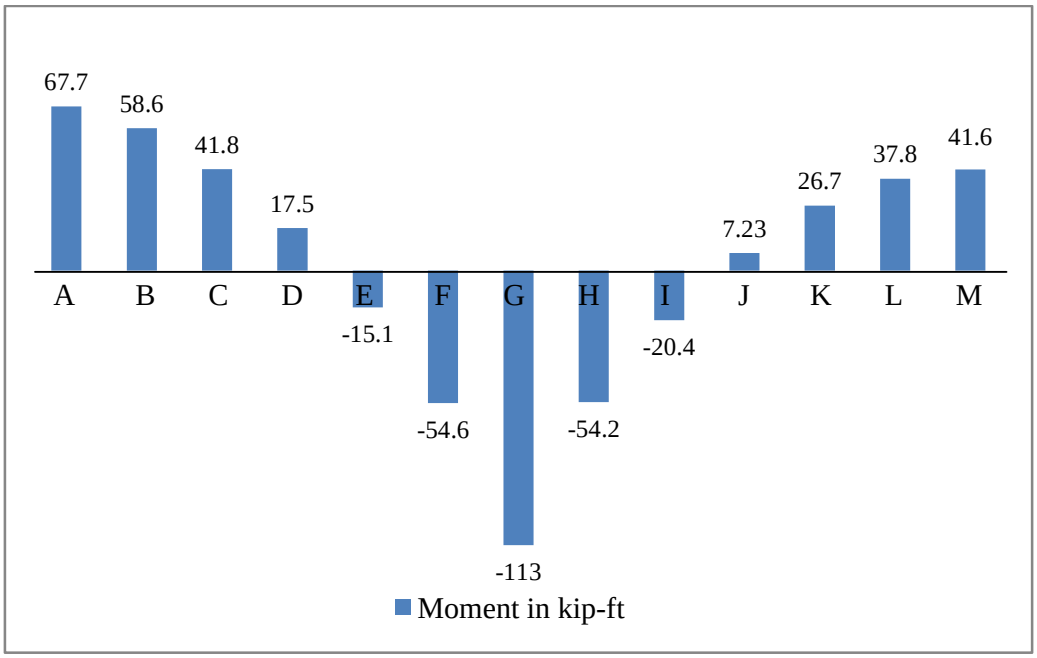

Figure 6.14 Moment in kip-ft under gravity load along the interior panel of flat plate structure

Under gravity load the percentages of moment are given below:

Negative factored moment ..... 67.4% of total factored static moment
Positive factored moment..... 32.6% of total factored static moment
Column strip negative moment..... 83.7% of negative factored moment
Middle strip negative moment..... 16.3% of negative factored moment
Column strip positive moment..... 53% of positive factored moment
Middle strip positive moment..... 47% of positive factored moment

There are some differences in between the above discussed percentages of moment and the percentages of moment based on direct design method as discussed in Sec. 6.2.1 for an interior panel.

A graphical representation of moments under lateral load is given below:

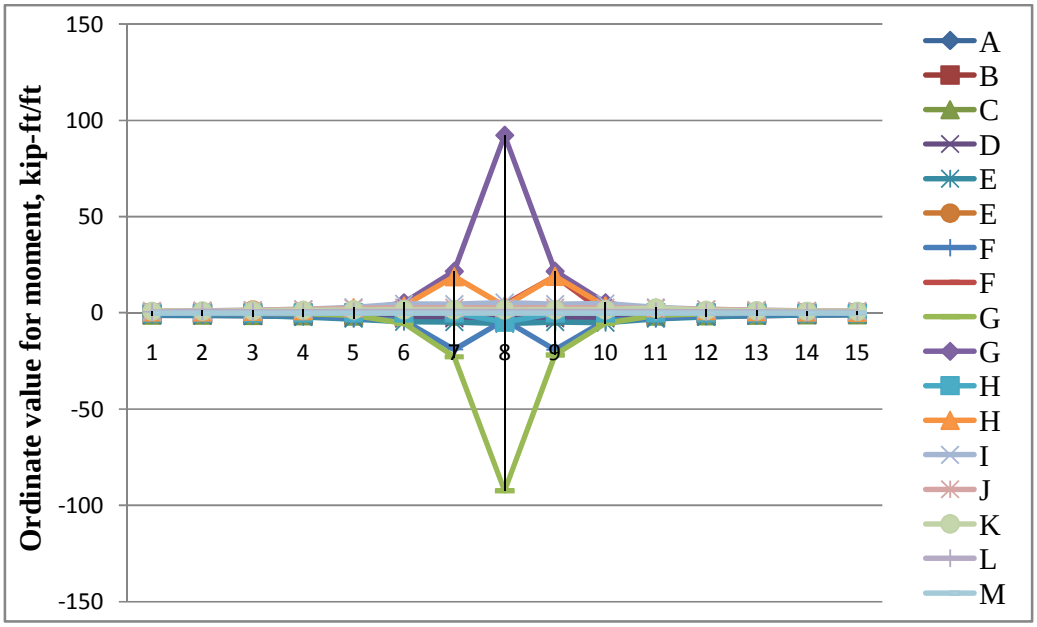

Figure 6.15 Ordinate value for moment in kip-ft/ft under lateral load along the interior panel of flat plate structure

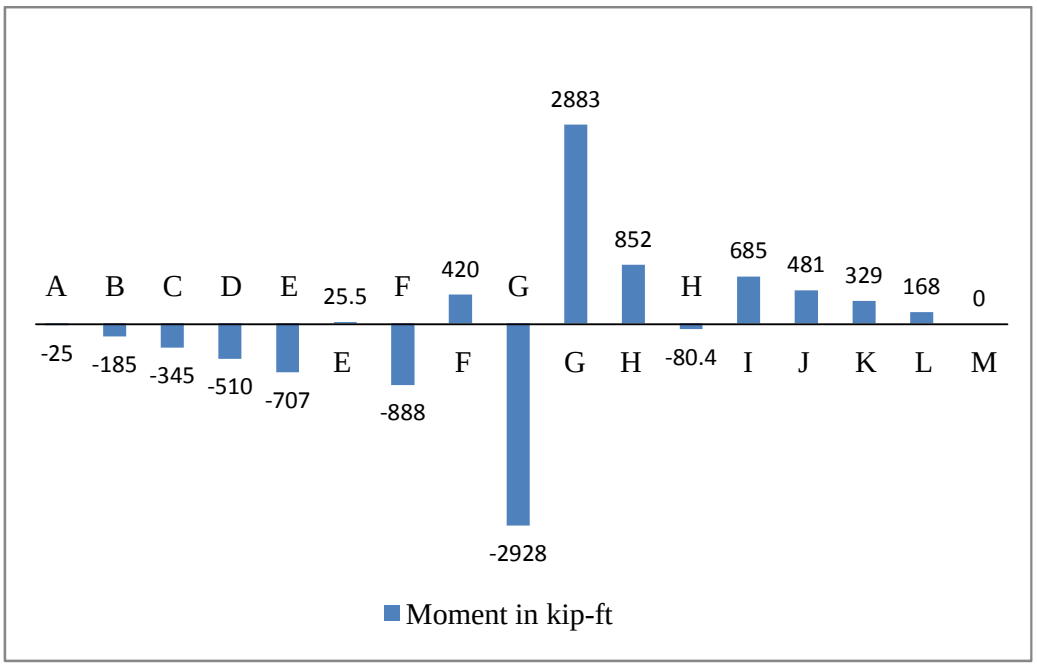

Figure 6.16 Moment in kip-ft under lateral load along the interior panel of flat plate structure

Again, under lateral load the percentages of unbalanced moment are given below:

Negative moment..... 100% at one side of the supporting end
Column strip negative moment..... 98.6% of negative moment
Middle strip negative moment..... 1.4% of negative moment
Positive moment..... 100% at other side of the supporting end
Column strip positive moment..... 99.1% of positive moment
Middle strip positive moment..... 0.9% of positive moment

From the above discussed percentages of moment in case of positive or negative moments for column strip, it can be decided that about 100% moment due to lateral load have transferred through column strip. It is also observed that in case of negative moment about 82% of column strip negative moment has transferred through effective width (c+3h) and 18% of column strip negative moment has transferred through rest of column strip. Similarly, in case of positive moment about 82.4% of column strip positive moment has transferred through effective width (c+3h) and 17.6% of column strip positive moment has transferred through rest of column strip.

6.5 Remark

Four separate slab-column joint of RC flat plates has been modeled numerically by using 'ABAQUS' software based on nonlinear finite element method and some numerical analysis has been performed to understand the behaviour of slab-column connections and the failure mechanisms under gravity or lateral loads. From numerical results it is evident that Model-4 having seismic detailing with drop panel have more strength and can take more gravity loads and lateral loads or unbalanced moment and it can also sustain more drift than the other three models. Most of the cases of loading history up to failure, Model-1 and Model-2 behaviour are similar as both models contain same amount of flexural reinforcement. In similar way, Model-3 behaviour is very close to Model-1 as Model-3 is not fully maintaining the ACI 318 (2008) code provisions. It is observed that the concentration of flexural reinforcement in the vicinity of the column seems to lead to a very small increase in the punching shear strength. This is because of the bar spacing has reduced and exceed the limit as specified by ACI 318-08 code provision, where the reinforcement ratio through effective width and column strip have exceed 37.5% of balanced steel ratio ($0.375\rho_b$) and has a net tensile strain less than 0.01 that generally indicates the overstress conditions on the joint.

The lateral displacements of the flat plate structure during seismic load will result in significant additional unbalanced moments in the slab-column joint. These additional unbalanced moments aggravate the potential for punching shear failure. From analysis it is found that for flat plate high-rise building having large span length, the slab-column joint is not sufficient to resist unbalanced moments under seismic load. However, combined shear wall and moment frame system have been shown better performance by minimizing the unbalanced moment at different story level to resist lateral forces. The flat plate high-rise building structure with shear wall has been designed only for gravity load based on direct design method may satisfy at seismic Zone-2 according to BNBC (2006) under combined gravity and lateral loads. On the other hand, it may not be satisfied at seismic Zone-3 according to BNBC (2006) under combined gravity and lateral loads even though there have

the shear wall structure. Therefore, the designer must careful on seismic Zone-3 according to BNBC (2006) which is most vulnerable zone for seismic action in Bangladesh.

The percentages of moment from present analysis which plays on column strip and middle strip is slightly different from moment as specified by direct design method under gravity loads. In case of lateral load it is found that about 100% moment has transferred through column strip where the significant amount (82%) of column strip moment has passed through effective width.

Chapter 7

CONCLUSIONS AND RECOMMENDATIONS

7.1 General

The performance of a numerical model to simulate behaviour of slab-column joint of RC flat plate based on nonlinear finite element method under gravity and lateral loads by using ABAQUS (2007) software has been investigated in this thesis. The numerical model is capable of predicting the behaviour of slab-column connection from linear to nonlinear stage through development of stresses, damage of concrete and degradation of strength. Parametric studies has been carried out considering different material and geometric parameters and also see the performance of slab-column connection with seismic detailing provisions of different building codes. The outcome of this thesis will be helpful to the design community to establish some restrictive rules for flat plate system in earthquake prone region and designing the connection.

7.2 Findings of the Work

The following findings are observed in this research work:

1) The behaviour of numerical model such as cracking pattern and tensile or compressive damage of concrete due to applied load, development of stresses and the load-deflection graph at centre of plate represents a good agreement with the test data.

2) Finite element results show slightly higher stiffness than the experimental results. This may be due to non-availability of some data used in the FE modeling. However, the effects of bond slip (between concrete and reinforcement), dowel action and aggregate interlock were absent in the finite element modeling.

3) All slabs specified in this thesis are modeled numerically by using Abaqus-Explicit approach. Explicit method requires a small time increment size that depends solely on the highest natural frequencies of the model and is independent of the type and duration of loading. The use of small increments is advantageous because it allows the solution to process without iterations and without requiring tangent stiffness matrices to be formed.

4) For a given reinforcement ratio and yield strength of steel, ultimate load increases with the increase in concrete compressive strength up to a certain limit. The increase in ultimate load is more prominent with lower strength concrete compared to higher strength concrete for different steel ratios.

5) From analysis, it is found that shear strength is proportional to $\sqrt{f'_c}$ which is similar with ACI 318 (2008) code equation and shear strength according to ACI 318 (2008) code equation is similar to ultimate load capacity having tension reinforcement ratio 0.5%. It has also been observed that an increase in tension reinforcement ratio above 0.5% increases the ultimate punching load capacity and ACI code underestimates the actual capacity.

6) Flexural reinforcement ratio has an important effect on punching shear strength of RC flat plates. Punching capacity increases with the increase of the percentage of flexural reinforcement. From analysis, it is seen that from plain concrete to lower percentage of reinforcement, slab load-carrying capacity has been increased rapidly whereas for higher percentage of reinforcement, this increase is gradual. Therefore, the increase in ultimate load is more prominent with lower percentage of reinforcement compared to higher percentage of reinforcement.

7) The punching load is not influenced by the yield strength of the flexural reinforcement if the slab does not experience yielding.

8) The influence of compression reinforcement on the ultimate load carrying capacity is not so significant. It has also been found that due to presence of compression steel there is also no significant change in stiffness and ductility.

9) Thickness is an important factor affecting the punching load capacity of a reinforced concrete flat plate where by increasing slab thickness punching shear strength is increased. From analysis, it is found that the increase in ultimate load is more prominent with lower slab thickness compared to higher slab thickness and it decreases with the increase of slab thickness.

10) The failure of slab-column joint has been observed to be different for different span-depth ratio. At lower slab thickness, flexure governs the failure. On the other hand, at higher slab thickness, shear governs the failure.

11) The increase in square column size and the longer side for rectangular column have increased the stiffness on slab-column joint and ultimate load carrying capacity. The increase in ultimate load is more prominent with smaller size square column compared to larger size square column. The benefit of increasing the longer side of rectangular column keeping the shorter side unchanged has been found to be insignificant in increasing punching capacity.

12) It is observed that increase in square column size increases the ultimate load capacity and the increase is almost proportional to punching perimeter. The capacity of a square column is significantly higher than the capacity of a rectangular column having same cross sectional area even though the rectangular section has higher punching perimeter.

13) The support condition has a significant influence on the punching shear strength of reinforced concrete flat plates. Different boundary condition has different influence on the punching capacity of slab-column connection. Therefore, boundary condition also is an important part of the model slab to get realistic result.

14) ACI 318-08 code formula for punching shear strength has been found to be conservative. Thus, there is a scope for improvement of shear strength computation formula of ACI 318-08 code.

15) A modified equation as suggested by Tian et al. (2008) to predict punching shear capacity has been investigated. Present study finds good correlation between FE results and those obtained by suggested equation. It is found that the contributions of concrete strength is best described by assuming connection punching capacity to be proportional to $(f'_c)^{0.25}$ instead of $\sqrt{f'_c}$ and strength of slab tensile reinforcement and c/d significantly affect the connection strength, as suggested by Tian.

16) The suggested equation of Tian to predict punching shear capacity appears to be safe when a reduction factor is used.

17) A modified equation has been proposed in the current work which is similar to that suggested by Tian et al. (2008) with some minor modification to predict punching shear capacity for rectangular column. The proposed modified equation for rectangular columns has been found to predict punching capacity correctly.

18) Four different slab-column joints of RC flat plates have been modeled numerically under different design specifications and analyzed to study the effects of different load combinations and loading sequence. From analysis, it is found that flat plate high-rise building structure might not be possible to design without drop panel.

19) No significant change have been found for slab-column joint of RC flat plate by considering fifty percent column strip reinforcement is passing through effective width (c+3h) which is designed based on direct design method under only gravity load.

20) It is observed that the concentration of flexural reinforcement in the vicinity of the column seems to lead to a very small increase in the punching shear strength, where the bar spacing has reduced and exceed the limit as specified by ACI 318-08 code provision.

21) From analysis it is found that for flat plate high-rise building having large span length, the slab-column joint is not sufficient to resist unbalanced moments under seismic load. However, combined shear wall and moment frame system have been shown better performance by minimizing the unbalanced moment at different story level to resist lateral forces.

22) The flat plate high-rise building structure with shear wall has been designed only for gravity load based on direct design method may satisfy at seismic Zone-2 according to BNBC (2006) under combined gravity and lateral loads. On the other hand, it may not be satisfied at seismic Zone-3 according to BNBC (2006) under combined gravity and lateral loads even though there have the shear wall structure.

23) In present analysis, it is found that the percentages of moment plays on column strip and middle strip is slightly different from moment as specified by direct design method under gravity loads and for lateral load it is found that about 100% moment have been transferred through column strip where the significant amount (82%) of column strip moment have passed through effective width (c+3h).

7.3 Conclusions

The following conclusions may be derived from this research work:

1) Numerical modeling of slab-column joint with emphasis on punching shear behaviour of reinforced concrete flat plates by using 'ABAQUS' software based on nonlinear finite element method has been done successfully and the numerical results have shown a good correlation with available experimental and numerical results.

2) A parametric study has been carried out considering different material and geometric parameters and after identifying effect of these parameters on the

behaviour of slab-column connection, an improvement is proposed on punching shear prediction equation of ACI 318 (2008)/BNBC (2006) code.

3) A study has been carried out to see the performance of slab-column connection designed considering seismic load. It has been found that strength of slab-column connection improves if seismic design is performed.

7.4 Recommendations for Future Studies

The following recommendations are made for future investigations:

1) The present study is only based on interior panel of flat plate slab system. Further research can be done by considering exterior or corner panel with or without edge beam and having column capital.

2) Skew plate and flat plate with opening can also be modeled numerically for the future research work.

3) Shear reinforcement has a significant effect on the punching shear strength of flat plate slab system. It increases ductility of the slab during failure. Therefore, further research work can be done by include shear reinforcement in the numerical model.

4) Post-punching failure is characterized by large deformation. Only material nonlinearity cannot represent the actual phenomena after punching shear failure. Therefore, geometric nonlinearity also needs to be included in the numerical model to get the realistic result.

5) A perfect bond have considered in between concrete and steel reinforcement in case of numerical model. Therefore, there have no slip as the experimental result have shown and that is why, the numerical result is stiffer than experimental result. In future analysis the bond should be relax by modify the numerical model.

6) In this study static nonlinear analysis has followed. For more investigation it can be extended to dynamic analysis.

REFERENCES

Abaqus Theory Manual (Volume-I-V), "Version 6.7", Simulia, USA, 2007.

ACI 318 (2008), "Building Code Requirements for Reinforced Concrete", American Concrete Institute, Farmington Hills, Michigan.

Adams, V. and Askenazi, A. (1998), Building Better Products with Finite Element Analysis, OnWord Press, 1999.

Aexander, S. D. B. and Simmonds, S. H. (1992), "Tests of Column-Flat Plate Connections", ACI Structural Journal, Bol. 89, No.5, pp. 495-502.

Aghayere, A. O. and MacGregor, J. G. (1990a), "Analysis of Concrete Plates under Combined in Plane and Transverse Loads", ACI Structural Journal, Vol. 87, No.5, pp. 539-547.

Aghayere, A. O. and MacGregor, J. G. (1990b), "Tests of Reinforced Concrete Plates under Combined In plane and Transverse Loads", ACI Structural Journal, Vol. 87,No.6, pp. 615-622.

AISI (1964) Anchorage and Alaska Earthquake.

Alam, A. K. M. J. (1997), "Punching Shear Behaviour of Reinforced Concrete Slabs", M. Sc Engineering Thesis, BUET, pp. 1-12.

Ali, M. A. and Alexander, S. D. B. (2002), "Behavior of Slab-Column Connections with partially Debonded Reinforcement under Cyclic Lateral Loading", Structural Engineering Report No. 243, University of Alberta, Jan. 2002,137 pp.

American Concrete Institute, Punching Shear in Reinforced concrete Slabs. ACI Structural Journal and ACI Material Journal.

Andra, H. P. (1982). On the behavior of Auflagerbereichs of flat slabs. Thesis, Univ--ersity of Stuttgart.

Australian Standard (AS) 3600-1988, Concrete Structures.

Bangladesh National Building Code (BNBC 2006), Housing and Building Research Institute and Bangladesh Standards and Testing Institution, Dhaka, Bangladesh.

Bangash, M. Y. H. (1989), Concrete and Concrete Structures: Numerical Modeling and Applications, Elsevier Science Publishers Ltd., London, England.

Banici, B. and Bayrak, O. B. (2003), "Punching Shear Strengthening of Reinforced Concrete Flat Plates Using Carbon Fiber Reinforced Polymers", ASCE Journal of Structural Engineering, Vol.129, No.9, pp.1173-1182.

Bathe, K. J. (1996), Finite Element Procedures, Prentice Hall, Upper Saddle River, New Jersey 07458, United States of America.

Bazant, Z. P. and Cao, Z. (1987), "Size Effect in Punching Shear Failure of Slabs", ACI Structural journal, January-February 1987, pp. 44-53.

Bortolotti, L. (1990), "Punching Shear Strength in Concrete Slabs", ACI Structural Journal, Vol. 87, No.2, pp. 208-219.

Broms, C. E. (1990a), "Punching of Flat Plates-A Question of Concrete Properties in Biaxial Compression and Size Effect", ACI Structural Journal, Vol. 87, No.3, pp. 292-304.

Broms, C. E. (1990b), "Shear Reinforcement for Deflection Ductility of Flat Plates", ACI Structural Journal, Vol. 87, No.6, pp. 696-705.

Broms, C. E. (2000), “Elimination of Flat Plate Punching Failure Mode”, ACI Structural Journal, Vol. 97, No.1, pp. 94-101.

Brown, S. J. and Dilger, W. H. (1994), “Seismic Response of Flat Plate Column Connections”, Proc., Canadian Society for Civil Engineering Annual Conference, Vol. 2, Winnipeg, pp. 388-397.

Brown, S. J. (2003), “Seismic Response of Slab Column Connection”, Ph.D. Thesis, University of Calgary, Calgary, pp. 341.

Brown, S. J. and Dilger, W. H., (2004), “Design of Slab-Column Connections to Resist Seismic Loading”, Proc., 13th World Conference on Earthquake Engineering, Paper 2832, Vancouver, pp. 13.

BS 8110 (1985), “Structural use of Concrete: Part 1: Code of Practice for Design and Construction,” British Standard Institution, London.

CAN3-A23.3-M84 (1984), “Design of Concrete for Buildings”, Canadian Standards Association, Rexdale.

CEB-FIP (1978), “Model Code foe concrete Structures”, International Committee of the Euro- concrete, Cement and Concrete Association, London.

CEB-FIP, “Model Code 1990”, Thomas Telford, London 1993.

Chen, W. F. (1982), Plasticity in Reinforced Concrete. McGraw-Hill Book Company, Inc. USA.

Cicekli, U., Voyiadjis, G. Z. and Rashid, K. A. A. R. (2007), “A plasticity and anisotropic damage model for plain concrete”, International Journal of Plasticity 23 (2007), pp. 1874–1900.

Coa, H. (1993), “Seismic Design of Slab Column Connection”, M.Sc. Thesis, University of Calgary, Calgary, pp. 185.

Dechka, D. C. (2001), “Response of Shear-Stud-Reinforced Continuous Slab-Column Frames to Seismic Loads”, Ph.D. Thesis, University of Calgary, Calgary, pp. 448.

Dilger, W. H. and Coa, H. (1994), “Behavior of Slab-Column Connections under Reversed Cyclic Loading”, Proc., 5th International Colloquium on Concrete, Cairo, Egypt, pp. 595-606.

Dilger, W. H. and Brown, S. J. (1995) “Earthquake Resistant Slab-Column Connections”, Festschrift Prof. Dr. HugoBachman, Institute of Structural Analysis und construction of new products, ETH Zurich, Sept., pp. 22-27.

EI-Salakawy, E. F., Polak, M. A. and Soudki, K. A. (2003), “New Shear Strengthening Technique for Concrete Slab-Column Connections”, ACI Structural Journal, Vol. 100, No.3, pp. 297-304.

Elgabry, A. A. and Ghali, A. (1990), “Design of Stud-Shear Reinforcement for Slabs”, ACI Structural Journal, Vol. 87, No.3, pp. 350-361.

Elstner, R. C. and Hognestad, E. (1956), “Shearing Strength of Reinforced Concrete Slabs”, ACI Structural Journal, Vol. 28, No.1, pp. 29-58.

Gardner, N. J. (1990), “Relationship of the Punching Shear Capacity of Reinforced Concrete Slabs with Concrete Strength”, ACI Structural Journal, Vol. 87, No.1, pp. 66-71.

Ghali, A., Elmasri, M. Z. and Dilger, W. H. (1976), “Punching of Flat Plates under Static and Dynamic Horizontal Forces”, ACI Journal, Proceedings, V. 73, No. 10, Oct. 1976, pp. 566-572.

Ghonoim, M. G. and MacGregor, J. G. (1994a), “Tests of Reinforced Concrete Plates Under Combined In plane and Lateral Loads”, ACI Structural Journal, Vol. 91, No.1, pp. 19-30.

Ghonoim, M. G. and MacGregor, J. G. (1994b), “Behaviour of Reinforced Concrete Plates Under Combined In plane and Lateral Loads”, ACI Structural Journal, Vol. 91, No.2, pp. 188-197.

Gonzalez-Vidosa, F., Kotsovos, M. D. and Pavlovie, M. N. (1988), “Symmetrical Punching of Reinforced Concrete Slabs: An Analytical Investigation Based on Nonlinear Finite Element Modeling”, ACI Structural Journal, May-Jun 1988, pp. 241-250.

Graf, O. (1938), Experiments on the hardiness of all sides lying thick iron-concrete slabs under concentrated loads. German Committee for Reinforced Concrete, Half 88.

Hammill, N. and Ghali, A. (1994), “Punching Shear Resistance of Corner Slab-Column Connections”, ACI Structural Journal, Vol. 91, No.6, pp. 697-707.

Harmon, T. G. and Zhangyuan, N. (1989), “Shear Strength of Reinforced Concrete Plates and shells Determined by Finite Element Analysis Using Layered Elements”, ASCE Journal of Structural Engineering, Vol. 115, N0.5, pp. 1141-1157.

Hawkins, N. M., Mitchell, D. and Hanna, S. H. (1975), “The Effect of Shear reinforcement on the Reversed Cyclic Loading Behavior of Flat Plate Structures”, Canadian Journal of Civil Engineering, Vol. 2, pp. 572-582.

Hillerborg, A. (1983), “Analysis of one single crack,” Fracture Mechanics of Concr--ete, ed. Y. Wittmann, and F. H. Elsevier, pp. 223-249, Amsterdam.

Hordijk, D. A. (1992), “Tensile and tensile fatigue behaviour of concrete; experime--nts, modeling and analysis”, Heron 37 (1), pp. 3-79.

Hueste, M. B. D. and Wight, J. K. (1999), “Nonlinear Punching Shear Failure Model for Interior Slab-Column Connections,” ASCE Journal of Structural Engineering, Vol. 125, No.9, pp. 997-1008.

Islam, D. S. M. S. (2004) “Nonlinear FiniteElement Analysis of Reinforced Concrete Plates in Punching Shear”, M.Sc Engineering Thesis, BUET, PP-1-30.

Jofriet, J. C., and McNeice, G. M. (1971), “Finite element analysis of reinforced concrete slabs.” *J. Struct. Div. ASCE*, 97(3), 785–806.

Kinnunen, S. and Nylander, H. (1960), “Punching of concrete slabs without shear reinforcement”. Transactions 158, Royal Institute of Technology, Stockholm.

Kinnunen, S. (1963), “Punching of concrete slabs with two-way reinforcement”. Transactions of Royal Institute of Technology, 198.

Kuang, J. S. and Morley, C. T. (1992), “Punching Shear Behaviour of Restrained Reinforced Concrete Slabs,” ACI Structural Journal, Vol. 89, No.1, pp. 13-19.

Kupfer, H. B. and Gerstle, K. H. (1973), “Behaviour of Concrete under Biaxial Stre--sses”, Journal of the Engineering Mechanics Division, Vol. 99, pp. 853-866.

Lee, J. and Fenves, G. L. (1998), “Plastic-damage model for cyclic loading of concr--ete structures”, Journal of Engineering Mechanics, Vol. 124 (8), pp. 892-900.

Loo, Y. C. and Falamaki, M. (1992), “Punching Shear Strength Analysis of Reinforced Concrete Flat Plates with Spandrel Beams”, ACI Structural Journal, Vol. 89, No.4, pp. 375-383.

Loo, Y. C. and Chiang, C. L. (1993), "Methods of Punching Shear Strength analysis of Reinforced Concrete Flat Plates-A Comparative Study", Structural Engineering and Mechanics, Vol. 1, No.1, pp. 75-86.

Loo, Y. C., and Guan, H. (1997), "Cracking and Punching Shear Failure Analysis of RC Flat Plates" ASCE Journal of Structural Engineering, Vol. 123, No.10, pp. 1321-1330.

Loseth, S., Slatto, A. and Syvertsen, G. (1982). Finite element analysis of punching shear failure of reinforced concrete slabs. Nordic concrete research, 82(1):18.1-18.17.

Lovrovich, J. S. and McLean, D. I. (1990), "Punching Shear Behaviour of Slabs with varying Span-Depth Ratios", ACI Structural Journal, Vol. 87, No.5, pp. 507-511.

Lubliner, J., Oliver, J., Oller, S. and Oñate, E. (1989), "A Plastic-Damage Model for Concrete", International Journal of Solids and Structures, vol. 25, pp. 299–329.

Mark, P. (2006), "Biaxially stressed by bending and shear forces reinforced concrete beams," Habilitationsschrift, Ruhr-University Bochum.

Marti, P. (1990), "Design of Concrete Slabs for Transverse Shear", ACI Structural Journal, Vol. 87, No.2, pp. 180-190.

Megally, S. (1998), "Punching Shear Resistance of Concrete Slabs to Gravity and Earthquake Forces", Ph.D. Thesis, University of Calgary, Calgary, Alberta, pp. 469.

Megally, S. and Ghali, A. (2000a), "Seismic Behavior of Edge Column-Slab Connections with Stud Shear Reinforcement", ACI Structural Journal, Vol. 97, No. 1

Megally, S. and Ghali, A. (2000b), "Punching Shear Design of Earthquake-Resistant Slab-Column Connections", ACI Structural Journal, Vol. 97, No. 5, pp. 720-730

Mitchell, D. and Cook, W. D. (1984), "Preventing Progressive Collapse of Slab Structures", ASCE Journal of Structural Engineering, Vol. 110, No.7, pp. 1513-1531.

Mitchell, D., Tinawi, R. and R. G. (1990) "Damage to Buildings Due to the 1989 Loma Prieta Earthquake- A Canadian Code Perspective", Canadian Journal of Civil Engineering, Vol. 17, No.10,Oct., pp. 813-834.

Mitchell, D., DeVall, R. H., Saatioglu, M., Simpson, R., Tinawi, R. and Tremblay, R. (1995) "Damage to concrete structures Due to Northridge Earthquake," Canadian Journal of Civil Engineering, Vol. 22, No.4, pp. 361-377.

Mortin, J. D. and Ghali, A. (1991), "Connection of Flat Plates to Edge Columns", ACI Structural Journal, Vol. 88, No.2, pp. 191-198.

Murray, K. A., Cleland, D. J., Gilbert, S. G. and Scott, R. H. (2003), "Improved Equivalent Frame Analysis Method for Flat Plate Structures in Vicinity of Edge Columns", ACI Structural Journal, Vol. 100, No.4, pp. 454-464.

Nilson, A. H. (1997). Design of Concrete structures, 13th Edition, McGraw-Hill Book Co. Singapore.

Olivera, D. R., Milo, G. S. and Regan, P. E. (2000), "Punching Strengths of Flat Plates with Vertical or Inclined Stirrups", ACI Structural Journal, Vol. 97, No.3, pp. 485-491.

Owen, D. R. J. and Hinton, E. (1980), Finite Elements in Plasticity. Theory and practice. Pineridge press limited, U.K.

Pan, A. and Moehle, J. P. (1989), “Lateral Displacement Ductility of Reinforced Concrete Flat Plates”, ACI Structural Journal, May-June 1989, pp. 250-258.

Philippe Menetrey (1994), “Numerical Analysis of Punching Failure in Reinforced Concrete Structures” M.Sc. Engineering Thesis, Colorado, Boulder.

Pillai, S. U., Kirk, W. and Seavuzzo, L. (1982), “Shear Reinforcement at Slab-Column Connections in a Reinforced Concrete Flat Plate Structure”, ACI Structural Jounal, January-February 1982, pp. 36-42.

Polak, M. A. (1998), “Modeling Punching Shear of Reinforced Concrete Slabs using Layered Finite Elements”, ACI Structural Journal, Vol. 95, No.1, pp. 71-80.

Pölling, R. (2000), “A practical, damage-oriented material description for reinforced concrete”, Dissertation, Ruhr-University Bochum.

Regan, P. E. (1981), “Behaviour of Reinforced Concrete Flat Slabs”, CIRIA Report No. 89, Construction Industry Research and Information Association, London.

Regan, P. E. and Jorabi, H. R. (1988), “Shear Resistance of One-Way Slabs under Concentrated Loads”, ACI Structural Journal, pp. 150-157.

Rangan, B. V. (1990), “Punching Shear Design in the New Australian Standard for Concrete Structures”, ACI Structural Journal, Vol. 87, No.2, pp. 140-144.

Robertson, I. N. (1997), “Analysis of Flat Slab Structures Subjected to Combined Lateral and gravity Loads”, ACI Structural Journal, Vol. 94, No.6, pp. 723-729.

Robertson, I. N., Kawai, T., Lee, J. and Enomoto, B. (2002), “Cyclic Testing of Slab-Column Connections with Shear Reinforcement”, ACI Structural Journal, Vol. 99, No.5, pp. 605-613.

Salim, W. and Sebastian, W. M. (2002), "Plasticity Model for Predicting Punching Shear Strengths of Reinforced Concrete Slabs", ACI Structural Journal, Vol. 99, No.6, pp. 827-835.

Schreiber, S.K. and Alexander, S. D. B. (2001), "Punching Shear Capacity of Slab-Column Connections with Steel-Fibre Reinforcement under Cyclic Lateral Loading", Structural Engineering Report No. 241, University of Alberta, Sept. 2001, 139 pp.

Seracino, R. (1995), "Towards improving nonlinear analysis of reinforced concrete shells", M.A.Sc. Thesis, Dept. of Civil Engrg., Univ. of Toronto.

Shaaban A. M. and Gesund, H. (1994), "Punching Shear Strength of Steel Fiber Reinforced Concrete Flat Plates", ACI Structural Journal, Vol. 91, No.3, pp. 406-414.

Shah, S. P., Swartz, S. E. and Ouyang, C. (1995), Fracture Mechanics of Concrete, John Wiley & Sons, Inc., New York, New York.

Siao, W. B. (1994), "Punching Shear Resistance of Flat Slabs: A Beam-Strip Analogy", ACI Structural Journal, Vol. 91, No.5, pp. 594-604.

Smith, B. S. and Coull, A. (1991), Tall Building Structures: Analysis and Design, John Wiley & Sons, INC. Singapore.

Tan, Y. and Teng, S. (2005), "Interior Slab-Rectangular Column Connections Under Biaxial Lateral Loadings", American Concrete Institute.

Tian, Y., Jirsa, J. O. and Bayrak, O. (2008), "Strength Evaluation of Interior Slab-Column Connection", ACI Structural Journal, Vol. 105, No. 6, pp. 692-700.

Timoshenko, S. and Krieger, S.W. (1959), Theory of Plates and Shells, McGraw-Hill Book Company, New York.

Van Mier, J. G. M. (1984), “Strain-softening of concrete under multiaxial loading c--onditions,” PhD-thesis, Techn. Univ. Eindhoven.

Vonk, R. A. (1993), “A micromechanical investigation of softening of concrete loa--ded in compression,” Heron Vol. 38 (3), pp. 3-94.

William, K. J. and Warnke, E. P. (1975), “Constitutive Model for the Triaxial Beha--vior of Concrete,” Proceedings, International Association for Bridge and Structural Engineering, Vol. 19, ISMES, Bergamo, Italy, pp. 174.

Winkler, K. and Stangenberg, F. (2007), “Numerical Analysis of Punching Shear Failure of Reinforced Concrete Slabs”, Ruhr-University Bochum, Universitätsstr. 150, 44780 Bochum, Germany, Institute for Reinforced and Prestressed Concrete Structures.

Wolfgang Schueller, (1986), High-Rise Building Structures, Second edition, Robert E. Krieger Publishing Company, Malabar, Florida.

Yamada, T., Nanni, A. and Endo, K. (1991), “Punching Shear Resistance of Flat Slabs: Influence of Reinforcement Type and Ratio”, ACI Structural Journal, Vol. 88, No.4, pp. 555-563.

Zienkiewicz, O.C. (1979), The Finite Element Method. TMII edition, McGraw-Hill Publishing Company Limited, New Delhi.

Zsutty, T. C. (1968), “Beam Shear Strength Prediction by Analysis of Existing Data”, ACI JOURNAL, Proceedings V. 65, No. 11, Nov. 1968, pp. 943-951.

Zsutty, T. (1971), “Shear Strength Prediction for Separate Categories of Simple Beam Tests”, ACI JOURNAL, Proceedings V. 68, No. 2, Feb. 1971, pp. 138-143.

Appendix A

SOME CALCULATIONS ON SLAB-COLUMN CONNECTION OF RC FLAT PLATE STRUCTURE

A-1 Slab-column connections designed only for gravity load (Model-1)

The calculations on flat plate slab design of fourteen storied building are given below which is based on direct design method:

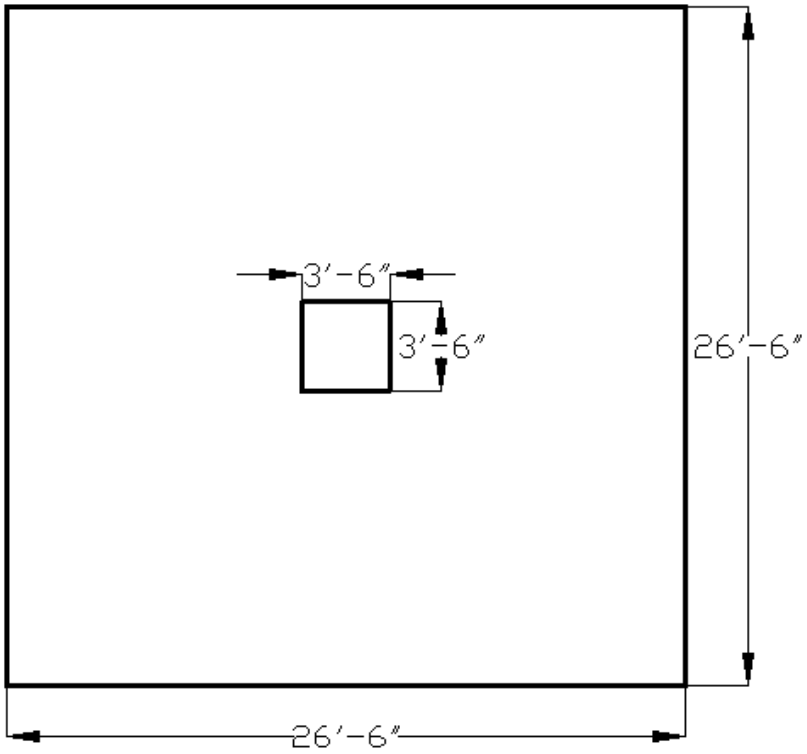

Figure A-1 Plan view of interior panel of flat plate slab system

A-1.1 Material strength:

Ultimate strength of concrete, $f'_c = 3500$ psi

Steel yield strength, $f_y = 60{,}000$ psi

A-1.2 Slab thickness calculation:

$h = l_n/33 = \{(26.5 \times 12)-42\}/33 = 8.36$ in ≈ 8.5 in

A-1.3 Load calculation:

F. F = 25 psf

P.W = 50 psf

Self Wt = $(10/12) \times 150$ = psf

DL = F.F + PW + self Wt = 25 + 50 + 125 = 200 psf

LL = 80 psf [As it is a commercial building]

$W_u = 1.4 \times DL + 1.7 \times LL$

$= 1.4 \times 200 + 1.7 \times 80$

$= 416$ psf

A-1.4 Column load check:

Column Load $= 416 \times (26.5)^2 \times 14$

$P_u = \alpha\varphi \{0.85 f'_c (A_g - A_{st}) + A_{st} f_y\}$

$4089.904 = 0.56 \times [0.85 \times 3.5\{(42\times42) - A_{st}\} + A_{st} \times 60]$

$\therefore A_{st} = 36.045$ in^2

$\rho = A_{st} / A_g = 36.045 / (42\times 42) = 0.0204$

$\therefore \rho = 2.04\ \% \approx 2\%$

(Column section is ok).

A-1.5 Shear check:

Critical section of slab is d/2 distance from column face. Where d is the effective depth of slab. Consider #4 bar to use and the diameter of the reinforcement would be 0.5 in. Figure A-2 represent some necessary data.

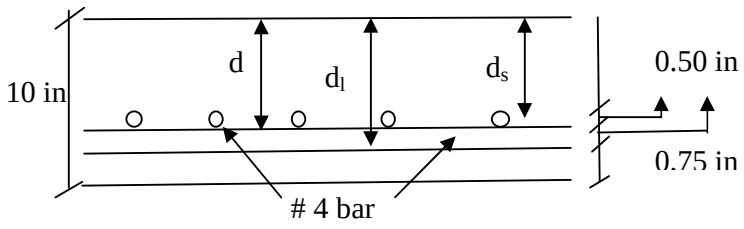

Figure A-2 Slab section of flat plate slab system

$d = 10 - 0.75 - 0.5 = 8.75$ in

$b_o = 4 \times (42 \times 8.75) = 203$ in

$V_u = 416 \times [(26.5 \times 26.5) - \{(42 + 8.75) / 12\}^2]$

$V_n \geq V_u / \varphi = 284.7 / 0.75 = 3.79.6$ kip

Allowable, $V_c = 4\sqrt{f'_c}\, b_o\, d = V_n$

$379.6 \times 1000 = 4\sqrt{3500} \times 203 \times d$

$\therefore d = 7.9$ in (This is less than provided value)

Here, h will be 9.15 in $<$ 10 in (Provided)

So, punching share will not occur.

(Ok)

By using the following equation to check punching shear failure, the ratio of critical perimeter can include.

$$Vc = \left(\frac{\alpha_s\, d}{b_o} + 2\right)\sqrt{f'_c}\, b_o\, d$$

[For interior slab, $\alpha_s = 40$]

By using the above discussed equation the effective depth is 8.49 in, which is less than the provided value. So, punching share failure will not occur.

(Ok)

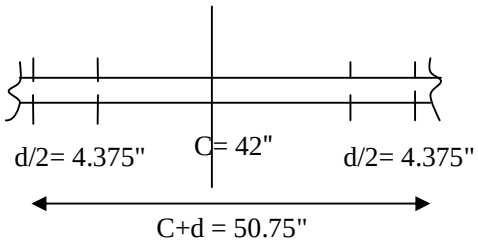

Figure A-3 Critical section for punching shear failure due to gravity load

A-1.6 Moment calculation:

In longitudinal direction, $d_l = 10 - 0.75 - d_b/2 = 10 - 0.75 - 0.5/2 = 9$ in

In transverse direction, $d_s = 10 - 0.75 - 1.5d_b = 10 - 0.75 - (1.5 \times 0.5) = 8.5$ in (assuming # 4 bar)

$M_o = 0.125\, W_u\, l_2\, ln^2$

$= 0.125 \times 416 \times 26.5 \times (26.5-3.5)^2 / 1000$

$\therefore M_o = 729$ kip-ft

In longitudinal direction, $d_l = 9$ in

Column strip negative moment

$-M_u = -0.75\ (0.65 \times M_o)$

$= -0.75(0.65 \times 729)$

$\therefore -M_u = -355.4$ kip-ft

$\therefore -M_n = -M_u/0.9 = -355.4/0.9 = 395$ kip-ft

Column strip width is half the transverse panel length: 13.25 ft or 159 in

Required $K_n = \frac{M_n}{bd^2} = (395 \times 12 \times 1000)/(159 \times 9^2) = 368 \ll 1041$ (Ok)

This result indicates such a greatly under-reinforced slab.

Assume, jd = 0.95d than,

$A_s = \frac{M_u}{\varphi f_y\, jd} = (355.4 \times 12)/(0.9 \times 60 \times 0.95 \times 9)$

$\therefore A_s = 9.24$ in^2 [Choose 47 No bars = 9.4 in^2]

$a = \frac{A_s f_y}{0.85 f'_c b}$

$= (9.4 \times 60)/(0.85 \times 3.5 \times 159)$

$\therefore a = 1.192$ in

$A_s = \frac{M_u}{\varphi f_y (d-a/2)}$

$= (355.37 \times 12)/\{0.9 \times 60 \times (9\text{-}1.192/2)\}$

$A_s = 9.397$ in^2

Required $A_s = 9.397$ in^2

Min $A_s = 0.0018 \times h \times b = 0.0018 \times 10 \times 159 = 2.862$ in^2

Provided straight bar

No of #4 ($A_b = 0.2$ in^2) $\longrightarrow$ 47

Average spacing = 159/46 = 3.46 in

47 # 4φ @ 3.456 in c/c [Column strip top bar]

A tabular form, as in Table A-1, expedites this type design and organizes the results in a manner that is easily available.

Table A-1 Steel calculation for different panel of flat plate slab system based on direct design method

	Longitudinal direction				Transverse direction			
	Column strip		Middle strip		Column strip		Middle strip	
	Negative	Positive	Negative	Positive	Negative	Positive	Negative	Positive
Distribution of moment M_o	-0.49 M_o	+0.21 M_o	-0.16 M_o	+0.14 M_o	-0.49 M_o	+0.21 M_o	-0.16 M_o	+0.14 M_o
M_o (kip-ft)	729				729			
M_u (kip-ft)	-355.4	+153.1	-118.5	+102	-355.4	+153.1	-118.5	+102
Required A_s (in^2)	9.4	3.89	2.99	2.57	10.1	4.13	3.2	2.73
Minimum A_s (in^2)	2.86	2.86	2.86	2.86	2.86	2.86	2.86	2.86
Provided A_s (in^2)	9.4	4	3.08	2.86	10.2	4.2	3.3	2.86
No. of straight bars #4 (A_b = 0.2 in^2)	47	20	--	--	51	21	--	--
Average Spacing (in)	3.46±	8.37±	--	--	3.18±	7.95±	--	--
No. of straight bars #3 (A_b = 0.2 in^2)	--	--	28	26	--	--	30	26
Average Spacing (in)	--	--	5.68±	6.1±	--	--	5.3±	6.1±

A-2 Slab-Column Connections of Intermediate Moment Resisting Frames (Model-3)

The calculations on flat plate slab design subjected to gravity and lateral loads of fourteen storied building are given below:

A-2.1 Load combinations:

1) 0.75 [1.4 DL+ 1.7 LL + 1.7(1.1 E)]

   Or, 1.05 DL+ 1.275 LL + 1.4025 E

   Gravity load portion → 0.75[1.4 DL+ 1.7 LL]

   Earthquake (Lateral) load portion → 0.75 [1.7(1.1E)]

2) 0.9 DL+ 1.3 (1.1E)

   Or, 0.9 DL + 1.43 E

   Gravity load portion → 0.9 DL

   Earthquake (Lateral) load portion → 1.43E

A-2.2 Moment due to gravity load:

Moment calculation under gravity load portion of load combination -1

W_u = 0.75 [1.4 DL + 1.7 LL]

= (0.75 × 416) psf

= 312 psf

$M_o = 0.125\ W_u\ l^2\ l_n^2$

$= \{0.125 \times 312 \times 26.5 \times (26.5 - 3.5)^2\}/1000$

= 546.7215 kip-ft

Column strip negative moment = − (0.75 × 0.65 × 546.7215) = − 266.53 kip-ft

Column strip negative moment through effective width (C+3h)

= −(266.53 × 72)/159 = −120.7 kip-ft

Moment calculation under gravity load portion of load combination -2

W_u = 0.9 DL

= (0.9 × 200) psf

= 180 psf

$M_o = 0.125\ W_u\ l^2\ l_n^2$

$= \{0.125 \times 180 \times 26.5 \times (26.5 - 3.5)^2\}/1000$

= 315.42 kip-ft

Column strip negative moment = − (0.75 × 0.65 × 315.42) = − 153.8 kip-ft

Column strip negative moment through effective width (C+3h)

= −(153.8 × 72)/159 = −69.64 kip-ft

A-2.3 Lateral load calculation:

The calculation on seismic lateral forces based on equivalent static frame method is given below:

DL = 200psf (F.F = 25psf, PW = 50psf, SW = 125psf)

Total seismic dead load at all floor level = 200psf

Total seismic dead load at roof level = 137.5psf

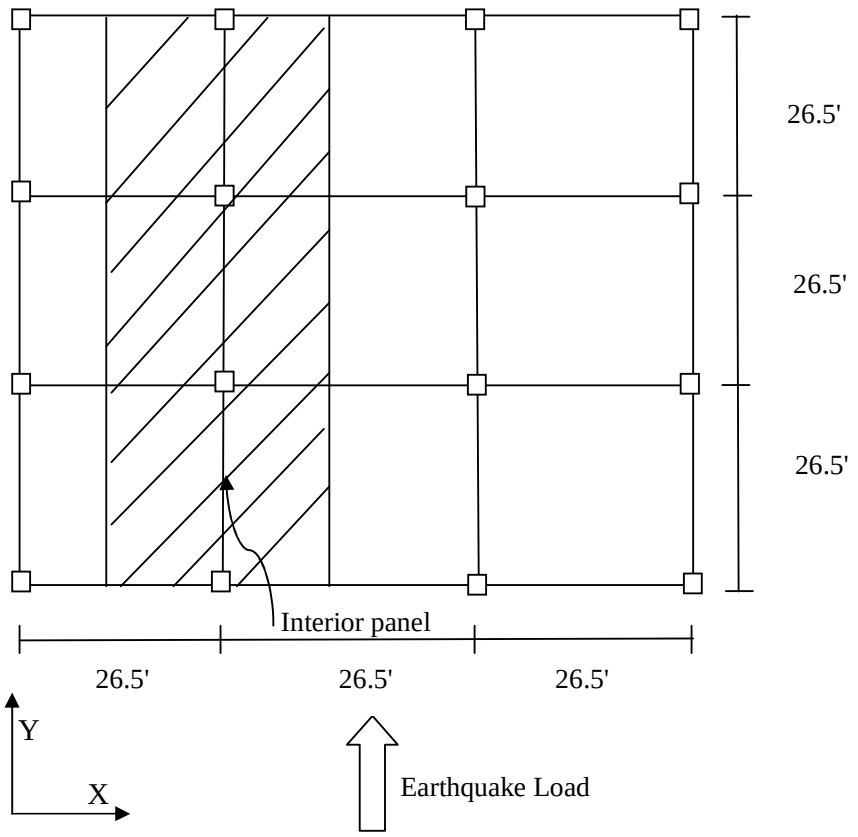

Figure A-4 Plan view of interior panel of a flat plate slab system

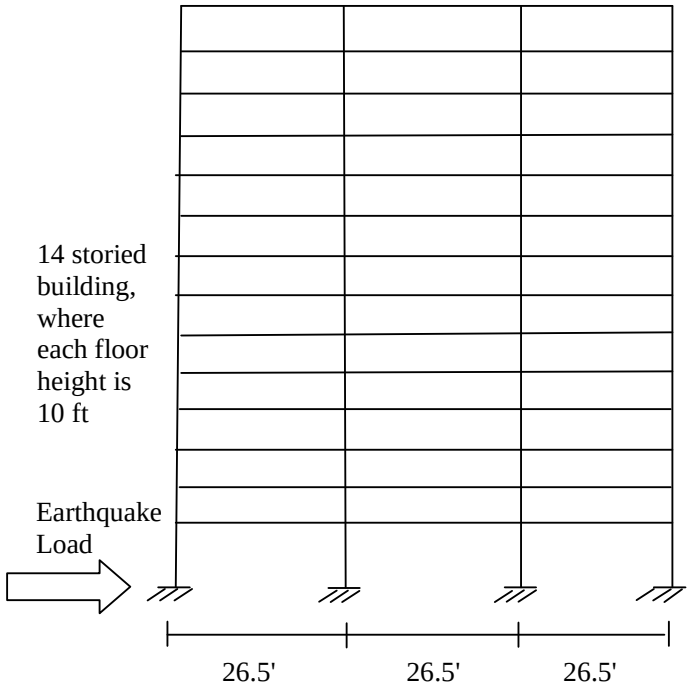

Figure A-5 Section view of interior panel of a flat plate slab system

Base share, $V = \frac{ZIC}{R} \times W$

Where,

Seismic zone factor Z = 0.15 (Zone 2)

Structural importance factor, I = 1.00

Response modification coefficient, R= 8

Site coefficient, S = 1.5 (Soft clay)

C_t = 0.073 (RC Moment Resisting Frame)

$T = C_t \times (h_n)^{3/4} = 0.073 \times (140/3.28)^{3/4} = 1.22$ sec

$C = \frac{1.25 \times S}{T^{\frac{2}{3}}} = \frac{1.25 \times 1.5}{(1.22)^{2/3}} = 1.6422 < 2.75$ (Ok)

$C/R = 1.6422/8 = 0.2053 > 0.075$ (Ok)

$V = \frac{ZIC}{R} \times W = \frac{0.15 \times 1 \times 1.6422}{8} \times \{(200 \times 13) + (137.5 \times 1)\}$ (79.5×26.5)

$\therefore V = 177.6$ kip

T > 0.7 sec

$F_t = 0.07 \times T \times V = 0.07 \times 1.22 \times 177.6 = 15.17$ kip < 0.25 V (44.4 kip)

$\sum W_i \times h_i = [\{200 \times 10 \times (1 + 2 + 3 + 4 + 5 + 6 + 7 + 8 + 9 + 10 + 11 + 12 + 13)\}+ \{137.5 \times 10 \times 14\}] \times (79.5 \times 26.5)$

$= 423.98\times 10^3$

$F_x = \frac{(V-F_t)\times W_x \times h_x}{\sum W_i \times h_i} = \frac{(177.6-15.17)\times W_x \times h_x}{423.98\times 10^3}$

$\therefore F_x = 3.83 \times 10^{-4}\, W_x \times h_x$

For all floor, $W_x = 200 \times (79.5 \times 26.5) = 421350$ lb

$F_x = 3.83 \times 10^{-4} \times 421350 \times h_x = 161.4\, h_x$

$F_1 = (161.4 \times 10)/1000 = 1.61$ kip, $F_2 = 1.614\times2 = 3.23$ kip, $F_3 = 1.614\times3 = 4.84$ kip, $F_4 = 1.614\times4 = 6.46$ kip, $F_5 = 1.614\times5 = 8.07$ kip, $F_6 = 1.614\times6 = 9.68$ kip, $F_7 = 1.614\times7 = 11.3$ kip, $F_8 = 1.614\times8 = 12.9$ kip, $F_9 = 1.614\times9 = 14.5$ kip, $F_{10} = 1.614\times10 = 16.1$ kip, $F_{11} = 1.614\times11 = 17.7$ kip, $F_{12} = 1.614\times12 = 19.4$ kip, $F_{13} = 1.614\times13 = 21$ kip,

For roof, $W_x = 1.37.5 \times (79.5 \times 26.5) = 289678.125$ lb

$F_{14} = F_t + F_x = 15.17 + 3.83 \times 10^{-4} \times (289678.125 \times 140)/1000 = 30.7$ kip

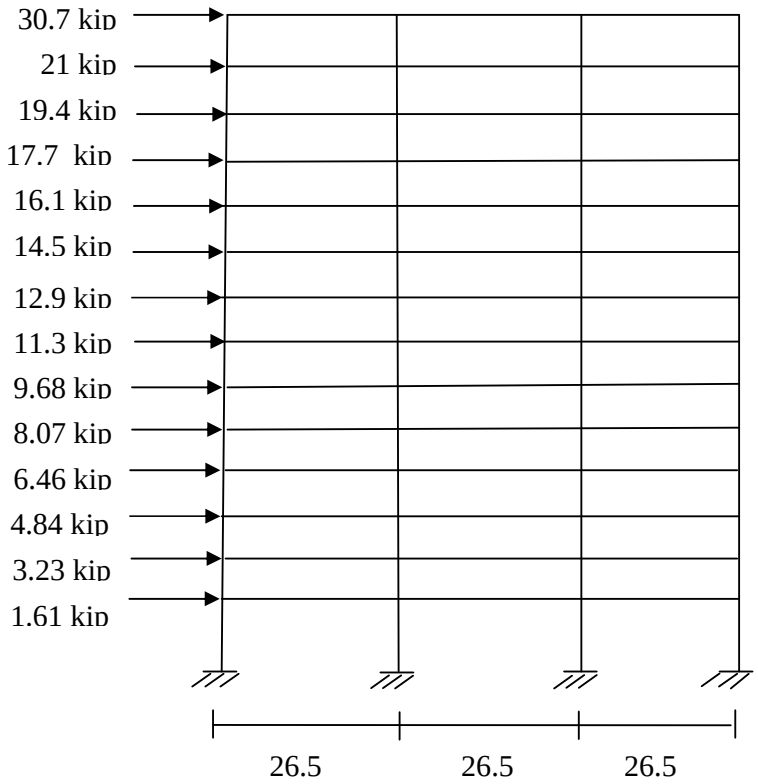

Figure A-6 Lateral loads due to seismic action on different story laval of interior panel of a flat plate slab system

A-2.4 Moment through column strip due to lateral load:

Due to both gravity and lateral loads, a huge amount of unbalanced moment has occurred at slab-column joint. The unbalanced moments have calculated with the above mentioned lateral loads by using ETABS software. The unbalanced moments at first story level are given below:

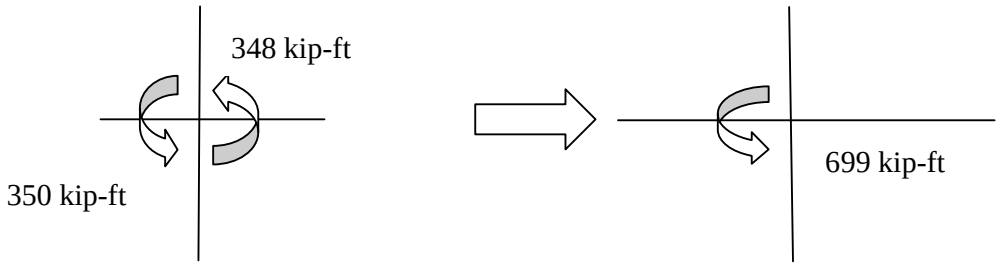

Here, $M_u = M_{slab} = 699$ kip-ft (Total unbalance moment)

Moment calculation under lateral load portion of load combination -1

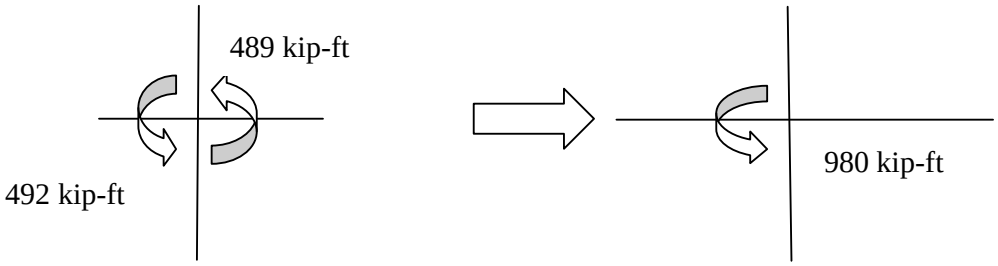

Moment calculation under lateral load portion of load combination -2

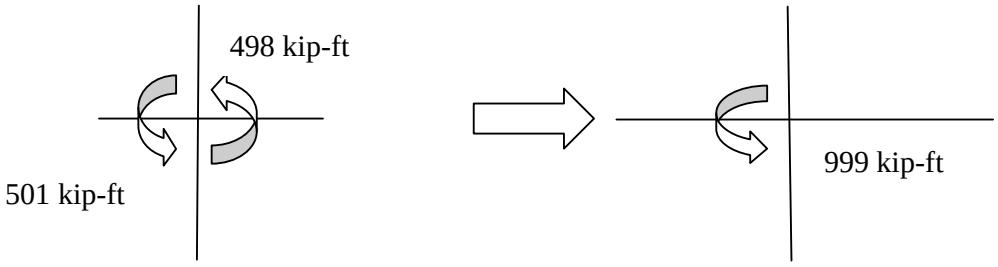

A-2.5 Combined gravity and lateral loads:

Moment calculation under both gravity and lateral loads of load combination -1

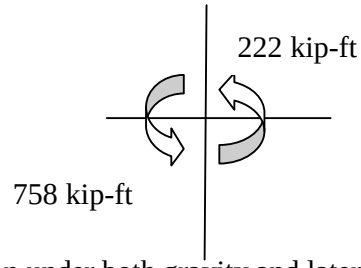

Moment calculation under both gravity and lateral loads of load combination -2

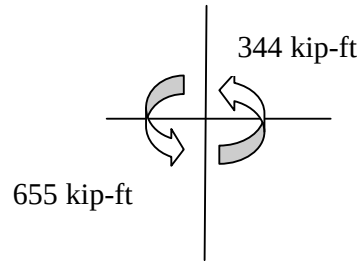

After a comparison of moments in between above mentioned two combinations, the design should be performed for 758 kip-ft negative moment and 344 kip-ft positive moment.

A-2.6 Balanced steel ratio:

$$\rho_b = \frac{0.85\,\beta_t\,f'_c}{f_y}\left(\frac{\varepsilon_{cu}}{\varepsilon_{cu}+\varepsilon_y}\right)$$

$$= \{(0.85 \times 0.85 \times 3.5)/60\} \times \{0.003/\,(0.003+0.00207)\}$$

$$\therefore \rho_b = 0.0249$$

[Where, $\varepsilon_y = \frac{f_y}{E_s} = 60 \times 10^3/29 \times 10^6 = 0.00207$]

$$0.375\rho_b = 0.00934$$

Table A-2 Steel calculation through column strip of flat plate slab system under combined gravity and lateral loads

	Longitudinal direction		Transverse direction	
	Column strip		Column strip	
	Left end of slab-column joint	Right end of slab-column joint	Left end of slab-column joint	Right end of slab-column joint
	Negative moment	Positive moment	Negative moment	Positive moment
M_u (kip-ft)	-758	+344	-758	+344
Required A_s (in^2)	22.3	9.15	24.4	9.7
Minimum A_s (in^2)	2.86	2.86	2.86	2.86
Provided A_s (in^2)	23	10	25	10
No. of straight bars #4 (A_b = 0.2 in^2)	115	50	125	50
Average Spacing (in)	1.39±	3.24±	1.28±	3.24±
Balanced steel ratio, ρ_b	0.0249	0.0249	0.0249	0.0249
$0.375\rho_b$	0.00934	0.00934	0.00934	0.00934
$\rho = \frac{A_s}{bd}$	0.016	0.007	0.0185	0.0074
Remarks	$\rho > 0.375\rho_b$ (Not ok)	$\rho < 0.375\rho_b$ (Ok)	$\rho > 0.375\rho_b$ (Not ok)	$\rho < 0.375\rho_b$ (Ok)

A-2.7 Moment through effective width due to lateral load:

According to ACI 318-08 code provision, 60% of the unbalanced moments have transferred through the effective width. 60% of the unbalanced moments at first story level are given below:

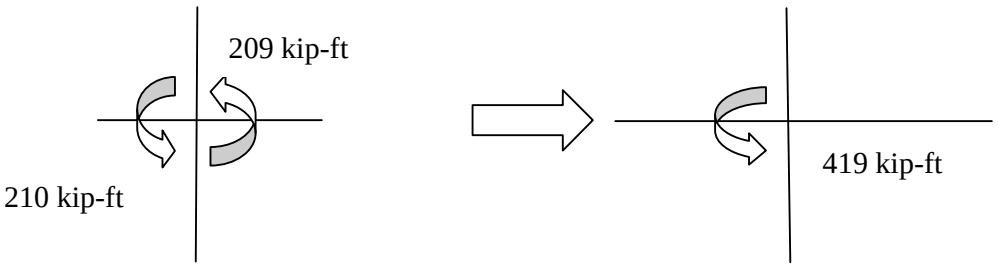

Here, $\gamma_f M_u = \gamma_f M_{slab} = 419$ kip-ft (Total unbalance moment through effective width)

Moment calculation under lateral load portion of load combination -1

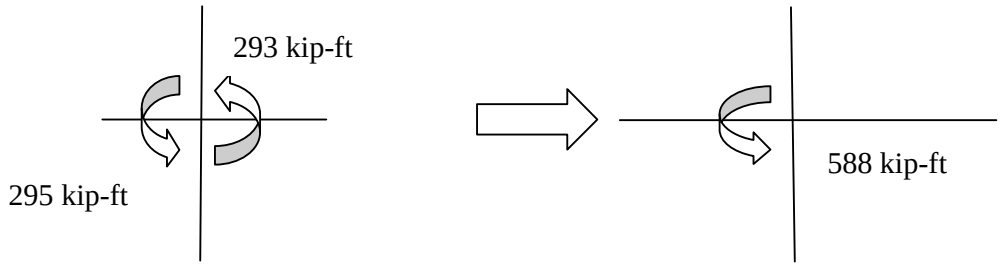

Moment calculation under lateral load portion of load combination -2

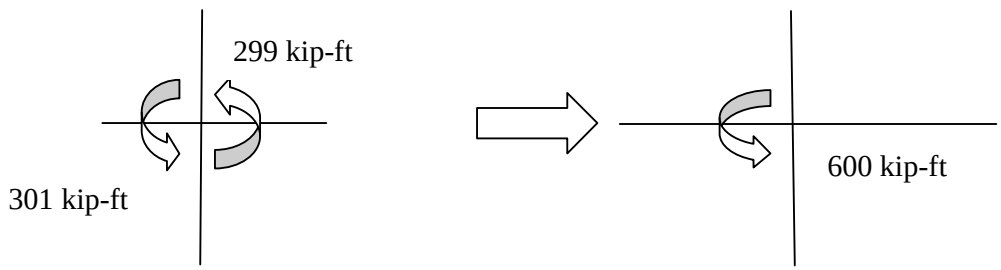

A-2.8 Combined gravity and lateral loads:

Moment calculation under both gravity and lateral loads of load combination -1

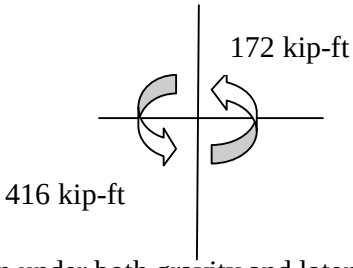

Moment calculation under both gravity and lateral loads of load combination -2

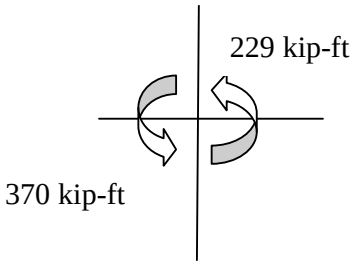

After a comparison of moments in between above mentioned two combinations, the design should be performed for 416 kip-ft negative moment and 229 kip-ft positive moment.

Table A-3 Steel calculation through column strip effective width of flat plate slab system under combined gravity and lateral loads

	Longitudinal direction		Transverse direction	
	Column strip effective width c+3h		Column strip effective width c+3h	
	Left end of slab-column joint	Right end of slab-column joint	Left end of slab-column joint	Right end of slab-column joint
	Negative moment	Positive moment	Negative moment	Positive moment
M_u (kip-ft)	-416	+229	-416	+229
Required A_s (in^2)	12.9	6.35	14.4	6.8
Minimum A_s (in^2)	1.3	1.3	1.3	1.3
Provided A_s (in^2)	13	7	15	7
No. of straight bars #4 (A_b = 0.2 in^2)	65	35	75	35
Average Spacing (in)	1.12±	2.11±	0.97±	2.11±
Balanced steel ratio, ρ_b	0.0249	0.0249	0.0249	0.0249
$0.375\rho_b$	0.00934	0.00934	0.00934	0.00934
$\rho = \frac{A_s}{bd}$	0.02	0.0108	0.0245	0.0114
Remarks	$\rho > 0.375\rho_b$ (Not ok)	$\rho > 0.375\rho_b$ (Not ok)	$\rho > 0.375\rho_b$ (Not ok)	$\rho > 0.375\rho_b$ (Not ok)

A-3 Slab-Column Connections with Drop Panel (Model-4)

The calculations on flat plate slab with drop panel design subjected to gravity and lateral loads of fourteen storied building are given below:

A-3.1 Load calculation:

F.F = 25 psf , PW = 50 psf

Self weight of slab = (10/12) × 150 = 125 psf

Self weight of drop panel = (4/12) × 150 = 50 psf

DL_1= F.F + PW + Self weight of slab = 25 + 50 + 125 = 200 psf

DL_2 = Self weight of drop panel = 50 psf

LL = 80 psf

Now, W_{u1} = 1.4 DL_1 + 1.7 LL = 1.4 × 200 + 1.7 × 80 = 416 psf

W_{u2} = 1.4 DL_2 = 1.4×50 = 70 psf

A-3.2 Shear check:

<u>1st critical shear check</u>

d = 14−0.75−0.5 = 12.75 in

b_o = 4 × (42+12.75) = 219 in

V_u= 416 ×[(26.5×26.5) – {(42+12.75)/12}^{2}] +70 ×[{4×(159×79.5) + (159 × 159)}/144 − {(42+12.75)/12}^{2}]

∴V_u= 318.9 kip

$V_n \geq V_u/\varphi$ = 425.2 kip

Allowable, $V_c = V_n = 4\sqrt{f'_c}\, b_o\, d$

425.2× 1000 = 4 $\sqrt{3500}$ ×219×d

∴ d = 8.2 in (Which is less than provided d)

Here, h will be 9.45 in < 14 in (provided)

So, punching share failure will not occur (ok)

Here,

$V_c = (2+4/\beta)\sqrt{f'_c}\, b_o\, d$, $(2+ 4/\beta) = 6 > 4$ (Does not govern) Here, β = 42/42 = 1

$V_c = (\frac{\alpha_s \times d}{bo} + 2)\sqrt{f'_c}\, b_o\, d$, $(\frac{\alpha_s \times d}{bo} + 2) = 4.33 > 4$ (Does not govern) ,$\alpha_s = 40$ (For interior panel)

$V_c = 4\sqrt{f'_c}\, b_o\, d$ (govern)

Here, $V_c = V_u = 4\sqrt{f'_c}\, b_o\, d = 4\sqrt{3500} \times 219 \times 12.75 = 660.77$ kip

$V_u / \varphi\, V_c = 318.9 / (0.75 \times 660.77) = 0.64$

2nd critical shear check:

$d = 10 - 0.75 - 0.5 = 8.75$ in

$b_o = 4 \times [42 + (2 \times 58.5) + 8.75] = 671$ in

$V_u = = 416 \times [(26.5 \times 26.5) - \{(42+117+8.75)/12\}^2] + 70 \times [\{4 \times 159 \times (79.5 - 4.375)\} / 144]$

$\therefore V_u = 234.1$ kip

$V_n \geq V_u / \varphi = 234.1 / 0.75 = 312.13$ kip

Allowable, $V_c = V_u = 4\sqrt{f'_c}\, b_o\, d$

$312.13 \times 1000 = 4\sqrt{3500} \times 671 \times d$

$\therefore d = 1.96$ in (Which is less than provided d)

Here, h will be 3.12 in < 10 in (provided)

So, punching share failure will not occur (ok)

If we use $V_c = (\frac{\alpha_s \times d}{bo} + 2)\sqrt{f'_c}\, b_o\, d$, $(\frac{\alpha_s \times d}{bo} + 2) = 2.52$ (govern) and effective depth will be 3.12in that is also less than the provided value . So punching share failure will not occur. (ok)

Here, $V_c = V_n = (\frac{\alpha_s \times d}{bo} + 2)\sqrt{f'_c}\, b_o\, d = 4\sqrt{3500} \times 671 \times 8.75$

$\therefore V_c = V_n = 875.32$ kip

$V_u / \varphi\, V_c = 234.1 / (0.75 \times 875.32) = 0.36$

Same gravity and lateral loads and moments have used as discussed in Sec A-2.

Table A-4 Steel calculation through column strip of flat plate slab system under combined gravity and lateral loads

	Longitudinal direction		Transverse direction	
	Column strip		Column strip	
	Left end of slab-column joint	Right end of slab-column joint	Left end of slab-column joint	Right end of slab-column joint
	Negative moment	Positive moment	Negative moment	Positive moment
M_u (kip-ft)	-758	+344	-758	+344
Required A_s (in^2)	13.9	6.1	14.6	6.33
Minimum A_s (in^2)	4	4	4	4
Provided A_s (in^2)	14	6.2	14.6	6.4
No. of straight bars #4 (A_b = 0.2 in^2)	70	31	73	32
Average Spacing (in)	2.3±	5.3±	2.2±	5.12±
Balanced steel ratio, ρ_b	0.0249	0.0249	0.0249	0.0249
$0.375\rho_b$	0.00934	0.00934	0.00934	0.00934
$\rho = \frac{A_s}{bd}$	0.0068	0.003	0.0073	0.0032
Remarks	$\rho < 0.375\rho_b$ (Ok)	$\rho < 0.375\rho_b$ (Ok)	$\rho < 0.375\rho_b$ (Ok)	$\rho < 0.375\rho_b$ (Ok)

Table A-5 Steel calculation through column strip effective width of flat plate slab system under combined gravity and lateral loads

	Longitudinal direction		Transverse direction	
	Column strip effective width c+3h		Column strip effective width c+3h	
	Left end of slab-column joint	Right end of slab-column joint	Left end of slab-column joint	Right end of slab-column joint
	Negative moment	Positive moment	Negative moment	Positive moment
M_u (kip-ft)	-416	+229	-416	+229
Required A_s (in^2)	7.8	4.1	8.14	4.3
Minimum A_s (in^2)	1.8	1.8	1.8	1.8
Provided A_s (in^2)	7.8	4.2	8.2	4.4
No. of straight bars #4 (A_b = 0.2 in^2)	39	21	41	22
Average Spacing (in)	1.89±	3.6±	1.8±	3.42±
Balanced steel ratio, ρ_b	0.0249	0.0249	0.0249	0.0249
$0.375\rho_b$	0.00934	0.00934	0.00934	0.00934
$\rho = \frac{A_s}{bd}$	0.0083	0.0045	0.0091	0.0049
Remarks	$\rho < 0.375\rho_b$ (Ok)	$\rho < 0.375\rho_b$ (Ok)	$\rho < 0.375\rho_b$ (Ok)	$\rho < 0.375\rho_b$ (Ok)

A-4 Column Reinforcement Calculation:

Longitudinal bar calculation

Column section has already chosen 42" X 42".

For $\rho = 3\%$

Here, $A_{st} = \rho Ag = 0.003 \times 42^2 \approx 54\ in^2$

Total cross-sectional area of longitudinal bar inside the column, $A_{st} = 54\ in^2$

use #14 bar which area is $2.25 in^2$

No of bar use = 54/2.25 = 24

So, use 24 #14φ

Tie bar calculation

4 bar have used as a tie bar.

(1) $48 \times (4/8) = 24$ in

(2) $16 \times 1.693 = 27.008$ in [#14 bar diameter is 1.693 in]

(3) b = 42 in [least dimension of column]

Use # 4 φ tie bar have used @ 22 in c/c.

Appendix B

SOME CALCULATIONS ON FLAT-PLATE STRUCTURE WITH SHEAR WALL

B-1 Flat-Plate Structure with Shear Wall

B-1.1 Load combinations:

1) 0.75 [1.4 DL+ 1.7 LL + 1.7(1.1 E)]

   Or, 1.05 DL+ 1.275 LL + 1.4025 E

   Gravity load portion → 0.75[1.4 DL+ 1.7 LL]

   Earthquake (Lateral) load portion → 0.75 [1.7(1.1E)]

2) 0.9 DL+ 1.3 (1.1E)

   Or, 0.9 DL + 1.43 E

   Gravity load portion → 0.9 DL

   Earthquake (Lateral) load portion → 1.43E

B-1.2 Moment due to gravity load:

Moment calculation under gravity load portion of load combination -1

W_u = 0.75 [1.4 DL + 1.7 LL]

= (0.75 × 416) psf

= 312 psf

$M_o = 0.125\, W_u\, l^2\, l_n^2$

$= \{0.125 \times 312 \times 26.5 \times (26.5 - 3.5)^2\}/1000$

= 546.7215 kip-ft

Column strip negative moment = − (0.75 × 0.65 × 546.7215) = − 266 kip-ft

Moment calculation under gravity load portion of load combination -2

W_u = 0.9 DL

= (0.9 × 200) psf

= 180 psf

$M_o = 0.125\, W_u\, l^2\, l_n^2$

$= \{0.125 \times 180 \times 26.5 \times (26.5 - 3.5)^2\}/1000$

$= 315.42$ kip-ft

Column strip negative moment $= -(0.75 \times 0.65 \times 315.42) = -154$ kip-ft

B-1.3 Lateral load calculation:

The calculations on seismic lateral forces considering seismic Zone-2 and Zone-3 according to BNBC 2006 based on equivalent static frame method are same as discussed in *Appendix A*. Base share value for Zone-2 and Zone-3 are 177.6 kip and 296.1 kip respectively. Lateral loads due to seismic action on different story level of interior panel of a flat plate slab system considering seismic Zone-2 and Zone-3 are given in Figure C-1 and Figure C-2 respectively.

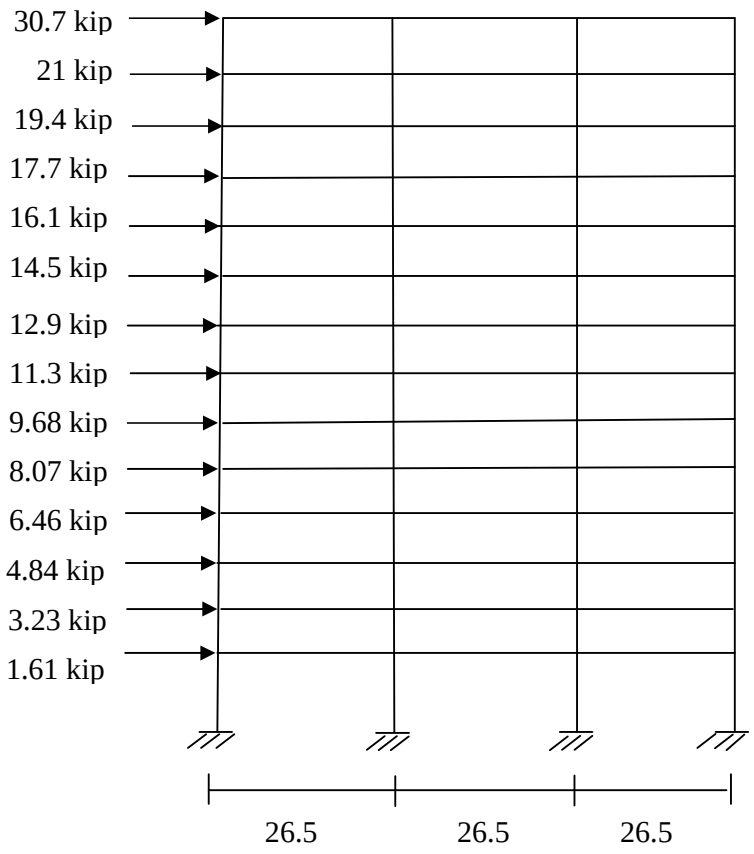

Figure B-1 Lateral loads due to seismic action on different story level of interior panel of a flat plate slab system under seismic Zone-2

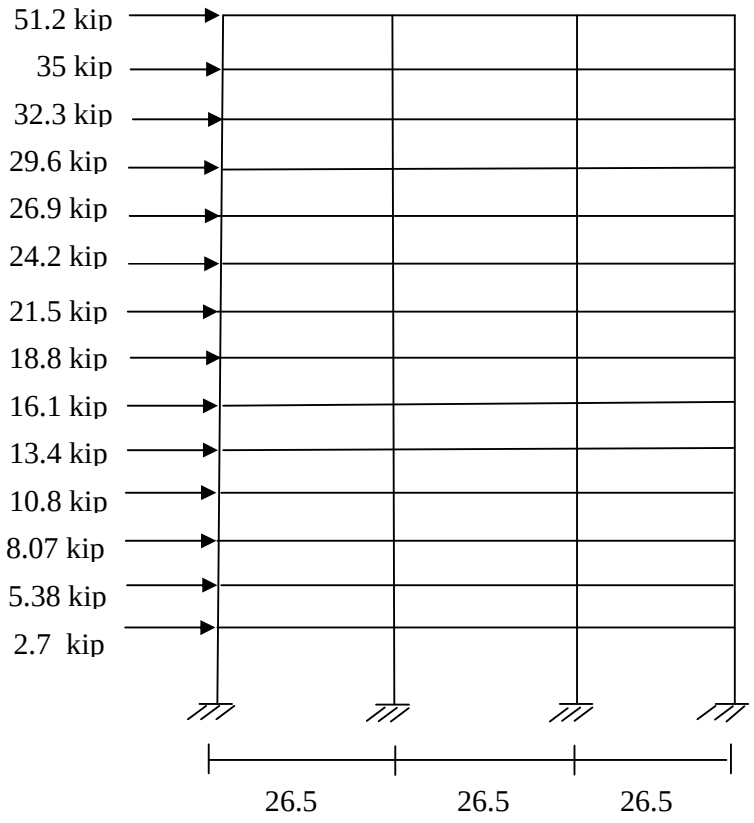

Figure B-2 Lateral loads due to seismic action on different story level of interior panel of a flat plate slab system under seismic Zone-3

In the above discussed frame, each floor has two interior columns and two exterior columns. From various observations it was found that the interior column lateral load effect is twice than the exterior column lateral load effect. Due to lateral load the unbalanced moment calculations under seismic Zone-2 and Zone-3 are given below.

B-1.4 Unbalanced moment calculation under seismic Zone-2:

Total Base share, V = 177.6 kip

Shear at each interior column of bottom story level = {(177.6 × 1)/3} = 59.2≈60 kip

As it has already discussed in Sec. 6.3.2 that about 80% unbalanced moment have transferred through shear wall and rest 20% have transferred through slab-column

joint. That is why; shear through each interior column of bottom story level is 12 kip.

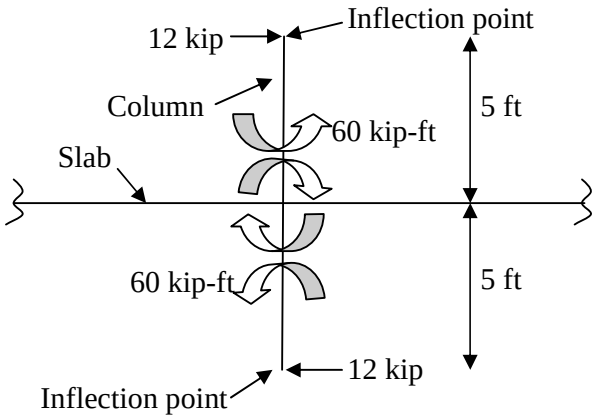

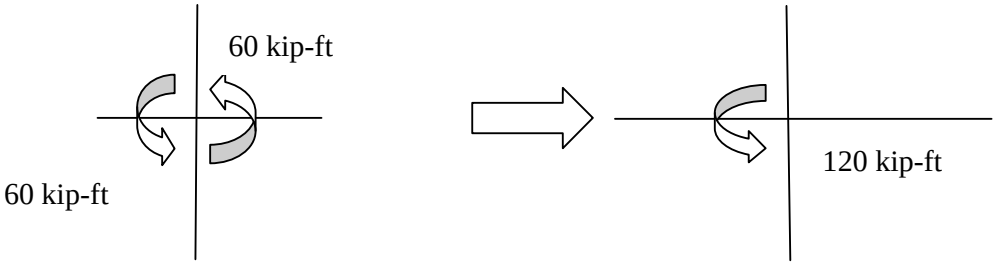

Here, $M_u = M_{slab} = 120$ kip-ft (Total unbalance moment)

Moment calculation under lateral load portion of load combination -1

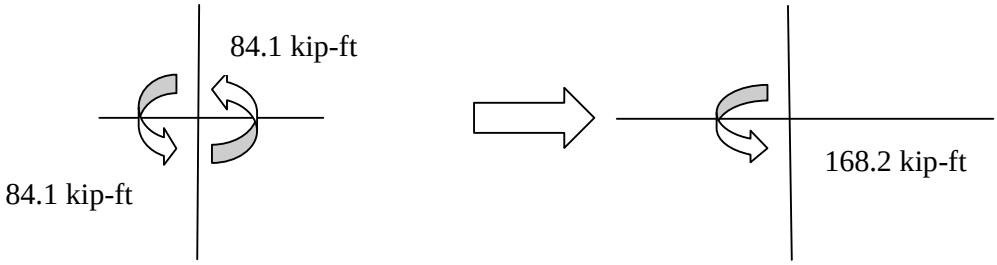

Moment calculation under lateral load portion of load combination -2

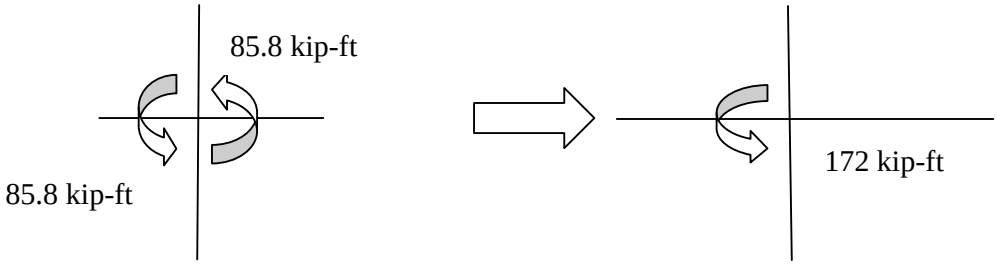

B-1.5 Combined gravity and lateral loads:

Moment calculation under both gravity and lateral loads of load combination -1

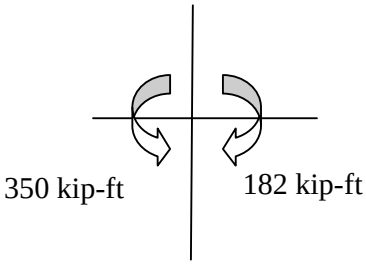

Moment calculation under both gravity and lateral loads of load combination -2

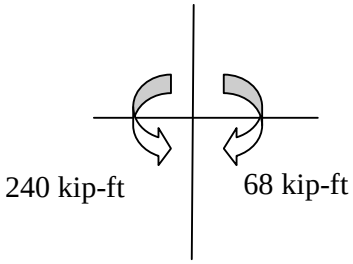

B-1.6 Unbalanced moment calculation under seismic Zone-3:

Total Base share, V = 296.1 kip

Shear at each interior column of bottom story level = {(296.1 × 1)/3} = 98.7≈99 kip

As it has already discussed in Sec. 6.3.2 that about 80% unbalanced moment have transferred through shear wall and rest 20% have transferred through slab-column joint. That is why; shear through each interior column of bottom story level is 19.8 kip.

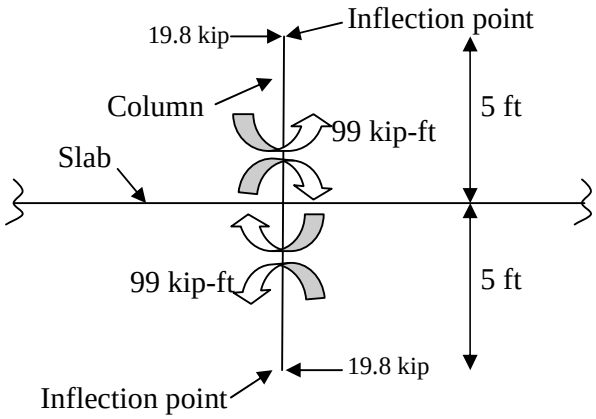

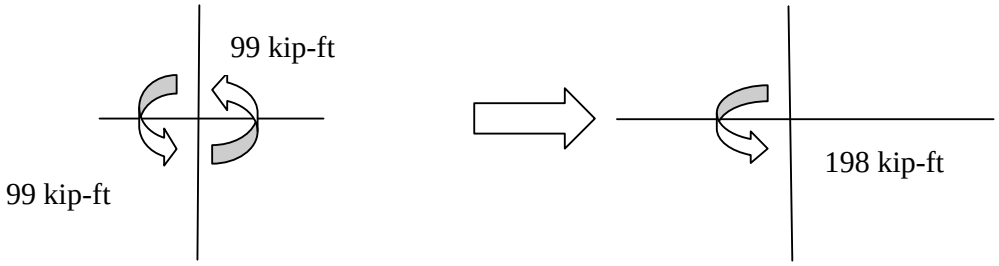

Here, $M_u = M_{slab} = 198$ kip-ft (Total unbalance moment)

Moment calculation under lateral load portion of load combination -1

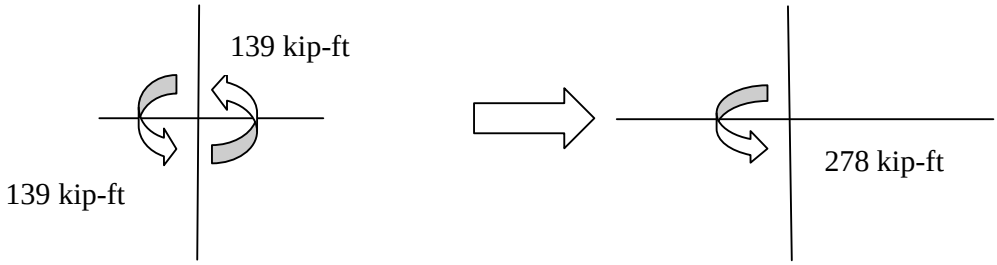

Moment calculation under lateral load portion of load combination -2

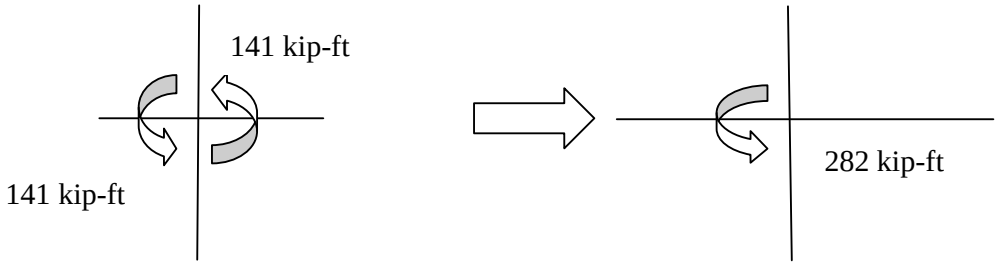

B-1.7 Combined gravity and lateral loads:

Moment calculation under both gravity and lateral loads of load combination -1

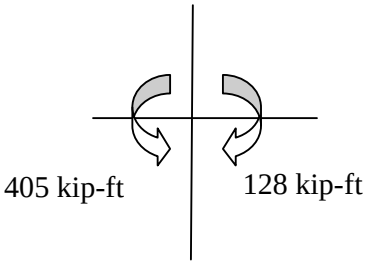

Moment calculation under both gravity and lateral loads of load combination -2

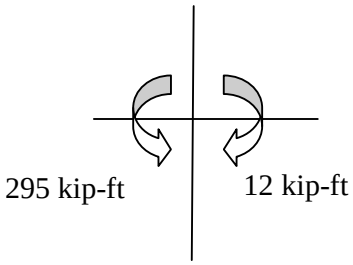

Based on direct design method, the column strip negative moment is 355 kip-ft. After a comparison between moments due to both gravity and lateral loads from above mentioned two combinations under seismic Zone-2 and Zone-3 and the moment based on direct design method, it is evident that Zone-2 is safe for design the high rise flat plate building having shear wall which is based on direct design method and Zone-3 is unsafe for design the same.